

Advanced functional porous materials for sensing and sequestration of toxic pollutants

A Thesis

Submitted in Partial Fulfillment of the Requirements for the
Degree of

Doctor of Philosophy

by

Arunabha Sen

Reg. ID: 20142007



Indian Institute of Science Education and Research (IISER), Pune

2021

Dedicated to

My parents, Aniruddha, Ananya and Poushali



Indian Institute of Science Education and Research (IISER), Pune

Certificate

It is hereby certified that the work described in this thesis entitled "*Advanced functional porous materials for sensing and sequestration of toxic pollutants*" submitted by *Mr. Arunabha Sen* was carried out by the candidate, under my supervision. The work presented here or any part of it has not been included in any other thesis submitted previously for the award of any degree or diploma from any other university or institution.

Date: 04.08.2021

A handwritten signature in blue ink, appearing to be "Sujit K. Ghosh", with a long horizontal stroke extending to the right.

Dr. Sujit K. Ghosh

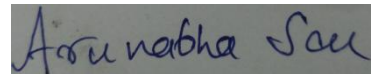
Research Supervisor

Email: sghosh@iiserpune.ac.in

Contact No.: +91(20)25908076

Declaration

I declare that this written submission represents my ideas in my own words and wherever other's ideas have been included; I have adequately cited and referenced the original sources. I also declare that I have adhered to all principles of academic honesty and integrity and have not misrepresented or fabricated or falsified any idea/ data/ fact/ source in my submission. I understand that violation of the above will cause for disciplinary action by the Institute and can also evoke penal action from the sources which have thus not been properly cited or from whom proper permission has not been taken when needed.



Date: 04.08.2021

Arunabha Sen

Reg. Id: 2014007

Acknowledgement

I would like to express gratitude from the core of heart to my research supervisor **Dr. Sujit K. Ghosh** for his continuous encouragement for improvement throughout my academic journey in Indian Institute of Science Education and Research (IISER) Pune. I believe his continual support always forwarded my research and it has been a learning process as well as freedom for me to work under his supervision. I believe that his inspirational supervision has taught me to think, plan and execute research projects with success. As an integrated-PhD student i joined his team as a master's student and his guidance was always there throughout the entire tenure even in the most difficult hours. Thank you very much Sir for having in faith in me throughout this entire time and most importantly for being such a great supervisor.

I sincerely acknowledge the former director of Indian Institute of Science Education and Research (IISER) Pune Prof. K. N. Ganesh and the current director Prof. J. B. Udgaonkar for developing excellent facilities and environment for research. I am also grateful to my research advisory committee (RAC) members, Dr. Benudhar Punji (NCL, Pune) and Dr. Moumita Majumder (IISER, Pune) for their valuable inputs and support during the annual meetings. I am also grateful to present chair Prof. H. N. Gopi and all other faculty members of the department of chemistry in IISER, Pune. I have learned a lot from all of them during my 2 year master's coursework period which I believe enriched my knowledge and love for the subject of Chemistry. I would also like to thank Dr. Angshuman Nag (IISER, Pune), Dr. Prasenjit Ghosh (IISER, Pune) and the senior students of their research team (Dr. Avishek Swarnakar and Dr. Niharika Joshi) who mentored my lab rotation projects in 'Physical chemistry' and 'Theoretical and Computational chemistry' during coursework. I would sincerely thank Dr. Partha Hazra, Dr. Shabana Khan, Dr. R Vaidyanathan, Dr. Seema Verma and Dr. Pramod Pillai of IISER, Pune from whom I have learned a great deal working as a teaching assistant. I would also my collaborator Dr. Mandar M. Shirolkar (Symbiosis, Pune) who helped me in completion of different research projects. I express my sincere gratitude to Ma'am (Dr. Sudarshana Mukherjee) for her friendly advices; and I wish Suvan and Suyosh all the best for their future.

It has been a great fortune and experience for me to be a member of the 'Microporous

Materials Lab' and I thank to all the past and present members of this great team. I would thank all of them (Dr. Sanjog Nagarkar, Dr. Biplab Joarder, Dr. Biplab Manna, Dr. Soumya Mukherjee, Dr. Avishek Karmakar, Arif Inamdar, Dr. Aamod V. Desai, Dr. Partha Samanta, Dr. Shivani Sharma, Dr. Samraj Mollick, Dr. Tarak Nath Mandal, Dr. Sreenu Bhanoth, Shilpa Sonar, Yogeshwar More, Prateek Agrawal, Subhajit Dutta, Sumanta Let, Writakshi Mandal, Sahel Fajal, Debanjan Mahato, Gourab Kumar Dam, Satyam Saurabh, Naveen Kumar, Priyanshu Chandra and Dr. Kriti Gupta. I would like to thank my senior Dr. Avishek Karmakar with whom I have worked during my master's project and learned a lot of things as well as Dr. Biplab Manna, Dr. Aamod V. Desai and Dr. Partha Samanta who have provided me inputs and counsel to improve and improvise for doing something good throughout this long journey of doctoral research. Apart from my seniors, I would mention my endless appreciation to all my current lab members, because without them this journey would not have been as possible. I would consider myself fortunate enough to have a friend in Subhajit with whom I had spent a lot of time and who always provided me endless heartiest inputs and efforts that guided me through the right ways in difficult times throughout the journey. I would mention Dr. Shivani Sharma and Sahel both of whom has provided me unconditioned help and inputs to move forward in terms of scientific work. I would like to acknowledge the on time assistance from Sumanta and Gourab in every necessary situation that helped me to achieve the desired goals. I would like to appreciate my friend Dr. Kriti Gupta specially for being selfless and helping me to overcome difficulties lying ahead in a lot of situations. I am especially thankful to Dr. Tarak Nath Mandal for giving me advices every time as a senior to improve my scientific visions and conscience. I am grateful to all of you for being so helpful and kind which helped me improve my scientific knowledge and also to become a good individual.

I would convey my regards towards my old school and college teachers who have encouraged me throughout different stages of life. I am also very much thankful to Dr. Arogyavaram Saha, Dr. Prasanta Ghosh, Dr. Amit Saharoy, Dr. Pulak Ganguly, Dr. Hrisikesh Chatterjee, Dr. Bikashbaran Ghosh, Dr. Bimal Kumar Sadhukhan and Dr. Rathindranath Ghosh of Ramkrishna Mission Residential College, Narendrapur (University of Calcutta) for teaching me and generating the love inside me for Chemistry. I would also thank all of my teachers from school for their education which helped me to move

forward. I would pay my deepest regards to Swami Satyatmananda, Swami Vedpurushananda (my first chemistry teacher in school), Satyanarayan Sarkar and Nirupam Chatterjee from Ramkrishna Mission Vidyalaya, Narendrapur with Rajat Bhattachaya and Siddhartha Bhattacharya from St. Lawrence High School for being such excellent teachers. I would also thank Dr. Amrit Mitra and Nilam Banerjee for helping me in academia.

I acknowledge IISER, Pune for providing me fellowship. I would also like to thank American Chemical Society (ACS), John Wiley & Sons (Wiley-VCH), Elsevier and Centralwestaustralia publisher for the various research articles and book chapters that I managed to publish in my PhD tenure. For the progress in such a long academic program, the support of technical and administrative staff is very important. I thank Dr. Umesha reddy Kacherki and Anuradha for library support, technical staff of the institute - Parveen Nasa, Archana, Mahesh Jadhav, Nilesh Dumbre, Swati, Anil, Yatish, Ganesh Dimbar, Suresh Prajapat, Sandeep, Nitin, Megha, Deepali and administrative staff - Mayuresh, Nayana, Tushar, Vrushali, Suresh, Prabhas, Priyadarshani for their help and assistance at multiple occasions. During my PhD tenure, I had the opportunity to attend national (MTIC-2017) conferences for which I thank my funding institute.

I wish to thank all my friends for their support and help at different stages of my life. I thank all my batch-mates (Integrated-PhD batch August-2014) and Chemphilic team-2018-19. I would like to acknowledge my childhood friend Sayak Dasgupta. I would deeply thank my school friends Rajan Paul, Debarnob Sarkar, Samrat Hembram, Sankhanil Saha, Ayan Das, Satyaki Khastagir, Pikon Medya, Kritavishek Mallick, Agnivo Sarkar, Arka Sarkar, Sohel Reja, Shrman Bhaduri, Soumyajit Nag, Arijit Mallick, Saptarshi Sarkar and friends during college life Shibam Chakraborty, Dibyajyoti Saha, Tirthankar Goon, Satyaki Sur, Pritam Dolui, Dipayan Mukherjee, Nilanjan Dey, Arpan Patra, Aishik Battacharya, Soumya Sinha and Treena Sarkar. I apologize in advance for not being able to take all of your names, but I feel it would not offend you to a great extent. Also, I would like to mention about my friends in campus Projjwal, Kingshuk, Krishnendu, Aslam, Saptashwa, Rijubrata, Soumya, Sudipa, Moitheli, Alakananda and Debashree for sharing innumerable rejoicing moments. I also thank my seniors Dr. Arindam Dasgupta, Dr. Supratik Sarkar, Dr.Sagar Satpati, Dr. Debanjan Chakrabarty, Dr.Soumendu Roy, Dr.Amit Bhunia, Rajarshi Dasgupta and Rahul Maity for their help.I also thank my juniors

Tamaghna, Arnab, Sumit, Pratim, Abhijit, Souvik, Indra, Joy, Pulak, Saikat, Rathijeet, Subhayan, Rithwik, Sanchayita, Joyeeta, Sukanya and wish them a prosperous future. I was a member of campus football community and IISM-2020. I wish all my sports comrades a great career in both sports and academia. I was an integral member of the football team 'Futbol Club De Proletariot' and wish my team to perform better every year in the championship.

Lastly, I am really grateful to my family members. My parents have experienced tremendous hardships and contributed their every drop of sweat and penny so that I can find the tough world more pleasant and experience least bitterness. I don't have enough words to express my gratitude towards them but without their constant sacrifices and support nothing would have been possible. I am grateful to grandmother and maternal uncle for teaching me the right path of morale and truth. And at the end I would and thank my little brother Aniruddha and my sisters Ananya and Poushali for making my life beautiful and wish them a great future ahead.

- Arunabha Sen

Contents

1. Introduction	
1.1 Advanced functional porous materials	1.1
1.2 Inorganic-organic hybrid porous materials	1.2
1.3 Porous organic materials (POMs)	1.5
1.4 Applications of AFPMs	1.9
1.5 Environmental pollution	1.10
1.5.1 Air pollution	1.11
1.5.2 Water pollution	1.12
1.6 Thesis overview	1.14
1.7 References	1.16
Part-I : Luminescent metal-organic frameworks (LMOFs) for sensing based applications	I.1
2. A 3D Metal-Organic Framework (MOF) as a luminescent sensor for selective Detection of Styrene	
2.1 Introduction	2.1
2.2 Experimental	2.3
2.3 Results and discussion	2.5
2.4 Conclusions	2.9
2.5 Appendix section	2.10
2.6 References	2.27
3. Post-synthetically modified MOF as a scaffold for selective bisulfite recognition in water	
3.1 Introduction	3.1
3.2 Experimental	3.3
3.3 Results and discussion	3.4
3.4 Conclusions	3.7

3.5	Appendix section	3.8
3.6	References	3.19
Part-II: : Functional porous organic polymers for sequestration based environmental applications		II.1
4. Functionalized ionic porous organic polymers exhibiting high iodine uptake from both vapor and aqueous medium		
4.1	Introduction	4.1
4.2	Experimental	4.3
4.3	Results and discussion	4.8
4.4	Conclusions	4.15
4.5	Appendix section	4.16
4.6	References	4.46
5. Imidazolium functionalized chemically robust ionic porous organic polymers (iPOPs) toward toxic oxo-pollutants capture from water		
5.1	Introduction	5.1
5.2	Experimental	5.3
5.3	Results and discussion	5.7
5.4	Conclusions	5.15
5.5	Appendix section	5.15
5.6	References	5.53
6. Summary and Perspectives		6.1

Synopsis

The research hypothesis is to design and synthesize functional porous materials and utilise them for sensing and sequestration of toxic air and water pollutants. The porous solids are further classified into a) *inorganic-organic hybrid porous materials*: built on metal-ligand co-ordination bond and b) *porous organic materials*: built on covalent bonding between synthons that sustain network solids. The main advantages rendered by such materials are their synthetic tuneability which leads to generation of pores within the infinite architecture enabling the materials to act as host matrix. The pores are occupied by guest molecules in case of neutral framework materials and counter-ions in case of ionic frameworks and the structures can be custom-designed by introducing desired functional groups. Such pre-selected supramolecular scaffolds offer the solid-state material chemists options to fine-tune the host-guest interaction. These properties of porous materials endow them with molecular recognition properties that include separation, molecular sensing as well as sequestration. In this work, a systematic study is carried out to develop new application specific advanced functional porous materials (AFPMS) based on different synthetic strategies. These newly designed functional porous materials are used as tool for molecular recognition of specific guest species that are harmful for our environment. In this regards attempts were made to design two distinct luminescent probe for selectively detecting styrene, a well known toxic air pollutant and bisulphite anion, (a hydrolysed derivative of a green house gas sulphur dioxide). Apart from air pollution, water pollution from industrial and radioactive waste is also a major problem which requires attention. In this context functional materials were synthesized for selective capture of such hazardous components from water based on principles of ion exchange and host guest interactions.

Chapter-1. Introduction

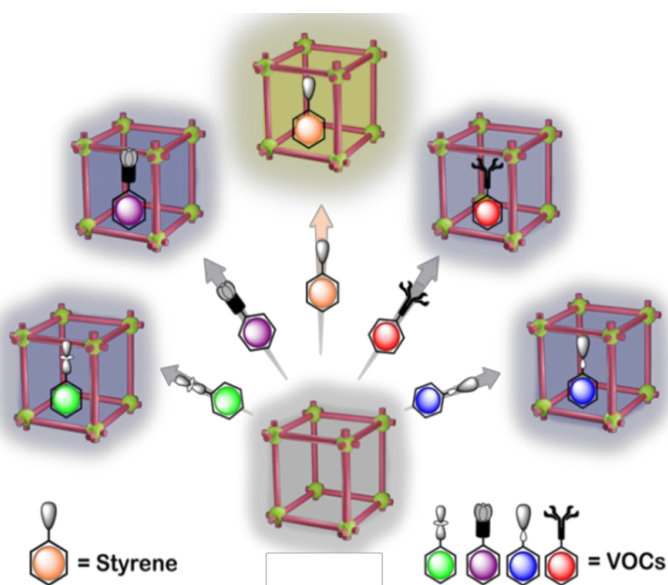
In this section a brief discussion on porous materials is included. This covers both inorganic-organic hybrid porous materials and porous organic materials. In case of inorganic-organic hybrid porous materials an overview have been provided for metal-organic frameworks (MOFs) and metal-organic polyhedras (MOPs) in terms of synthetic strategies and structural aspects along with the scope of their applications. For porous organic materials, several subclasses including covalent-organic frameworks (COFs), hydrogen-bonded organic frameworks (HOFs), porous organic cages (POCs) and porous organic polymers (POPs) would be discussed with their applications. One of the potential applications of porous materials is to detect and capture of different air and water pollutants leading to clean environment. In this regard a section would be introduced regarding the sources and harmful effect of different type of environment pollutants. An overview will be provided about the advantages and importance of functional porous materials and the strategies for usage in such applications.

Part-I: Luminescent metal-organic frameworks (L-MOFs) for sensing based applications

Luminescent MOFs (LMOFs) is a subclass of MOFs and they are utilized for molecular recognition. The advantages provided by LMOFs include their strategic application specific design as well as simplicity in terms of applications. The host-guest interaction within the porous scaffold of LMOFs offer a fast as well accurate response towards incoming guest analyte rendering tremendously potential for real time application. The aforementioned section of the thesis contains two chapters i.e. chapter-2 utilizing a LMOF to detect styrene, a toxic VOC and air pollutant while in chapter-3, a post-synthetically modified LMOF is utilized to detect bisulphite anion in water medium.

Chapter-2. A 3D Metal-Organic Framework (MOF) as a luminescent sensor for selective Detection of Styrene

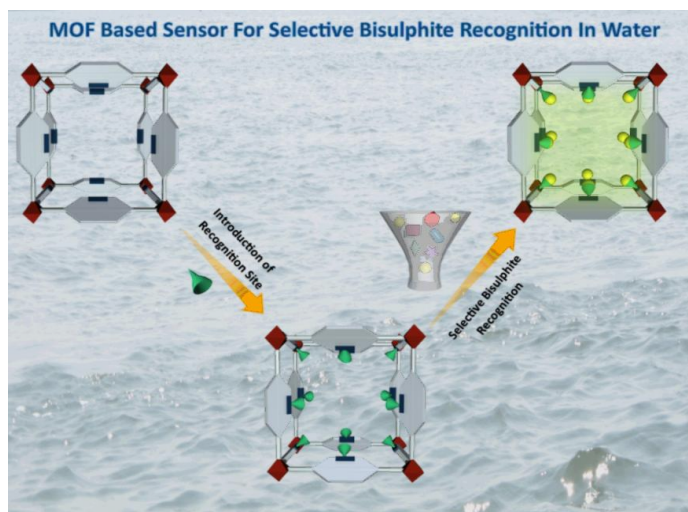
In this chapter, Zinc based MOF was synthesized using a neutral nitrogen-donor (N-donor) linker and inorganic hexafluorosilicate (SiF_6^{2-}) anion. The MOF has Zn(II) coordinated octahedral geometry with the equatorial position occupied by linker's pyridyl nitrogen while the axial positions are co-ordinated by SiF_6^{2-} anions. Such a coordinative arrangement leads to a three dimensional (3D) framework with generation of rectangular pores with 1D channel along crystallographic *a*-axis. Such porous architecture decorate with functional groups along with presence of Zn^{2+} metal nodes propelled us for luminescence studies with the aromatic volatile organic compounds (VOCs). The blue emissive parent MOF shows a selective and distinctive yellow luminescent response in presence of styrene in both solution and air-dried phase retaining its structural integrity. The MOF can act as potential luminescence probe for detection of such toxic air pollutants for real time application. (*Manuscript under preparation*).



Chapter- 3. Post-synthetically modified MOF as a scaffold for selective bisulfite recognition in water

Bisulfite anion (HSO_3^-) is produced by hydrolysis of sulphur dioxide (SO_2), a recognized air pollutant. Such anions are used as antioxidant in food and beverage industries but it is observed that bisulphite anion generates biological disorder in human at high concentration. So recognition of bisulfite is essential in water medium. MIL (Materials Institut Lavoisier) is a series of porous and chemically stable carboxylate linker based MOFs, well explored for a variety of molecular recognition based applications. In this work, $\text{NH}_2\text{-MIL-68(In)}$ having pendant amine functionality was chosen and post synthetically modified by affixing functional aldehyde moieties. The post synthetically tailored MOF $\text{NH}_2\text{-MIL-68(In)@CHO}$ exhibited a turn on photoluminescence response selectively towards bisulfite anion in water. This recognition was consistent even in occurrence of other competing anions in water. It was also observed that $\text{NH}_2\text{-MIL-68(In)@CHO}$ retains its structural integrity post bisulphite recognition.

Reference: [Arunabha Sen](#), [Aamod V. Desai[†]](#), [Partha Samanta[†]](#), [Subhajit Dutta](#), [Sumanta Let](#) and [Sujit K. Ghosh](#), *Polyhedron.*, 2018, **156**, 1-5.



Part-II: Functional porous organic polymers for sequestration based environmental applications

Porous organic polymers (POPs) are porous organic materials build on purely organic building blocks connected by covalent linkages. Based on synthetic strategies and methodologies POPs can be neutral as well as ionic where extra framework counter ions are present for charge balance. The metal free light weight nature of POPs with presence of functional cores and backbone as well as robust architecture leads to high chemical and hydrolytic stability. Presence of all these properties leads such materials for utilization in sequestration based applications. In this section, in chapter 4 such materials are utilized for

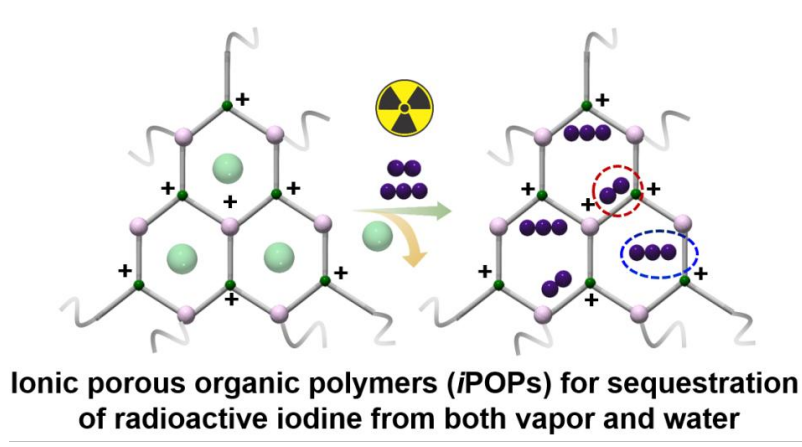
uptake of iodine (as a surrogate for radio-iodine, a nuclear fission product) from vapour phase and water. In chapter 5, cationic POPs are utilized for capturing oxo-anions of heavy metals (chromate) and radioactive fission products (perhenate anion is used as surrogate for radioactive pertechnetate) which causes severe water pollution through principle of ion exchange.

Chapter-4. Functionalized ionic porous organic polymers exhibiting high iodine uptake from both vapor and aqueous medium

Radioactive iodine generated from nuclear fission represents a threat to the environment due to their high half life. So capture of such radioactive isotopes is an important problem and hence the quest for an ideal adsorbent is on. Also the volatile nature of iodine also leads to accumulation in water in form of polyiodide. Hence an ideal material should be able to identify and capture iodine from both vapour phase and water. In this work two chemically stable ionic polymers compound-1 and compound-2 were utilized to detect as well as capture iodine in both of the aforementioned phases. The compounds show an instant colorimetric change in presence of iodine as well as high uptake capacity in both vapour phase and water. Such multifunctional material for both detection and sequestration of radioactive iodine is important for real time application.

Reference: [Arunabha Sen,[†] Shivani Sharma,[†] Subhajit Dutta, Mandar M. Shirolkar, Gourab K. Dam, Sumanta Let and Sujit K. Ghosh, *ACS Appl. Mater. Interfaces.*, 2021, **13**, 29, 34188-34196.](#)

DOI: 10.1021/acsami.1c07178.

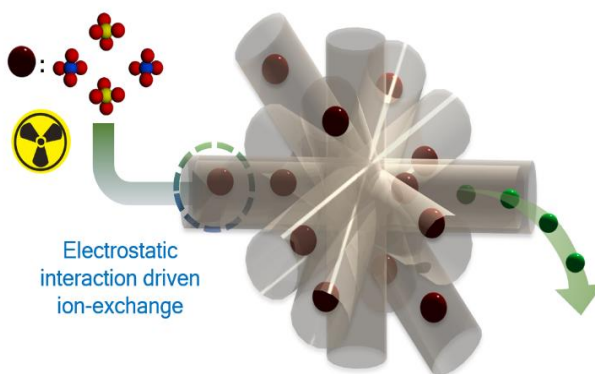


Chapter 5. Imidazolium Functionalized Chemically Robust Ionic Porous Organic Polymers (iPOPs) toward Toxic Oxo-pollutants Capture from Water

In this work, two ionic porous polymers were synthesized via quaternization of a triazine based tripodal bromide based precursor with imidazol and benzimidazol . The resultant polymers contain a cationic aromatic functional group rich backbone with bromide as the extra framework anions. The polymers

exhibited high thermal and chemical stability and provided an excellent platform for capture of oxo-anionic pollutants from water medium. Chromate generated from industrial effluents is enlisted by the EPA (Environment Protection Agency) as a top priority water pollutant while Per technetate a well known radioactive waste with high half-life and water solubility. These two oxo-anions were chosen in this work for sequestration based functional studies in water. Perrhenate was used as surrogate anion for per technetate anion for this work. Both the polymers showed fast kinetics as well as appreciable uptake amounts for the anions retaining their structural integrity. The uptake was unaltered in presence of other concurrent anions in water and recyclable up to four cycles citing the potential for the materials for usage in real time applications.

Reference: [Arunabha Sen,[†] Subhajit Dutta,[†] Subhajit Dutta, Gourab K. Dam, Partha Samanta, Sumanta Let, Shivani Sharma, Mandar M. Shirolkar and Sujit K. Ghosh, *Chem. Eur. J.*, 2021, **27**, 53, 13442-13449;DOI: 10.1002/chem.202102399.](#)



Toxic Oxo-pollutants trapping by ionic POPs

Chapter 6. Summary and perspectives

In this section a summary has been provided based on the studies herein. This work primarily focuses on systematic design, synthesis and application of new advanced functional porous materials (AFPMS) to address the threat of environmental pollution. Based on that functional AFPMS were strategically designed and utilized for recognition of toxic air pollutants and sequestration of harmful water pollutants. Such studies based on of AFPMS for recognition of toxic pollutants could provide a way to develop aforementioned materials as a new platform to address the concerning issues of environmental pollution in near future.

Abbreviations

Anal.	Analysis
Calc.	Calculated
DMF	N,N'-dimethylformamide
MeOH	Methanol
EtOH	Ethanol
FT-IR	Fourier transform infra-red spectroscopy
mg	Miligram
g	Gram
SCXRD	Single-Crystal X-Ray Diffraction
RT	Room Temperature
min	Minutes
mL	Milliliter
mmol	Milli moles
MOF	Metal-Organic Framework
MOP	Metal-Organic Polyhedra
COF	Covalent-Organic Framework
MOG	Metal-Organic Gel
POP	Porous organic polymer
<i>i</i> POP	Ionic porous organic polymer
PAF	Porous aromatic framework
COP	Covalent-Organic Polymer
CMP	Conjugated microporous polymer
PPN	Porphyrin-Phthalocyanine network
HCP	Hyper-cross-linked polymer
PXRD	Powder X-Ray Diffraction
RT	Room Temperature
TGA	Thermo-gravimetric Analysis
UV	Ultraviolet
FE-SEM	Field Emission Scanning Electron Microscopy
NMR	Nuclear Magnetic Resonance
EDX	Energy Dispersive X-ray Analysis
VOC	Volatile organic compound

PVDF	Polyvinylidene fluoride
IPM	IISER Pune Materials
IPM-326	Name of the MOF used in this work in Chapter-2

Rights and Permissions

Chapter 3:

Reprinted (adapted) with permission from *Polyhedron.*, 2018, **156**, 1-5.
(<https://doi.org/10.1016/j.poly.2018.08.069>). Copyright 2018: Elsevier.

Chapter4:

Reprinted (adapted) with permission from *ACS Appl. Mater. Interfaces.*, 2021, **13**, 29, 34188-34196.(DOI: 10.1021/acsami.1c07178) Copyright 2021: American Chemical Society.

Chapter 5:

Reprinted (adapted) with permission from *Chem. Eur. J.*, 2021, DOI: 10.1002/chem.202102399, Copyright 2021: John Wiley and Sons. Licence number 5124690485737 dated 9th August 2021.

Research Publications

([†] - indicates equal contribution)

Included in Thesis:

1. Post-synthetically modified metal-organic framework as a scaffold for selective bisulphite recognition in water.
Arunabha Sen, Aamod V. Desai[†], Partha Samanta[†], Subhajit Dutta, Sumanta Let and Sujit K. Ghosh.
Polyhedron., 2018, **156**, 1-5.
2. Functionalized ionic porous organic polymers exhibiting high iodine uptake from both vapor and aqueous medium.
Arunabha Sen[†], Shivani Sharma[†], Subhajit Dutta, Mandar M. Shirolkar, Gourab K. Dam, Sumanta Let and Sujit K. Ghosh.
ACS Appl. Mater. Interfaces., 2021, **13**, 29, 34188-34196.
DOI: 10.1021/acsami.1c07178.
3. Imidazolium functionalized chemically robust ionic porous organic polymers (iPOPs) toward toxic oxo-pollutants capture from water

Arunabha Sen[†], Subhajit Dutta[†], Gourab K. Dam, Partha Samanta, Sumanta Let, Shivani Sharma, Mandar M. Shirolkar and Sujit K. Ghosh.

Chem. Eur. J., 2021, **27**, 53, 13442-13449.

DOI: 10.1002/chem.202102399 (Just accepted).

4. A 3D Metal-Organic Framework (MOF) as a luminescent sensor for selective Detection of Styrene.

Arunabha Sen[†], Sahel Fajal[†], Subhajit Dutta, Aamod V. Desai and Sujit K. Ghosh.

(Manuscript under preparation)

Not Included in Thesis:

5. Advanced porous materials: a promising candidate for sequestration of industrial hazardous dye effluents.

Arunabha Sen, Partha Samanta and Sujit K. Ghosh.

Book chapter, 2019, 177-228. Edited by: Dr. Vikash Mittal, Book Title: Porous Polymer Networks.

6. Hydrogen-Bonded Organic Frameworks (HOFs): A New Class of Porous Crystalline Proton-Conducting Materials.

Avishek Karmakar, Rajith Illathvalappil[†], Bihag Anothumakkool[†], **Arunabha Sen**[†], Partha Samanta, Aamod V Desai, Sreekumar Kurungot and Sujit K Ghosh.

Angew. Chem. Int. Ed., 2016, **55**, 10667-10671.

7. Ultrahigh Ionic Conduction in Water-Stable Close-Packed Metal-Carbonate Frameworks.

Biplab Manna[†], Aamod V Desai[†], Rajith Illathvalappil, Kriti Gupta, **Arunabha Sen**, Sreekumar Kurungot and Sujit K Ghosh.

Inorg. Chem., 2017, **56**, 9710-9715.

Chapter 1

Introduction

1.1 Advanced functional porous materials (AFPMs)

Porosity is a concept inherited in nature with naturally abundant porous materials include rocks and biological systems.^[1] Such porous architectures are generated as result of extended structure and packing of molecules leading to formation of voids and represent an exciting class in the research area of materials development.^[2] An important classification of porous materials is based on its pore size or the distance between opposite surfaces of the pore. Based on this, the materials with the pore size less than 2 nanometer (nm) is called microporous materials while the materials with pore size between 2 to 50 nm are called mesoporous materials. The materials with pore size greater than 50 nm are called macroporous materials.^[3] The early class of porous materials include zeolites and Aluminophosphates (ALPOs) constructed from covalent bonding between inorganic nodes.^[3-5] The past two decades have witnessed a significant uplift in the synthesis of various class of new porous materials commonly termed as advanced functional porous materials (AFPMs) through utilisation of novel synthetic strategies and functional building blocks.^[1,6] The construction of these materials are carried out in two important strategies which are a) Utilisation of functional organic synthons and inorganic nodes to construct organic-inorganic hybrid porous frameworks and b) Usage of organic functionalised building blocks via covalent linking as well as noncovalent interactions to synthesize metal free porous organic materials (Figure 1.1). The former class include metal-organic architectures like metal-organic Frameworks (MOFs) and metal-organic polyhedras (MOPs) while the later being functionalised porous organic materials (POMs).^[7-11] POMs consist of crystalline porous organic architectures like covalent-organic Frameworks (COFs), hydrogen-bonded organic Frameworks (HOFs), porous organic cages (POCs) as well as amorphous porous organic systems which include various kinds of porous organic polymers (POPs).^[12-15] One of the important aspects for construction of the aforementioned AFPMs depend on the judicious choice of constituent building blocks. The building blocks are engineered in such a way that a target specific functionality is introduced into the framework backbone to device a functional interactive porous scaffold within the materials in accordance with the application in hand.^[6,7] Such fabrication of porous materials leads to generation of two kinds of porosity termed as a) extrinsic porosity and b) intrinsic porosity. The word extrinsic indicates ‘between the molecules’ while the word intrinsic refers to ‘within the molecules’. Based on this, extrinsic porosity refers to the porosity generated in the molecular architectures as a result of packing between the molecules while intrinsic porosity refers to the generation of pores as a consequence of the shape and geometry of the building blocks.^[16-17] All these synthetic design strategies are utilised to develop different class of AFPMs for usage in a large number of applications in the field of molecular recognition as a host matrix.^[1-2, 6-7]

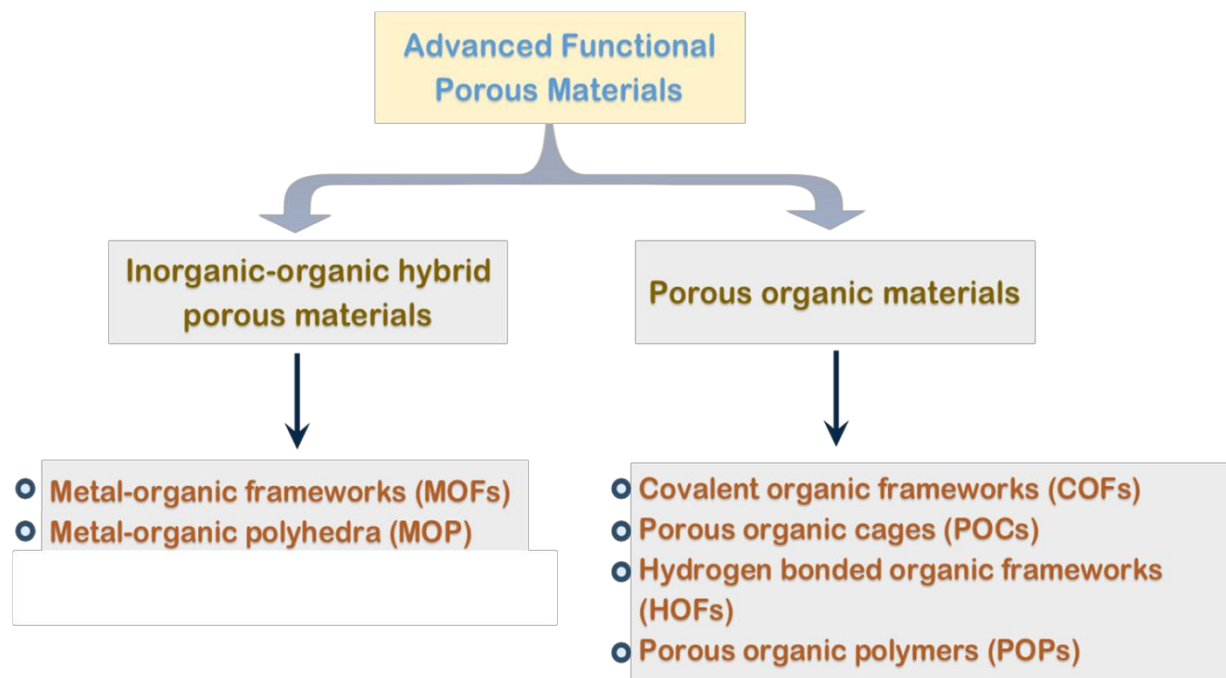


Figure 1.1: Schematic representation for classification of different types of advanced functional porous materials.

1.2 Inorganic-organic hybrid porous materials

Inorganic-organic hybrid porous materials consist of both organic linkers and inorganic metal nodes/clusters. Such class of porous materials can be further classified in metal-organic Frameworks (MOFs) and metal-organic polyhedras (MOPs). The following porous materials would be discussed in brief in this section.

1.2.1 Metal-organic framework (MOF)

MOFs are special class of AFPMs and subclass of co-ordination polymers bearing potential voids. Such porous structures are constructed via co-ordination bond formation between inorganic metal nodes or clusters and organic struts and represent a class of hybrid porous materials.^[18, 19] MOFs are synthesized at room temperature or through solvothermal crystallisation methods from ligand and metal precursor solutions.^[20] After the formation of the framework, the porous voids are normally occupied by the solvent molecules of the synthetic reaction medium. These guest solvents are to be removed via desolvation by vacuum treatment or heating to access the space inside the pores of the MOF for different applications.^[21] MOFs are categorised in three different generations based on the structural features of the synthesized framework. The first generation framework loses its structural integrity post desolvation and does not exhibit permanent porosity. The second generation frameworks retains its structural integrity in case of both addition and removal of guest molecules while the third generation also known as ‘Dynamic

frameworks' show flexible behaviour by transforming into an alternate structure post desolvation or in presence of any external stimulus. Another important characteristic of such frameworks is their reversible dynamism that is upon resolution or removal of external stimulus, the framework reverts back to its parent structure.^[22] Another method for synthesizing functional MOFs is the 'post synthetic modification (PSM)' approach where a MOF synthesized by aforementioned pre-synthetic strategies, bear a functional reactive subunit within the porous architecture which is further utilised for chemical transformation to generate structurally identical but functionally different porous MOFs (Figure 1.2).^[23] The main utility of PSM is that it allows harnessing the otherwise unavailable functional MOFs which are difficult to synthesize by conventional synthetic routes.^[24]

Functional MOFs can be classified based on their charges on the framework backbone leading to generation of neutral MOFs and ionic MOFs (*i*-MOFs).^[25] The organic struts utilised in MOF chemistry to bind the metal nodes normally consist of carboxylate ($-\text{COO}^-$) functionalities and different heterocyclic donors containing nitrogen atoms for co-ordinating with the metal centre.^[26-27] The nature of the framework can be tuned strategically based on the nature of organic counterpart utilised in MOF fabrication. Utilisation of carboxylic acid based ligands often produces neutral MOFs as the binding occurs between cationic metal nodes with anionic carboxylate functionalities resulting in charge neutrality. On the other hand *i*-MOFs can be classified to cationic and anionic frameworks based on their electrostatic nature. Cationic MOFs are generated when there are excess of positive charges in the framework backbone along with the presence of additional counter anion to maintain the charge neutrality. Such frameworks are formed by neutral nitrogen donor based ligand systems where the positive charge of the metal centre is not neutralised post co-ordination by neutral nitrogen atoms of the ligand. On the other hand anionic frameworks are formed if the ligand contains multiple anionic sites so that the metal nodes post co-ordination fails to satisfy the condition of charge neutrality and excess counter cations are required additionally to be present within the framework for electrostatic charge balance (Figure 1.2).^[25]

MOFs are utilised for a wide spectrum of applications based on their structural features as well as high surface area. The pore dimension associated with MOFs as well as pendant functionalities in the backbone of framework enables the potential exploration of host guest chemistry.^[28] MOFs are often utilised for storage of gases as well as challenging gas separation from mixture of gases which are extremely important from industrial perspectives. The most relevant application of MOFs includes separation of carbon dioxide, a well known greenhouse gas from a mixture of gases like nitrogen, methane and hydrogen which addresses the issue of carbon capture and sequestration (CCS).^[29] MOFs are also utilized for separation of the xylene isomers, styrene and ethylbenzene as well as benzene and

cyclohexane molecules.^[30-31] Separation of aforementioned triad and pairs are very difficult through conventional distillation techniques due to their close resemblance in their boiling point. The porous cavity present within MOFs are also utilised for host guest recognition offering selective sensing response toward different incoming analytes including both cationic and anionic species, explosives as well as biomolecules.^[32] The encapsulation of analytes within the porous voids enables MOF to act as carrier molecule helping in drug delivery based biological applications.^[33] The presence of functionalised moieties within porous network of MOFs aid them acting as tool for heterogeneous catalytic applications.^[34] In case of ionic frameworks the presence of extra framework counter-ions provide scope for ion exchange based applications that is highly relevant for environment friendly molecular recognition involving sensing and sequestration of toxic hazardous molecules.^[35] MOFs are also one of the front runners in developing materials for electrochemical, clean energy and ion conduction based applications.^[36-37] Also the encapsulation of guest species like nano particles and functional molecules inside porous cavity of MOFs leads to development of composite materials, applied in energy and environment related applications.^[38]

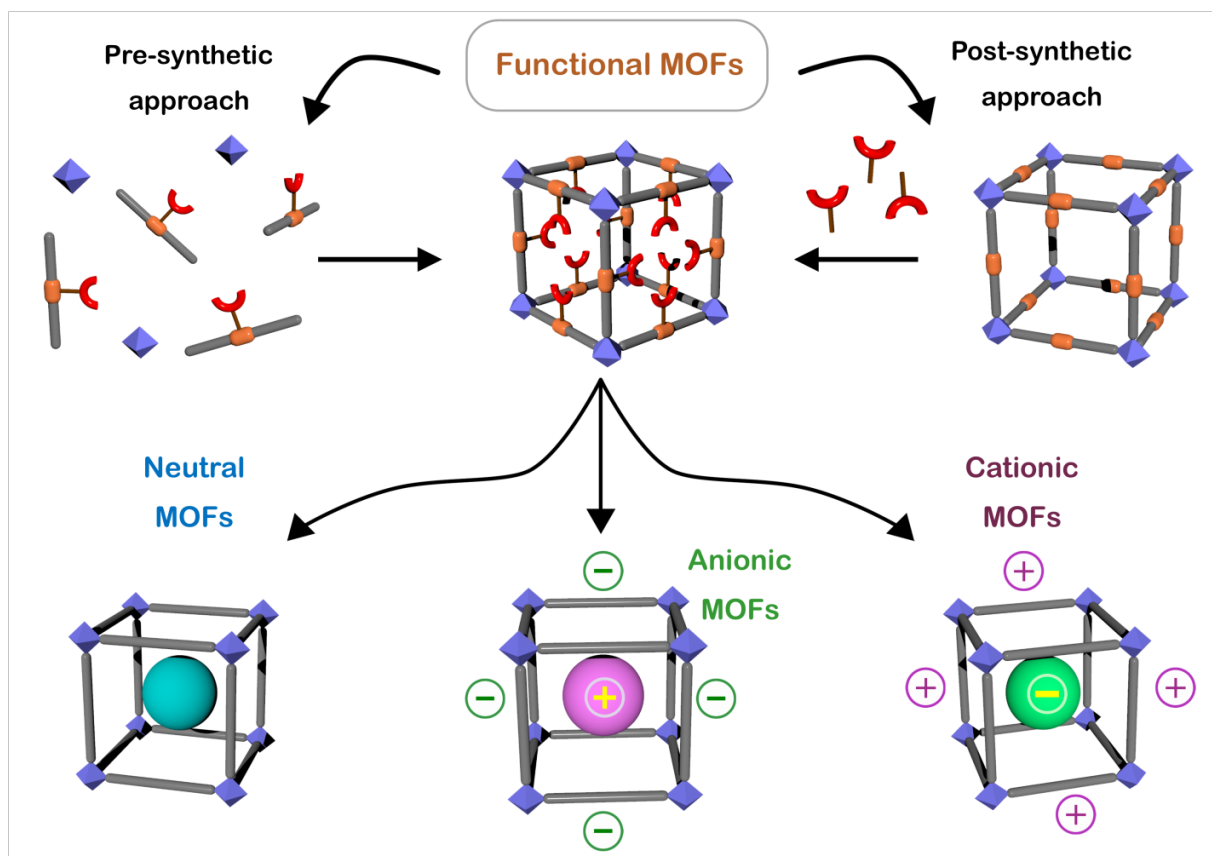


Figure 1.2: Schematic representation showing strategies for construction of different types of MOFs.

1.2.2 Metal-organic polyhedra (MOP)

Metal-organic polyhedras (MOPs) are an important class of inorganic-organic hybrid porous architectures.^[9] These are discrete supramolecular entity constructed from organic ligands like carboxylic acids and nitrogen heterocyclic moieties and metal ion based clusters as the secondary building unit (SBU).^[39] These molecules are synthesized via strategic choice and utilization of aforementioned ligands of definite geometry and symmetry along with metal precursors in a perfect stoichiometry.^[9,39] MOPs can be synthesized both via room temperature crystallization as well as solvothermal methods while post synthetic transformations are also carried out in pre-synthesized materials to enhance stability or achieve desired functionalities.^[40] MOPs have definite polyhedral shape with defined vertices and faces and they generate porous cavities based on molecular assembly.^[9,39] The solution processable nature of MOPs also provides excellent platform for host-guest chemistry enabling various applications including molecular storage, separation, heterogeneous catalysis, ion transport and drug delivery.^[9a]

1.3 Porous organic materials (POMs)

Porous organic materials are built from functional organic molecules rendering light weight property to such materials. Another distinctive feature is the metal free nature of such materials. Based on the synthetic strategy, structural order of such frameworks could be controlled to a great extent. As a result of that, POMs can be crystalline in case of covalent-organic Frameworks (COFs), hydrogen-bonded organic Frameworks (HOFs), porous organic cages (POCs) and amorphous for porous organic polymers (POPs) (Figure 1.3). The aforementioned materials would be introduced in this section.

1.3.1 Covalent organic framework (COF)

Covalent organic frameworks (COFs) are an exciting class of crystalline POMs constructed from organic building blocks. COFs are constructed from condensation reaction of monomers with multiple reactive sites which helps in the formation of the polymeric network.^[41] The principle of dynamic covalent chemistry is utilized in case of COF synthesis where reversible chemical reactions are utilized to generate the most thermodynamically stable polymeric network. Such methodology leads to the generation of a highly crystalline ordered polymeric structure through bond breaking and bond making procedure. The difference between noncrystalline porous polymers and crystalline COFs results from the reaction pathway where the former is the kinetically controlled product while the later is the thermodynamically controlled product.^[42] The synthetic condition for preparation of COFs depends on two factors which are reaction conditions and choice of the building blocks. COFs could be constructed using room

temperature, solvo-thermal, mechano-chemical, iono-thermal and microwave synthetic techniques while the parent monomers involved are of distinct symmetry. Such symmetry induced monomers leads to formation of COFs of variation topology and symmetry based on different types of organic reactions.^[43-44] The utilization of boronic acid and ester based reactions, schiff base reaction condition involving amine, hydrazine and hydrazone linkages, amide and imide formation reactions, trimerisation reactions in case of crystalline covalent triazine frameworks (CTFs) as well as different organometallic coupling reactions has been explored to synthesize COFs. Apart from that, post-synthetic modification (PSM) is also carried out to synthesize task specific COFs.^[43] COFs could be 2D involving planar structure with high pi-pi stacking among alternate layers leading to formation of highly ordered structure. Apart from that 3D COFs are also well explored where the framework contains tetrahedral building blocks involving sp^3 carbons or silane based covalent linkages helping in propagation of the polymeric structure in all three dimensions.^[44] The structural robustness arises in COFs due to the presence of stabilizing noncovalent interaction amongst the different layers leading to its stability in varying chemical environment including water, acidic and basic conditions.^[45-46]

COFs are utilized for diverse applications due to their structural robustness and light weight nature. COFs are utilized for storage of carbon dioxide, hydrogen, ammonia and methane as well as for heterogeneous catalysis based applications attributed to their large surface area. COFs are also utilized for sensing of toxic analyte and environmental applications. Ionic COFs are also used for different ion exchange based applications.^[15,44] The 2D nature of COFs enables the utilization as materials for semiconductors, optoelectronics, photoconduction as well as clean energy based applications. For practical applications thin films are constructed from COFs that are utilized for different molecular recognition and energy based applications.^[47]

1.3.2 Hydrogen-bonded organic framework (HOF)

HOFs represent another emerging interesting crystalline class of POMs. Unlike other POMs, HOFs are built from organic building blocks utilizing noncovalent interactions and hydrogen bonding.^[13] HOFs are built from monomers containing a hydrogen bond donor and a hydrogen bond acceptor moiety.^[13,48] The functional groups utilized for construction of HOFs involves carboxylic acid and amide based moieties, guanidinium-organosulphonate moieties, diaminotriazine (DAT) based moieties and nitrogen hetrocyclic moieties. The basic principle of synthesizing HOFs depends on the control as well as stability of hydrogen bonds in propagation of the network.^[49] Another important factor regarding the construction of HOFs with permanent porosity is that the hydrogen bond assisted supramolecular architecture should be stable after guest solvent removal to access the porous voids post solvent removal. All these factors

contributes together to synthesize functional HOFs for molecular recognition and clean energy based applications. HOFs are utilized in field of separation of different gas molecules, particular in separation of hydrocarbons and carbondioxide from nitrogen.^[50] HOFs are also utilized for sensing and capture of different molecules including enzyme encapsulation as well as for clean energy based application including proton conduction.^[13, 51]

1.3.3 Porous organic cage (POC)

Porous organic cages (POCs) are an important class of porous solids built from organic building blocks through covalent and noncovalent interactions.^[14,17] POCs exhibit intrinsic porosity on account of packing of the constituent building blocks in solid state generating the porous cavity within the architecture.^[52] Along with that the discreteness of POCs helps in the improvement of their solution processible property.^[53] The synthesis of POCs depends on important factors including geometry of the parent molecules, inclusion of a balance between rigidity as well as flexibility in the bonds involved in formation of the cage, choices of appropriate reaction conditions including solvent, temperature as well as stoichiometry of the starting materials.^[52-54] Cages are synthesized by utilization of organic reactions including reversible imine bond formation and irreversible carbon carbon bond forming organometallic coupling reactions through crystallization in both room and high temperature.^[54] The stability of cages is very important to achieve the permanent porous nature for the POCs. The voids within the POCs are preoccupied by guest molecules and to access those it is extremely important to remove the guest solvents inside.^[53] During the process of desolvation it's important for the POCs to retain its structural integrity and that is possible with effective packing of the molecules, presence of rigid bonds within the architecture and stabilizing noncovalent interactions.^[52-55] Also post synthetic modifications have been carried out in presynthesized POCs to achive functional POCs with enhancement in porosity, stability as well achieve task specific property.^[56] POCs are utilized for molecular recognitions involving separation of gases as well as small molecules.^[57-58]

1.3.4 Porous organic polymer (POP)

Porous organic polymers represent a wide class of amorphous AFPMs constructed by tethering functional organic moieties like hetrocycles, macrocycles and fused aromatic systems through covalent linkages.^[59] These class of materials include the polymers with intrinsic microporosity (PIMs), conjugated microporous polymers (CMPs), hyper-crosslinked polymers (HCPs), covalent triazine frameworks (CTFs) and porous aromatic frameworks (PAFs). These organic porous compounds are synthesized via different types of organic reactions both in solution as well as solid state including Friedel crafts reactions in cases of HCPs, trimerisation of nitrile functionalities in case of CTFs as well as different types of

organometallic crosscoupling reactions like Sonogashira-Hagihara coupling, Yamamoto coupling and Suzuki coupling for PIMs, PAFs and CMPs.^[11,15,59] The strategic choice of functional synthons with multiple reaction sites facilitates the propagation of infinite network structure. Depending upon the structure of building blocks as well as free rotation of the pendant chemical bonds, the materials can be two dimensional as well as three dimensional in nature.^[60] The main advantage provided by POPs is that it contains the features of both porous materials as well as the organic polymers. The presences of porous voids generate sufficient space for host guest interaction while the polymeric backbones provide rigid structural architectures. Porosity can be optimised and tuned in this type of materials through variation of following factors including monomer structure and shape, the synthetic route as well as the reactivity of the components.^[59, 61] The reaction conditions which includes concentration of starting materials, amount of solvent and catalyst if used as well as temperature can cause subtle effect in the porous nature of the generated porous solids. POPs are well known for their high surface area leading to generation of excellent porosity and robust nature displaying of high stability in varying chemical environment. The metal free nature of POPs also helps them to act as low density materials while in some cases the short range order in the structures of POPs generated due to nature of packing in molecular level helps them to gain solution processibility.^[60] This is important for real time applications as such materials can be utilised in both solution and solid state as well as in form of thin films.^[15]

Alike MOFs, POPs are also utilised for different applications including storage of multiple gases like hydrogen, methane as well as separation of carbon dioxide from other gases. POPs are employed as a scaffold for heterogeneous catalysis due to the presence of large pores to accommodate functional molecules important for catalytic applications as well as structural stability and excellent reusability.^[59, 62] Both hydrophilic and hydrophobic functionalities could be incorporated within the pores of POPs promoting applications in field of molecular recognition including molecular separation, sensing as well as selective capture of a particular molecule from both water and organic medium.^[59, 63-64] The presence of extended conjugation within backbones of POPs also helps in achieving different photophysical and light harvesting applications while strategic incorporation of appropriate functional moieties also propels these materials to be used in different electrochemical applications.^[59, 65-66]

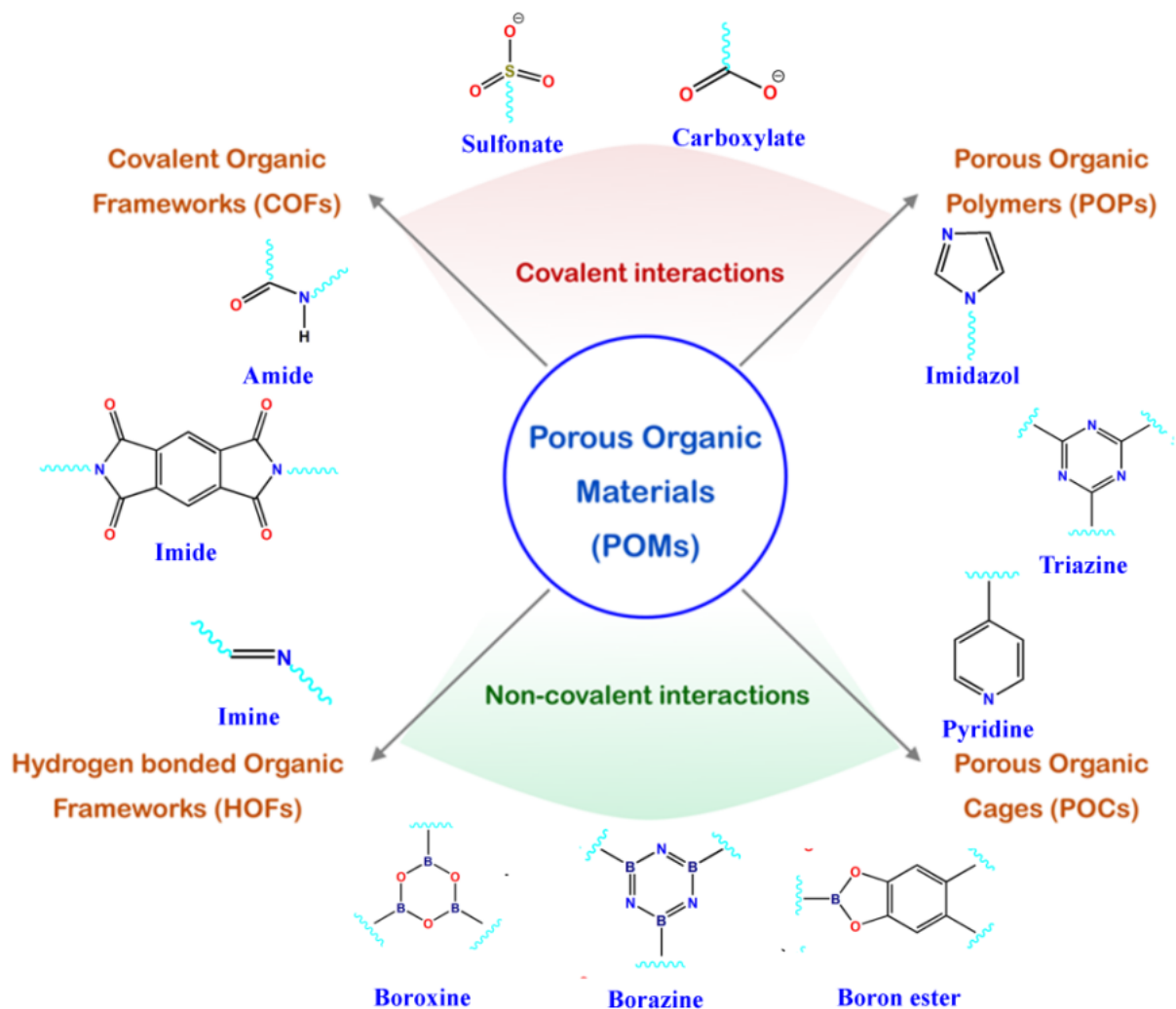


Figure 1.3: Schematic representation for different types of porous organic materials along with the important functional building blocks utilized for synthesis.

1.4 Applications of AFPMs

AFPMS are utilised for a variety of applications (Figure 1.4). This includes molecular storage, separation and sensing based applications.^[9a,15,29,31,32,44,50,58,59,62] The aforementioned materials are also used for heterogeneous catalysis, biomedical and energy based applications.^[13,33,34,36,47,65,66] The porous nature and functionality decorated architecture of AFPMS hold tremendous potential in usage as host matrix for recognition as well as sequestration of environmental pollutants. This includes air pollutants like green house gases, volatile organic compounds and radioactive vapours as well as water pollutants like pharmaceutical and radioactive wastes along with the oxo-anions of heavy metals.^[35] Such functional applications of AFPMS are explored to limited extent and there is a huge scope for AFPMS to represent as

ideal host materials to recognise and capture toxic and harmful pollutants and showing promises to tackle the problems based on environmental pollution.

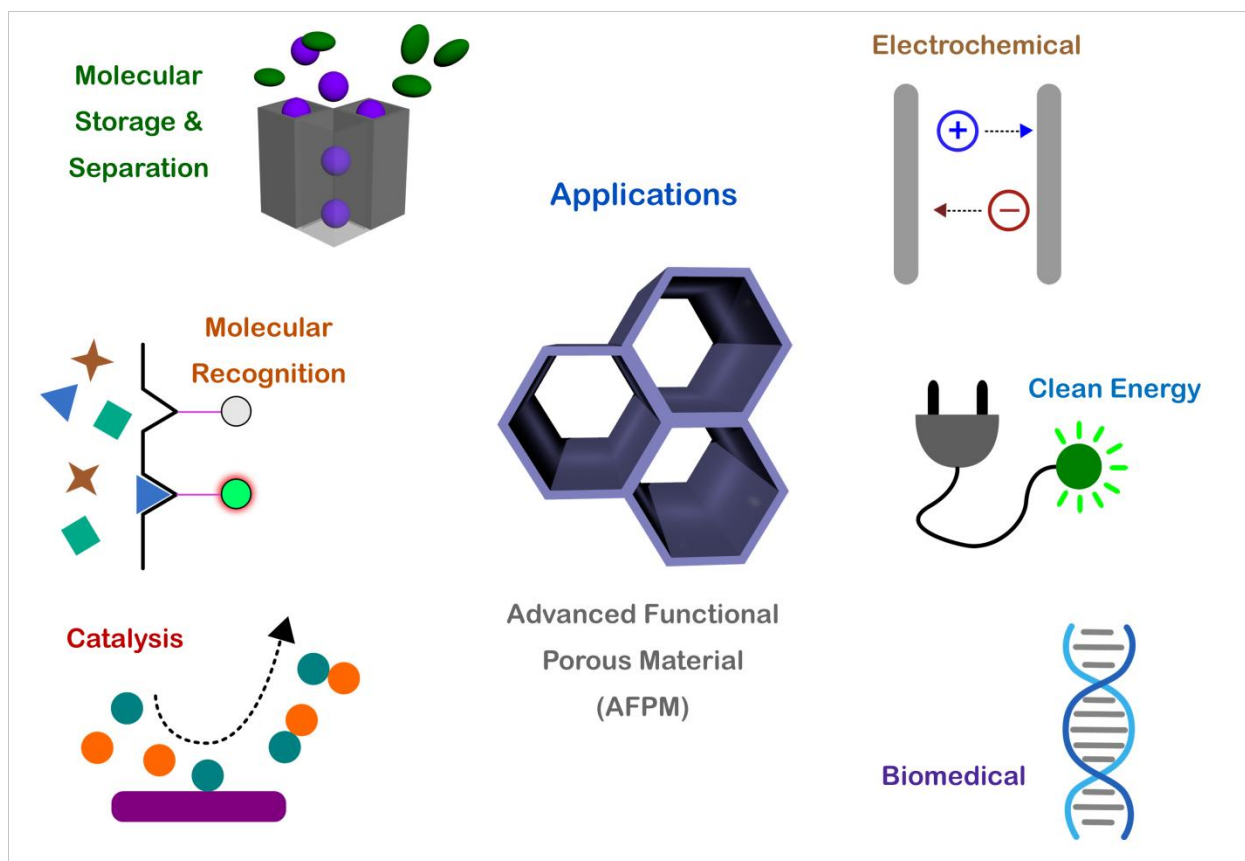


Figure 1.4: Schematic representation for different applications of AFPMs.

1.5 Environmental pollution

The last few decades exhibited industrialisation for improvement of economic prosperity which simultaneously leads to the dreadful consequences of environmental pollution. Environmental pollution implies introduction of harmful substances into the environment through natural and manmade sources which hampers the regular environmental process.^[67a] The major forms of environment pollution are air, water and soil pollution^[67b] Air pollution is caused by natural sources volcanic eruptions, forest fire and artificial manmade sources introducing green house gases and volatile organic compounds in air.^[68-69] The continuous drainage of toxic industrial, pharmaceutical, biological and polymeric wastes in natural water bodies is the main reason for water pollution and it leads to huge damage of the marine ecosystem.^[67b-c] Soil pollution is mainly done through dumping of chemical wastes, fertilizers and pesticides by human sources compromising the natural pH of the soil.^[67a-b] These different types of pollution causes great damage to nature, ecosystems and human life and hence addressing such threats are tremendously

important.^[67d-e] In this section a brief discussion in details would be carried about air and water pollution and the strategies of utilisation of AFPMs in remediation of such global problems.^[67f]

1.5.1 Air pollution

Air mainly consists of nitrogen (~78 %) and oxygen (~21 %) by volume along with presence of small amounts of inert gases like helium and argon along with carbon dioxide, methane, hydrogen and water vapour.^[68a] The word air pollution signifies the introduction of toxic harmful species to air which causes severe damage to living beings and environment. Air pollution represents one of the major global concerns in this century due to its adverse effects over environment and also causing huge deaths across the globe.^[68] Air pollution is generally caused by the green house gases, the fine particulate matter and ozone (Figure 1.5). The green house gases (carbon dioxide, methane, nitrogen based oxides and fluorinated gases) traps heat into atmosphere and releases heat waves leading to unnatural climate change threatening the environment to a large extent.^[69] Another major concern is the depletion of the ozone layer in stratosphere. The ozone layer through filtration protects earth from harmful solar ultraviolet rays. Owing to air pollution the emitted halogen based carbon compounds participates in chemical reactions in atmosphere causing depletion of aforementioned ozone layer.^[70] The fine particulate matters are generated due to emission of sulphur dioxide and nitrogen based oxides while ozone is produced from the reaction of nitrogen based oxides and the volatile organic compounds (VOCs) in the atmosphere.^[71] The fine particulate matters affect the human cardiovascular system while ozone causes asthma and permanent damage to respiratory systems.^[70] The nitrogen and sulphur based oxides often reacts with atmospheric water and oxygen causing acid rain which contaminates the natural body as well as perturbs soil composition. The major sources of aforementioned air pollutants are different industrial sources, automobiles as well as natural sources like volcanic eruptions and forest fires. Owing to this the recognition as well as identification of toxic air pollutants like nitrogen, carbon and sulphur based oxides as well as the volatile organic compounds are of tremendous importance.^[67] The World health organisation (WHO), the United nations (UN) and the world bank along with environmental agencies of different countries are working together in this regard to construct a clean and green world for the future.^[72] AFPMs represent a new class of materials in recognition of toxic air pollutants due to their task specific synthetic tuneability and well as large surface area and functionally decorated pores (Figure 1.6). Carbon dioxide (CO₂) is a well known greenhouse gas which is generated from combustion and demands huge attention towards the scientific problem of carbon capture and sequestration (CCS). CO₂ capture is carried out in two ways which are capture of CO₂ from mixture of gases from gas reserves including hydrogen and methane known as precombustion and capture of CO₂ from exhaust gas mixtures mainly containing nitrogen called post combustion. Advanced functional porous materials including MOFs, MOF

based mixed matrix membranes and POPs containing functional CO₂ interaction sites have been successfully employed to tackle the CCS issues in different varying conditions of both pre and post combustion.^[29, 76] Another major air pollutant includes aromatic and aliphatic VOCs. Due to their volatile nature, such compounds are easily emitted in atmosphere from industries and household activities. AFPMs have been utilised as materials for trapping of VOCs involving both physical and chemical adsorption methods owing to structural tuneability and decorated functional pores.^[35b, 73] These materials are also employed for capture of toxic air pollutants including sulphur dioxide, ammonia, hydrogen sulphide, radioiodine and mercury vapours.^[35b, 74] Apart from sorption, detection of toxic air pollutants are also important.^[67] Different types of mass spectrometric and spectroscopic techniques are utilised for detection of aforementioned compounds.^[75] Among them fluorescence spectroscopy with features including quick and accurate response along with simplicity of operation provide scope for luminescent AFPMs toward sensing of toxic gases like sulphur dioxide, carbon monoxide and carbon dioxides as well as VOCs.^[67] The surface area provided by AFPMs allows sufficient preconcentration of incoming analytes helping in production of distinctive transduction signals important for development of fluorescent air pollutant sensors applicable for real time applications in future.^[77]

1.5.2 Water pollution

Water pollution has come forth as one of the most genuine global crisis in the 21st century and leads to huge casualties including damage of marine ecosystem and loss of human lives.^[78] The major sources of water pollution include drainage of industrial as well as radioactive waste from nuclear power plants along with daily life human activities.^[79] The major chemical water pollutants include both toxic organic and inorganic components (Figure 1.5). The organic compounds include antibiotics, pharmaceuticals, pesticides, herbicides and dyes. The inorganic counterpart consist of toxic metal cations including mercury, lead and cadmium (Hg²⁺, Pb²⁺, Cd²⁺) as well as cationic radionuclides like caesium, uranium and strontium ions (Cs⁺, UO₂⁺, Sr²⁺). Among the inorganic anionic pollutants the oxoanions of heavy metals like chromium, arsenic, selenium (CrO₄²⁻, Cr₂O₇²⁻, AsO₄³⁻, SeO₃²⁻, SeO₄²⁻) and the radioactive anions pertechnetate (⁹⁹TcO₄⁻) and different polyiodides of radioiodine (¹³¹I, ¹²⁹I) also features in the list.^[80] All these pollutants are well known for affecting human physiology and causing large number of global deaths. They are responsible for extreme environmental casualties and present a major obstruction in the path of accessing clean drinking water as enlisted by US environmental protection agency (US-EPA).^[81] Access to clean water is very important for survival and for that reuse and refining water by purification serves as an efficient alternate pathway to tackle the problem.

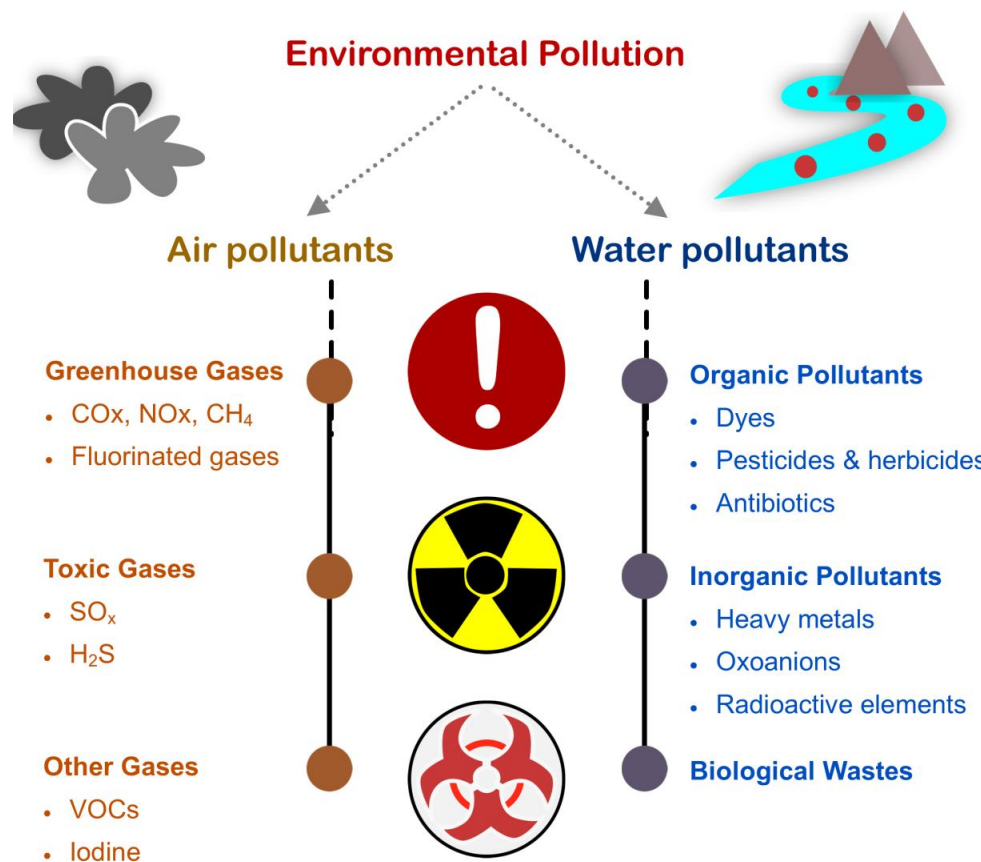


Figure 1.5: Schematic representation showing different types of environmental pollution along with the major sources.

In this context detection and sequestration of water pollutants can be regarded as a scientific problem of top priority. In the field of detecting water pollutants, two factors are of tremendous importance. Firstly the techniques should be simple, error free and producing quick output signal.^[77] Secondly the material should be robust and stable in water retaining high selectivity towards the targeted pollutant. As mentioned earlier fluorescence spectroscopy hold distinct advantages as a method for detecting such pollutants.^[82] Hence luminescent AFPMs are employed for sensing of various toxic water pollutants. Apart from detection, sequestration as well as degradation of such pollutants from water through advanced oxidation and photocatalytic processes is also important.^[35a] For that purpose efficient and cost friendly adsorption based technique is utilised for selective sequestration of toxic water pollutants over sedimentation, precipitation, coagulation and membrane technologies.^[83-84] Among the adsorbents, layered double hydroxides (LDH), inorganic clays, resins and zeolites are utilised for sequestration of water pollutants. But these materials lack superiority in performance in terms of sorption kinetics, capacity and selectivity of uptake.^[85] This is mainly due to the fact that in such materials the fine tuning

during synthesis that can lead to a specific as well as improved performance is confined to a great extent. [86] The advantages rendered by AFPMs include their large porous functionally decorated architecture which is utilised for selective sequestration of particular pollutant of choice in large quantity from a pool of other analytes present in water with least generation of secondary pollutants. [87-88] Additionally, AFPMs can be recycled efficiently with retention of performance post first cycle. Keeping all these electronic and steric factors in account AFPMs can be utilised as host matrix for sequestration of water pollutants (Figure 1.6). [35a, 89-90]

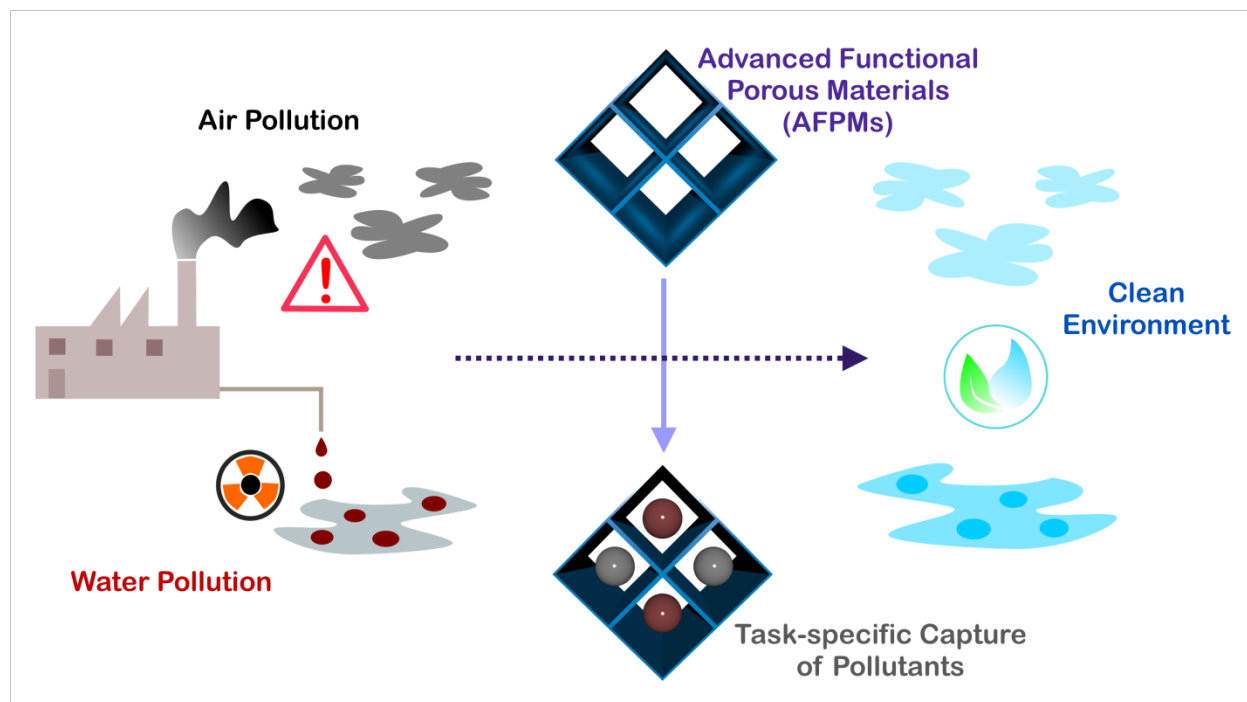


Figure 1.6: Schematic representation for utilization of AFPMs for remediation of environmental pollution.

1.6 Thesis Overview

All the scientific works included in this thesis focus on the utilization of AFPMs as a tool for detection and sequestration of toxic environment pollutants. Task specific AFPMs are designed and synthesized for identification and encapsulation of both toxic air and water pollutants. In the first part of the work functionalised luminescent MOFs are constructed through diversified pre and post synthetic route and employed toward identification of toxic air pollutants through chemosensor and chemodosimetric approach. In the second part of the work robust and hydrolytically stable porous organic polymers with aromatic backbone are used for efficient encapsulation of toxic water pollutants in a selective manner. Such strategic studies related to fabrication and investigation of AFPMs as a tool for environmental remediation is explored very less in the literature to the best of our knowledge.

In the second chapter, a luminescent MOF was constructed from functionalised N-donor linker and zinc metal nodes. The resultant MOF was three dimensional and neutral containing one dimensional channel to accommodate guest molecules. The electron deficient nature of the framework enables strong host guest interaction with electron rich styrene molecule. This leads to generation of distinct as well as selective yellow luminescent signal in presence of styrene molecule among a library of aromatic VOC molecules. Thus the MOF can be utilised as luminescence based probe for detection of styrene, a toxic air-pollutant. In the third chapter a chemodosimetric luminescent probe was constructed by post-synthetically attaching aldehyde group to a water stable luminescent MOF NH₂-MIL-68(In) where MIL stands for 'Materials Institut Lavoisier'. The MOF NH₂-MIL-68(In)@CHO was used to identify bisulphite anion, a hydrolysed product of sulphurdioxide selectively through reaction based approach where post bisulphite interaction an enhancement was observed in luminescence intensity of the probe.

Apart from sensing of toxic pollutants, selective sequestration of such compounds serves as an alternate strategy to control the problem of environmental pollution. Based on that in the fourth chapter, two cationic chemically stable ionic porous organic polymer (*i*POPs) were utilised to detect and capture iodine both in vapour phase and water. Iodine serves as a surrogate for radio iodine liberated post nuclear fission and gets accumulated in air as iodine vapour and water bodies in the form of stable polyiodides. The aforementioned *i*POPs showed quick colorimetric changes in presence of both iodine vapour as well as iodine in water. In addition to that it shows selective as well as appreciable amount of iodine uptake in both phases. The uptake behaviour is reversible and consistent upto four cycles with no drop in performance. Apart from iodine, oxoanions of heavy metals produced from industries and nuclear powerplants are deposited in natural water bodies causing enormous pollution and hampers marine ecosystem. Thus designing of materials to address the problem is essential. Based on that in the fifth chapter two hydrolytic and chemically stable cationic POPs were designed to selectively capture chromate anion, an enlisted industrial water pollutant. Along with that the aforementioned POPs were also employed for perrhenate uptake as a surrogate anion for radioactive, toxic and water soluble prrtechnetate anion. The uptake amount of both anions by the POPs lies within appreciable range in the literature. The uptake process was kinetically facile as well as selective for the oxoanions in presence of concurrent anions commonly available in water and thus provides scope for real time application.

1.7 References

- [1] D. Zhao, P. K. Thallapally, C. Petit and J. Gascon, *ACS Sustainable Chem. Eng.*, 2019, **7**, 7997-7998.
- [2] A. I. Cooper, *ACS Cent. Sci.*, 2017, **3**, 544-553.
- [3] M. E. Davis, *Nature.*, 2002, **417**, 813-821.
- [4] M. E. Davis and R. F. Lobo, *Chem. Mater.*, 1992, **4**, 756-768.
- [5] A. Corma, *Chem. Rev.*, 1997, **97**, 2373-2419.
- [6] A. G. Slater and A. I. Cooper, *Science*, 2015, **348**, aaa8075.
- [7] J. Jhiang, Y. Zhao and O.M. Yaghi, *J. Am. Chem. Soc.*, 2016, **138**, 3255-3265.
- [8] H.-C. Zhou and S. Kitagawa, *Chem. Soc. Rev.*, 2014, **43**, 5415-5418.
- [9] (a) N. Ahmad, H. A. Younus, A. H. Chughtai and F. Verpoort, *Chem. Soc. Rev.*, 2015, **44**, 9-25; (b) D. J. Tranchemontagne, Z. Ni, M. O’Keeffe and O. M. Yaghi, *Angew. Chem., Int. Ed.*, 2008, **47**, 5136-5147.
- [10] J. H. Jung, J. H. Lee, J. R. Silverman and G. John, *Chem. Soc. Rev.*, 2013, **42**, 924-936.
- [11] R. Dawson, A. I. Cooper and D. J. Adams, *Prog. Polym. Sci.*, 2012, **37**, 530-563.
- [12] S. Yuan, X. Li, J. Zhu, G. Zhang, P. V. Puyvelde and B. V. Bruggen, , *Chem. Soc. Rev.*, 2019, **48**, 2665-2681.
- [13] J. Luo, J.-W. Wang, J.-H. Zhang, S. Laia and D.-C. Zhong, *CrystEngComm.*, 2018, **20**, 5884–5898.
- [14] M.A. Little and A. I. Cooper, *Adv. Funct. Mater.*, 2020, **30**, 1909842.
- [15] D. Wu, F. Xu, B. Sun, R. Fu, H. He and K. Matyjaszewski, *Chem. Rev.*, 2012, **112**, 3959-4015.
- [16] M. J. Bojdys, M. I. E. Briggs, J. T. A. Jones, D. J. Adams, S. Y. Chong, M. Schmidtman and A. I. Cooper, *J. Am. Chem. Soc.*, 2011, **133**, 16566-16571.
- [17] J. R. Holst, A. Trewin and A. I. Cooper, *Nat. Chem.*, 2010, **2**, 915-920.
- [18] H. Furukawa, K. E. Cordova, M. O’Keeffe and O. M. Yaghi, *Science.*, 2013, **341**, 6149.
- [19] H.-C. Zhou, J. R. Long and O. M. Yaghi, *Chem. Rev.*, 2012, **112**, 673-674.
- [20] J. Ren, X. Dyosiba, N. M. Musyoka, H. W. Langmi, M. Mathe and Shijun Liao, *Coord. Chem. Rev.*, 2017, **352**, 187-219.

- [21] D. Wu, P.-F. Zhang, G.-P. Yang, L. Hou, W.-Y. Zhang, Y.-F. Han, P. Liu and Y.-Y. Wang, *Coord. Chem. Rev.*, 2021, **434**, 213709.
- [22] S. Horike, S. Shimomura and S. Kitagawa, *Nat. Chem.*, 2009, **1**, 695-704.
- [23] Z. Wang and S. M. Cohen, *Chem. Soc. Rev.*, 2009, **38**, 1315–1329.
- [24] S. M. Cohen, *J. Am. Chem. Soc.*, 2017, **139**, 2855-2863.
- [25] A. Karmakar, A. V. Desai and S. K. Ghosh, *Coord. Chem. Rev.*, 2016, **307**, 313-341.
- [26] Y. He, B. Li, M. O’Keeffe and B. Chen, *Chem. Soc. Rev.*, 2014, **43**, 5618-5656.
- [27] J. -P. Zhang, Y. -B. Zhang, J. -B. Lin and X.-M. Chen, *Chem. Rev.*, 2012, **112**, 1012-1033.
- [28] A. Karmakar, P. Samanta, A. V. Desai and S. K. Ghosh, *Acc. Chem. Res.*, 2017, **50**, 2457-2469.
- [29] B. Seoane, J. Coronas, I. Gascon, M. E. Benavides, O. Karvan, J. Caro, F. Kapteijna and J. Gascon, *Chem. Soc. Rev.*, 2015, **44**, 2421-2454.
- [30] S. Mukherjee, D. Sensharma, O.T. Qazvini, S. Dutta, L. K. Macreadie, S. K. Ghosh, R. Babarao, *Coord. Chem. Rev.*, 2021, **437**, 213852.
- [31] S. Mukherjee, A. V. Desai and S. K. Ghosh, *Coord. Chem. Rev.*, 2018, **367**, 82-126.
- [32] M. D. Allendorf, C. A. Bauer, R. K. Bhaktaa and R. J. T. Houka, *Chem. Soc. Rev.*, 2009, **38**, 1330-1352.
- [33] L. Wang, M. Zheng and Zhigang Xie, *J. Mater. Chem. B.*, 2018, **6**, 707-717.
- [34] B. Li, M. Chrzanowski, Y. Zhang and S. Ma, *Coord. Chem. Rev.*, 2016, **307**, 106-129. .
- [35] (a) P. Samanta, A. V. Desai, S. Let and S. K. Ghosh, *ACS Sustainable Chem. Eng.*, 2019, **7**, 7456-7458; (b) Y. Zhang, X. Cui and H. Xing, *Mater. Chem. Front.*, 2021, Advance Article; <https://doi.org/10.1039/D1QM00516B>.
- [36] X. Cao, C. Tan, M. Sindorob and H. Zhang, *Chem. Soc. Rev.*, 2017, **46**, 2660-2677.
- [37] (a) T. Yamada, K. Otsubo, R. Makiurac and H. Kitagawa, *Chem. Soc. Rev.*, 2013, **42**, 6655-6669; (b) W. Liu and X. -B. Yin, *Trends in Analytical Chemistry.*, 2016, **75**, 86-96.
- [38] Q. -L. Zhu and Q. Xu, *Chem. Soc. Rev.*, 2014, **43**, 5468-5512.

- [39] (a) N. Ahmad, A. H. Chughtai, H. A. Younus and F. Verpoort, *Coord. Chem. Rev.*, 2014, **280**, 1-27; (b) H. Duan, Y. Li, Q. Li, P. Wang, X. Liu, L. Cheng, Y. Yu and L. Cao, *Angew. Chem. Int. Ed.*, 2020, **132**, 10187-10196.
- [40] S. Mollick, S. Fajal, S. Mukherjee and S.K. Ghosh, *Chem. Asian*, 2019, **14**, 3096 – 3108.
- [41] M. J. Mancheño, S. Royuela, A. de la Peña, M. Ramos, F. Zamora and J. L. Segura, *J. Chem. Educ.* 2019, **96**, 1745–1751.
- [42] S. J. Lyle, P. J. Waller and O. M. Yaghi, *Trends in Analytical Chemistry.*, 2019, **1**, 172-184.
- [43] X. Feng, X. Ding and D. Jiang, *Chem. Soc. Rev.*, 2012, **41**, 6010–6022.
- [44] X. Chen, K. Geng, R. Liu, K. T. Tan, Y. Gong, Z. Li, S. Tao, Q. Jiang and D. Jiang, *Angew. Chem., Int. Ed.*, 2020, **59**, 5050-5091.
- [45] X. Ma and T. F. Scott, *Commun. Chem.*, 2018, **1**, 1-15. doi.org/10.1038/s42004-018-0098-8.
- [46] T. He, K. Geng and D. Jiang, *Trends in Analytical Chemistry.*, 2021, **3**, 431-444.
- [47] H. Wang, Z. Zeng, P. Xu, L. Li, G. Zeng, R. Xiao, Z. Tang, D. Huang, L. Tang, C. Lai, D. Jiang, Y. Liu, H. Yi, L. Qin, S. Ye, X. Rena and W. Tanga, *Chem. Soc. Rev.*, 2019, **48**, 488–516.
- [48] X. Luo, X. Jia, J. Deng, J. Zhong, H. Liu, K. Wang, D. Zhong, *J. Am. Chem. Soc.*, 2013, **135**, 11684–11687.
- [49] (a) Y. He, S. Xiang and B. Chen, *J. Am. Chem. Soc.*, 2011, **133**, 14570–14573; (b) P. Li, Y. He, H. D. Arman, R. Krishna, H. Wang, L. Weng and B. Chen, *Chem. Commun.*, 2014, **50**, 13081-13084; (c) P. Li, Y. He, Y. Zhao, L. Weng, H. Wang, R. Krishna, H. Wu, W. Zhou, M. O. Keeffe, Y. Han and B. Chen, *Angew. Chem. Int. Ed.*, 2015, **54**, 574 –577; (d) P. Li, Y. He, J. Guang, L. Weng, L. J. C. Zhao, S. Xiang and B. Chen, *J. Am. Chem. Soc.*, 2014, **136**, 547–549.
- [50] (a) K. T. Holman, A. M. Pivovar, J. A. Swift and M. D. Ward, *Acc. Chem. Res.*, 2001, **34**, 107-118; (b) K. Ma, P. Li, J. H. Xin, Y. Chen, Z. Chen, S. Goswami, X. Liu, S. Kato, H. Chen, X. Zhang, J. Bai, M. C. Wasson, R. R. Malnodado, R. Q. Snurr and O. K. Farha, *Cell Reports Physical Science.*, 2020, **1**, 100024; (c) T. Khadivjam, H. C. Quang, T. Maris, Z. Ajoyan, A. Howarth, and J. D. Wuest, *Chem. Eur. J.*, 2020, **26**, 7026-7040.
- [51] R-B. Lin and B. Chen, *Nat. Chem.*, 2019, **11**, 1078-1080.
- [52] J. D. Evans, C. J. Sumby and C. J. Doonan, *Chem. Lett.*, 2015, **44**, 582–588.

- [53] 2.M. E. Briggs and A. I. Cooper, *Chem. Mater.*, 2017, **29**, 149–157.
- [54] T. Hasell and A. I. Cooper, *Nat Rev Mater.*, 2016, **1**, 16053.
- [55] T. Tozawa, J. T. A. Jones, S. I. Swamy, S. Jiang, D. J. Adams, S. Shakespeare, R. Clowes, D. Bradshaw, T. Hasell, S. Y. Chong, C. Tang, S. Thompson³, J. Parker, A. Trewin, J. Bacsá, A. M. Z. Slawin, A. Steiner and A. I. Cooper, *Nature Mater.*, 2009, **8**, 973-978.
- [56] H. Wang, Y. Jin, N. Sun, W. Zhang and J. Jiang, *Chem. Soc. Rev.*, 2021, Advance Article. <https://doi.org/10.1039/D0CS01142H>
- [57] G. Zhang, Y. Ding, A. Hashem, A. Fakim and N. M. Kashab, *Cell Reports Physical Science.*, 2021, **2**, 100470.
- [58] L. Chen, P. S. Reiss, S. Y. Chong, D. Holden, K. E. Jelfs, T. Hasell, M. A. Little, A. Kewley, M. E. Briggs, A. Stephenson, K. M. Thomas, J. A. Armstrong, J. Bell, J. Busto, R. Noel, J. Liu, D. M. Strachan, P. K. Thallapally and A. I. Cooper, *Nature Mater.*, 2014, **13**, 954-960.
- [59] S. Das, P. Heasman, T. Ben and S. Qiu, *Chem. Rev.*, 2017, **117**, 1515-1563.
- [60] Y. Yuan and G. Zhu, *ACS Cent. Sci.*, 2019, **5**, 509-518.
- [61] X. Zou, H. Rena and G. Zhu, *Chem. Commun.*, 2013, **49**, 3925—3936.
- [62] N. Fontanals, R. M. Marcé, F. Borrulla and P. A. G. Cormack, *Polym. Chem.*, 2015, **6**, 7231–7244.
- [63] L. Tan and B. Tan, *Chem. Soc. Rev.*, 2017, **46**, 3322-3356.
- [64] N. Chaoui, M. Trunk, R. Dawson, J. Schmidt and A. Thomas, *Chem. Soc. Rev.*, 2017, **46**, 3302-3321.
- [65] T. Zhang, G. Xing, W. Chen and L. Chen, *Mater. Chem. Front.*, 2020, **4**, 332-353.
- [66] T. Liu and G. Liu, *Nat. Commun.*, 2020, **11**, 1-3.
- [67] (a) <https://www.britannica.com/print/article/468070>; (b) P. O. Ukaogo, U. Ewuzie and C. V. Onwuka, *Elsevier.*, 2020, **21**, 419-429; (c) A. Vaseashta, M. Vaclavikova, S. Vaseashta, G. Gallios, P. Roy and O. Pummakarnchana, *Sci. Technol. Adv. Mater.*, 2007, **8**, 47-59; (d) R. Saxena, S. Srivastava, D. Trivedi, E. Anand, S. Joshi and S. K. Gupta, *Acta Ophthalmologica Scandinavica.*, 2003, **81**, 491-494; (e) <https://www.worldwildlife.org/threats/pollution>; (f) X. Ma, Y. Chai, P. Li and Bo Wang, *Acc. Chem. Res.*, 2019, **52**, 1461–1470.

- [68] (a) J. Lelieveld and U. Pöschl, *Nature.*, 2017, **551**, 291-293; (b) H.-Y. Li, S. -N. Zhao, S. -Q. Zang and J. Li, *Chem. Soc. Rev.*, 2020, **49**, 6364-6401.
- [69] <https://www.britannica.com/print/article/10772>
- [70] I. Manisalidis, E. Stavropoulou, A. Stavropoulos and E. Bezirtzoglou, *Frontiers in public health.*, 2020, **8**; doi.org/10.3389/fpubh.2020.00014.
- [71] B. C. McDonald, A. De Gouw, J. B. Gilman, S. H. Jathar, A. Akherati, C. D. Cappa, J. L. Jimenez, J. L. Taylor, P. L. Hayes, S. A. McKeen, Y. Y. Cui, S. W. Kim, R. Gentner, G. I. VanWertz, A. H. Goldstein, R. A. Harley, G. J. Frost, J. M. Roberts, T. B. Ryerson and M. Trainer, *Science.*, 2018, **359**, 760-764.
- [72] <https://www.epa.gov/clean-air-act-overview/air-pollution-current-and-future-challenges#protecting>.
- [73] C. Lai, Z. Wang, L. Qin, Y. Fu, B. Li, M. Zhang, S. Liu, L. Li, H. Yi, X. Liu, X. Zhou, N. An, Z. An, X. Shi and C. Feng, *Coord. Chem. Rev.*, 2021, **427**, 213565.
- [74] X. Suo, Y. Yu, S. Qian, L. Zhou, X. Cui, and H. Xing, *Angew. Chem., Int. Ed.*, 2021, **133**, 7062-7067.
- [75] L. Zhua, D. Shena and K. H. Luo, *J. Hazard. Mater.*, 2020, **389**, 122102.
- [76] S. Keskin, T. M. van Heest and D. S. Sholl, *ChemSusChem.*, 2010, **3**, 879-891.
- [77] W. P. Lustig, S. Mukherjee, N. D. Rudd, A. V. Desai, J. Li and S. K. Ghosh, *Chem. Soc. Rev.*, 2017, **746**, 3242.
- [78] J.B. Derraik, *Mar. Pollut. Bull.*, 2002, **44**, 842–852.
- [79] R.P. Schwarzenbach, B.I. Escher, K. Fenner, T.B. Hofstetter, C.A. Johnson, U. Gunten and B. Wehri, *Science.*, 2006, **313**, 1072–1077.
- [80] M. Mon, R. Bruno, J. Ferrando-Soria, D. Armentano and E. Pardo, *J. Mater. Chem. A.*, 2018, **6**, 4912-4947.
- [81] L. H. Keith and W. A. Teillard, *Environ. Sci. Technol.*, 1979, **13**, 416–423.
- [82] P. Samanta, S. Let, W. Mandal, S. Dutta and S. K. Ghosh, *Inorg. Chem. Front.*, 2020, **7**, 1801-1821.

- [83] E. M. Dias and C. Petit, *J. Mater. Chem. A*, 2015, **3**, 22484–22506.
- [84] A. Waheed , N. Baig, N. Ullah and W. Falath, *Journal of Environmental Management.*, 2021, **287**, 112360.
- [85] S. R. J. Oliver, *Chem. Soc. Rev.*, 2009, **38**, 1868–1881.
- [86] Q. Gao, J. Xu and X.-H. Bu, *Coord. Chem. Rev.*, 2019, **378**, 17-31.
- [87] D. Banerjee, D. Kim, M. J. Schweiger, A. A. Kruger and P. K. Thallapally, *Chem. Soc. Rev.*, 2016, **45**, 2724–2739.
- [88] Q. Sun, B. Aguila and S. Ma, *Trends in Chemistry.*, 2019, **1**, 292-303.
- [89] L. Rani, J. Kaushal, A. L. Srivastav and P. Mahajan, *Environ Sci Pollut Res.*, 2020, **27**, 44771-44796; <https://doi.org/10.1007/s11356-020-10738-8>.
- [90] T. Skorjanc, D. Shetty and A. Trabolsi, *Chem.*, 2021, **7**, 882-918.

Part-I

**Luminescent metal-organic frameworks
(LMOFs) for sensing based applications**

Luminescent MOFs (LMOFs) are a special subclass of MOFs involving fluorescence and phosphorescence based photophysical processes and advantageous in terms of electronic property modulation. The electronic property in such frameworks can be tuned by judicious choice of task specific luminescent aromatic organic struts and metal nodes, the incoming guest molecules and also the counter ions in case of ionic frameworks.^[1] All these factors help in designing an analyte specific chemical environment within the pores of LMOFs leading to generation of selectivity towards incoming analyte. The different types of photophysical processes that occur in case of LMOFs include ligand to metal charge transfer (LMCT), metal to ligand charge transfer (MLCT), ligand to ligand charge transfer (LLCT), guest induced luminescence change and sensitization in case of lanthanide MOFs (also known as antenna effect).^[2] LMOFs help in improved performance in case of molecular recognition due to preconcentration effect leading to sufficient accumulation of guest analyte within the pores leading to prominent luminescence response. The host MOF acts as an immobilized rigid luminescence probe reducing the molecular motion and enhancing the radiative decay process resulting in high intensity luminescence output.^[3] In case of LMOFs, molecular recognition between host and analyte occurs in a heterogeneous phase which is important for easy operation as well as real time application. Based on host-guest recognition LMOFs are utilized for sensing of different types of guest molecules. Such recognition processes by LMOFs can be classified into two categories: a) chemosensor where the host framework-guest analyte recognition is noncovalent in nature and such interaction produces a detectable change in luminescence; b) chemodosimeter where the host framework contains a reaction site where the guest analyte binds through an irreversible chemical reaction and generates a distinctive luminescence change with respect to the emission of the parent framework. These factors lead to the utilization of LMOFs as materials for sensors for recognition of chemical species as well as optoelectronic applications.^[3-4]

This section consists of two chapters, i.e. chapter 2 and chapter 3. In chapter 2, LMOFs designed by a pre-synthetic approach are deployed for recognition of styrene, a toxic air pollutant through host-guest recognition. While in chapter 3, a post-synthetically designed MOF is utilized as a chemodosimeter to recognize bisulphite anion, a hydrolysed derivative of sulphur dioxide selectively in water medium. In both chapters, the studies focus on designing L-MOFs synthesized through different approaches for identification of toxic air-pollutants.

References:

- [1] M. D. Allendorf, C. A. Bauer, R. K. Bhakta and R. J. T. Houka, *Chem. Soc. Rev.*, 2009, **38**, 1330-1352.
- [2] Z. Hu, B. J. Deibert and J. Li, *Chem. Soc. Rev.*, 2014, **43**, 5815-5840

[3] W. P. Lustig, S. Mukherjee, N. D. Rudd, A. V. Desai, J. Li and S. K. Ghosh, *Chem. Soc. Rev.*, 2017, **746**, 3242.

[4] A.Karmakar, P. Samanta, S. Dutta and Sujit K Ghosh, *Chem. Asian J.*., 2019, **14**, 4506-4519.

Chapter 2

A 3D Metal-Organic Framework (MOF) as a luminescent sensor for selective Detection of Styrene

2.1 Introduction

One of the major global concerns of the current world is air pollution, which is caused by both natural and anthropogenic sources.^[1-3] Among the well-known air pollutants, volatile organic compounds (VOCs) represents organic compounds having boiling point less than or equal to 250 °C at 1 atm according to the European union (EU) and are mentioned as harmful species by both World Health Organization (WHO) and the US-Environment protection agency (US-EPA).^[4-5] Common VOCs includes aliphatic as well as aromatic hydrocarbon compounds produced from industries and domestic sources and those are responsible for generation of photochemical smog and ozone layer depletion.^[6-7] In addition to that, exposure to such toxic air-pollutants affect human cardiovascular, alimentary and metabolic system leading to death.^[8-9] All these detrimental effects caused by the carcinogenic VOCs in case of both human life and environment makes the detection of such air pollutants extremely important for the initiatives of a clean environment. In this context, styrene which is a well known derivative of benzene with an olefinic unsaturation is regarded as a toxic aromatic VOC with permissible limit of 39 ppb in the air.^[10-12] Styrene is normally used as precursors in rubber and plastic industries to make polystyrene products.^[13] But over exposure to such compound can cause both short term and long term illness in human body including nausea, vomiting, damage of respiratory and nervous system, eventually leading to death.^[14] Recently in 2020, leakage of styrene gas in the air from a polymer industry in Vishakhapatnam, India led to grave consequence. Mass-scale breathing troubles, severe illnesses and death of large number of people were reported. On account of this, detection of even miniscule amount of styrene leakage becomes important to avoid large-scale disasters.^[15-16] The state-of-the-art techniques for styrene detection include mass spectrometry, spectroscopic and chromatographic methods. However these methods lack on several frontiers including time-scale of detection, cumbersome in terms of portability thus demanding the development of other easy techniques.^[5, 10, 17-18] In this respect, fluorescence spectroscopy score over other techniques in terms of simplicity in operation as well as quick and accurate response.^[19] Thus designing of new fluorescent materials and enriching the library of luminescent materials for fast and accurate detection of styrene is required.^[10,20-21]

Metal-organic framework or porous coordination polymer are organic-inorganic hybrid materials constructed from functionalised organic linkers and metal nodes/clusters with presence of porous voids within framework architecture.^[22,23] The crystalline nature and large surface area of such materials enables preconcentration of incoming analyte within functionalised pore surface of host MOFs, thus achieving sensitivity towards the targeted guest molecules. Along with that, the host guest interaction in heterogeneous phase enables MOFs as luminescent materials for sensing based applications.^[24, 25] In the literature, it is well reported that zinc metal nodes with fulfilled d^{10} electronic configuration is widely used

to construct luminescent MOFs.^[19] On the other hand the utilization of photoactive naphthalene di-imide (NDI) based N-donor ligand is carried out in literature for chemical sensing, sorption and clean energy based applications.^[26] In the literature, it is well explored that electron deficient naphthalene di-imide (NDI) based frameworks interacts with electron rich guest VOCs producing exciplex charge transfer features that generates luminescence response in the visible range (400nm-700nm). Such strategy is utilised to construct luminescence based sensor materials for VOC recognition.^[33] In addition, the usage of binding anion (SiF_6^{2-}) is carried out along with N-donor linkers to ensure formation of charge neutral three dimensional (3D) porous frameworks with structural propagation along all three directions.^[26] Keeping this things in mind, in this work we developed a neutral luminescent MOF IPM-326 (where IPM stands for IISER Pune Materials) constructed from a functional N-donor based linker containing both NDI functionality with pyridyl linkages and $\text{ZnSiF}_6 \cdot \text{H}_2\text{O}$, where SiF_6^{2-} is utilised strategically as binding anion. The presence of electron deficient di-imide core in the framework led to favourable host guest interaction between the framework and incoming electron rich styrene molecules generating distinct yellow luminescent response that can be utilised as a signal in developing selective MOF based recognition probe for styrene molecules (Figure 2.1).

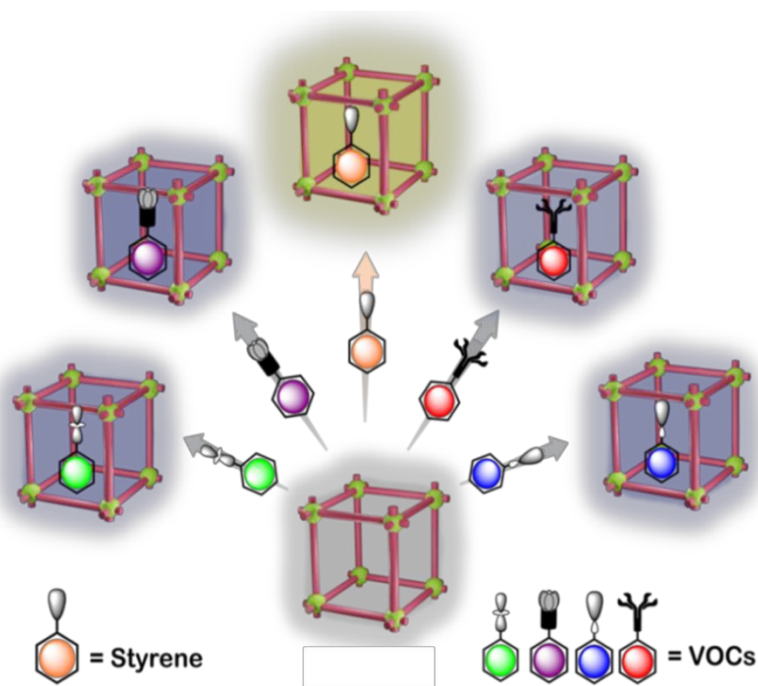


Figure 2.1. Schematic representation of luminescent response by compound in presence of VOCs.

2.2 Experimental

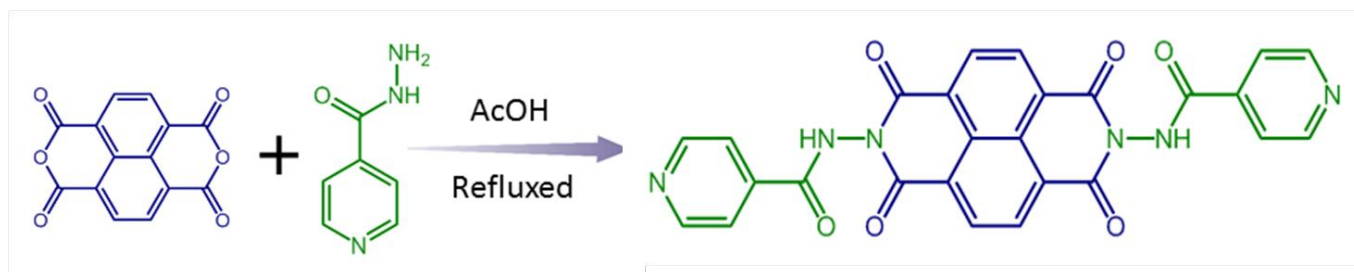
2.2.1 Materials

Zinc hexafluorosilicate hydrate, 1,4,5,8-Naphthalenetetracarboxylic dianhydride, isoniazid and all solvents were commercially available and were used as it is without any further purification.

2.2.2 Synthesis

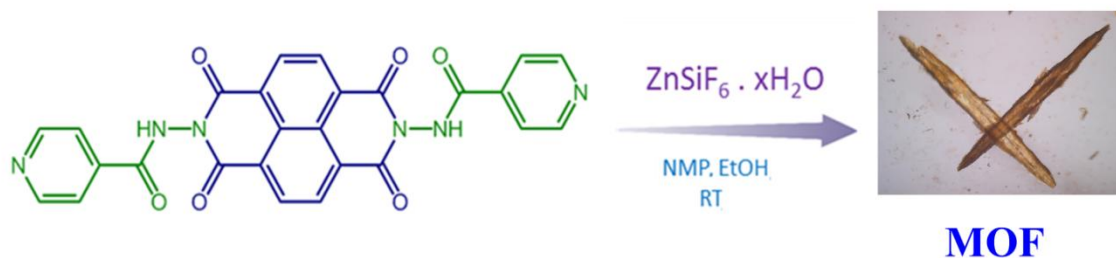
Synthesis of N,N' -(1,3,6,8-tetraoxo-1,3,6,8-tetrahydrobenzo[*lmn*][3,8]phenanthroline-2,7-diyl)diisonicotinamide (L).

1,4,5,8-Naphthalenetetracarboxylic dianhydride (1.34 g, 5 mmol) and Isonicotinic hydrazide (1.57 g, 11.5 mmol) were refluxed in 30 mL of acetic acid for 24 hours. The light brown colored reaction mixture was concentrated in a rotary evaporator and thereafter diluted with water to give brown precipitate. The precipitate was filtered and vacuum dried to obtain the product. The ligand was used for crystallization without further purification (Scheme 2.1).^[27]



Scheme 2.1. Synthesis scheme of ligand (L).

Synthesis of MOF (IPM-326). The ligand (L) (0.05 mmol, 25.3 mg) was dissolved in 5 ml NMP (N-Methyl-2-Pyrrolidone) through sonication and carefully added to a crystallisation tube. After that $ZnSiF_6 \cdot H_2O$ (0.05 mmol, 10.37 mg) in 5 ml ethanol was slowly added to the ligand solution. The tube was kept at room temperature for a week to generate single crystals of the MOF $\{[Zn(L)_2](SiF_6)] \cdot xG\}_n$ (G-Guest) (Scheme 2.2). Yield ~ 35%.



Scheme 2.2. Synthesis scheme of MOF.

Desolvation of MOF (IPM-326): The as-synthesized crystals of MOF were kept in ethanol for 3 days with exchanging the solvent at an interval of 12 hours. After solvent exchange was done, the crystals were desolvated using SCLEAD-2BD supercritical CO₂ drying equipment with liquefied CO₂ at 50 °C and 14 MPa followed by heating around 80 °C in vacuum for 12 hours. The desolvated phase of the MOF was used for fluorescence study.

Preparation of guests@MOF (IPM-326): 5 mg desolvated MOF crystals were soaked in a vial consisting of 2 ml of each analyte for 7 days at room temperature to prepare the guests@MOF phase. After that the samples were collected, air dried and further characterized using PXRD, TGA and fluorescence measurements.

Construction of the thin film: An experimental protocol reported in the literature has been utilized to manufacture the MOF based thin film.^[35b] The MOF was treated with polyvinylidene fluoride (PVDF) (0.15 g) in N,N-Dimethylformamide (DMF) (1.9 mL) via stirring for 12 hours and then the mixture was poured into a glass plate to generate a flat sheet membrane at room temperature. The system was washed with water and films of area of 2x1 cm² were prepared for sensing experiments.

2.2.3. Physical Measurements

Single-crystal X-ray diffraction collection and processing was done by CrysAlisPro (Rigaku OD, 2021). To the collected reflections, a multi-scan absorption correction was applied. The structure was solved with the ShelXT^[38] structure solution program utilizing Intrinsic Phasing using Olex2.^[39] The refinement was done using Least Squares minimization by the ShelXL^[40] refinement package. Anisotropic refinements were done to all non-hydrogen atoms. Generation of the organic hydrogen atoms were done geometrically. The disordered solvents were introduced to solvent mask. The residual electron count in the unit cell resulted in 407 electrons corresponding to 16 ethanol molecules.

Powder X-ray diffraction was recorded on Bruker D8 Advanced X-Ray diffractometer using Cu K α radiation ($\lambda = 1.5406 \text{ \AA}$) in 5° to 30° 2 θ range. Gas adsorption measurements were recorded using BelSorp-max instrument from Bel Japan. The Fourier transform infra-red (FT-IR) spectra were recorded

on NICOLET 6700 FT-IR Spectrophotometer using KBr Pellets. Thermo gravimetric analyses (TGA) measurements are done on Perkin-Elmer STA6000 TGA analyser under N₂ atmosphere with heating rate of 10 °C/min. Morphologies of the crystals were recorded with Zeiss Ultra Plus field-emission scanning electron microscopy (FESEM). All fluorescence measurements were done on JobinYvon Fluoromax-4 spectrofluorometer with stirring attachment at room temperature.

2.3 Results and discussion

The MOF (IPM-326) was constructed from naphthalene di-imide based linker (L) and ZnSiF₆.H₂O through slow diffusion method (See experimental section for more details) to generate single crystals which were characterised by SC-XRD measurements after two weeks. The single crystal data reveals that the MOF crystallised in I2/m space group. The asymmetric unit of the MOF contains 1/4 of Zn(II) metal ion and SiF₆²⁻ anions along with 1/2 of ligand (L) unit respectively resulting in formation of neutral MOF having formula as {[Zn(L)₂](SiF₆)}.xG_n (G-Guest) (Appendix 2.1). The co-ordination environment of the zinc metal node was found to be octahedral wherein the equatorial co-ordination sites were occupied by four pyridyl nitrogen from four independent ligand while the axial sites were occupied by fluorine atoms of SiF₆²⁻ anions (Appendix 2.2). The co-ordination by the pyridyl nitrogen from the ligand (L) forms a two-dimensional layered structure while the binding from bridging anion SiF₆²⁻ from the third dimension act as a pillar interconnecting the two layers (Appendix 2.3b). Such co-ordination arrangement leads to formation of three dimensional structure with rectangular pore aperture and one dimensional channel pore along crystallographic *a* axis (Appendix 2.3a). Such arrangements lead to generation of guest accessible sites with pore walls decorated by the variety of functional groups (carbonyl groups of amide and imide linkages, fluorine atoms of SiF₆²⁻) from the ligand moiety.

Post elucidation of the structure through SC-XRD technique, the MOF was synthesized in bulk scale. The phase purity of the synthesized MOF was determined by powder X-ray diffraction (PXRD). The PXRD data exhibited similar peak profile of the as-synthesized phase when compared to the simulated phase confirming retention of structural integrity in bulk phase (Appendix 2.4). Thermogravimetric analysis (TGA) of the compound showed a gradual weight loss between 30 °C to 350 °C which may be attributed to the presence of ethanol and NMP solvent molecules. After that the crystals were exchanged thoroughly with ethanol for 3 days and subjected to critical phase drying (CPD) followed by vacuum desolvation at 80 °C to obtain the desolvated phase of the MOF (Appendix 2.5). The desolvated phase also retains structural integrity as evident from PXRD data (Appendix 2.4). The FTIR spectra of both the as-synthesized and desolvated phase of the MOF corroborated similarity in peak profile compared to the FTIR spectrum of the ligand (Appendix 2.6). The desolvated phase of the framework also exhibited an

uptake of ~ 60 ml/g CO_2 as observed from sorption studies at 195 K, 1 bar (Appendix 2.7). The FESEM image confirmed a rod like morphology of the MOF, while EDX data and elemental mapping confirmed presence as well as uniform distribution of constituent elements (C, N, O, Zn, Si, F) in the surface of the crystals (Appendix 2.8-10).

The presence of electron deficient naphthalene di-imide core along with luminescent zinc metal node in the MOF prompted us to study the influence of electron rich VOCs on its photophysical properties. We envisioned that interaction between incoming electron rich guests with the electron deficient moieties within the host framework might affect the photoluminescence properties thereby generating a unique fluorescence response. For this we recorded the UV-visible spectrum of the ligand that showed absorption peaks around 355 nm and 380 nm corresponding to n to π^* and π to π^* transitions in the ligand (Appendix 2.11).^[28] The solid-state UV-visible spectra of the ligand as well as the MOF also exhibited broad absorption profile with peak maxima around 355 nm (Appendix 2.13). Next, we recorded the emission spectra of the ligand in acetonitrile by excitation at 355 nm which exhibited a broad spectrum with emission maxima at 420 nm and a shoulder emission peak around 540 nm (Appendix 2.12).

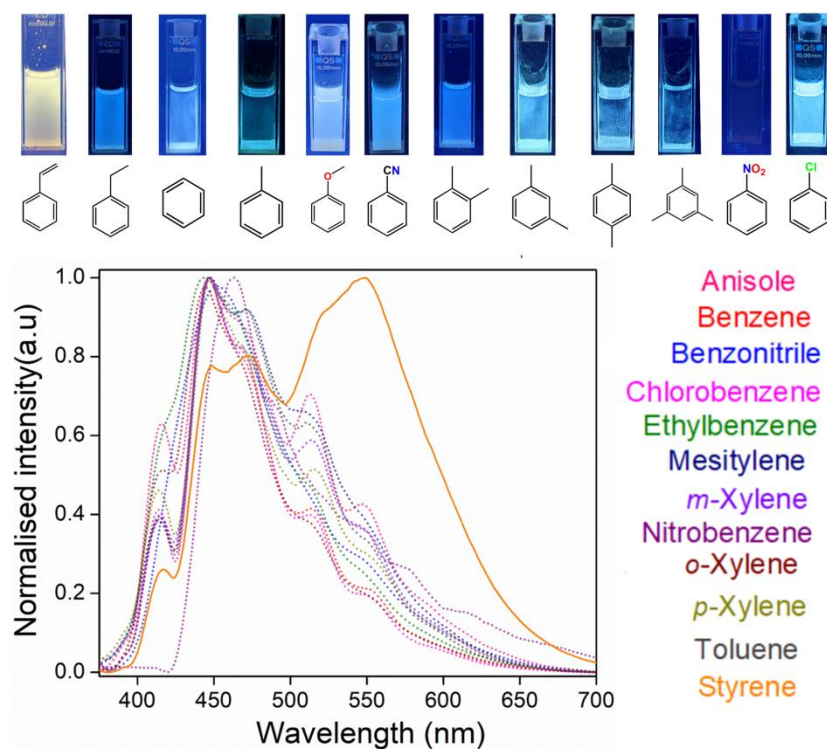


Figure 2.2. Photoluminescence spectra of MOF in different aromatic VOC solvent along with images under UV lamp (λ_{ex} - 365 nm).

In the literature, origin of such emission peaks in naphthalene di-imide based ligands are attributed to intramolecular and intermolecular electronic transitions within the ligand fluorophore.^[29] Next we sought to study the photophysical interaction of the MOF with aromatic VOCs. The VOC solvents were strategically chosen in such a way that there is a variation of secondary functional group leading to variation of the stereo electronic nature of the guest which might lead to distinctive luminescent response. For that we dipped 5 mg MOF in 2 ml VOC solvent for a week at room temperature so that sufficient preconcentration of guest solvent can occur within the pores of the MOF, which lead to suitable host guest interaction. After that we incorporated the MOF@VOC system in a photoluminescence cuvette and recorded the emission spectra under stirring condition from 380 nm to 700 nm by excitation at 365 nm. We observed a broad emission profile with emission maxima around 440 nm similar to the ligand in case of all aromatic VOCs, with a difference in emission intensity except in case of styrene (Appendix 2.14-25). In case of styrene, significant emission intensity was observed in case of both peaks around 440 nm and 545 nm resulting in distinctive yellow fluorescent response unlike all other VOCs where a bluish emission signal was observed (Appendix 2.25). This observation establishes the MOF as selective luminescent probe towards styrene molecule (Figure 2.2). Such distinguished fluorescent response by the MOF based probe towards styrene could be reasoned due to probable host guest interaction between the host matrixes with incoming styrene molecules.^[30] The naphthalene di-imide based MOF is electron deficient in nature and styrene is electron rich with presence of aromatic ring as well as secondary double bond absent in all other VOCs. Such host guest arrangements leads to electronic charge transfer from the electronic rich moiety towards the electron deficient moiety that can be monitored through fluorescence spectroscopy. In this case the probable explanation for such selective yellow luminescent response could be attributed to styrene molecules occupying the pores of the MOF and electronically interacting with the functionalised framework through C-H π interaction and π - π stacking leading to enhancement of intermolecular electronic transition as well as the intensity of the emission peak around 545 nm leading to such yellow luminescence signal.^[31,32] In the literature such host guest chemistry based molecular decoding phenomenon based on fluorescence studies are well explored by Kitagawa and co-workers.^[33,34]

Inspired by these observations we sought to check whether such luminescent behaviour is persistent in the MOF in guest loaded solid state. We collected the solid MOF powder dipped in aromatic solvents (benzene, toluene, ethylbenzene and styrene) by filtration and air dried it for solid state UV-visible studies. It was observed that the styrene loaded MOF shows a shoulder hump around 471 nm along with broad absorption profile with peak maxima around 355 nm (Appendix 2.26). This can be reasoned to interaction of styrene guest molecules with host MOF.^[29,30] Solid state luminescence studies reveal that the MOF@VOC luminescence behaviour in solid-state is consistent with the solution state photo physical

response and the retention of yellow fluorescence output in case of MOF@styrene is retained even in solid-state (Figure 2.3). Previous literature studies for styrene detection is carried out based on organic probes using chemodosimetric approach or utilising lanthanide MOF based probes where post styrene exposure causes an inhibition in ligand to metal charge transfer thus causing decrease in fluorescent intensity of metal based emission peak utilised for studying the photophysical process.^[10,20,21] This study utilises the concept of host guest interaction within the pores of linker functionalised MOF with incoming analyte (styrene) rendering guest specific distinctive visible luminescence response. Such approach for detection of styrene is unexplored in the literature and can lead to development of new avenues for designing chemosensors based on host guest chemistry.

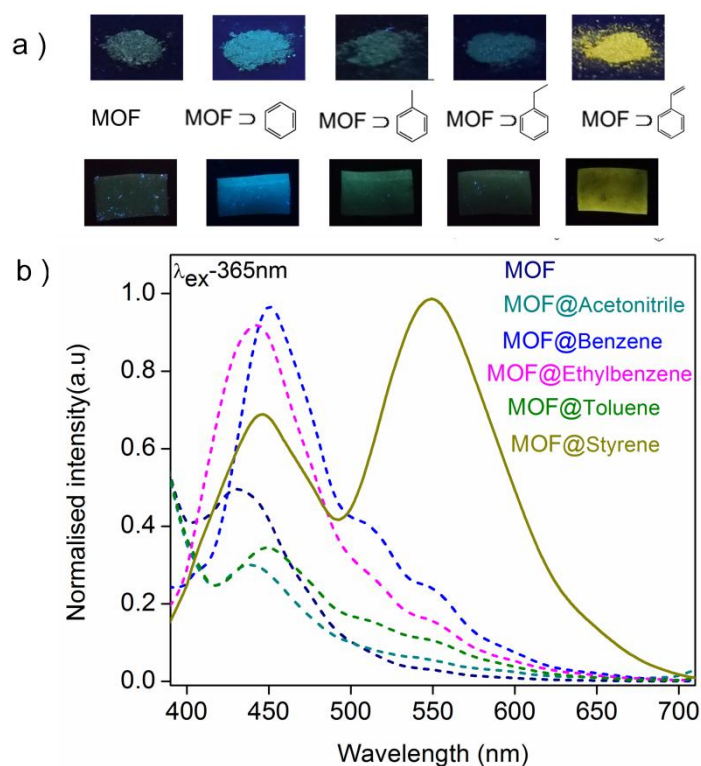


Figure 2.3. (a) Photographs of VOC treated MOF in solid state and in thin film under UV lamp (λ_{ex} - 365 nm). (b) Emission spectra of VOC treated MOF in solid state.

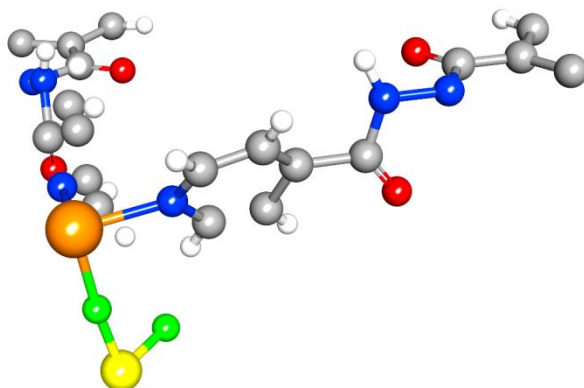
Based on this observation we constructed a thin film based on the MOF and treated with different VOCs including benzene, toluene, ethylbenzene and styrene (Appendix 2.27-28).^[35] It was observed that the yellow luminescence response was persistent in case of styrene loaded MOF-based thin film, while blue luminescence signal was observed for other aforementioned VOC incorporated thin films under UV lamp (Figure 2.3). Such consistent luminescence response both in case of solution and thin film by the MOF enables its potential in usage in real time application for styrene detection.^[35]

After the photoluminescence studies, the MOF@VOC compound were subjected to further characterizations to elucidate the structural stability of the MOF post VOC exposure. PXRD analysis of MOF@VOC compounds reveals similar profile compared to the parent phase revealing structural integrity post VOC inclusion (Appendix 2.29). TGA profile of VOC loaded MOFs showed initial loss in weight % around 80 °C to 150 °C that can be corroborated to loss corresponding to the VOCs residing inside the pores post loading (Appendix 2.30). FTIR studies post styrene loading reveals shift in C=O stretching frequency in MOF@styrene compared to the desolvated phase of the MOF (Appendix 2.31). Such shifting in FTIR peaks in case of particular solvent is observed in the literature and can be attributed as a result of host guest interaction^[36,37] The FESEM images of MOF@VOC compounds shows similar rod morphology post interaction with the VOCs (Appendix 2.32). Thus it can be said that the MOF act as selective styrene detection probe retaining its structural integrity.

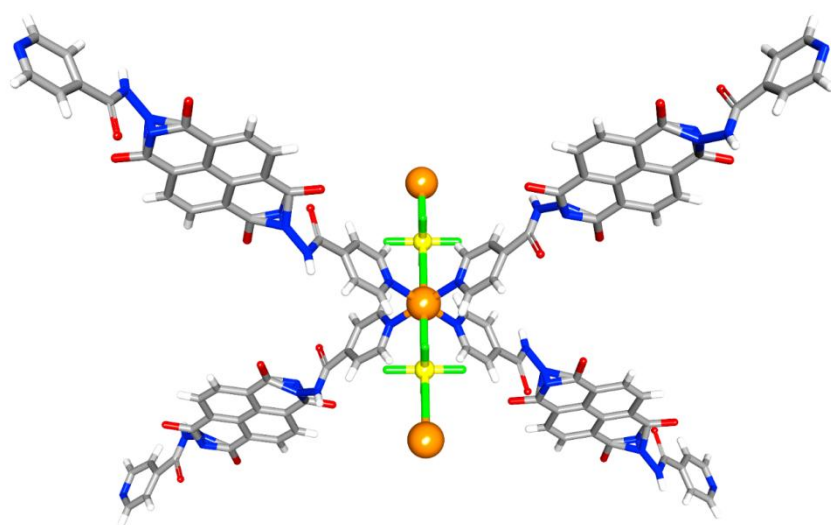
2.4 Conclusions

In this work, a 3D luminescent zinc based MOF (IPM-326) was constructed from functional N-donor di-imide based linker containing pyridyl linkages. The MOF consist of carbonyl and fluorine functionalities based one-dimensional porous channel which was utilised for host guest interaction with incoming aromatic electron rich guest VOCs. Such molecular recognition phenomenon was probed utilising fluorescence studies where it was rationale that such framework analyte interaction will produce distinguished photophysical response as output. In case of styrene as a guest analyte, the MOF exhibited visible yellow luminescent signal which was different from blue luminescence response in case of all other VOCs. Such selective readout is attributed to interaction of the electron deficient framework with electron rich styrene molecule and evident also from fluorescence profile. To the best of our knowledge such studies in development of styrene recognition probes based on framework analyte interaction are rare in literature. This work will definitely enrich the concept of designing MOF based chemosensors based on host guest chemistry.

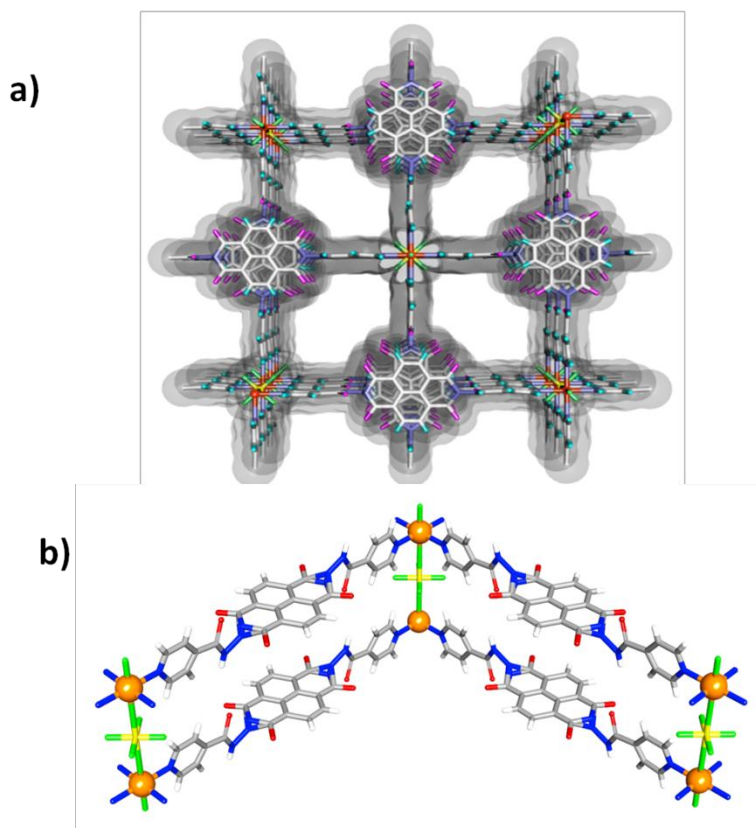
2.5 Appendix section



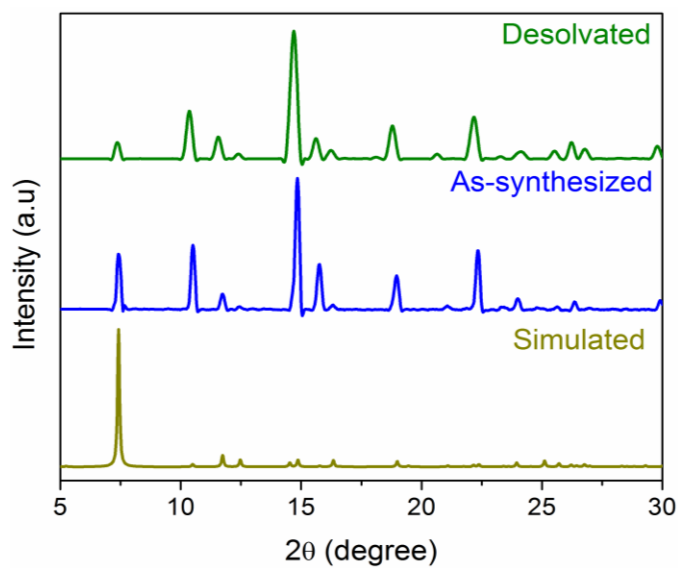
Appendix 2.1. Asymmetric unit of MOF (IPM-326) (color: Light gray - C, Red- O, Blue - N, White - H, Orange - Zn, and Green-F, Yellow-Si).



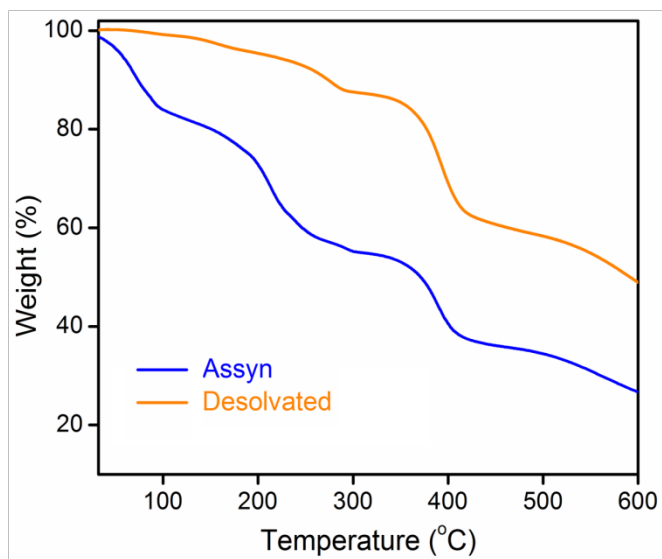
Appendix 2.2. Coordination environment of MOF (color: Light gray - C, Red - O, Blue - N, White - H, Orange - Zn, and Green - F, Yellow - Si).



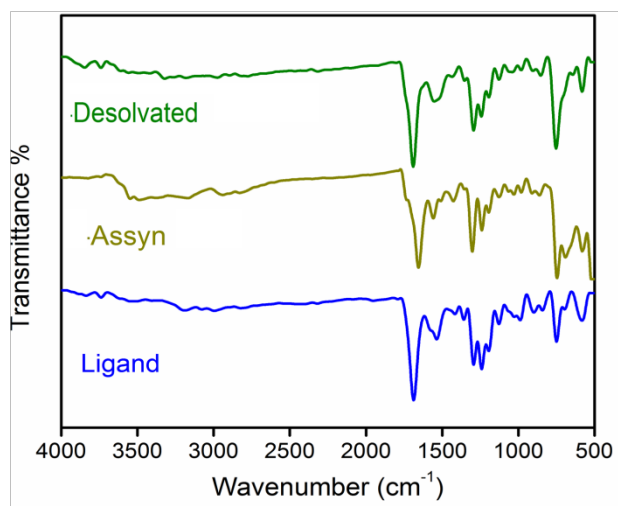
Appendix 2.3. a) Packing diagram of MOF (IPM-326) (color: Light gray - C, Pink - O, Blue - N, Sky-blue - H, Orange - Zn, and Green-F, Yellow-Si). b) SiF_6^{2-} anions interconnecting the metal nodes in IPM-326 (color: Light gray - C, Red - O, Blue - N, White - H, Orange - Zn, and Green-F, Yellow-Si).



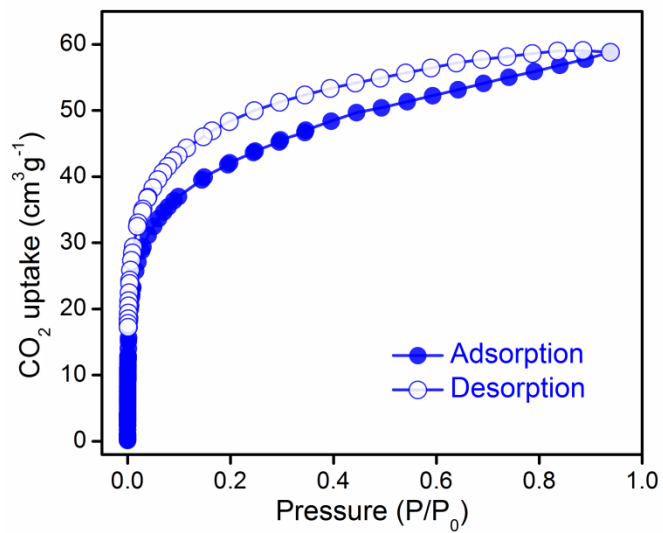
Appendix 2.4. PXRD profile of MOF in all phases.



Appendix 2.5. TGA profile of MOF in all phases.



Appendix 2.6. FTIR profile of the ligand and the MOF in all phases.

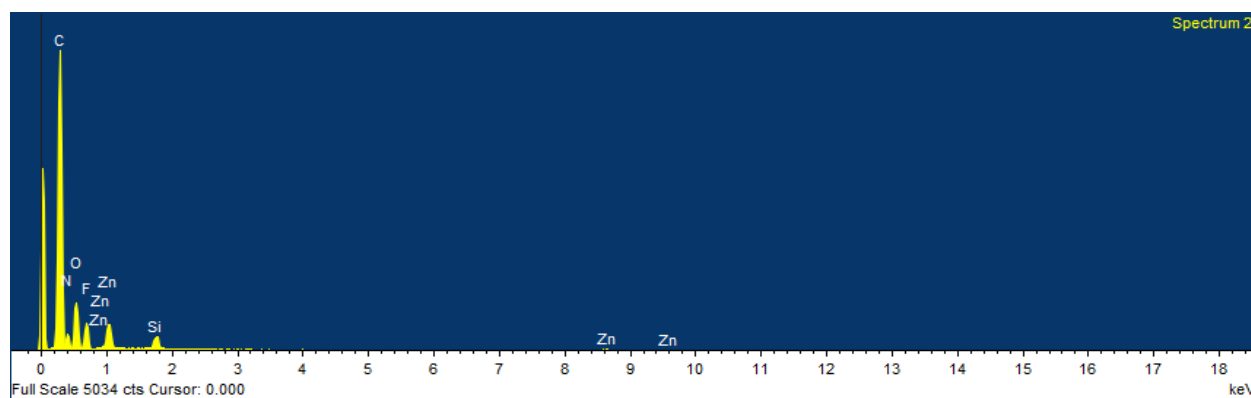


Appendix 2.7. CO₂ sorption profile of MOF at 195 K.

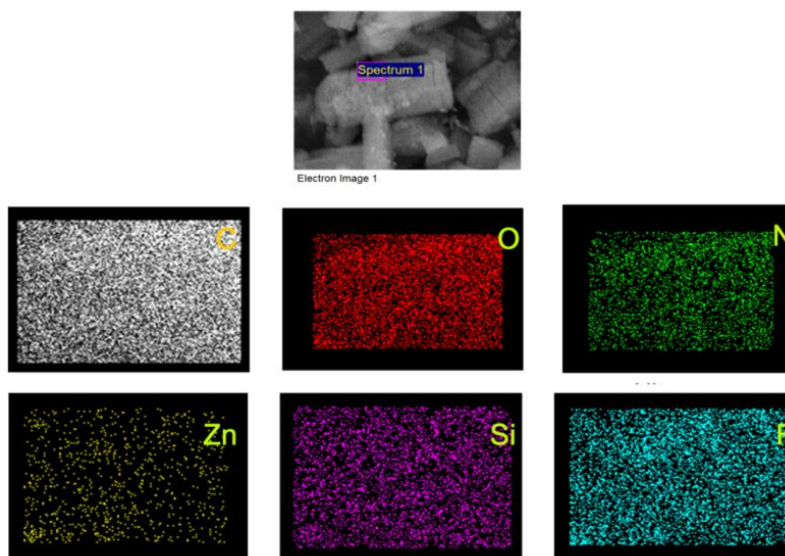


Appendix 2.8. FESEM images of MOF.

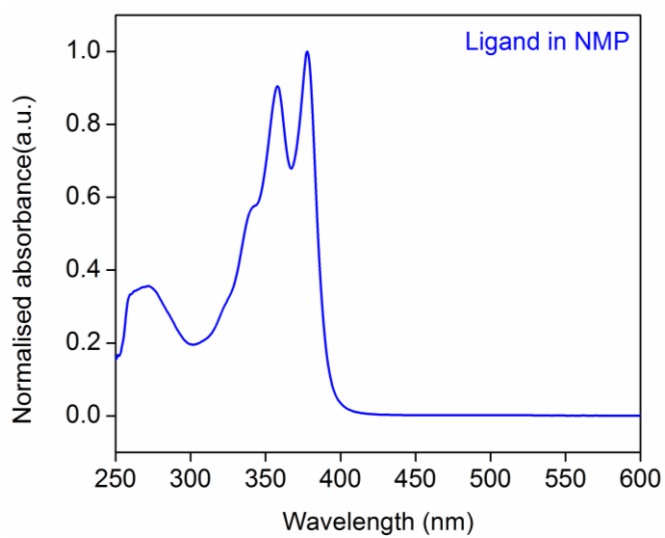
Element	Weight%
C	51.31
N	15.23
O	17.95
F	10.20
Si	0.97
Zn	4.33
Totals	100.00



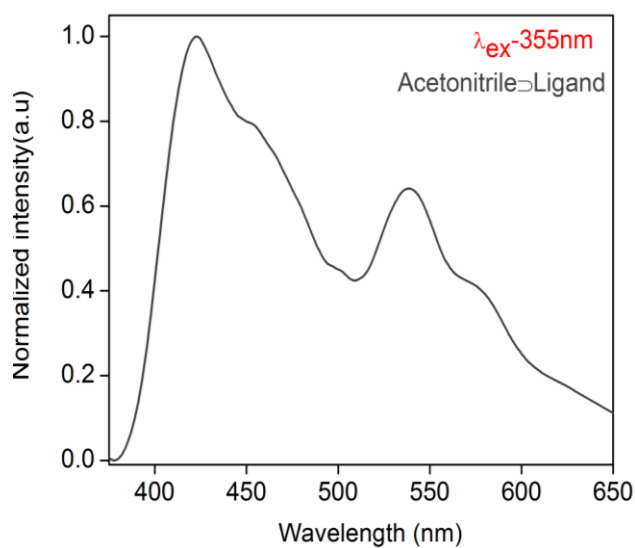
Appendix 2.9. EDX data of MOF



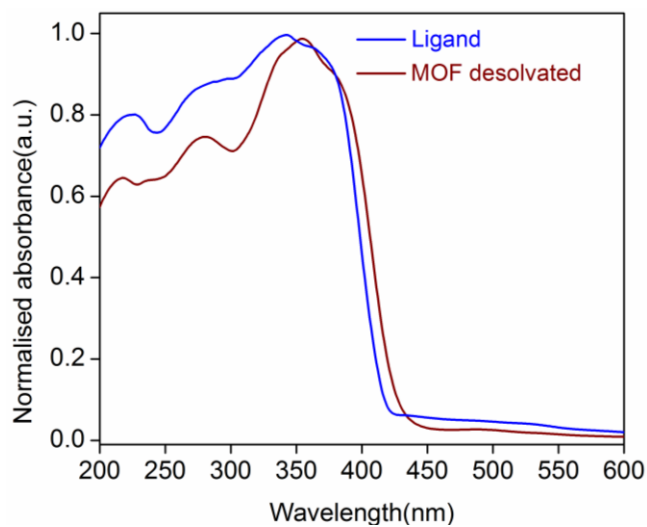
Appendix 2.10. Elemental mapping profile of MOF



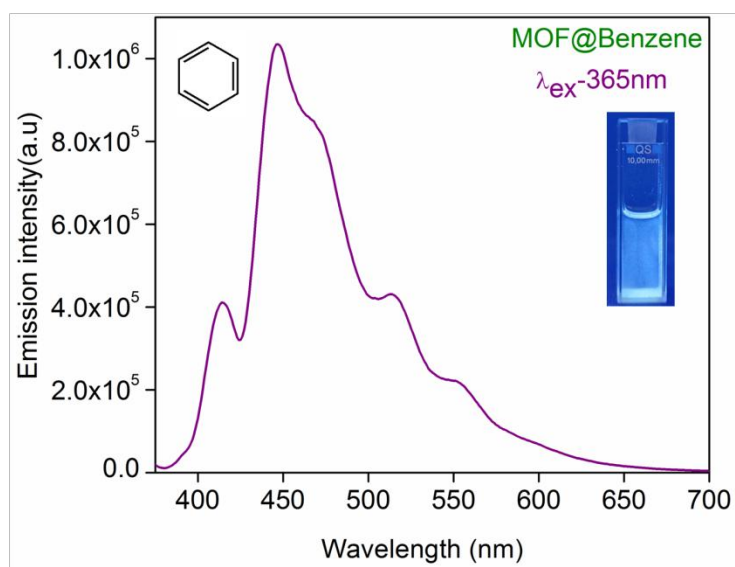
Appendix 2.11. UV-visible profile of ligand in NMP.



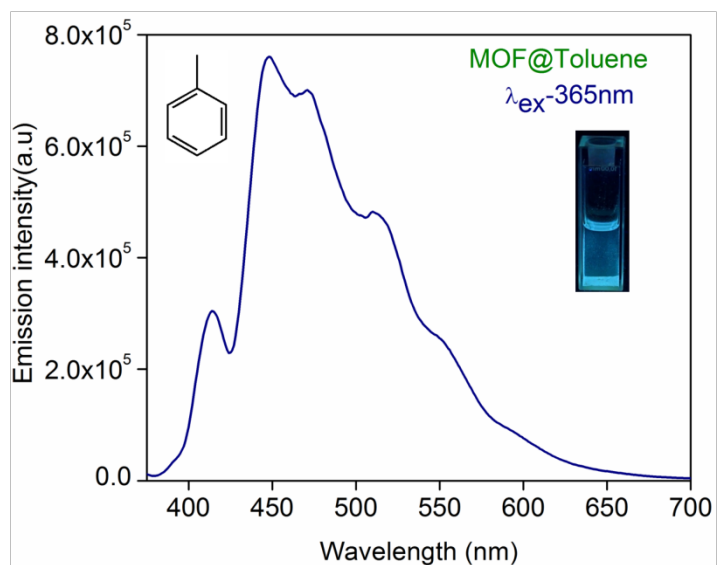
Appendix 2.12. Fluorescence spectra of ligand ($\lambda_{exc} = 355$ nm).



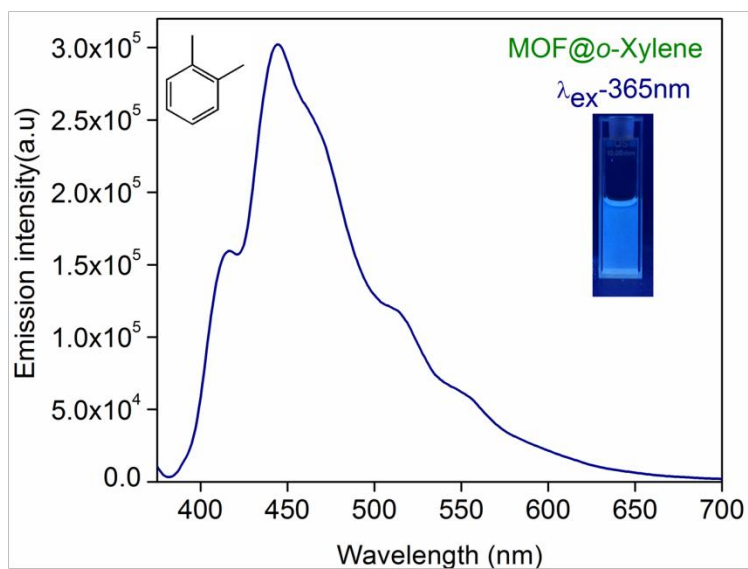
Appendix 2.13. Solid state UV-visible spectra of ligand and MOF.



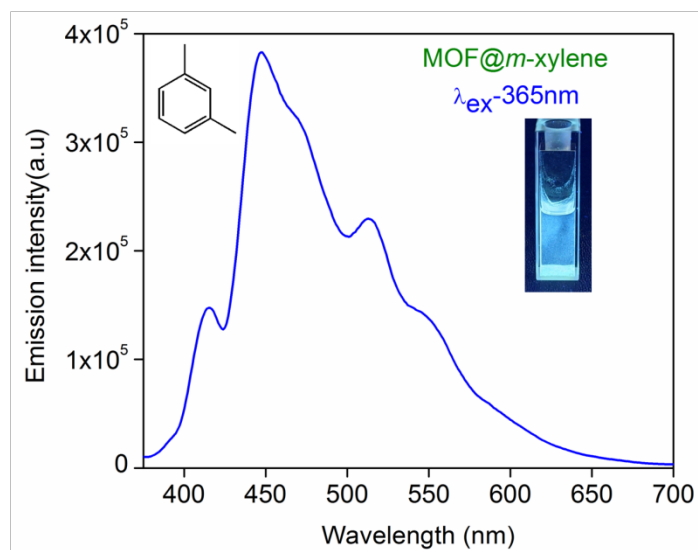
Appendix 2.14. Luminescence spectra of MOF dispersed in benzene ($\lambda_{exc} = 365\text{ nm}$).



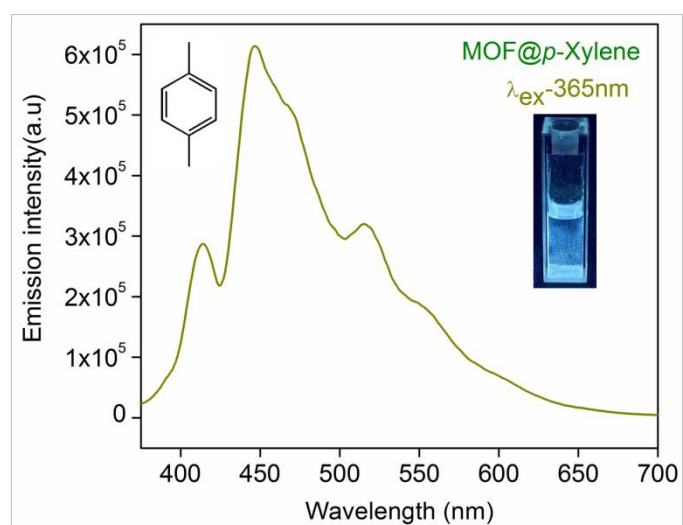
Appendix 2.15. Luminescence spectra of MOF dispersed in toluene ($\lambda_{exc} = 365$ nm).



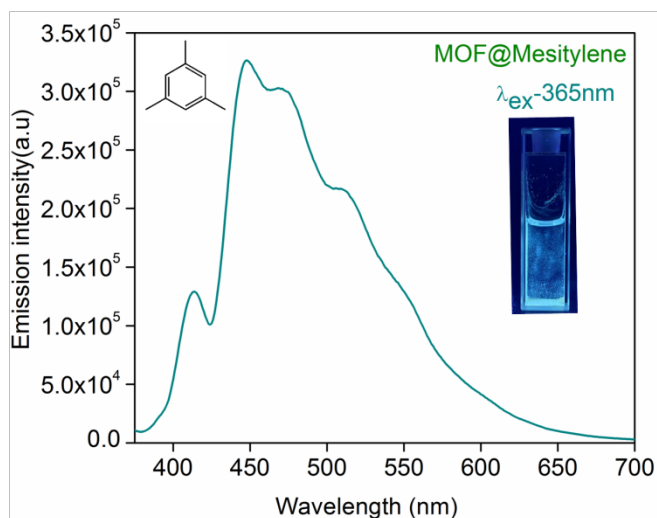
Appendix 2.16. Luminescence spectra of MOF dispersed in *o*-xylene ($\lambda_{exc} = 365$ nm).



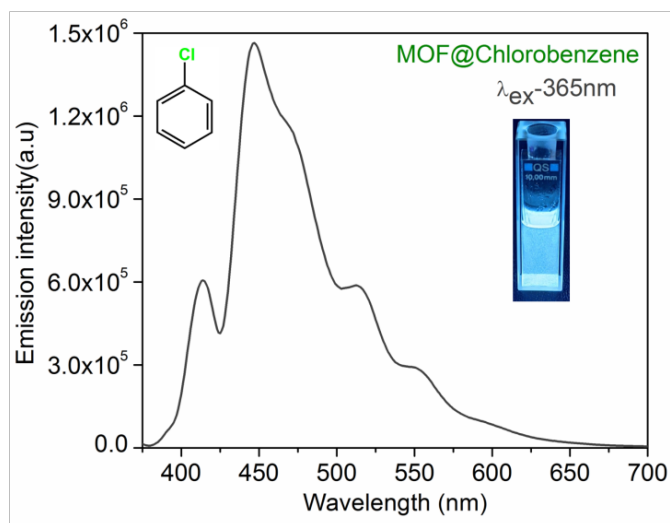
Appendix 2.17. Luminescence spectra of MOF dispersed in *m*-xylene ($\lambda_{exc} = 365$ nm).



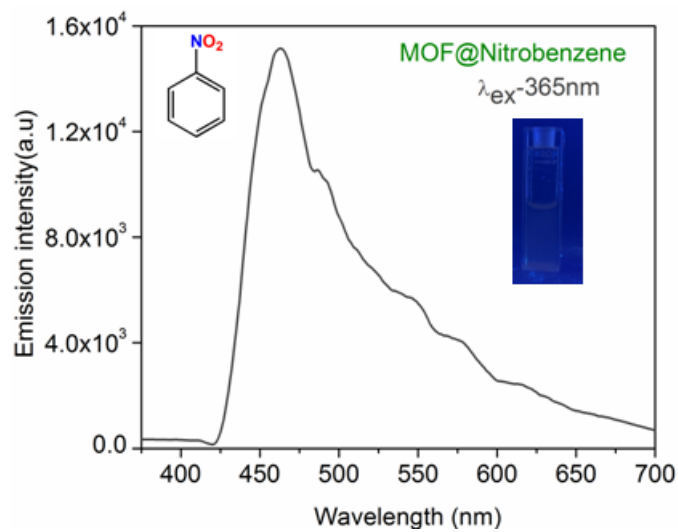
Appendix 2.18. Luminescence spectra of MOF dispersed in *p*-xylene ($\lambda_{exc} = 365$ nm).



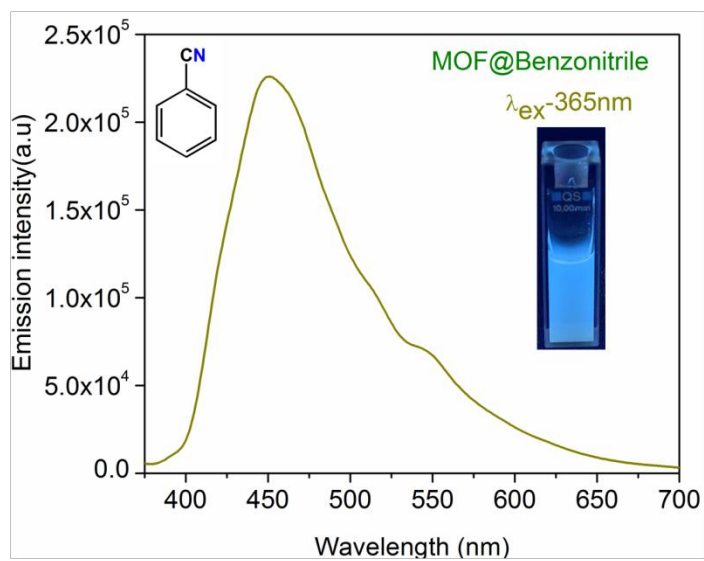
Appendix 2.19. Luminescence spectra of MOF dispersed in mesitylene ($\lambda_{exc} = 365 \text{ nm}$).



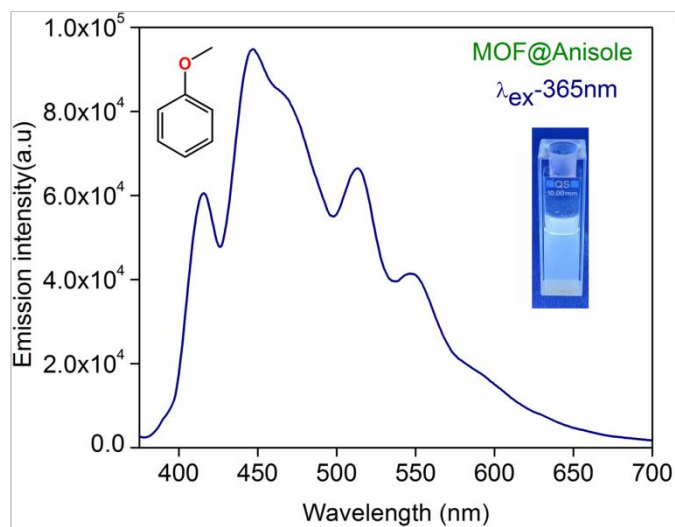
Appendix 2.20. Luminescence spectra of MOF dispersed in chlorobenzene ($\lambda_{exc} = 365 \text{ nm}$).



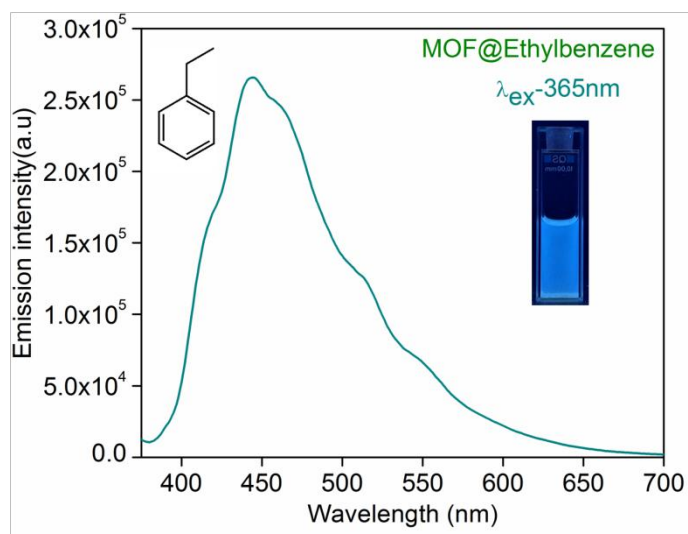
Appendix 2.21. Luminescence spectra of MOF dispersed in nitrobenzene ($\lambda_{\text{exc}} = 365 \text{ nm}$).



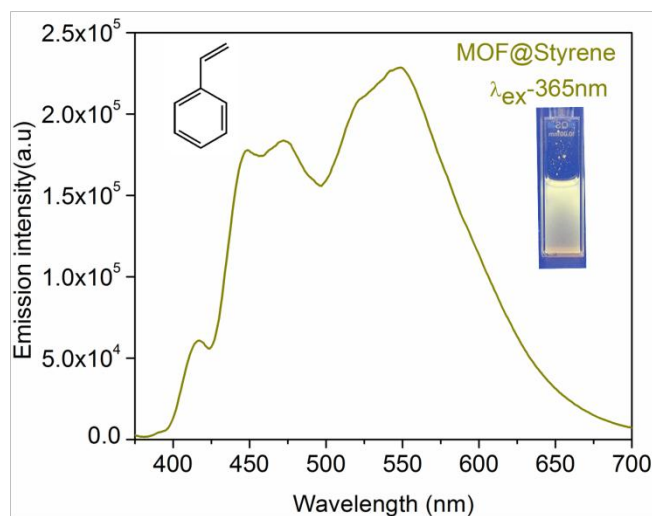
Appendix 2.22. Luminescence spectra of MOF dispersed in benzonitrile ($\lambda_{\text{exc}} = 365 \text{ nm}$).



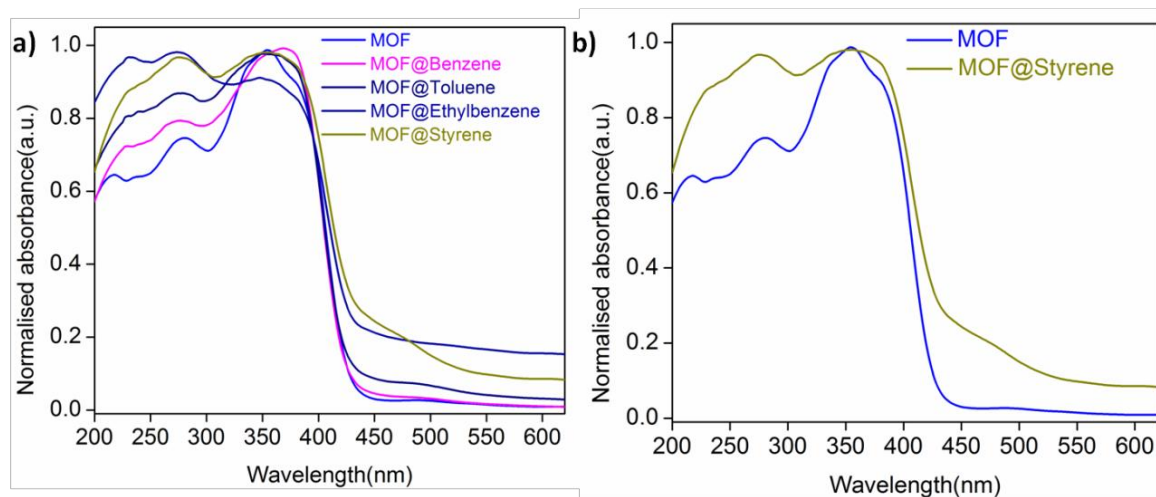
Appendix 2.23. Luminescence spectra of MOF dispersed in anisole ($\lambda_{exc} = 365$ nm).



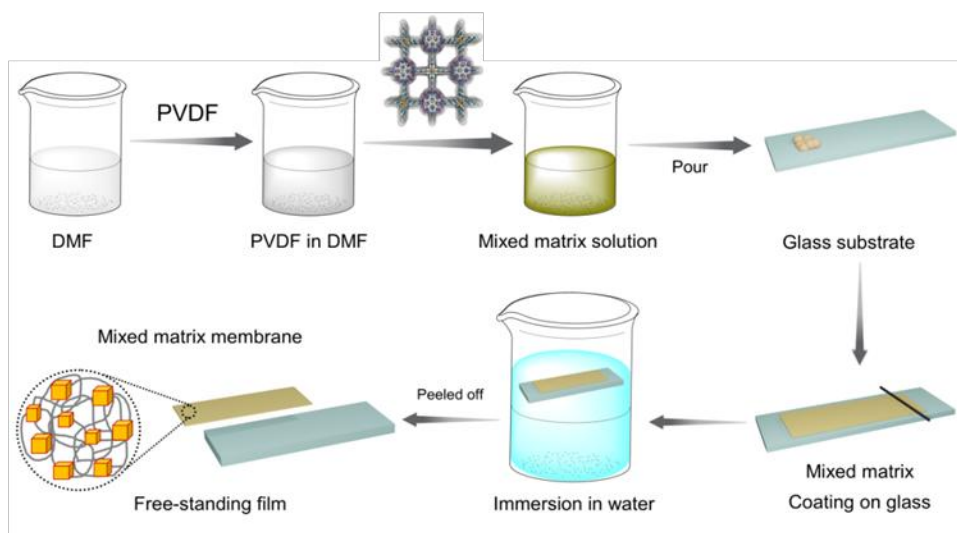
Appendix 2.24. Luminescence spectra of MOF dispersed in ethylbenzene ($\lambda_{exc} = 365$ nm).



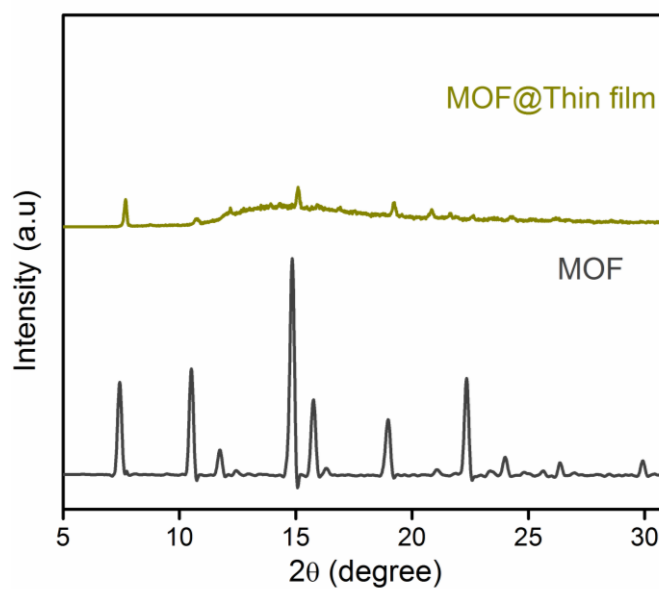
Appendix 2.25. Luminescence spectra of MOF dispersed in styrene ($\lambda_{\text{exc}} = 365 \text{ nm}$).



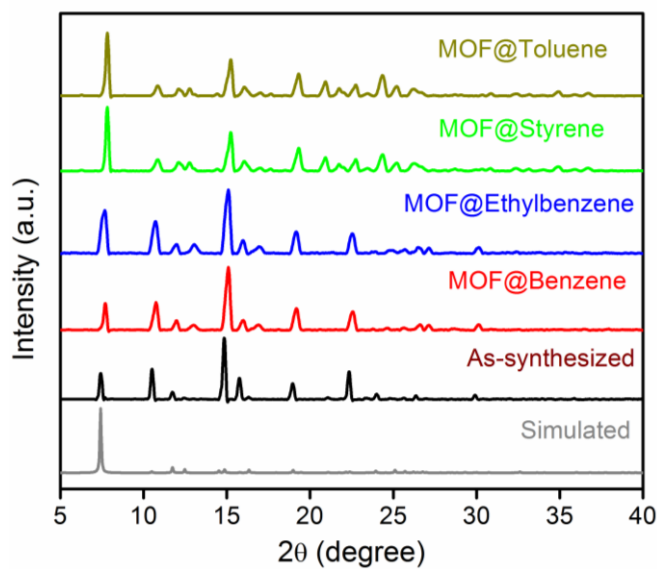
Appendix 2.26. Solid state UV-visible profile of MOF after VOC loading. a) Solid state UV-visible profile of MOF in pristine and VOC loaded phases. b) Comparison between solid-state UV-visible profile of MOF, pre and post styrene exposure.



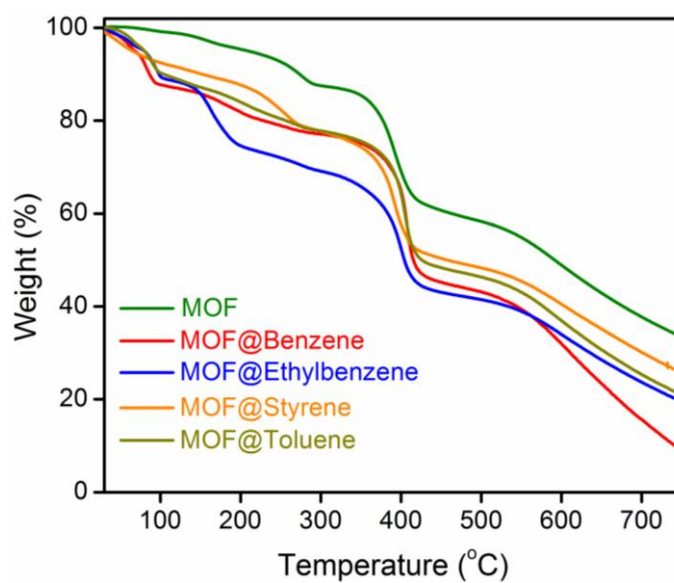
Appendix 2.27. (a) Procedure for construction of MOF based thin film for styrene detection. (b) Images of MOF based thin film before and after different VOC treatment.



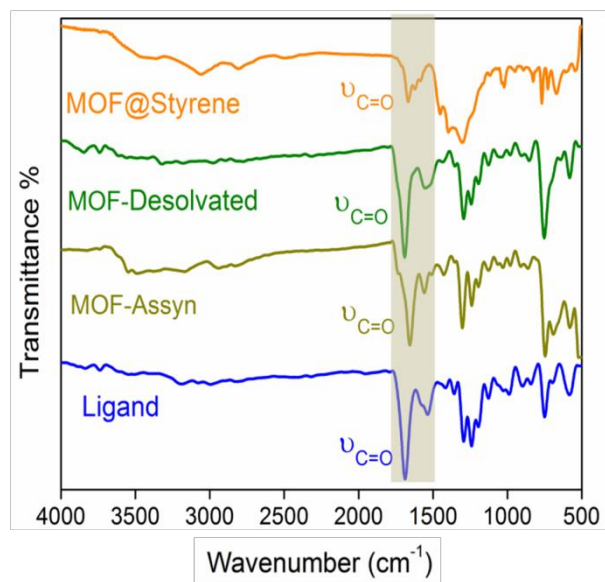
Appendix 2.28. PXRD of MOF based thin film, along with parent MOF.



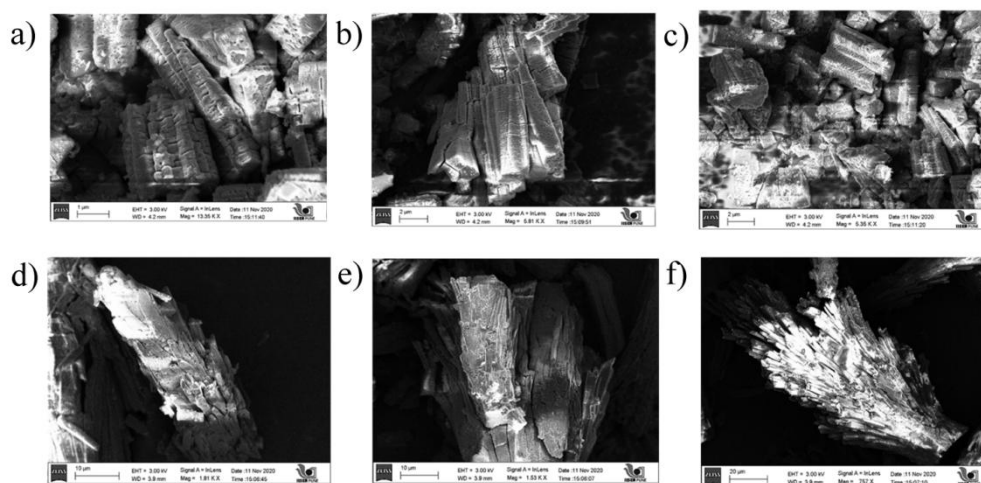
Appendix 2.29. PXRD data of MOF before and after VOC exposure.



Appendix 2.30. TGA data of MOF before and after VOC exposure. The boiling points of the VOCs are a) 80.1 °C for benzene b) 136 °C for ethylbenzene c) 110.6 °C for toluene d) 145 °C for styrene.



Appendix 2.31. FTIR data of ligand with MOF before and after styrene exposure.



Appendix 2.32. FESEM images of MOF before and after VOC exposure; a) MOF b) MOF@Styrene c) MOF@Toluene d) MOF@*p*-xylene e) MOF@ethylbenzene f) MOF@benzene.

Appendix Table 2.1. Crystal data and structure refinement for MOF (IPM-326).

CCDC number: 2115944 (IPM-326)

Chemical formula $C_{52}H_{28}F_6N_{12}O_{12}SiZn$ M_r 1220.32Crystal system, space group Monoclinic, $I2/m$

Temperature (K) 150

 a, b, c (Å) 7.3770 (6), 24.000 (2), 23.987 (2) β (°) 90.503 (8) V (Å³) 4246.7 (7)

Z 2

Radiation type Mo $K\alpha$ μ (mm⁻¹) 0.36

Crystal size (mm) 0.14 × 0.12 × 0.10

Data collection

Diffractometer : Saxi-CrysAlis PRO-abstract goniometer imported SAXI images

Absorption correction: Multi-scan

CrysAlis PRO 1.171.41.113a (Rigaku Oxford Diffraction, 2021) Empirical absorption correction using spherical harmonics, implemented in SCALE3 ABSPACK scaling algorithm.

 T_{min}, T_{max} : 0.603, 1.000No. of measured, independent and observed: $[I > 2\sigma(I)]$ reflections 38998, 4134, 2893 R_{int} : 0.161 $(\sin \theta/\lambda)_{max}$ (Å⁻¹): 0.610

Refinement

 $R[F2 > 2\sigma(F2)], wR(F2), S$: 0.130, 0.360, 1.31

No. of reflections : 4134

No. of parameters: 257

No. of restraints : 26

H-atom treatment: H-atom parameters constrained

 $\Delta\rho_{max}, \Delta\rho_{min}$ (e Å⁻³): 0.88, -0.82

2.6 References

- [1] J. J. Lelieveld and U. Pöschl, *Nature.*, 2017, **551**, 291-293.
- [2] <https://www.britannica.com/print/article/10772>
- [3] <https://www.epa.gov/clean-air-act-overview/air-pollution-current-and-future-challenges#protecting>
- [4] B. C. McDonald, A. De Gouw, J. B. Gilman, S. H. Jathar, A. Akherati, C. D. Cappa, J. L. Jimenez, J. L. Taylor, P. L. Hayes, S. A. McKeen, Y. Y. Cui, S. W. Kim, R. Gentner, G. I. VanWertz, A. H. Goldstein, R. A. Harley, G. J. Frost, J. M. Roberts, T. B. Ryerson and M. Trainer, *Science.*, 2018, **359**, 760-764.
- [5] A. Azzouz, K. Vikrant, K. -H. Kim, E. Ballesteros, T. Rhadfi and A. K. Malik. *TrAC Trends in Analytical Chemistry.*, 2019, **118** , 502-516.
- [6] V. V. Tran, D. Park and Y. -C. Lee, *Int. J. Environ. Res. Public Health.*, 2020., **17**, 2927.
- [7] G. Churkina, F. Kuik, B. Bonn, A. Lauer, R. Grote, K. Tomiak, and T. M. Butler, *Environ. Sci. Technol.*, 2017, **51**, 6120-6130.
- [8] E. V. Berezina, K. B. Moiseenko, A. I. Skorokhod, N. F. Elansky and I. B. Belikov, *Dokl. Earth Sc.*, 2017, **474**, 599–603.
- [9] M. Śmiełowska, M. Marć and B. Zabiegała, *Environ. Sci. Pollut. Res.*, 2017, **24**, 11166–11176.
- [10] K. Chen, Z. Gao, J. Sun, X. Hou, and J. Chen, *Chem. Commun.*, 2020, **56**, 13037-13039.
- [11] X. Li, L. Zhang, Z. Yang, P. Wang, Y. Yan and J. Ran, *Sep. Purif. Technol.*, 2020, **235**, 116213.
- [12] F. Radica, S. Mura, D. Carboni, L. Malfatti, S. Garroni, S. Enzo, G. D. Ventura, G. Tranfo, A. Marcelli, P. Innocenzi, *Microporous Mesoporous Mater.*, 2020, **294**, 109877.
- [13] R. Babae, B. Bonakdarpour, B. Nasernejad and N. Fallah, *J. Hazard. Mater.*, 2010, **184**, 111–117.
- [14] B. Liu, Y. Y. Li, L. Gao, F. Zhou and G. T. Duan, *J. Hazard. Mater.*, 2018, **358**, 355–365.

- [15] <https://www.bbc.co.uk/news/world-asia-india-52569636>
- [16] T. Rasheed and F. Nabeel, *Coord. Chem. Rev.*, 2019, **401**, 213065.
- [17] Y. Wang, X. Du, Y. Long, X. Tang, Z. Chen and Y. Jiang, *Sens. Actuators B-Chem.*, 2015, **206**, 252-257.
- [18] Z. Moradi, V. Kiarostami and M. Amini, *Food Analytical Methods.*, 2017, **10**, 41-48
- [19] W. P. Lustig, S. Mukherjee, N. D. Rudd, A. V. Desai, J. Li and S. K. Ghosh, *Chem. Soc. Rev.*, 2017, **46**, 3242-3285.
- [20] Y. Su, J. Yu, Y. Li, S. F. Z. Phua, G. Liu, W. Q. Lim, X. Yang, R. Ganguly, C. Dang, C. Yang and Y. Zhao, *Commun. Chem.*, 2018, **1**, 1-13.
- [21] L. Feng, C. Dong, M. Li, L. Li, X. Jiang, R. Gao, R. Wang, L. Zhang, Z. Ning, D. Gao and J. Bi, *J. Hazard Mater.*, 2019, **388**, 121816.
- [22] (a) A. Schoedel, M. Li, D. Li, M. O’Keeffe and O. M. Yaghi, *Chem. Rev.*, 2016, **116**, 12466–12535; (b) S. Kitagawa, R. Kitaura, S. –i. Noro, *Angew. Chem., Int. Ed.*, 2004, **43**, 2334-2375; (c) S. Horike, S. Shimomura and S. Kitagawa, *Nature Chem.*, 2009, **1**, 695–704.
- [23] (a) H. –C. Zhou, J. R. Long, O. M. Yaghi, *Chem. Rev.*, 2012, **112**, 673-674; (b) Z. Chen, S. L. Hanna, L. R. Redfern, D. Alezi, T. Islamoglu, O. K. Farha, *Coord. Chem. Rev.*, 2019, **386**, 32–49.
- [24] A. Karmakar, P. Samanta, A. V. Desai, and S. K. Ghosh, *Acc. Chem. Res.*, 2017, **50**, 2457–2469.
- [25] S. Yuan, L. Feng, K. Wang, J. Pang, M. Bosch, C. Lollar, Y. Sun, J. Qin, X. Yang, P. Zhang, Q. Wang, L. Zou, Y. Zhang, L. Zhang, Y. Fang, J. Li and H. –C. Zhou, *Adv.Mater.*, 2018, **30**, 1704303.
- [26] (a) B. –Q. Song, Q. –Y. Yang, S. –Q. Wang, M. Vandichel, A. Kumar, C. Crowley, N. Kumar, C. –H. Deng, V. GasconPerez, M. Lusi, H. Wu, W. Zhou and M. J. Zaworotko, *J. Am. Chem. Soc.*, 2020, **142**, 6896–6901; (b) Y. Zhou and L. Han, *Coord. Chem. Rev.*, 2021, **430**, 213665; (c) B.Garai, A.Mallick and

- R. Baneerjee, *Chem. Sci.*, 2016, **7**, 2195-2200; (d) L. Jiang, Y. Tian, T. Sun, Y. Zhu, H. Ren, X. Zou, Y. Ma, K. R. Meihaus, J. R. Long and G. Zhu, *J. Am. Chem. Soc.*, 2018, **140**, 15724–15730.
- [27] S. Bhattacharjee, B. Maitia and S. Bhattacharya, *Nanoscale.*, 2016, **8**, 11224–11233.
- [28] C. Fu, H. Y. Wang, G. S. Zhang, L. Li, Y. N. Sun, J. W. Fu and H. Zhang, *CrystEngComm.*, 2018, **20**, 4849–4856.
- [29] J. –J. Liu, Y. –B. Shan, C. –R. Fan, M. –J. Lin, C. –C. Huang and W. –X. Dai, *Inorg. Chem.*, 2016, **55**, 3680–3684.
- [30] T. Ono, M. Sugimoto and Y. Hisaeda, *J. Am. Chem. Soc.*, 2015, **137**, 30, 9519-9522
- [31] S. Mukherjee, B. Joarder, A. V. Desai, B. Manna, R. Krishna and S. K. Ghosh, *Chem Inorg. Chem.*, 2015, **54**, 4403–4408.
- [32] A. Dey, S. Chand, B. Maity, P. M. Bhatt, M. Ghosh, L. Cavallo, M. Eddaoudi and N. M. Khashab, *J. Am. Chem. Soc.*, 2021, **143**, 11, 4090–4094.
- [33] Y. Takashima, V.M. Martínez, S.Furukawa, M. Kondo, S. Shimomura, H. Uehara, M. Nakahama, K. Sugimoto and S. Kitagawa, *Nat. Commun.*, 2011, **2**, 1-8.
- [34] S. Jensen, K. Tan, W. P. Lustig, D. S. Kilin, J. Li, Y. J. Chabal and T. Thonhauser, *Chem. Mater.*, 2019, **31**, 7933-7940.
- [35] (a) E. Fernandez, P. G. Siaz, N. Perinka, S. Wuttke and R. F. de Luis, *Adv. Funct. Mater.*, 2021, 2010703; (b) M. S. Denny Jr and S. M. Cohen, *Angew. Chem. Int. Ed.*, 2015, **54**, 9029 –9032.
- [36] R. D. Pensack, K. M. Banyas and J. B. Asbury, *Phys. Chem. Chem. Phys.*, 2010, **12**, 14144–14152.
- [37] Y. Li, H. Zhang and Q. Liu, *Spectrochimica Acta Part A: Molecular and Biomolecular Spectroscopy.*, 2012, **86**, 51-55.
- [38] G. M. Sheldrick, *Acta Cryst.*, 2015, **A71**, 3-8.
- [39] O. V. Dolomanov, L. J. Bourhis, R. J. Gildea, J. A. K., Howard and H. Puschmann, *J. Appl. Cryst.*, 2009, **42**, 339-341.
- [40] G. M. Sheldrick, *Acta Cryst.*, 2015, **C71**, 3-8.

Chapter 3

Post-synthetically modified MOF as a scaffold for selective bisulfite recognition in water

3.1 Introduction

The versatile role played by anions both in biological and environmental aspects makes anion recognition an important area of scientific interest. Hence anion recognition chemistry has seen tremendous development over the past few decades.^[1] Sulphur dioxide (SO₂), a known major air pollutant further on hydrolysis produces its oxo-anion namely bisulfite (HSO₃⁻).^[2-3] Bisulfite anion plays a crucial role in regulation of different cardiovascular processes in our body at low concentration.^[4] Also it is used extensively in food, beverage and pharmaceutical industries as an antioxidant and antimicrobial agent.^[5] However, at high concentration it is well established to have marked adverse effects.^[6] This includes attack in the cells and tissues of human respiratory system leading to asthmatic and allergic tendencies.^[7] Further it is also found that bisulfite anion affects the human cardiovascular and alimentary systems leading to abdominal pain, diarrhea, dermatitis, hypertension as well as other biological disorders.^[8] Based on all these fact some countries have imposed serious restrictions on usage of bisulfite in food products either to a very low level or prohibited it.^[9] So from a bigger perspective recognition of bisulfite in water medium is very important. Many analytical techniques which include electrophoresis and electrochemical methods, chromatography etc.have been developed for determination of bisulfite.^[10] Due to lack of simplicity to a great extent and time consuming procedure have hindered the application of aforementioned techniques . On the other hand fluorescence spectroscopy is a simple, cost effective and sensitive technique with fast response time and can be an alternate powerful tool to serve this purpose.^[11] Various luminescent organic probes with specific functionalities have been designed in the past for selective sensing of bisulfite anions. This includes inclusion of functional moieties like aldehyde and levulinate group or group containing unsaturated covalent bonds into the probe.^[12] The reason behind choice of such groups is the facile chemical reactions of the bisulfite anion with all these functionalities which results in achieving a fast and accurate response in fluorescence intensity. But low water solubility often causes difficulty for such organic probes to detect bisulfite in water medium.^[13] So designing luminescent probes for selective anion recognition in water medium is indeed required.

Metal-organic frameworks (MOFs) are a distinguished class of crystalline porous material that has emerged over the last decade.^[14] Constructed from organic struts and metal nodes, MOFs represent an excellent tunable structure-property co-relationship. The choice of metal nodes as well as the design of the organic counterpart can be devised strategically to target and obtain any specific functionality. This can be utilized for the usage of MOFs in terms of molecular storage and separation, sensors, ion-conduction, molecular transport and various other applications.^[15] Luminescent MOFs (LMOFs) are a subclass of MOFs with wide range of applications in terms of molecular sensing, fabrication of optical devices etc.^[16] The long range ordering and porosity generated from the coordination nanospace within

these MOFs makes them an excellent platform for host-guest chemistry.^[17] The strategic design and incorporation of luminescent building blocks tune the electronic properties of the framework while the presence of secondary functional sites imparts selectivity to the host framework towards a particular incoming guest inducing high sensitivity towards the analyte. Linker modulation plays a huge role in design of luminescent MOFs which is carried out via two approaches: a) pre-synthetic approach where MOFs are constructed from linkers bearing targeted functional sites and b) post-synthetic approach where modifications are carried out in synthesized MOFs to render desired functionalities within the framework.^[18] Hence with all these attributes MOFs can perform as an excellent luminescent sensor to incoming guest molecules. For recognition of a particular analyte in water medium water stability of the luminescent probe is a primary criterion. MIL-series (MIL stands for 'Materials Institut Lavoisier') are a well-known family of MOFs for its chemical stability, high porosity and availability of free tunable functionality within the system.^[19-24] Keeping all these things in mind herein we have chosen a carboxylate based MOF NH₂-MIL-68(In) bearing free accessible amine moiety.^[25] Aldehyde groups were attached to it through post synthetic modification approach.^[26-29] The facile reaction between bisulfite anion and aldehyde group is known to generate turn on response in the fluorescence intensity.^[30] Turn on response is desired for its high signal to noise ratio and also to minimize false response as the detection occurs relative to a dark background.^[31] Herein we report selective aqueous phase detection of bisulfite anion with a post synthetically modified MOF NH₂-MIL-68(In)@CHO (Figure 3.1). To the best of our knowledge detection of this anion by post-synthetically modified MOF is demonstrated for the first time in the literature.

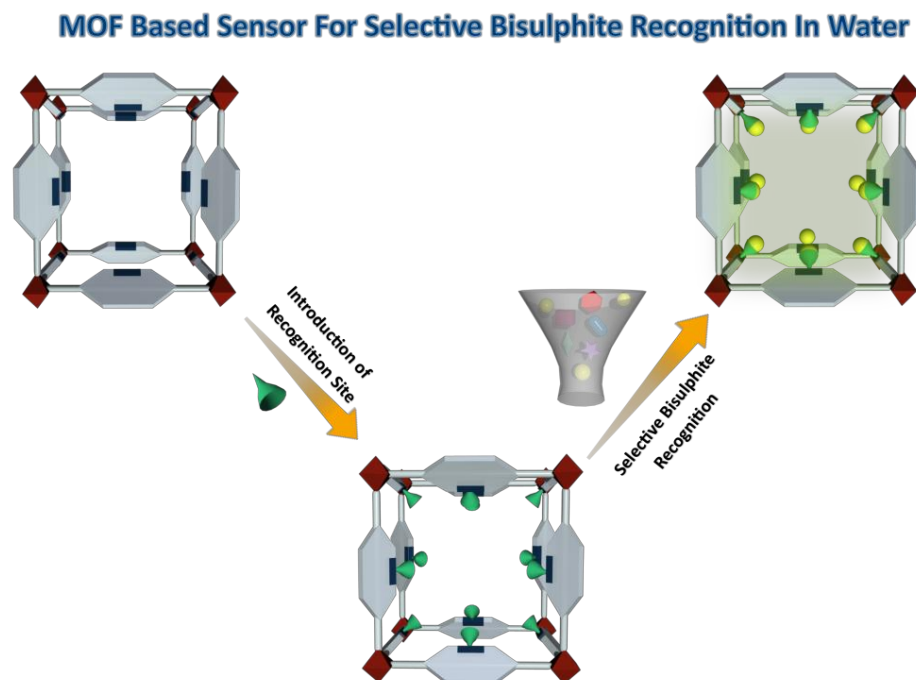


Figure 3.1. Schematic representation for selective recognition of bisulphite anion in water by a MOF based probe..

3.2 Experimental

3.2.1. Materials: All the chemicals used in this work were obtained commercially. 2-aminoterephthalic acid, glyoxal solution (40 wt % in water) and $\text{In}(\text{NO}_3)_3 \cdot x\text{H}_2\text{O}$ was purchased from Sigma Aldrich and are used without any further purification.

3.2.2 Physical Measurements: Powder X-ray diffraction (PXRD) data were recorded at Bruker D8 Advanced X-Ray diffractometer using $\text{Cu K}\alpha$ radiation ($\lambda = 1.5406 \text{ \AA}$) in 5° to 30° 2θ range. The IR-spectra were acquired by using NICOLET 6700 FT-IR spectrophotometer using KBr pellet in $400\text{-}4000 \text{ cm}^{-1}$ range. Gas adsorption measurements were carried out using BelSorp-max instrument from Bel Japan. All fluorescence measurements were carried on JobinYvon Fluoromax-4 spectrofluorometer. The SEM images were collected in FEI Quanta 3D dual beam FESEM at 30KV.

3.2.3 Synthesis

3.2.3.1 Synthesis of $\text{NH}_2\text{-MIL-68(In)}\text{-}(1\text{-NH}_2)$: This MOF was synthesized by following a reported protocol.^[32]

3.2.3.2 Synthesis of $\text{NH}_2\text{-MIL-68(In)}\text{ @CHO}(1\text{-CHO})$: $\text{NH}_2\text{-MIL-68(In)}\text{-}(1\text{-NH}_2)$ and glyoxal solution was taken in molar ratio of 1:1.25 and was subsequently refluxed in 1:1 methanol-ethanol system for 24

hours. The obtained solid 1'-CHO was filtered and washed with methanol and ethanol for several times. The washed solid was dipped in methanol for 48 hours to ensure removal of other solvent and unreacted molecules with methanol. The dipped solvent was changed at an interval of 8 hours with fresh methanol. The methanol exchanged phase was then filtered, air-dried and desolvated by heating at 80°C under vacuum for 24 hours to obtain guest free phase 1-CHO. This phase (1-CHO) was characterized and used for all experiments.

3.2.4. Analyte preparation:

Stock solutions of different anions HSO_3^- , Cl^- , SCN^- , NO_3^- , N_3^- , $\text{S}_2\text{O}_3^{2-}$ and HS^- were prepared from their respective sodium and potassium salts in 10 ml distilled water of concentration 1 mM.

3.2.5. Limit of Detection (LOD) Calculation:

The limit of detection was estimated by a reported protocol.^[36] For calculating limit of detection, HSO_3^- (20 – 200 μL , 1 mM stock solution) was added to 1-CHO (2 mg, in 2 mL water). Then we recorded the fluorescent intensity. We plotted the fluorescence intensity against increasing concentration of HSO_3^- , and received a linear trend. We fitted the trend at its low concentration to generate a linear plot. Slope (m) was calculated from the plot. Standard deviation (σ) was determined using five blank measurements of probe. Limit of detection (LOD) is calculated according to the formula:

Limit of Detection: ($3\sigma/m$)

3.3 Results and discussion

The NH_2 -MIL-68(In)(1- NH_2) was synthesized via solvothermal reaction according to protocol reported in the literature from its precursors $\text{In}(\text{NO}_3)_3 \cdot x\text{H}_2\text{O}$ and 2-aminoterephthalic acid.^[32] After synthesis of the compound the pristine phase (1'- NH_2) was collected by filtration and air-dried. PXRD analysis was done and the patterns of 1'- NH_2 matched well with the simulated pattern of MIL-68(In) confirming the bulk phase purity of 1'- NH_2 . Then the compound was dipped into methanol for 3-4 days and further heated at 100 °C for 12 hours in vacuum to obtain the desolvated phase 1- NH_2 . 1- NH_2 was characterized by PXRD, TGA and IR analysis (Appendix 3.1, 3.3, 3.6). The PXRD profile confirmed structural integrity of the desolvated phase (Appendix 3.1). The TGA profile showed no weight loss until 250 °C confirming absence of occluded solvent molecules inside the framework (Appendix 3.3). 1- NH_2 was further post synthetically modified when treated with glyoxal to achieve the parent phase 1'-CHO (Figure 3.2a). Thus obtained compound was dipped into methanol for 48 hours and desolvated under vacuum around 80 °C to obtain guest free phase 1-CHO (Appendix 3.4). The integrity of the framework 1-CHO was also confirmed by PXRD analysis (Appendix 3.2). Field emission scanning electron microscopy (FE-SEM)

images confirmed its needle like morphology (Appendix 3.21). The IR spectra of 1- CHO showed appearance of peaks around $\sim 1710\text{ cm}^{-1}$ and $\sim 1630\text{ cm}^{-1}$ which corresponds to C=O and C=N stretching frequencies of imine and aldehyde functionality respectively (Appendix 3.6).^[26] The nitrogen sorption isotherms of 1- CHO at 77K showed much lesser uptake as compared to $\text{NH}_2\text{-MIL-68(In)}$ (1-NH_2) which is well studied.^[33] This may be attributed to the pore hindering effect after post-synthetic modification (Appendix 3.5).^[34]

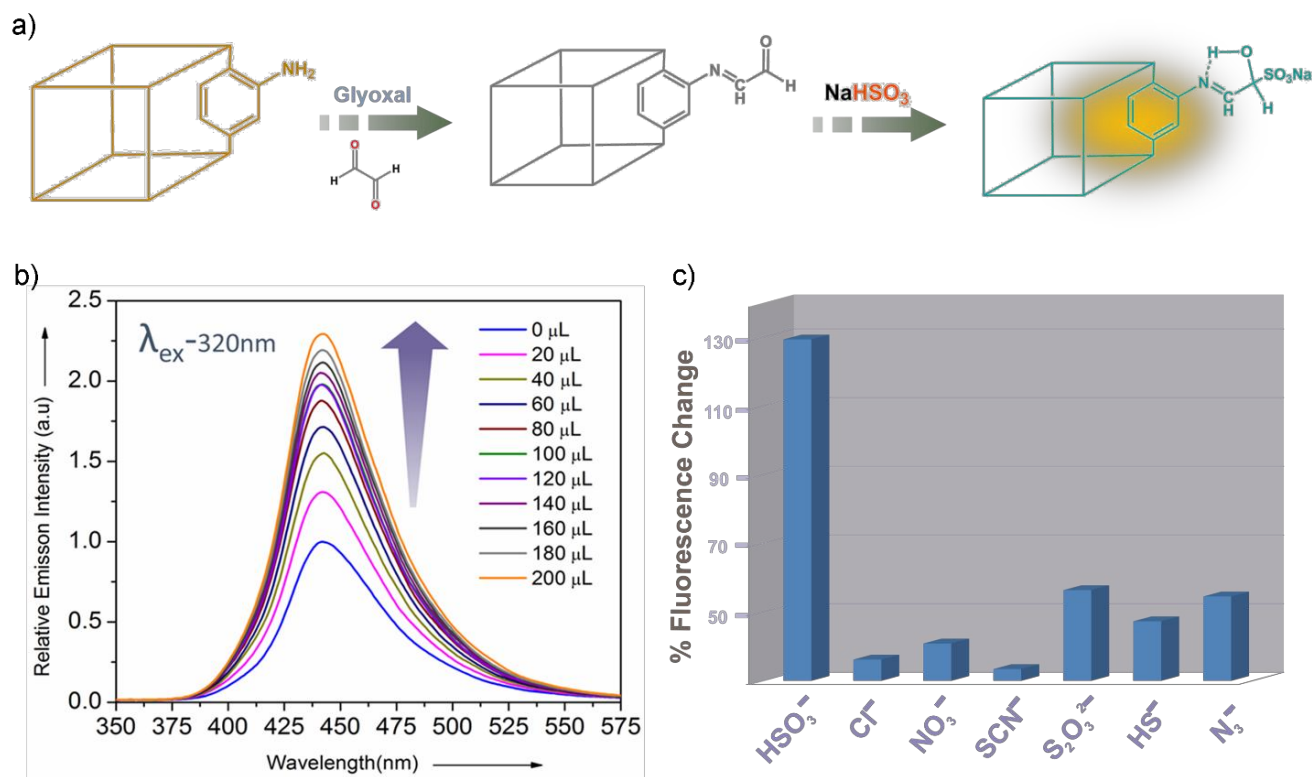


Figure 3.2. a) Probable mechanism of turn on response in presence of HSO_3^- ion; b) Emission spectra of the $\text{NH}_2\text{-MIL-68(In)@CHO}$ in presence of bisulfite anion in water medium when excited at 320 nm; c) Increase in fluorescence intensity upon addition of bisulfite ion and other anions to $\text{NH}_2\text{-MIL-68(In)@CHO}$ in water.

Next we sought to check the affinity of this probe towards bisulfite anion with fluorescence studies. Initial luminescence spectra of 1- CHO in water was recorded by exciting at 320 nm (λ_{ex} : 320 nm; spectra recorded in the range of 335-620 nm) (Appendix 3.7). Further, 2 mg desolvated 1- CHO was taken in a fluorescence cuvette and subsequently 2 mL water was added to it. Then to the dispersed MOF in water, a stock solution (1 mM) of bisulfite anion in water (20 μL to 200 μL) was added and spectra were recorded after every addition (Figure 3.2b). With each addition of bisulfite anion ion, enhancement in the fluorescence intensity of $\text{NH}_2\text{-MIL-68(In)@CHO}$ (1- CHO) was observed. This turn-on response in

fluorescence intensity may be attributed to the restriction of rotation of C=N bond which is present in 1-CHO prior to addition of bisulfite ion. The bisulfite anion react in a facile manner with the free aldehyde moiety and generates a free and available -OH group. This attached hydroxyl group takes part in hydrogen bonding with the nitrogen of the imine bond thus inhibiting its rotation. This hydrogen bonding induced restriction of C=N bond movement is probably leading to the turn-on response observed in this case. Such hydrogen bond assisted interactions between imine bond containing probes and guest analyte is well studied in the literature (Figure 3.2a).^[30, 35]

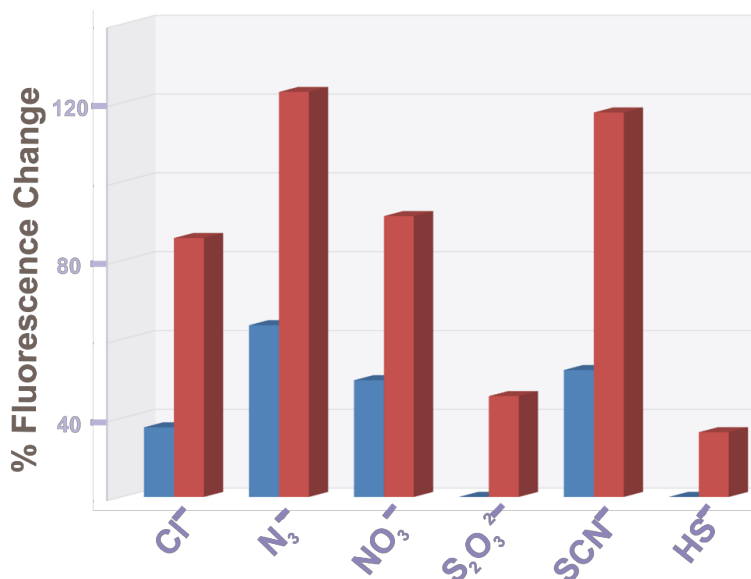


Figure 3.3. Increase in fluorescence intensity upon addition of bisulfite in presence of other anions to NH₂-MIL-68(In)@CHO.

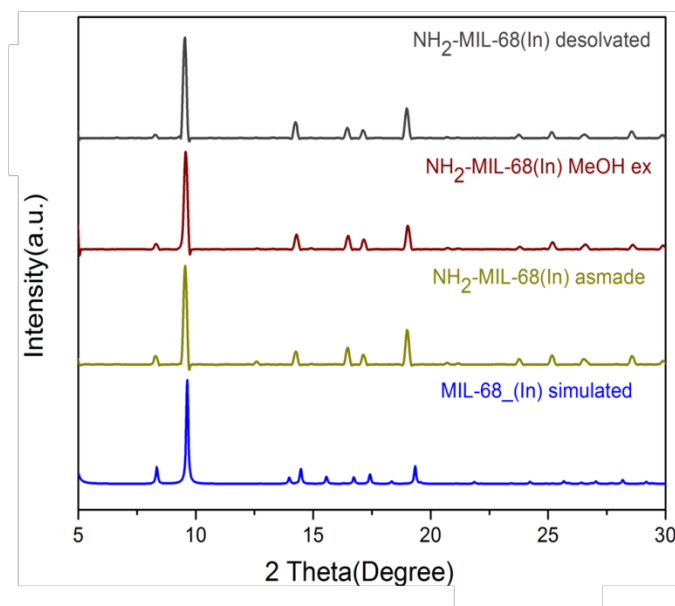
After the photoluminescence studies, the bisulfite treated phase of 1-CHO was subjected to PXRD and FE-SEM analysis to check the stability of the treated phase. FE-SEM studies confirmed the identical needle morphology of the bisulfite treated phase with the desolvated phase of 1-CHO (Appendix 3.21), while the PXRD pattern reveals no structural change of the framework post bisulfite treatment (Appendix 3.2). IR spectra of the bisulfite treated phase of 1-CHO showed peak around $\sim 1130\text{ cm}^{-1}$ which corresponds to the S=O stretching frequency confirming the probable mechanism of bisulfite recognition. (Appendix 3.6) The sensitivity of a probe depends on its limit of detection (LOD) value. In this case calculation of LOD as per literature protocols shows a value of 0.047 ppm (Appendix Table 3.2).^[36] Also selective recognition towards a particular anion in presence of other competing anions is important for practical application of any luminescent probe.^[37] To examine the selectivity of the probe 1-CHO luminescence studies were carried out with other anions both in presence and absence of bisulphite (Appendix 3.8-19). These studies were performed with 1mM solution of Cl⁻, SCN⁻, NO₃⁻, N₃⁻, S₂O₃²⁻ and HS⁻

ions in water. Briefly, 2 mg of 1-CHO in 2 mL of water was taken for measurement. To the dispersed MOF, 200 μL of the competing anion from the stock solution was added and the corresponding spectra were recorded to verify the response of MOF towards other anions. Individual anion based luminescence studies with other anions showed negligible enhancement in fluorescence intensity of 1-CHO indicating the selectivity of 1-CHO only towards bisulfite anion. To validate the observation a follow up competitive experiment was performed with bisulfite anion in presence of other anions. In the similar manner to the dispersed phase of 1-CHO (2 mg) in 2 ml water, 100 μL of competing anion solution was added following the addition of 100 μL HSO_3^- ion solution from the prepared stock. Initially the fluorescence intensity of 1-CHO showed negligible enhancement with addition of particular amount of the competing anion. But with the addition of equivalent amount of bisulfite anion drastic enhancement in the fluorescence intensity was observed (Figure 3.3). By combining both these responses we got the sensitivity of 1-CHO towards HSO_3^- ion even with other competing ions. Hence this experiment clarifies the ability of 1-CHO towards selective bisulfite recognition even with existing other anions.

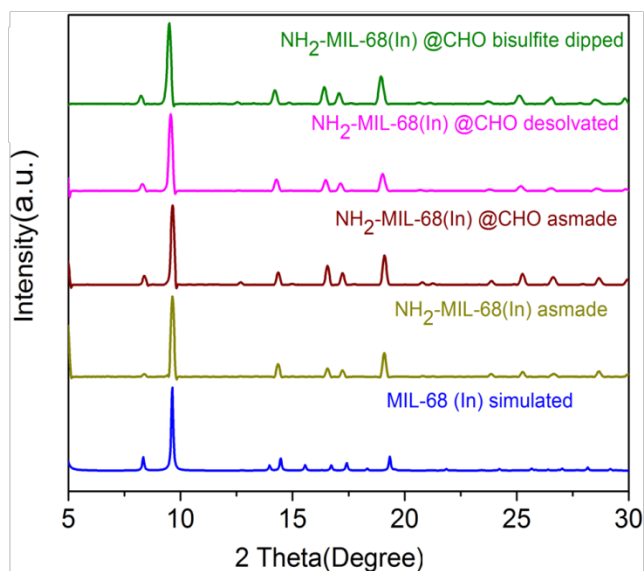
3.4 Conclusions

In conclusion we have synthesized a post-synthetically modified MOF (1-CHO) from a water stable robust porous parent MOF $\text{NH}_2\text{-MIL-68(In)}$ (1- NH_2). 1-CHO is used for selective recognition of bisulfite anion in aqueous medium. Selective recognition of bisulfite anion through such reaction based approach by a MOF based luminescent probe is rarely explored. We believe that this work can contribute in the development process of constructing of MOF based sensors for practical applications.

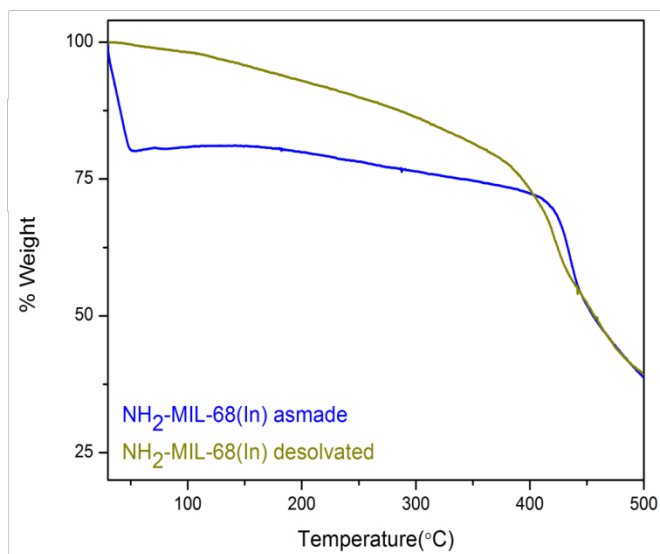
3.5 Appendix section



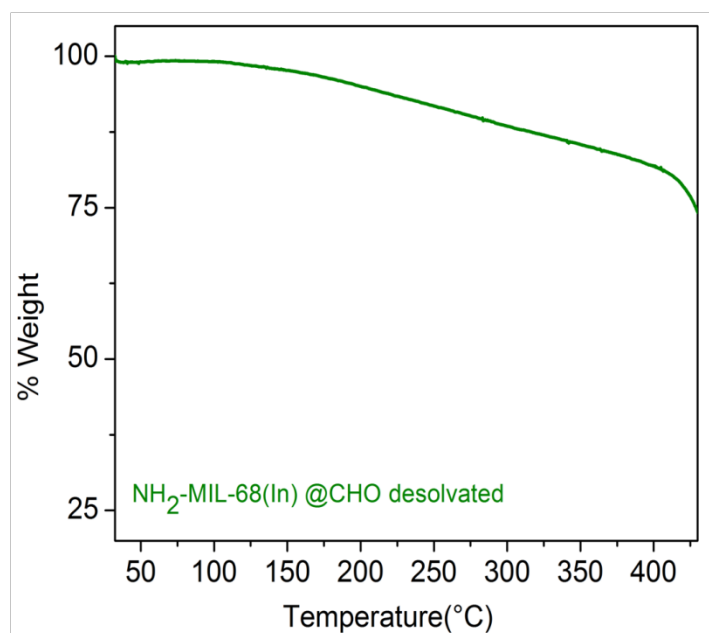
Appendix 3.1. Powder X-ray diffraction patterns of simulated MIL-68(In) (blue), asmade phase (dark yellow), methanol exchanged phase (wine red) and desolvated phase of NH₂-MIL-68(In) (dark gray).



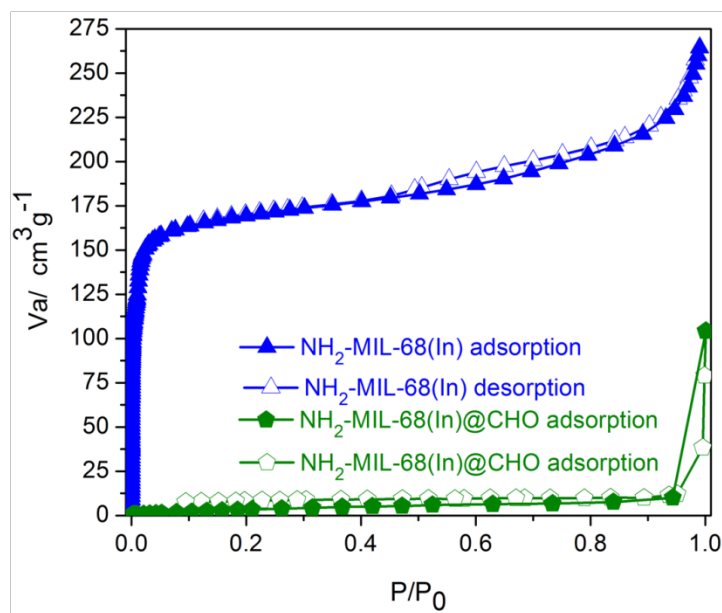
Appendix 3.2. Powder X-ray diffraction patterns of simulated MIL-68(In) (blue), asmade phase of NH₂-MIL-68(In) (dark yellow), asmade phase of NH₂-MIL-68(In)@CHO (wine red), desolvated phase of NH₂-MIL-68(In)@CHO (magenta) and bisulfite treated phase (green) of NH₂-MIL-68(In)@CHO.



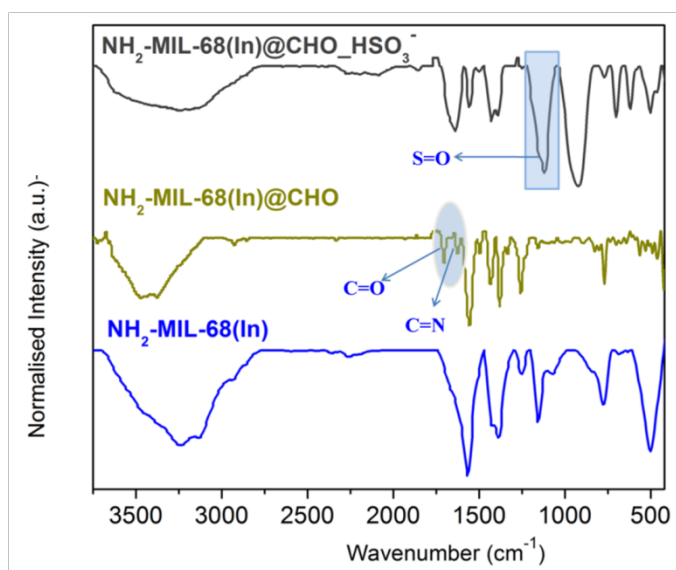
Appendix 3.3. TGA profile of the asmade phase (blue) and the desolvated phase (green) of NH₂-MIL-68(In).



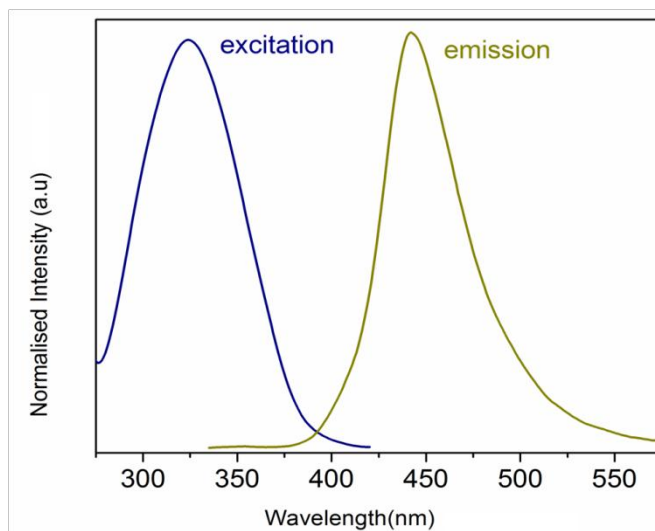
Appendix 3.4. TGA profile of the desolvated phase of NH₂-MIL-68(In)@CHO.



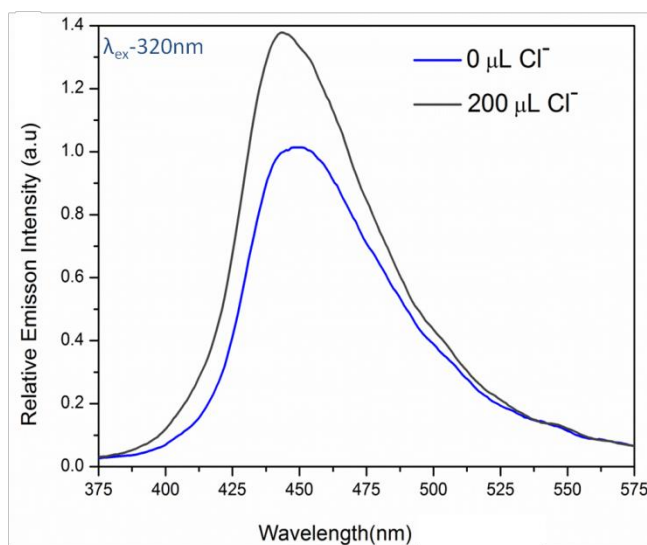
Appendix 3.5. N_2 sorption isotherm of NH_2 -MIL-68(In) and NH_2 -MIL-68(In)@CHO at 77K.



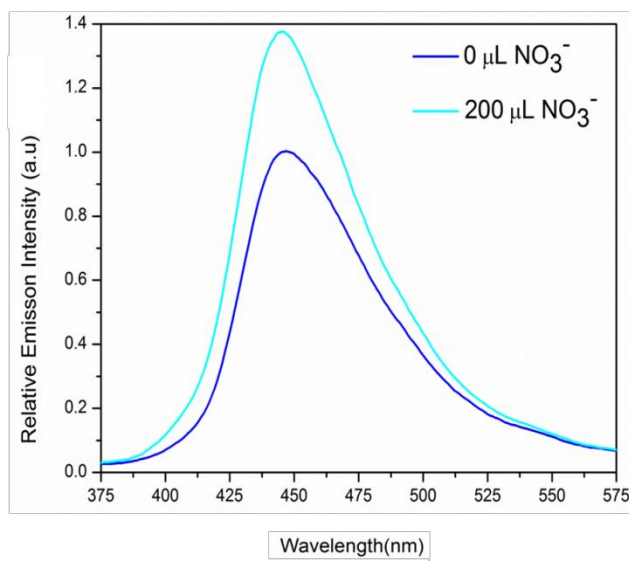
Appendix 3.6. IR-spectra of NH_2 -MIL-68(In) (blue), NH_2 -MIL-68(In)@CHO (dark yellow) and bisulfite treated phase (dark gray) of NH_2 -MIL-68(In)@CHO.



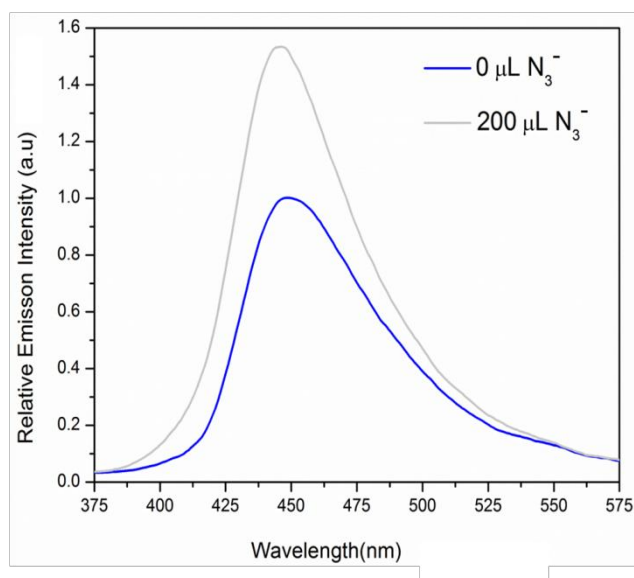
Appendix 3.7. Excitation and emission spectra of the $\text{NH}_2\text{-MIL-68(In)@CHO}$. When the dispersed phase of $\text{NH}_2\text{-MIL-68(In)@CHO}$ in water was excited at 320 nm an emission maxima at 442 nm was obtained.



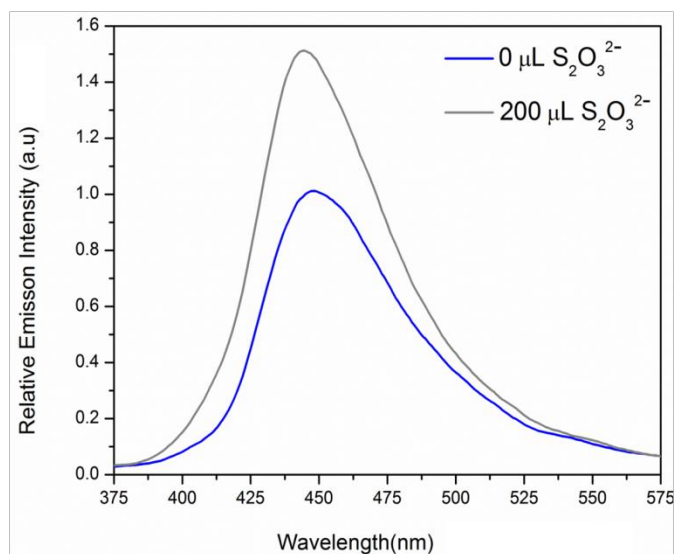
Appendix 3.8. Change in fluorescence upon addition of Cl^- anion to $\text{NH}_2\text{-MIL-68(In)@CHO}$ in water when excited at 320 nm.



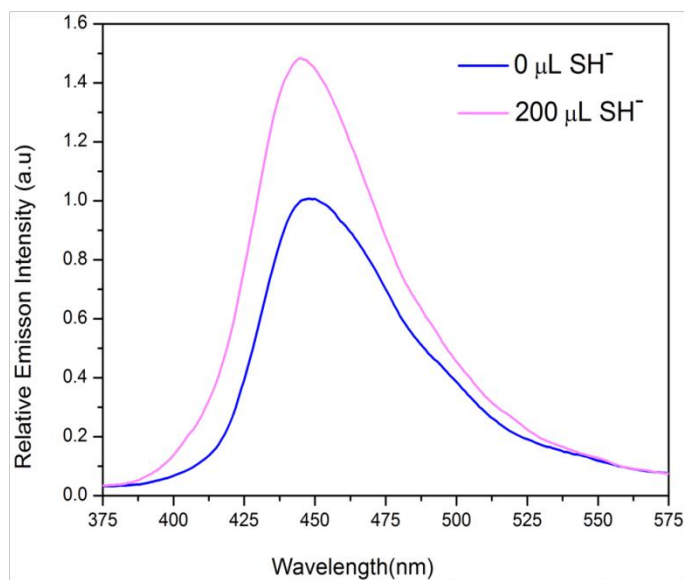
Appendix 3.9. Change in fluorescence upon addition of NO_3^- anion to $\text{NH}_2\text{-MIL-68(In)@CHO}$ in water when excited at 320 nm.



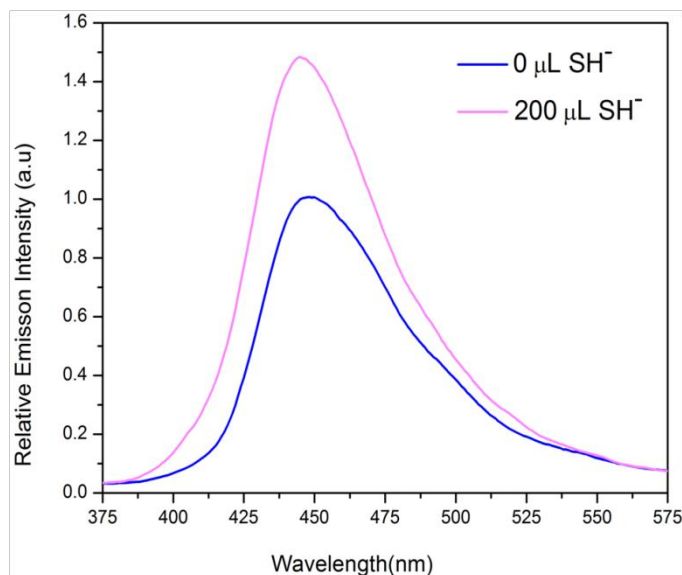
Appendix 3.10. Change in fluorescence upon addition of azide anion to $\text{NH}_2\text{-MIL-68(In)@CHO}$ in water when excited at 320 nm.



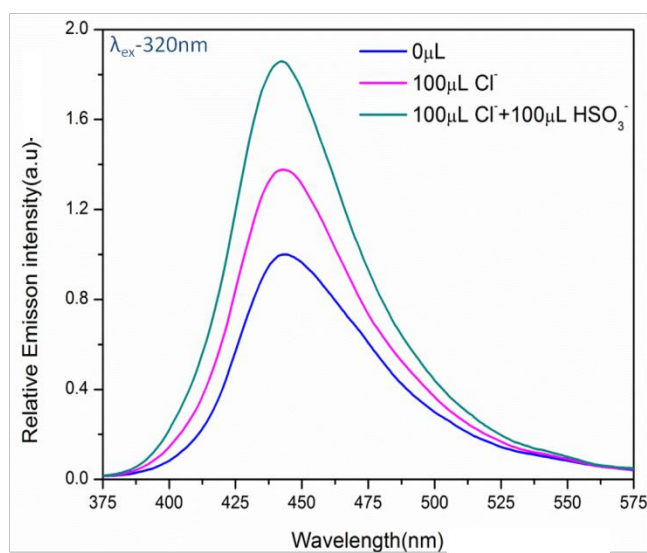
Appendix 3.11. Change in fluorescence upon addition of thiosulfate anion to $\text{NH}_2\text{-MIL-68(In)@CHO}$ in water when excited at 320 nm.



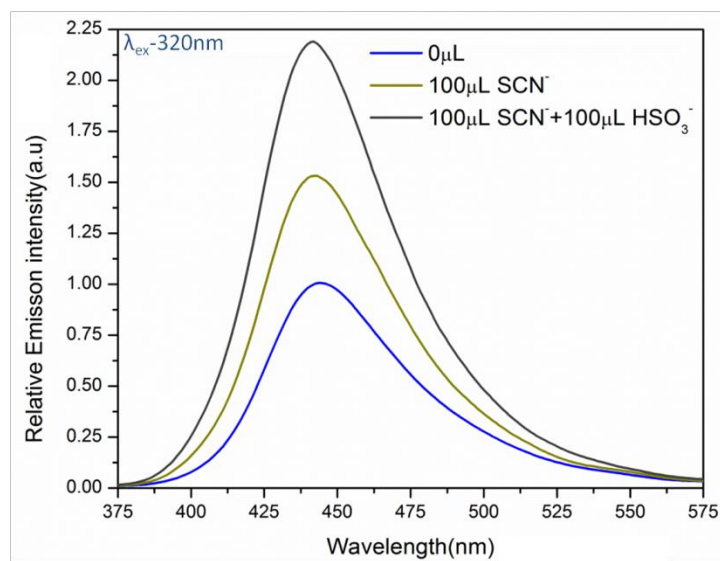
Appendix 3.12. Change in fluorescence upon addition of HS^- anion to $\text{NH}_2\text{-MIL-68(In)@CHO}$ in water when excited at 320 nm.



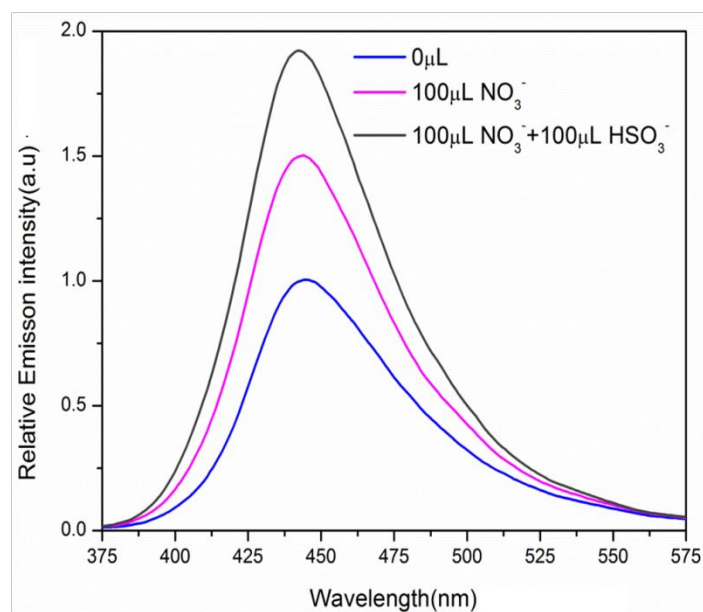
Appendix 3.13. Change in fluorescence upon addition of SCN⁻ anion to NH₂-MIL-68(In)@CHO in water when excited at 320 nm.



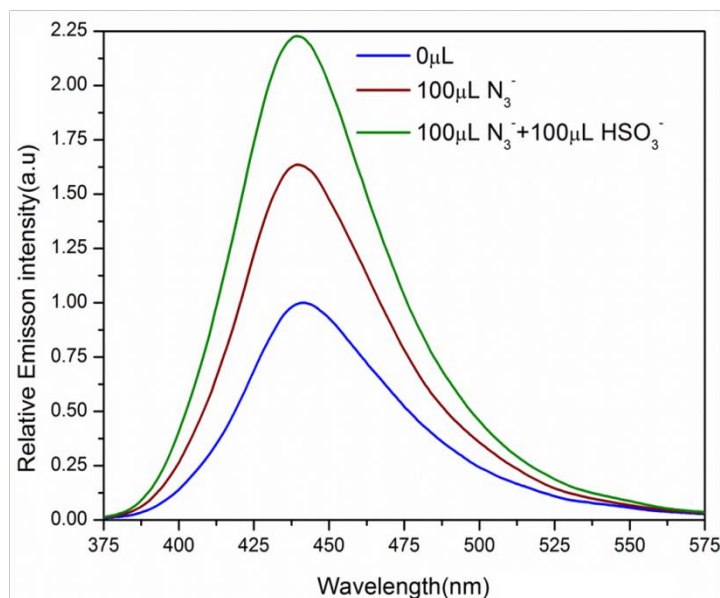
Appendix 3.14. Change in fluorescence upon addition of Cl⁻ anion in presence of HSO₃⁻ to NH₂-MIL-68(In)@CHO in water when excited at 320 nm.



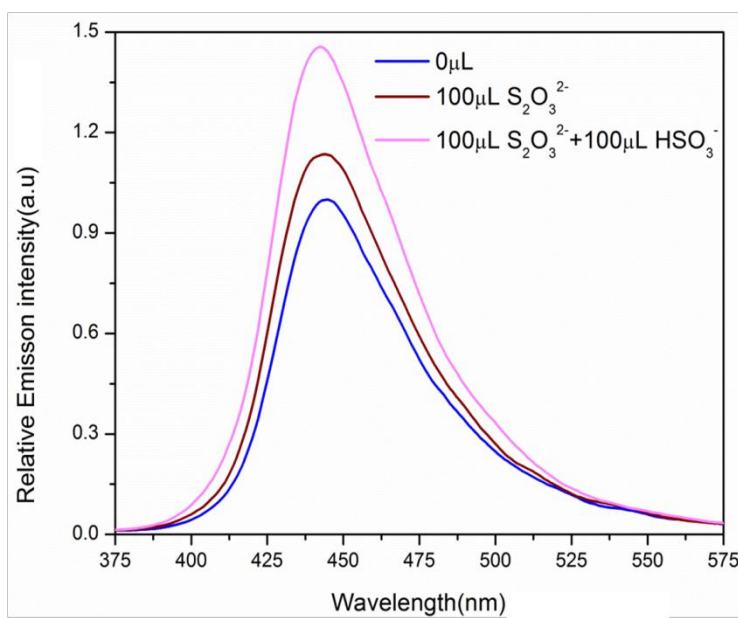
Appendix 3.15. Change in fluorescence upon addition of SCN⁻ anion in presence of HSO₃⁻ to NH₂-MIL-68(In)@CHO in water when excited at 320 nm.



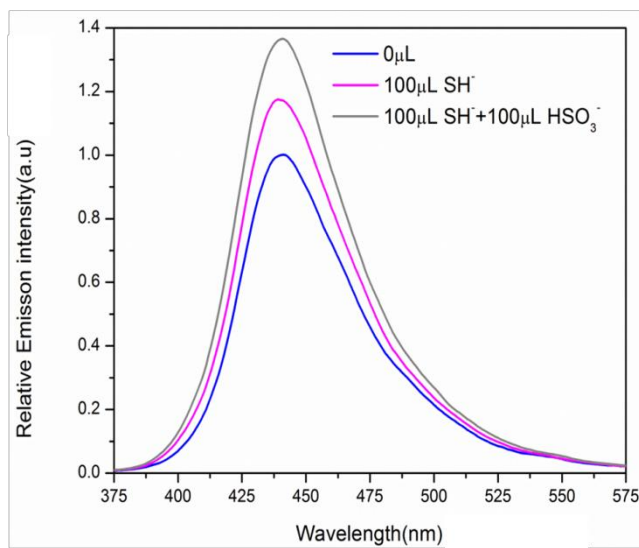
Appendix 3.16. Change in fluorescence upon addition of NO₃⁻ anion in presence of HSO₃⁻ to NH₂-MIL-68(In)@CHO in water when excited at 320 nm.



Appendix 3.17. Change in fluorescence upon addition of N₃⁻ anion in presence of HSO₃⁻ to NH₂-MIL-68(In)@CHO in water when excited at 320 nm.

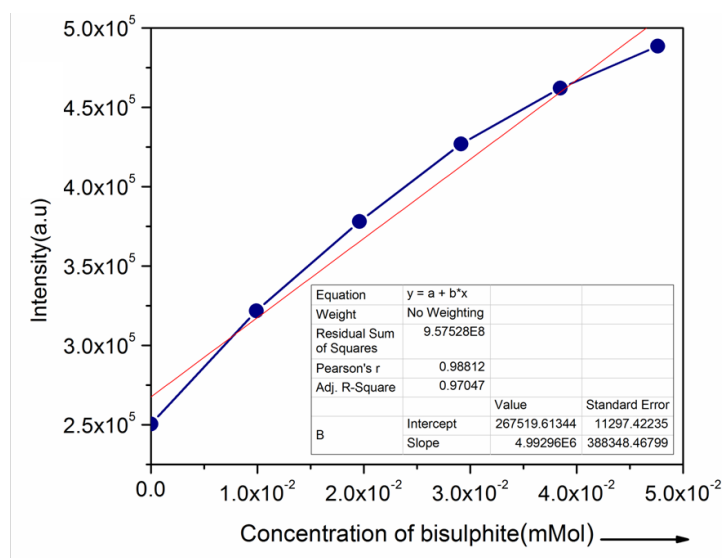


Appendix 3.18. Change in fluorescence upon addition of S₂O₃²⁻ anion in presence of HSO₃⁻ to NH₂-MIL-68(In)@CHO in water when excited at 320 nm.

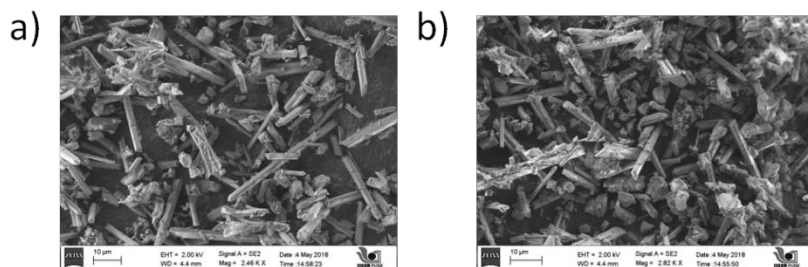


Appendix 3.19. Change in fluorescence upon addition of HS^- anion in presence of HSO_3^- to $\text{NH}_2\text{-MIL-68(In)@CHO}$ in water when excited at 320 nm.

Limit of Detection (LOD) calculation:



Appendix 3.20. Concentration vs intensity plot for the probe when HSO_3^- ion (1 mM stock solution) has been added in water medium (λ_{ex} : 320 nm, λ_{em} : 442 nm; $R^2=0.97047$).



Appendix 3.21. FESEM images of $\text{NH}_2\text{-MIL-68(In)@CHO}$ before and after fluorescence experiments in water

Calculation of standard deviation:

Appendix Table 3.1: Standard deviation for probe

Blank Readings (only probe)	Fluorescence Intensity
Reading 1	52418.48832
Reading 2	52631.23808
Reading 3	51965.47915
Reading 4	51341.27696
Reading 5	53950.81953
Standard deviation (σ)	968.2032342

Calculation of Limit of Detection:

Appendix Table 3.2: Detection limit calculation for probe

Slope from Graph (m)	4.99296E6	mM^{-1}
Limit of Detection ($3\sigma/m$)	5.82E-04 0.047	mM ppm

3.6 References

- [1] N. Busschaert, C. Caltagirone, W.V. Rossom and P. A. Gale, *Chem. Rev.*, 2015, **115**, 8038-8155.
- [2] Z. Meng, G. Qin, B. Zhang and J. Bai, *Mutagenesis.*, 2004, **19**, 465-468.
- [3] Y.-Q. Sun, J. Liu, J. Zhang, T. Yang and W. Guo, *Chem. Commun.*, 2013, **49**, 2637-2639.
- [4] D. Zhang, L. Wenya, K. Chen, J. Cheng, Y. Zhao and Y. Ye, *RSC Adv.*, 2016, **6**, 103905-103909.
- [5] P. Xie, G. Gao, W. Zhang, G. Yang and Q. Jin, *J. Chem. Sci.*, 2015, **127**, 1267-1273.
- [6] (a) Y. Yang, F. Huo, J. Zhang, Z. Xie, J. Chao, C. Yin, H. Tong, D. Liu, S. Jin, F. Cheng and X. Yan, *Sens. Actuators. B.*, 2012, **166**, 665-670; (b) G. Li, Y. Chen, J. Wang, Q. Lin, J. Zhao, L. Ji and H. Chao, *Chem. Sci.*, 2013, **4**, 4426-4433. (c) Y. Sun, Y. Li, X. Ma and L. Duan, *RSC Adv.*, 2016, **6**, 79830-79835.
- [7] (a) J. Chao, Z. Li, Y. Zhang, F. Huo, C. Yin, Y. Liu, Y. Li and J. Wang, *J. Mater. Chem. B.*, 2016, **4**, 3703-3712; (b) X. Yang, Y. Cui, Y. Li, L. Zheng, L. Xie, R. Ning, Z. Liu, J. Lu, G. Zhang, C. Liu and G. Zhang, *Spectrochimica Acta, Part A.*, 2015, **137**, 1055-1060; (c) S. Paul, K. Ghoshal, M. Bhattacharyya and D. K. Maiti, *ACS Omega.*, 2017, **2**, 8633-8639.
- [8] (a) L. E. S. Figueroa, C. Gimenez, A. Agostini, E. Aznar, M. D. Marcos, F. Sancenon, R. M. Manez and P. Amoros, *Angew. Chem. Int. Ed.*, 2013, **52**, 13712-13716; (b) H. Vally, N. L. A. Misso and V. Madan, *Clinical & Experimental Allergy.*, 2009, **39**, 1643-1651.
- [9] (a) Y. Sun, D. Zhao, S. Fan, L. Duan and R. Li, *J. Agric. Food Chem.*, 2014, **62**, 3405-3409; (b) J. Wang, Y. Hao, H. Wang, S. Yang, H. Tian, B. Sun, and Y. Liu, *J. Agric. Food Chem.*, 2017, **65**, 2883-2887.
- [10] (a) X. Ma, C. Liu, Q. Shan, G. Wei, D. Wei and Y. Du, *Sens. Actuators B.*, 2013, **188**, 1196-1200; (b) B. Palenzuela, B.M. Simonet, A. Rios and M. Valcarcel, *Anal. Chim. Acta.*, 2005, **535**, 65-72; (c) S. Faldt, B. Karlberg and W. Frenzel, *Fresenius. J. Anal. Chem.*, 2001, **371**, 425-430; (d) U. T. Yilmaz and G. Somer, *Anal. Chim. Acta.*, 2007, **603**, 30-35.
- [11] A. P. de Silva, H. Q. N. Gunaratne, T. Gunnlaugsson, A. J. M. Huxley, C. P. McCoy, J. T. Rademacher and T. E. Rice, *Chem. Rev.*, 1997, **97**, 1515-1566.
- [12] (a) H. Agarwalla, S. Pal, A. Paul, Y. W. Jun, J. Bae, K. H. Ahn, D. N. Srivastava and A. Das, *J. Mater. Chem. B.*, 2016, **4**, 7888-7894; (b) K. Kaur, S. Chaudhary, S. Singh and S.K. Mehta, *J. Lumin.*, 2015, **160**, 282-288; (c) M.Y. Wu, T. He, K. Li, M. B. Wu, Z. Huang and X-Qi Yu, *Analyst.*, 2013, **138**, 3018-3025; (d) X. Cheng, H. Jia, J. Feng, J. Qin and Z. Li, *Sens. Actuators B.*, 2013, **184**, 274-280; (e)

M.-Y. Wu, K. Li, C.-Y. Li, J.-T. Hou and X.-Q. Yu, *Chem. Commun.*, 2014, **50**, 183-185; (f) M. G. Choi, J. Hwang, S. Eor and S.-K. Chang, *Org. Lett.*, 2010, **12**, 5624-5627; (g) J. Xu, K. Liu, D. Di, S. Shao, Y. Guo, *Inorg. Chem. Commun.*, 2007, **10**, 681-684; (h) Y. Sun, C. Zhong, R. Gong, H. Mu and E. Fu, *J. Org. Chem.*, 2009, **74**, 7943-7946; (i) X. Pan, Y. Zhong, Y. Jiang, G. Zuo, J. Li and W. Dong, *Mater. Chem. Phys.*, 2018, **213**, 83-88.

[13] E. J. O'Neil and B. D. Smith, *Coord. Chem. Rev.*, 2006, **250**, 3068-3080.

[14] (a) M. Eddaoudi, J. Kim, N. Rosi, D. Vodak, J. Watcher, M. O'Keeffe and O. M. Yaghi, *Science.*, 2002, **295**, 469-472; (b) J. R. Long and O. M. Yaghi, *Chem. Soc. Rev.*, 2009, **38**, 1213-1214; (c) S. Horike, S. Shimomura and S. Kitagawa, *Nat. Chem.*, 2009, **1**, 695-704; (d) D. Bradshaw, S. E.-Hankari and L. L.-Spagnolo, *Chem. Soc. Rev.*, 2014, **43**, 5431-5443; (e) A. Karmakar, P. Samanta, A. V. Desai, S. K. Ghosh, *Acc. Chem. Res.*, 2017, **50**, 2457-2469; (f) S.-L. Li and Q. Xu, *Energy Environ. Sci.*, 2013, **6**, 1656-1683.

[15] (a) P. Silva, S. M. F. Vilela, J. P. C. Tome and F. A. A. Paz, *Chem. Soc. Rev.*, 2015, **44**, 6774-6803; (b) R. J. Kuppler, D. J. Timmons, Q.-R. Fang, J.-R. Li, T. A. Makal, M. D. Younga, D. Yuana, D. Zhao, W. Zhuang and H.-C. Zhou, *Coord. Chem. Rev.*, 2009, **253**, 3042-3066.

[16] (a) L. E. Kreno, K. Leong, O. K. Farha, M. Allendorf, R. P. V. Duyne and J. T. Hupp, *Chem. Rev.*, 2012, **112**, 1105-1125; (b) M. D. Allendorf, C. A. Bauer, R. K. Bhakta and R. J. T. Houk, *Chem. Soc. Rev.*, 2009, **38**, 1330-1352; (c) Y. Cui, Y. Yue, G. Qian and B. Chen, *Chem. Rev.*, 2012, **112**, 1126-1162; (d) W. P. Lustig, S. Mukherjee, N. D. Rudd, A. V. Desai, J. Li and S. K. Ghosh, *Chem. Soc. Rev.*, 2017, **46**, 3242-3285.

[17] (a) H. Cai, Y.-L. Huang and D. Li, *Coord. Chem. Rev.*, 2017, **378**, 207-221; (b) H. Cai, M. Li, X.-R. Li, W. Chen, G.-H. Chen, X.-C. Huang and D. Li, *Angew. Chem. Int. Ed.*, 2015, **127**, 10600-10605.

[18] (a) J. G. Nguyen and S. M. Cohen, *J. Am. Chem. Soc.*, 2010, **132**, 4560-4561; (b) Z. Wang and S. M. Cohen, *Chem. Soc. Rev.*, 2009, **38**, 1315-1329; (c) S. M. Cohen, *J. Am. Chem. Soc.*, 2017, **139**, 2855-2863.

[19] C. Volkringer, M. Meddouri, T. Loiseau, N. Guillou, J. Marrot, G. Fe'rey, M. Haouas, F. Taulelle, N. Audebrand and M. Latroche, *Inorg. Chem.*, 2008, **47**, 11892-11901.

[20] T. Devic, P. Horcajada, C. Serre, F. Salles, G. Maurin, B. Moulin, D. Heurtaux, G. Clet, A. Vimont, J.-M. Grene'che, B. L. Ouay, F. Moreau, E. Magnier, Y. Filinchuk, J. Marrot, J.-C. Lavalley, M. Daturi and G. Fe'rey, *J. Am. Chem. Soc.*, 2009, **132**, 1127-1136.

- [21] K. Barthelet, J. Marrot and G. D. Riou, *Chem. Commun.*, 2004, **5**, 520-521.
- [22] C. Janiak and J. K. Vieth, *New J. Chem.*, 2010, **34**, 2366-2388.
- [23] A. M. Katzenmeyer, J. Canivet, G. Holland, D. Farrusseng and A. Centrone, *Angew. Chem. Int. Ed.*, 2014, **53**, 2852-2856.
- [24] J. W. Yoon, H. Chang, S.-J. Lee, Y. K. Hwang, D.-Y. Hong, S.-K. Lee, J. S. Lee, S. Jang, T.-U. Yoon, K. Kwac, Y. Jung, R. S. Pillai, F. Faucher, A. Vimont, M. Daturi, G. Férey, C. Serre, G. Maurin, Y.-S. Bae and J.-S. Chang, *Nat. Mater.*, 2017, **16**, 526-531.
- [25] (a) M. Savonnet, D. B. -Bachi, C. Pinel, V. Lecocq, N. Bats and D. Farrusseng, 2009, FR Patent 09/05.101 (2009); (b) M. Savonnet, D. B.-Bachi, N. Bats, J. P.-Pellitero, E. Jeanneau, V. Lecocq, C. Pinel and D. Farrusseng, *J. Am. Chem. Soc.*, 2010, **132**, 4518-4519; (c) L. Wu, M. Xue, S.-L. Qiu, G. Chaplais, A. S.-Masseron and J. Patarin, *Microporous Mesoporous Mater.*, 2012, **157**, 75-81; (d) R. Liang, L. Shen, F. Jing, W. Wu, N. Qin, R. Lin and L. Wu, *Appl. Catal. B.*, 2015, **162**, 245-251.
- [26] W. Morris, C. J. Doonan, H. Furukawa, R. Banerjee and O. M. Yaghi, *J. Am. Chem. Soc.*, 2008, **130**, 12626-12627.
- [27] A. M. Fracaroli, P. Siman, D. A. Nagib, M. Suzuki, H. Furukawa, F. D. Toste and O. M. Yaghi, *J. Am. Chem. Soc.*, 2016, **138**, 8352-8355.
- [28] F.-G. Xi, H. Liu, N.-N. Yang and E.-Q. Gao, *Inorg. Chem.*, 2016, **55**, 4701-4703.
- [29] C. Liu, Q. Liu, A. Huang, *Chem. Commun.*, 2016, **52**, 3400-3402.
- [30] Y.-Q. Sun, P. Wang, J. Liu, J. Zhang and W. Guo, *Analyst.*, 2012, **137**, 3430-3433.
- [31] (a) A. Karmakar, B. Joarder, A. Mallick, P. Samanta, A. V. Desai, S. Basu and S. K. Ghosh, *Chem. Commun.*, 2017, **53**, 1253-12566; (b) S. S. Nagarkar, T. Saha, A. V. Desai, P. Talukdar, S. K. Ghosh, *Sci. Rep.*, 2014, **4**, 1-6; (c) S. S. Nagarkar, A. V. Desai, S. K. Ghosh, *Chem. Eur. J.*, 2015, **21**, 9994-9997; (d) S. Sharma, S. K. Ghosh, *ACS Omega.*, 2018, **3**, 254-258.
- [32] C. Yang, J. Cheng, Y. Chena and Y. Hua, *RSC Adv.*, 2016, **6**, 61703-61706.
- [33] B. Li, D. Ma, Y. Li, Y. Zhang, G. Li, Z. Shi, S. Feng, M. J. Zaworotko and S. Ma, *Chem. Mater.*, 2016, **28**, 4781-4786.
- [34] D. Jiang, L. L. Keenan, A. D. Burrows and K. J. Edler, *Chem. Commun.*, 2012, **48**, 12053-12055.
- [35] P. Wang, J. Liu, X. Lv, Y. Liu, Y. Zhao and W. Guo, *Org. Lett.*, 2012, **14**, 520-523.

[36] A. V. Desai, P. Samanta, B. Manna and S. K. Ghosh, *Chem. Commun.*, 2015, **51**, 6111-6114.

[37] A. Karmakar, N. Kumar, P. Samanta, A. V. Desai and S. K. Ghosh, *Chem. Eur. J.*, 2016, **22**, 864-868.

Part-II

**Functional porous organic polymers for
sequestration based environmental
applications**

Porous organic polymers (POPs) are constructed from functional organic nodes with multiple sites for propagation of the polymeric structures occurs through covalent bonds as discussed earlier. [1] Based on that POPs can be both neutral as well as ionic in terms of charge. In general, the charge neutral POPs are utilised for accommodation of neutral guest molecules while in case of ionic POPs (*i*POPs) the aromatic backbone is either cationic or anionic in nature and the electrical neutrality is achieved by the extra framework counter ions with opposite charge. [1-2] Both categories of POPs are constructed by varied synthetic strategies. Neutral POPs are constructed by condensation reactions of monomers and also post-synthetically modified by attaching desired functionality for targeted applications. [3] One of the strategies to construct cationic POPs are quaternization reaction between bipodal, tripodal and tetrapodal aromatic halide subunits with multiple nitrogen based heterocyclic units containing compounds leading to generation of free halide as counter-ion. [4] It is well reported in the literature that cationic POPs are also synthesized by postsynthetic alkylation of pristine POPs containing tertiary amine groups. [5] Anionic POPs are synthesized by deprotonation of POPs containing alcohol, thiol, carboxylic acid, sulphonic acid and phosphonic acid based functional groups and further exchanging them with metal salts to obtain extra framework cations. [6-7] Based on these synthetic designs POPs are widely utilised as materials for detection and sequestration of toxic pollutants from water and thus represents tremendous potentials in terms of tackling environmental pollution. [8] The main reason that can be attributed for tremendous application of POPs includes two main factors. Firstly, POPs are highly stable in water as well as in harsh acidic and alkaline environment due to their robust nature as well as structural rigidity obtained from covalent bonding. Secondly, the building blocks can be chosen in such a way that the constructed POP is decorated with functional groups that can incorporate both hydrophilic as well as hydrophobic guest molecules. [9-10]

Based on all this rationale this section is also consist of two chapters i.e. chapter 4 and chapter 5. In chapter 4, cationic POPs are utilized for detection and sequestration of iodine (^{127}I) from vapour phase and water as surrogate for radioiodine (^{129}I , ^{131}I). In chapter 5, two cationic POPs were designed for capture of chromate ion and perrhenate anion. Chromate (CrO_4^{2-}) is enlisted as one of the priority pollutant by US-EPA (US- Environment protection agency) due to its toxic effects while perrhenate (ReO_4^-) is used as surrogate for pertechnetate (TcO_4^-), a highly water soluble radioactive anion with high half-life ($t_{1/2}=2.1 \times 10^5$ years) generated post nuclear fission.

References:

[1] S. Das, P. Heasman, T. Ben and S. Qiu, *Chem. Rev.*, 2017, **117**, 1515-1563.

[2] P. Samanta, P. Chandra, S. Dutta, A. V. Desai, S. K. Ghosh, *Chem. Sci.*, 2018, **9**, 7874–7881.

-
- [3] X. Zou, H. Rena and G. Zhu, *Chem. Commun.*, 2013, **49**, 3925—3936.
- [4] H. Zhao, L. Li, Y. Wang and R. Wang, *Sci. Rep.*, 2014, **4**, 5478.
- [5] D. Banerjee, S. K. Elsaidi, B. Aguila, B. Li, D. Kim, M. J. Schweiger, A. A. Kruger, C. J. Doonan, S. Ma and P. K. Thallapally, *Chem. Eur. J.*, 2016, **22**, 17581–17584.
- [6] Z. Yan, Y. Yuan, Y. Tian, D. Zhang and G. Zhu, *Angew. Chem., Int. Ed.*, 2015, **54**, 12733-12737 .
- [7] P. Samanta , P. Chandra , A. V. Desai and S.K. Ghosh, *Mater. Chem. Front.*, 2017, **1**, 1384-1388
- [8] A. Waheed , N. Baig, N. Ullah and W. Falath, *Journal of Environmental Management.*, 2021, **287**, 112360.
- [9] P. Samanta, A. V. Desai, S. Let and S. K. Ghosh, *ACS Sustainable Chem. Eng.*, 2019, **7**, 7456-7458.
- [10] T. Skorjanc, D. Shetty and A. Trabolsi, *Chem.*, 2021, **7**, 882-918.

Chapter 4

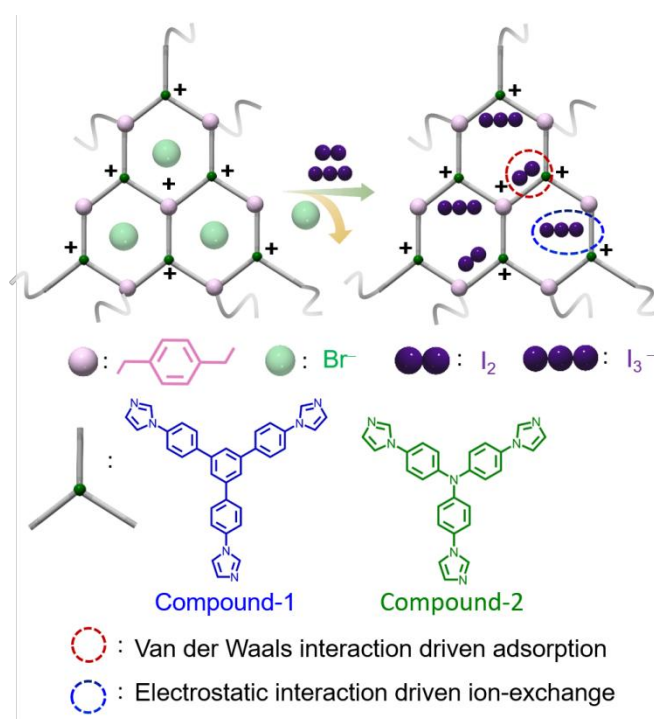
Functionalized ionic porous organic polymers exhibiting high iodine uptake from both vapor and aqueous medium

4.1 Introduction

Nuclear energy is regarded as an efficient zero emission-based clean energy source.^[1] Recent projection estimate a substantial rise of ~80% in nuclear energy by the year 2050, reaching a massive ~715 GW(e)/annum.^[2] Typically, nuclear energy generated via uranium (^{235}U) fission produces several harmful radioactive isotopes alongside, that includes selenium (^{79}Se), technetium (^{99}Tc), iodine (^{129}I , ^{131}I), krypton (^{85}Kr), and so-on.^[3] Among them, ^{129}I is regarded as extremely dangerous because of its large half-life ($\sim 1.57 \times 10^7$ years) and high volatility.^[4,5] Also, ^{131}I , although exhibiting a shorter half-life span (~ 8 days),^[6] is even more problematic as it can interfere with metabolic processes causing various adverse effects such as coma and untimely death as witnessed during the tragic Chernobyl nuclear disaster.^[4,7] Moreover, a significant spike in concentrations of volatile radionuclides (^{131}I , ^{129}I , ^{137}Cs) was observed all across Europe, especially in water bodies post-Chernobyl.^[6,7] Further, ^{131}I shows utility in cancer therapy and is regularly generated in hospitals, which is unequivocally risky as well.^[8] Classically, iodine exists as molecular iodine (I_2) in the vapor phase^[9]; however, recent studies have also hinted at the presence of iodide (I^-) and triiodide anion (I_3^-) in the vapor phase.^[6,10] While, in the aqueous medium, iodine tends to form polyiodides, among which triiodide (I_3^-) is one of the most predominant species.^[6,11] The state-of-the-art materials employed for iodine sequestration include silver-based zeolites (Ag-Z), activated carbons, zerovalent iron (ZVI), clays.^[12-14] Although displaying high chemical stability, these traditional sorbents fail to reach high sorption capacity and selectivity on account of low surface area and weak interactions.^[15] Additionally, the incorporation of expensive silver metal lowers the cost-effectiveness, thus making them unsustainable for the long-term use.^[16] This renders development of cost-efficient and highly selective sorbents for radioactive iodine capture from both vapor and aqueous phase of high topical relevance.

As a seminal class of porous materials, metal-organic frameworks (MOFs), covalent-organic frameworks (COFs), porous organic polymers (POPs), porous organic materials (POMs), and others have shown vast potential in several applications, including molecular recognition-based capture studies.^[17-25] In particular, recent literature reflects an upsurge in researcher's interest globally in developing advanced porous sorbents to address the long-standing radionuclide issue, among which radioactive iodine capture holds prominence as well.^[4,14,26-28] Specifically, the aforementioned porous materials have been extensively trialed for iodine capture (I_2); however, these studies are limited to the vapor phase or from organic medium (methanol (MeOH), cyclohexane).^[5,9,29-35] Notably, systematic investigations showing the capture of I_3^- from aqueous medium are limited.^[36-39]

Further, to the best of our knowledge, the sorbents mentioned above have not been trialed for iodine (I_3^-) sequestration from challenging matrices such as seawater representing real-world samples. To this end, we sought to explore ionic porous organic polymers (*i*POPs) as our host material for I_2/I_3^- capture, owing to their exclusive features including high physicochemical stability, charged network, a tuneable backbone that have been previously explored for several applications.^[28,40-42] We hypothesized that the presence of a polarizable pore surface (aromatic rings), Lewis basic nitrogen sites, ionic backbone (presence of exchangeable anions) in synergy might serve as an interactive host matrix for both I_2/I_3^- . Albeit these functionalities are known for their ability to polarize large molecules such as I_2 , but their effect on I_3^- remains largely underexplored.^[33] To test this, we rationally prepared two imidazolium-based *i*POPs, termed compound-1 and compound-2, via quaternization reaction between ligand-1 and ligand-2 (ESI) with 1,4-Bis-bromomethyl-benzene (linking node) (Scheme 4.1). These compounds were probed for their ability to capture iodine at both fuel reprocessing conditions and from challenging matrices such as seawater, which has been hitherto unexplored in porous materials.



Scheme 4.1. Schematic representation of ionic porous organic frameworks exhibiting efficient and selective iodine capture.

4.2 Experimental

4.2.1 Materials

All the reagents and solvents were available commercially and used without further purification unless otherwise specified.

4.2.2 Synthesis

Synthesis of compound-1: At first, we prepared 1,1'-(5'-(4-(1H-Imidazol-1-yl)phenyl)-[1,1':3',1''-terphenyl]-4,4''-diyl)bis(1H-imidazole) (ligand 1) as per the literature protocol.^[43] Further, compound-1 was synthesized via invoking a reported protocol with slight modification.^[44] 1,1'-(5'-(4-(1H-Imidazol-1-yl)phenyl)-[1,1':3',1''-terphenyl]-4,4''-diyl)bis(1H-imidazole) (0.3986 mmol, 201 mg) was reacted with 1,4-Bis-bromomethyl-benzene (0.7955 mmol, 210mg) in 20mLN-N'-dimethylformamide (DMF) at 100°C for 24 h. After cooling this mixture to room temperature, 1mL benzyl bromide was added, and the reaction mixture was further heated at 80°C for 12 h. The solid crude product obtained was collected and thoroughly washed with different solvents viz. water, DMF, N-N'-dimethylsulfoxide (DMSO), tetrahydrofuran (THF) and acetonitrile (MeCN) to get rid of oligomers. The solids was thereafter exchanged with dichloromethane (DCM), THF, and MeOH and heated at ~80°C in the presence of vacuum to obtain the desolvated phase of the compound. The solids were characterized by ¹³C NMR to establish purity.

Synthesis of compound-2: This compound was recently reported by Qiu and co-workers during the preparation of this manuscript and applied for separate functional studies.^[45] At first, we prepared Tris(4-(1H-imidazol-1-yl) phenyl) amine (ligand 2) as per the following literature protocol.^[46] Compound-2 was synthesized by following a similar synthetic scheme used for the preparation of compound-1. Tris-(4-imidazol-1-yl-phenyl)-amine (0.399mmol, 177mg) was reacted with 1,4-Bis-bromomethyl-benzene (0.7955 mmol, 210mg) in 20mL DMF at 100°C for 24 h. The reaction mixture was cooled down to room temperature, and to this, 1 mL benzyl bromide was added, and this mixture was further heated at 80 °C for 12 h. The solid crude product obtained was collected and thoroughly washed with different solvents i.e., water, DMF, DMSO, THF and MeCN to get rid of oligomers. The solids were further exchanged with DCM, THF, and MeOH, and heated ~80 °C in vacuum to obtain the desolvated phase of the compound. The solids were characterized by ¹³C NMR to establish purity.

4.2.3 Physical measurements

Thermogravimetric analysis profile was recorded on Perkin-Elmer STA6000, TGA analyser under N₂ atmosphere with heating rate of 10°C/min. ¹³C NMR spectra were recorded on a JEOL 400 MHz or Bruker 400MHz spectrometer. The IR Spectra were acquired by using NICOLET 6700 FT-IR spectrophotometer using KBr pellet in 400-4000 cm⁻¹ range. UV spectra were recorded on Shimadzu UV 2600 Spectrophotometer having stirring attachment. The SEM images and EDX data were obtained using FEI Quanta 3D dual beam ESEM. All fluorescence measurements were done on Jobin YvonFluoromax-4 spectrofluorometer. Four probe DC conductivity measurements were done on pressed pellets of compounds in Keithley 6221 sourcemeter instrument.

4.2.4 Computational details

Discovery Studio 2016 (Accelrys) have been used to perform the structural simulation to determine binding energy of interactions electrostatic – potential surface (ESP) and binding sites. Firstly, the molecular structure of the polymeric unit was fully relaxed using DMOL3 using B3LYP hybrid function by keeping Multiplicity function in Auto mode, double numeric plus polarizing (DNP) basis set and water as solvent. Further, structural simulation on the relaxed structure was performed using single – point energy calculations at a fine-quality calculation level.

To locate the initial position of the anion in the monomer unit of compound-1 and compound-2, simulated annealing technique was used. The static binding energies (ΔE) at 0 K in vacuum were calculated using the following expression

$$\Delta E = E_{Compound + Anion} - E_{Compound} - E_{Anion}$$

where E_x refers, to the total energies of the *Compound+Anion* complex, the charged *Compound* + alone, and the *Anion* molecule respectively.

The electrostatic potential (ESP) on the van der Waals (VDW) surfaces (isodensity = 0.001 a.u.) of monomers of compound-1 and compound-2 was derived based on its ground state electron density.

4.2.5 Iodine capture based study

4.2.5.1. Vapour phase uptake studies

10 mg of compound-1 and compound-2 were weighed in separate glass vials, and these vials were exposed to molecular iodine for 24 h at 70°C in a closed system. Iodine uptake capacity was calculated using the formula:

$$W = \frac{(m_2 - m_1)}{m_1} \times 100 \% \quad - (1)$$

Where W is the iodine uptake, m_1 and m_2 are the mass of compounds before and after being exposed to iodine vapour. The experiment was repeated five times.

4.2.5.2. Aqueous phase based I_3^- capture studies

The I_3^- solutions were freshly prepared before experiments by mixing an equivalent amount of iodine (I_2) and potassium iodide (KI) in water via sonication.

4.2.5.3. Kinetic studies

For the time-dependent study for I_3^- removal, we took 2.2 mL (0.2 mL of 5 mM I_3^- and 2 mL water) of an aqueous solution of 5 mM freshly prepared I_3^- ion solution in a cuvette. We recorded the initial absorbance value with the help of UV-Vis spectroscopy. Then, 0.5 mg of compound-1 or compound-2 was added to the cuvette. After exposing the compounds, we recorded the absorbance spectra of the supernatant solution at regular time intervals. We calculated the % removal data of I_3^- , decrease in the concentration of the I_3^- vs. time and uptake of I_3^- from this study using the following equations:

$$D_t = \frac{(C_0 - C_t)}{C_0} \times 100\% = \frac{(A_0 - A_t)}{A_0} \times 100\% \quad - (2)$$

$$\frac{C_0 - C_t}{C_0} = \frac{A_0 - A_t}{A_0} \quad - (3)$$

$$C_t = C_0 \times [1 - (A_0 - A_t/A_0)] \quad - (4)$$

$$Q_t = (C_t - C_0) \times \frac{V}{m} \quad - (5)$$

D_t is the exchange capacity, C_0 and A_0 are the initial concentration and absorbance of the I_3^- solution respectively and C_t and A_t are the concentration and absorbance of the I_3^- solution at specific times, respectively. Q_t is the uptake amount in time t in mg/g, V is the volume of the solution in mL, and m is the mass of the compound in g. The kinetics data were fitted to a pseudo-second-order kinetic model using the following equation.

$$Q_t = \frac{(k_2 Q_e^2 t)}{(1 + k_2 Q_e t)} \quad - (6)$$

where t is time in hours, Q_t and Q_e are the adsorption amount at time t and equilibrium, respectively, and K_2 is the pseudo-second-order rate constant.

4.2.5.4. Uptake capacity studies:

1 mg of compound-1 and compound-2 were kept in contact with 2 mL of I_3^- solutions bearing different concentrations (2 to 5 mM solution) for 24 h under stirring conditions. After 24 h, compounds were filtered out, and the filtrate was analyzed by UV-Vis studies. The absorbance was recorded by diluting the solution, and the uptake amount was calculated from the initial and final absorbance value of the filtrate using equations (2),(3), (4), and (5).

The sorption process was analyzed using the Langmuir equation:

$$Q_e = \frac{Q_m C_e}{k_d + C_e} \quad - (7)$$

C_e (mM) and Q_e (mg g^{-1}) represent the I_3^- ion concentration at equilibrium and amount of I_3^- ion adsorbed at equilibrium, respectively. Q_m (mg g^{-1}) is the maximum amount of I_3^- ion per unit mass of adsorbent to form a complete monolayer. K_d (mg/L) is a constant related to the affinity of the binding sites.

4.2.5.5. Titration study for calculation of uptake capacity for iodine

Compound-1: 5 mg compound-1 was dipped in a 10mL aqueous solution containing 16.6 mg KI and 25.4 mg I_2 for 48 h at room temperature. After that, the residual solid was filtered and washed thoroughly with water, MeOH and ethanol and dried in a vacuum. The filtrate was collected and was titrated against 0.05(M) sodium bisulfite solution using 2% aqueous starch solution as an indicator. The resultant solution contains 7.62 mg I_2 as per calculation. Hence I_2 uptake by 5 mg of compound-1 is 17.78 mg. Therefore, the capacity of I_2 uptake by compound-1 in water is 3.55 g g^{-1} .

Compound-2: 5 mg of compound-2 was dipped in a 10mL aqueous solution containing 13.28 mg KI and 20.32 mg I_2 for 48 h at room temperature. After that, the I_2 -loaded phase was filtered and washed thoroughly with water, MeOH and ethanol and dried in vacuum. The filtrate was collected and was titrated against 0.05(M) sodium bisulfite solution using 2% aqueous starch solution as an indicator. The resultant solution contains 5.08 mg I_2 as per calculation. Hence I_2 uptake by 5 mg of compound-2 is 15.24 mg. Therefore, the capacity of I_2 uptake by compound-2 in water is 3.04 g g^{-1} .

4.2.5.6. Selectivity Studies

In this study, 2 mg each of compound 1 and compound-2 were kept in contact separately with a binary solution containing 1 mL of I_3^- solution (5 mM) and 1 mL of competing anion solution (Cl^- , NO_3^- and SO_4^{2-}) (5 mM) for 24 h under stirring conditions. Then, after 24 h, the compounds were filtered, and the filtrate was analyzed by UV-Vis studies using the protocol discussed above. The efficiency of the capture

process in the presence of competing anions was measured with respect to a blank where 1 mL water is used instead of the competing anion solution. The absorbance was recorded by diluting the solution, and the uptake amount was calculated from the initial and final absorbance value of the filtrate using equations (2), (3), (4), and (5). The iodine uptake in presence of mixture of competing ions was also carried using the same protocol. 2 mg each of compound-1 and compound-2 was exposed to a mixture containing 1 ml I_3^- solution (5 mM) and 1 ml of all aforementioned competing ions (5 mM each) for 24 h. The efficiency of the uptake process was compared against a standard system wherein 1 ml of water was used as blank instead of competing ions in the above-mentioned experiment.

4.2.5.7. K_d calculation formula

$$K_d = \left(\frac{C_0 - C_f}{C_f} \right) \times \frac{v}{m} \quad (8)$$

All the distribution coefficient values were collected using the formula mentioned in equation (8). Herein, K_d is the distribution coefficient, C_0 and C_f represents initial and final concentration, respectively. v represents the volume of solution, whereas m is the mass of the sorbent.

4.2.5.8. Reversibility studies

Vapor phase- The compounds were recycled post-iodine capture by treating with methanolic solution of tetrabutylammonium bromide solution. After release of iodine, the solids were utilized as it is to check to retention of uptake capacity for two cycles.

Aqueous medium- For this study, 10 mg of compound-1 and compound 2 were kept separately in contact with 5 mL of I_3^- ion solution (2mM) concentration for 24 h under stirring conditions. After 24h, compounds were filtered out, and the filtrate was analyzed via UV-Vis measurements to calculate the uptake amount using equations (2), (3), (4), and (5). Then the I_3^- loaded phase of 1 and 2 was dipped in tetrabutylammonium bromide solution in water and methanol solvent mixture to release the I_3^- anions and regenerate the parent compound for I_3^- uptake in the next cycle. Such recyclability studies were repeated for four cycles to check the performance of the compounds.

4.2.5.9. Sea water experiment

A stock solution of 5mM I_3^- was prepared using seawater as the matrix. Then 1 mg of compound-1 and compound-2 were separately kept in contact with 2mL of I_3^- ion seawater stock solution for 24 h under stirring conditions. After 24 h, compounds were filtered out, and the filtrate was analysed by UV-Vis

studies. The absorbance was recorded by diluting the solution, and the uptake amount was calculated from the initial and final absorbance value of the filtrate using equations (2),(3),(4), and (5).

4.2.5.10. Conductivity Studies

Electrical Conductivity measurement was carried out for both the parent compound-1 and 2 in pellets in four probe setups. For compound-1 and compound-2, no significant conductivity was observed in the parent phase. After the measurements, both the compounds were exposed to 8mM I_3^- solution under inert condition for 24 h. Then, the iodine exposed phase of compound-1 and compound-2 were washed thoroughly with alcoholic solvents (to get rid of surface adsorbed iodine) and dried in vacuum. After that, the pellets (8 mm diameter) were formed, which were used for four-probe measurements.

4.3 Results and discussion

Compound-1 and compound-2 were synthesized in a round-bottomed flask via quaternization reaction by invoking a reported protocol after slight modifications (Appendix scheme 4.1, 4.2, details in the Experimental section). The unreacted precursors and plausible oligomers were removed by washing with solvents of distinct polarity (Experimental section for more details). The as-obtained solids were examined by solid-state ^{13}C -NMR (CP-MAS) measurements that revealed peaks around 123 ppm and 130 ppm corresponding to the presence of benzene and imidazole rings in both the compounds (Appendix 4.1, 4.2). More importantly, an emergence of a peak around 52 ppm provided evidence regarding the formation of aliphatic methylene linkages crucial for propagating the polymeric network. Further, the air-dried compounds were soaked in low boiling solvents (MeOH, THF) before evacuating under vacuum at ~ 80 °C, which yielded the desolvated phase of compounds, i.e., used as it for further characterizations. Thermogravimetric (TGA) analysis of the as-synthesized compounds showed an initial weight loss (~ 9 %) around ~ 90 °C, which may be due to the loss of occluded solvent molecules, followed by negligible weight loss until ~ 300 °C (Appendix 4.3, 4.4). Field emission scanning electron microscopy (FESEM) showed the presence of particles having spherical morphology, while energy dispersive X-ray (EDX) spectroscopy confirmed the homogeneous distribution of carbon, nitrogen, and bromine in the compounds (Appendix 4.5, 4.6). The average diameter of polymeric microspheres of compound-1 and compound-2 was calculated to be ~ 1.36 μm and ~ 3.16 μm respectively from the particle size distribution analysis (Appendix 4.7, 4.8). Further, fourier transform infrared (FTIR) spectroscopy revealed peaks ~ 1500 cm^{-1} and ~ 1070 cm^{-1} , which corresponds to C=N stretching frequency of imidazole rings and quaternary imidazolium cations, respectively (Appendix 4.9). The peak at ~ 1410 cm^{-1} represents the stretching frequency of the methylene ($-CH_2-$) functionalities present in the polymeric compound. Further, low-

temperature nitrogen measurements N_2 (77 K) revealed very low uptakes of around $48 \text{ cm}^3\text{g}^{-1}$ and $\sim 20 \text{ cm}^3\text{g}^{-1}$ for compound-1 and compound-2, respectively. We speculate that this might be due to the presence of large counter ions (Br^-) within the pores, which can impact the accessible void space, rendering these ionic polymers non-porous (Appendix 4.10, 4.11). This observation is consistent with the literature of porous polymers wherein almost negligible uptake of N_2 was observed due to presence of counter ions that block the pores.^[47]

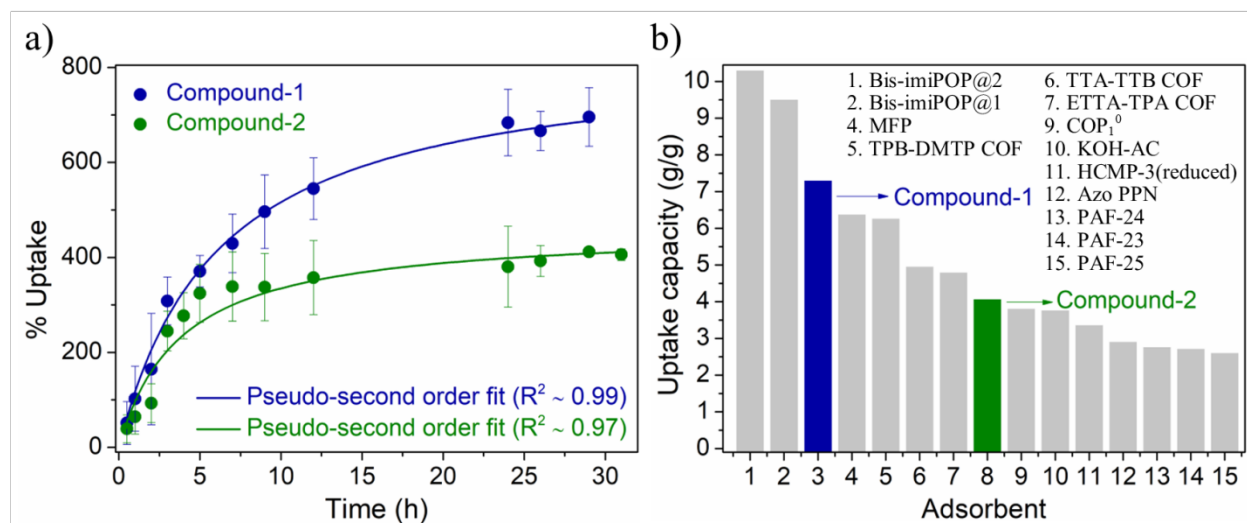


Figure 4.1: (a) Gravimetric uptake for iodine (I_2) vapors at fuel reprocessing temperatures ($\sim 70 \text{ }^\circ\text{C}$, 1 bar). (b) Comparison of maximum uptake capacity for compound-1 and compound-2 with benchmark adsorbents in the field of porous materials (Appendix Table 4.5).

To assess the chemical stability of the compounds, both *i*POPs were dipped in an acidic and basic media of 1(N) HCl and 1(N) NaOH, respectively, for 24 h, and thereafter the residual solids were characterized by TGA, FESEM, and FTIR studies. Post-treatment TGA profiles were found to be analogous to the parent compounds (Appendix 4.12a, 4.13a). Furthermore, FT-IR measurements confirmed retention of all the characteristic peaks compared to desolvated compounds (Appendix 4.12b, 4.13b), while FESEM analysis confirmed the presence of particles with spherical morphology (Appendix 4.14). Moreover, both the compounds showed a negligible loss in their residual weight percentage after soaking in various protic and aprotic solvents for 24 h, thus highlighting the stability of *i*POPs (Appendix 4.15, 4.16). Hereafter, these ionic porous polymers were investigated for their iodine capture behaviour.

To evaluate and quantify iodine uptake behavior of compound-1 and compound-2, these were exposed to iodine vapor at $\sim 70 \text{ }^\circ\text{C}$ for 24 h (nuclear fuel reprocessing conditions) through vial in vial method (Experimental section for more details). Interestingly, we observed an instant colorimetric change in the

color of the compounds from yellowish-white to black, attributed to the occlusion of iodine molecules within the network of the compounds (Appendix 4.17). The iodine uptake (gravimetrically) in the vapor phase was quantified to be $\sim 7 \text{ g g}^{-1}$ and $\sim 4 \text{ g g}^{-1}$ for compound-1 and compound-2, respectively (Figure 4.1). Notably, these experimentally determined uptake values are among the highest in the literature of porous materials (Figure 4.1b, Appendix Table 4.5). Further, the I_2 uptake profile was fit with a pseudo-second-order kinetic model with a correlation coefficient ($R^2 \sim 0.99$) and the rate constants (k_2) were determined to be $2.36 \times 10^{-4} \text{ g g}^{-1} \text{ h}^{-1}$ and $5.27 \times 10^{-4} \text{ g g}^{-1} \text{ h}^{-1}$ for compound-1 and compound-2, respectively. The iodine exposed samples were thoroughly studied by FESEM and EDX analysis, which confirmed the presence of spherical morphology and a homogenous distribution of iodine (Appendix 4.18, 4.19). Intriguingly, TGA analysis of iodine-loaded samples exhibited a drastic weight loss near 200°C , absent in the parent phase and could be assigned to the loss of occluded iodine molecules (Appendix 4.20). Next, we sought to check the affinity of these compounds towards iodine in an aqueous medium. Based on the excellent features exhibited by these *i*POPs, including the presence of cationic network (presence of exchangeable bromide anions), presence of polar sites, and high dispersing tendency in water, we speculated that the I_3^- anions might replace the bromide anions via ion-exchange. To check this hypothesis, compound-1 and compound-2 were exposed to I_3^- solution (formed by mixing equal proportional KI and I_2 in water, Experimental section for more details). An immediate change in the color of the supernatant from an initial dark yellow to almost colorless was noted within few minutes, while the solids turned from yellow to black (Appendix 4.21, 4.22). Additionally, a rapid decrease in the fluorescence intensity of the desolvated phase was observed upon dipping in I_3^- solution for both the compounds (Appendix 4.22, 4.23). These experiments indicate that these compounds can provide prompt, reliable colorimetric as well as fluorometric detection of I_3^- anion in water. Such a fast-responsive sensor for I_3^- holds significance in recognition of radioactive hazards in the real world. Encouraged by this preliminary observation, we probed the performance of these compounds towards I_3^- capture in water by UV-Visible (UV-Vis) spectroscopy. For this, we prepared 0.5 mM I_3^- solution in water and exposed both sorbents to this solution while monitoring characteristic absorbance peaks for I_3^- at 287 nm and 351 nm .^[11] The time-dependent UV-Vis studies demonstrated rapid removal of I_3^- from the supernatant as a fast decline in the intensity of the aforementioned peaks was observed (Figures 4.2a, 4.2b, Appendix Table 4.3, 4.4). Nearly 98 % removal of I_3^- was observed within 5 min by compound-1, while for compound-2 ~ 93 % of I_3^- was sequestered within 10 min (Appendix 4.24, 4.25). Overall, ~ 99 % of I_3^- was removed after 30 min of exposure to both the compounds (Appendix Table 4.3, 4.4). In brief, these compounds exhibit ultrafast kinetics as desired from an efficient sorbent. Further, the capture process followed a pseudo-second-order kinetic model with a correlation coefficient of $R^2 \sim 1$ (Figure 4.2c).

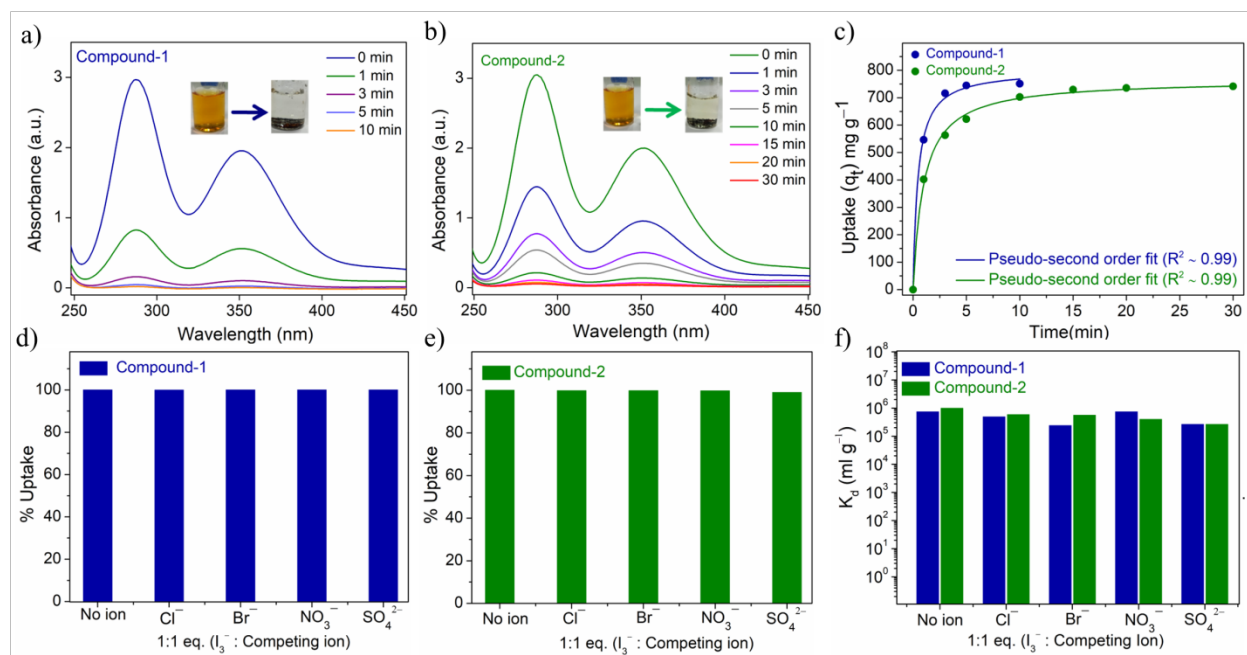


Figure 4.2: (a), (b) UV-Vis plot for I_3^- uptake as a function of time respectively. (c) Pseudo-second order kinetic fitting for I_3^- uptake. (d), (e) Relative uptake for I_3^- anion in a binary mixture of competing anions. (f) Comparative distribution coefficient (K_d) profile for I_3^- uptake in binary mixture of competing ions.

We also analyzed the distribution coefficient (K_d) values corresponding to the I_3^- capture. Typically, the distribution coefficient value is indicative of the affinity of a sorbent material towards sorbate, and a $K_d > 10^3$ mL/g is regarded as exceptional.^[47,48] For both the sorbents, K_d was found in the order of $\sim 10^5$ mL/g, indicative of high affinity for I_3^- anion (Figure 4.2f). We also probed the equilibrium uptake capacities via studying concentration-dependent uptake experiments (Details in experimental section). The corresponding equilibrium uptake capacities as calculated from UV-Vis studies were around 3.5 g g⁻¹ and ~ 3.4 g g⁻¹ for compound-1 and compound-2, respectively (Appendix 4.26). Moreover, these values were consistent with the theoretically determined values (from Langmuir fit) for compound-1 and compound-2, i.e. ~ 3.90 g g⁻¹ and ~ 3.96 g g⁻¹, respectively (Appendix 4.27). We also confirmed the saturation uptake capacity for I_3^- via titration method and found it to be similar, i.e., 3.5 g g⁻¹ for compound-1 and 3.04 g g⁻¹ for compound-2 (Experimental section for more details). To the best of our knowledge, these uptake capacities corresponding to iodine (triiodide) capture in the water represent the benchmark in the field of porous materials (Appendix Table 4.6). This excellent performance may be attributed to the presence of exchangeable bromide anions that impart intrinsic ionic character and the synergy between aromatic rings, nitrogen-rich sites that promote host-guest interactions. Hereafter, the I_3^- loaded phase of the *i*POPs

was collected and characterized via solid-state UV-Visible spectroscopy, which showed the emergence of a broad absorption peak in the visible region along with a peak around 352 nm corresponding to I_3^- anion (Appendix 4.28). Generally, such broad absorption spectra are associated with the formation of charge-transfer complexes.^[49] We speculate that the formation of such a charge-transfer complex between *i*POPs and I_3^- guest anions might be arising on account of ligand molecule's redox-active nature and the presence of highly polarizable I_3^- anions.^[46] Further, FESEM analysis confirmed retention of spherical morphology while EDX spectra showed homogeneous distribution of iodine in the residual solids, also confirmed from elemental mapping results (Appendix 4.29-4.32). Raman spectra of the I_3^- loaded compounds revealed peaks at 112 and 143 cm^{-1} , corresponding to the symmetric and asymmetric stretching frequency of I_3^- anions (Appendix 4.33).^[11]

Further, we probed the selectivity of *i*POPs for I_3^- capture to get an idea regarding the applicability of the solid adsorbent in real-time. Typically, contaminated water contains several counter anions, including chloride (Cl^-), bromide (Br^-), nitrate (NO_3^-), sulphate (SO_4^{2-}), which may cause hindrance in the uptake of I_3^- by *i*POPs.^[43] To check this, the capture of I_3^- was investigated from a binary mixture of anions (equimolar solution of I_3^- and other competing ions viz. Cl^- , Br^- , NO_3^- , and SO_4^{2-}). The experiment revealed >99 % retention in the removal performance for I_3^- by both the compounds (Figure 4.2d, 4.2e). Furthermore, we also calculated K_d for all the binary-competing mixtures, and it was found in the order of $\sim 10^5$ mL/g, comparable to the K_d value for only I_3^- (Figure 4.2f). This data indicates exceptional binding (high affinity) for I_3^- by both the polymers even in the presence of competing ions. We also investigated the performance of the compounds for I_3^- capture in the presence of multiple concurrent anions (Cl^- , Br^- , NO_3^- , and SO_4^{2-}) (details in Experimental section). Both the compounds exhibited similar uptake capacity with complete retention of performance when compared with binary-mixture-based selectivity studies (Appendix 4.34). To further assess the performance of the polymers in real-time conditions, we collected seawater samples from Mumbai, India (ESI). At first, both *i*POPs were soaked in this solution (spiked with iodine), and the residual solids post-filtration were analyzed by FESEM, EDX. FESEM analysis revealed that both *i*POPs maintain their morphological features in seawater samples (Figure 4.3a, Appendix 4.35). EDX and elemental mapping showed a homogenous distribution of iodine in the exposed samples (Figure 4.3b, Appendix 4.35, 4.36). Further, UV-Vis studies of the supernatant unveiled that within 24 h, our materials can capture >95% of I_3^- anion from a 5 mM solution (Figure 4.3c). Moreover, both compounds exhibit an uptake capacity of ~ 3.5 g g^{-1} and ~ 3.4 g g^{-1} for I_3^- , which is exceptional considering the challenging matrix viz. seawater (Figure 4.3d). Additionally, the K_d was calculated in the order of $\sim 10^5$ mL/g, which is unusually high considering the matrix that contains high concentrations of

competing ions and fouling agents (Figure 4.3d). Overall, this data highlights the ability of the *i*POPs to perform in real-world samples.

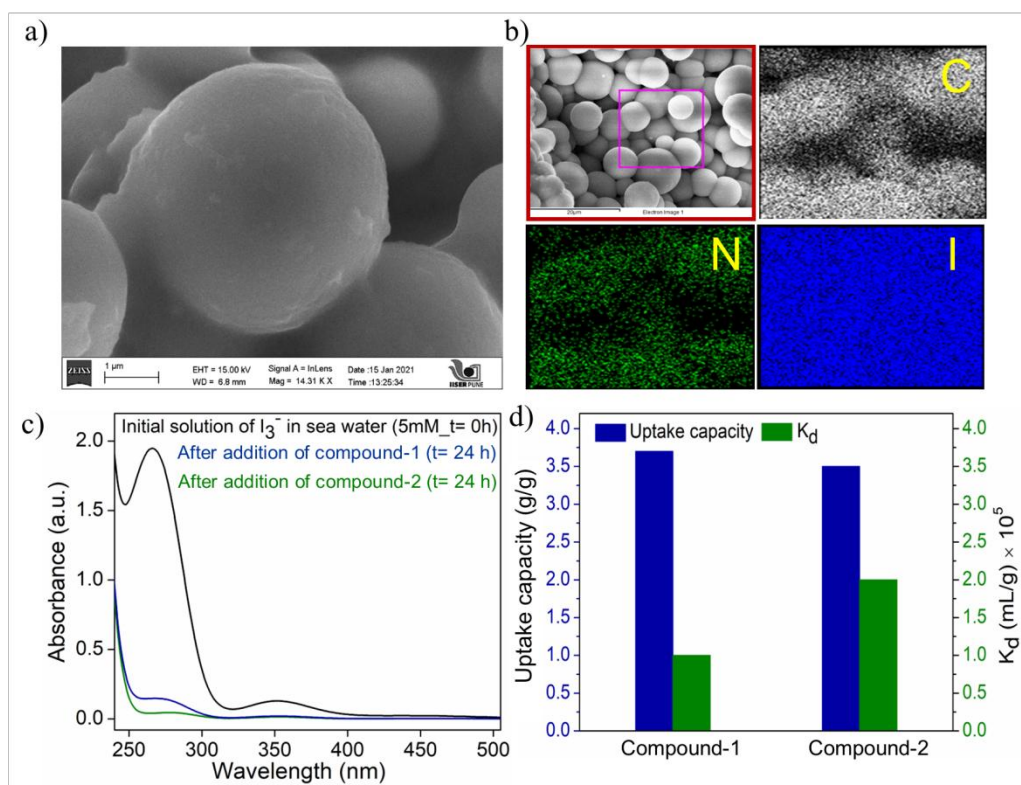


Figure 4.3: (a),(b) FESEM images and elemental mapping profile of compound-2 exposed to iodine spiked seawater sample. (c) UV-Vis spectra of iodine uptake from seawater matrix by both the compounds for 24 h. (d) Bar diagram showing comparative iodine uptake capacity from seawater matrix and corresponding distribution coefficient value (K_d) for both the compounds.

Further, another aspect, i.e., recycling, plays a vital role in increasing the cost-effectiveness of a material. We were successful in achieving rapid desorption of adsorbed I_3^- anion by using an aqueous methanolic solution of tetrabutylammonium bromide for both materials (Appendix 4.37). Also, *i*POPs demonstrated >99% retention in removal performance up to four cycles (Appendix 4.38). We analyzed both compounds post recyclability studies by FESEM, FTIR studies. FESEM analysis showed spherical morphology, while FTIR showed retention of peaks corresponding to various functionality (Appendix 4.39-4.41). Thus, both the compounds display facile recycling and can be utilized for real-time capture of I_3^- from water. Similar results were also obtained for recyclability studies in the case of iodine uptake in the vapor phase with ~80 % retention in performance after three cycles (Appendix 4.42).

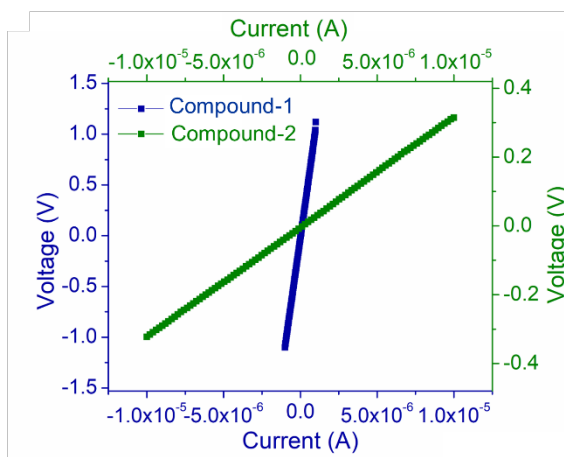


Figure 4.4: Current-Voltage (I-V) plots of ionic porous polymers after iodine loading.

Further, it has been well reported in the literature that loading of I_2 or polyiodide anions in π -electron-rich network can alter the electrical conductivity (σ) properties of the host matrix.^[30,49-51,47] This prompted us to evaluate σ of the iodine-loaded phase of *i*POPs. Four-probe measurements on pelletized samples of both iodine loaded samples of compound-1 and compound-2 yielded bulk σ values $\sim 9.76 \times 10^{-6} \text{ S cm}^{-1}$ and $\sim 2.46 \times 10^{-4} \text{ S cm}^{-1}$ (Figure 4.4). Interestingly, the value for iodine-loaded compound-2 was almost ~ 100 folds higher than σ of molecular iodine in solid-state ($7.69 \times 10^{-6} \text{ S cm}^{-1}$).^[52] The higher σ value for compound-2 post iodine treatment compared to compound-1 may be because of extra nitrogen functionality that is missing in compound-1. Remarkably, the conductivity values of iodine treated compound-2 are among the most promising candidates reported hitherto in the domain of porous organic polymers (Appendix Table 4.7). These compounds indeed display potential in generating exciting electrical properties post waste I_3^- capture.

To gain further insights into experimental findings, theoretical studies invoking the DFT model were conducted on a single monomer polymeric network (to reduce the calculation time) (Figure 4.5). The geometry-optimized structures for energy minimized units of compound-1 and compound-2 with I_2 and I_3^- revealed plausible binding sites (Figure 4.5, Appendix 4.43-4.44). The electrostatic potential (ESP) distribution of the 1 and 2 with I_2 and I_3^- interactions reveal several exciting features. The interaction sites show energy maxima. For compound-1, relative ESP value for I_2 and I_3^- were observed to be 4.57 eV and 3.0 eV, respectively. Whilst for compound-2, relative ESP value for I_2 and I_3^- were observed to be 3.7 eV and 2.8 eV, respectively. Moreover, the interaction of these anions with *i*POPs developed small energy packets within monomers preferable for interaction with other monomer units. The simulation also divulges several key supramolecular non-covalent interactions, including hydrogen-bonding interactions,

van der Waals interaction, which formed the binding interaction sites that afforded stabilization of these analytes (I_2 , I_3^-).

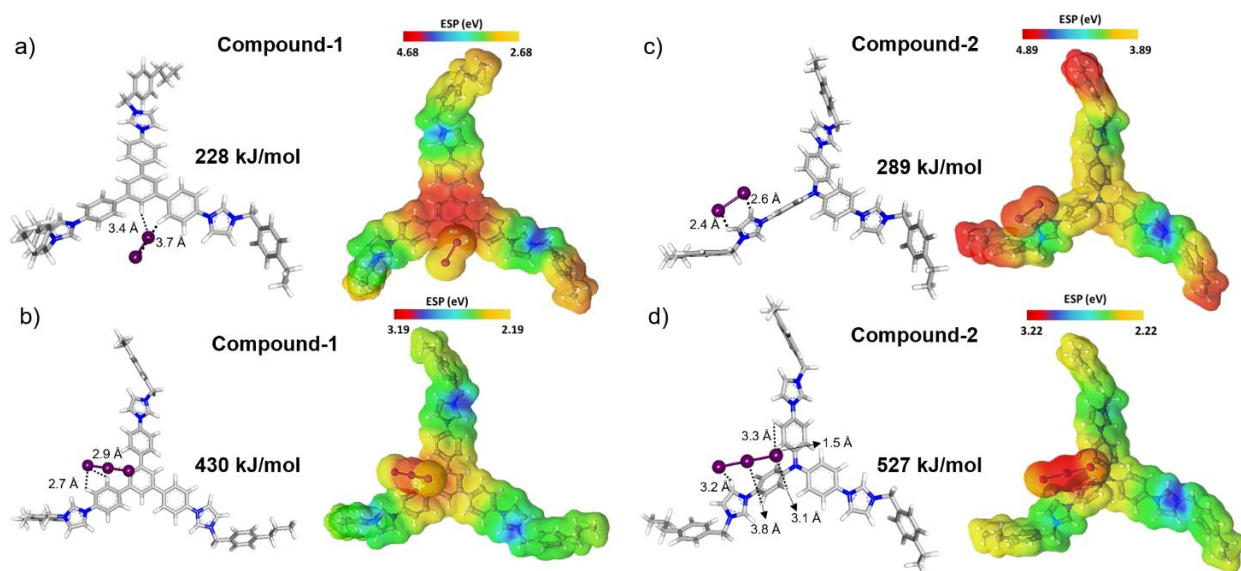


Figure 4.5: DFT studies for iodine loaded phase (Binding energies are in (- kJ/mol): a), c) Minimum binding energy site for I_2 in compound-1 and compound-2, respectively. b), d) Minimum binding energy site for I_3^- for compound-1 and compound-2, respectively.

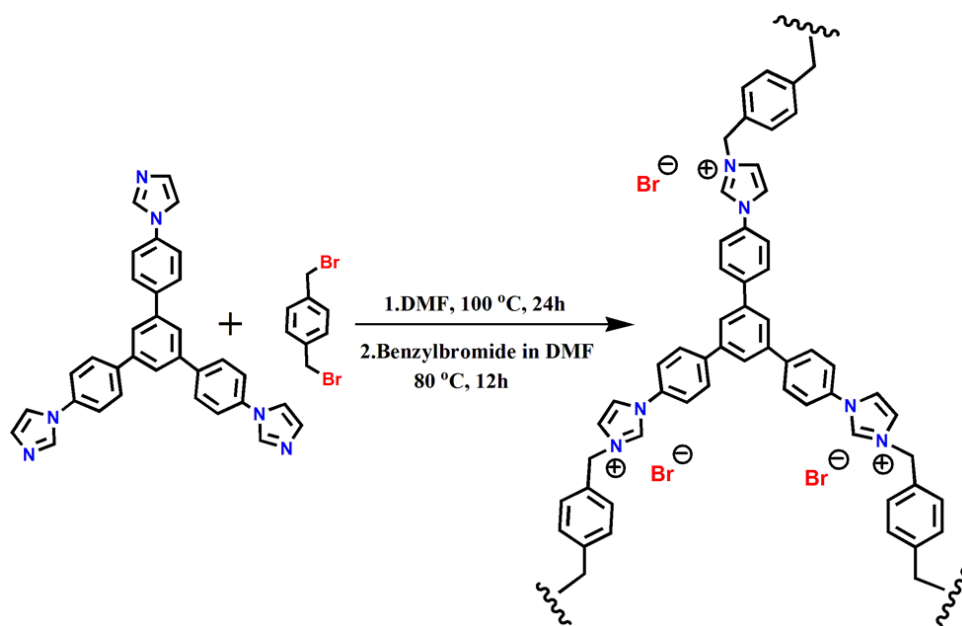
Interestingly, the corresponding binding energies for both I_2 and I_3^- anion within the geometry-optimized unit of compound-1 and 2 were quite exceptional, explaining the unusual affinity and uptake performance (Figure 4.5). Further, we also evaluated the binding energies of 1 and 2 for different competing ions such as Cl^- , NO_3^- , Br^- , SO_4^{2-} (Appendix Table 4.7). Interestingly, the binding energy of *i*POPs was at a relatively higher end for I_3^- anion as compared to other competing ions, thereby substantiating the observed selectivity in experimental observation (in binary mixtures as well as in seawater). Overall, this data endorses our experimental findings and aids our understanding regarding the observed selective and efficient capture performance by compound-1 and compound-2 toward iodine (I_2 and I_3^-).

4.4 Conclusions

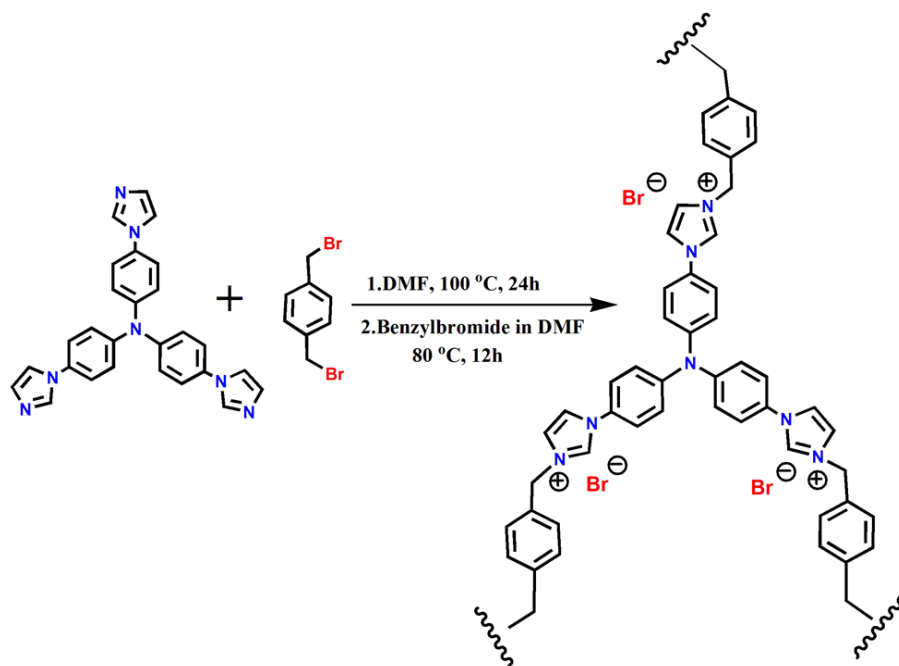
In summary, we have utilized two rationally designed ionic polymers for iodine capture whose compositional features include multiple binding sites (imidazolium cation, phenyl groups, and bromide anions). These features in synergy afforded excellent iodine capture from challenging conditions found during fuel reprocessing and in contaminated seawater. To the best of our knowledge, this is the first porous ionic polymer to be trialed for iodine sequestration from seawater, which represents real-world

conditions. In addition, the polymers display excellent selectivity and facile recyclability, which render them efficient and cost-effective. Further, we also observed an enhancement in the electrical conductivity values post-iodine loading according to reported literature. Fundamentally, our studies highlight the importance of rational design in solid-state materials to achieve multi-functionality, which remains an untapped prospect.

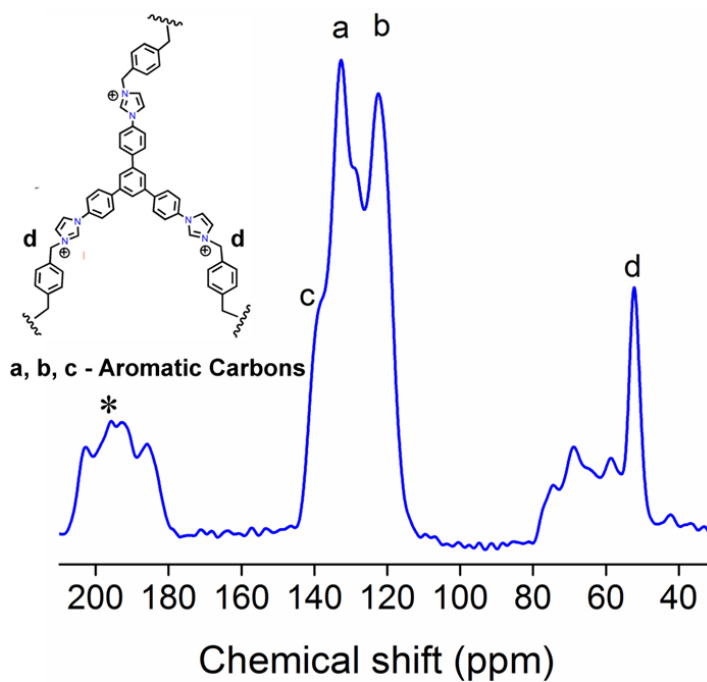
4.5 Appendix section



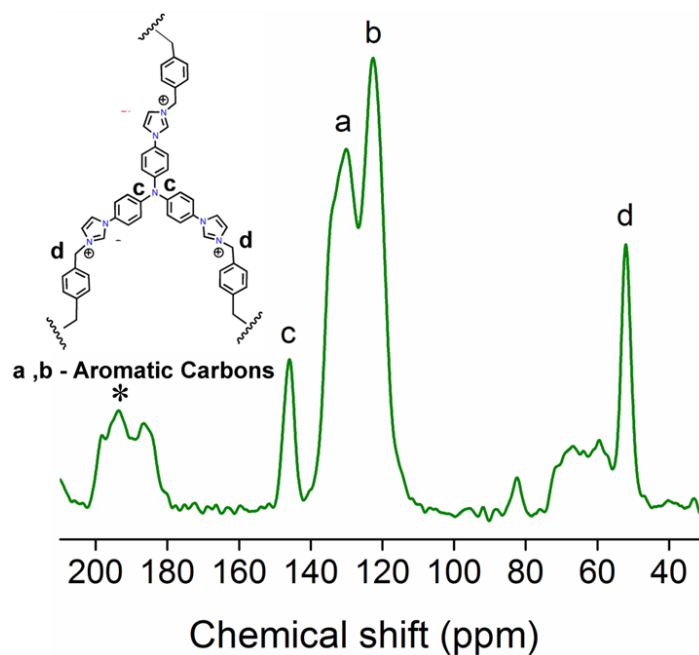
Appendix scheme 4.1. Schematic representation showing synthesis for compound-1.



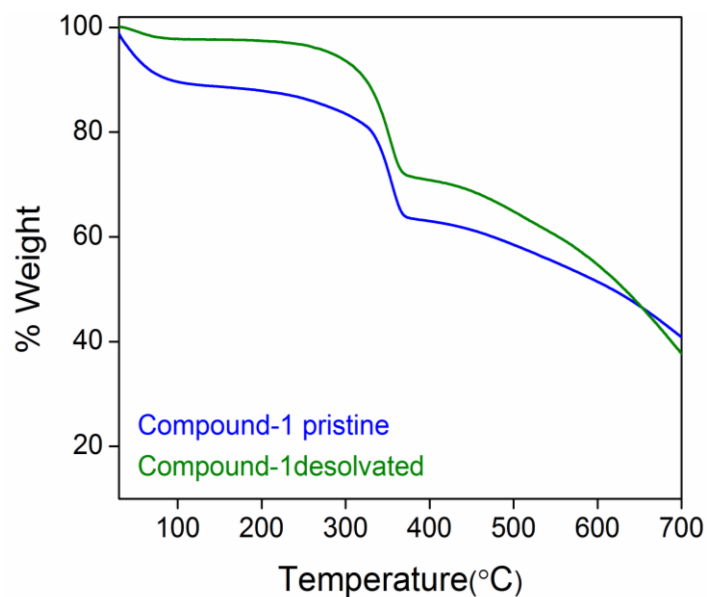
Appendix Scheme 4.2. Schematic representation showing synthesis for compound-2.



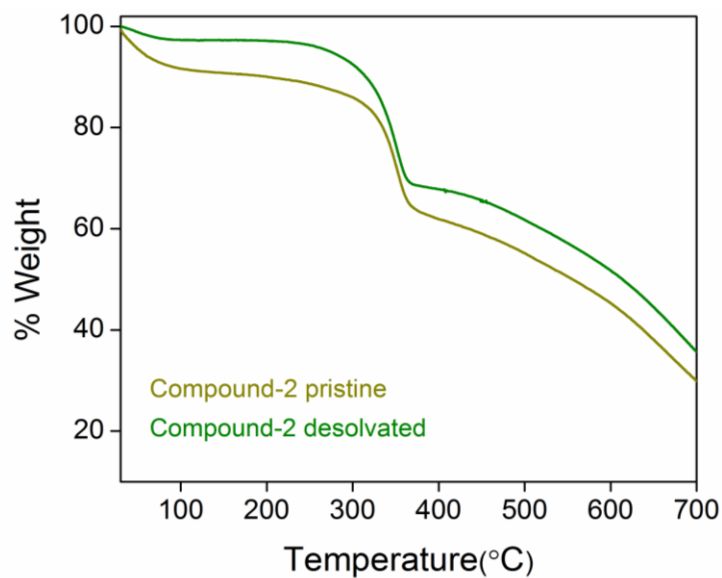
Appendix 4.1. Solid state ^{13}C -NMR of pristine compound-1 (The * peaks indicate side bands).



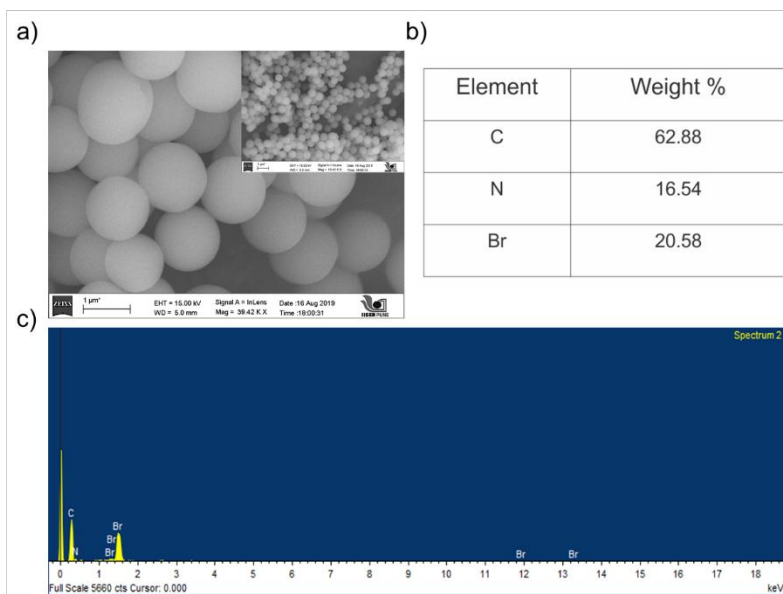
Appendix 4.2. Solid state ^{13}C -NMR of pristine compound-2 (The * peaks indicate side bands).



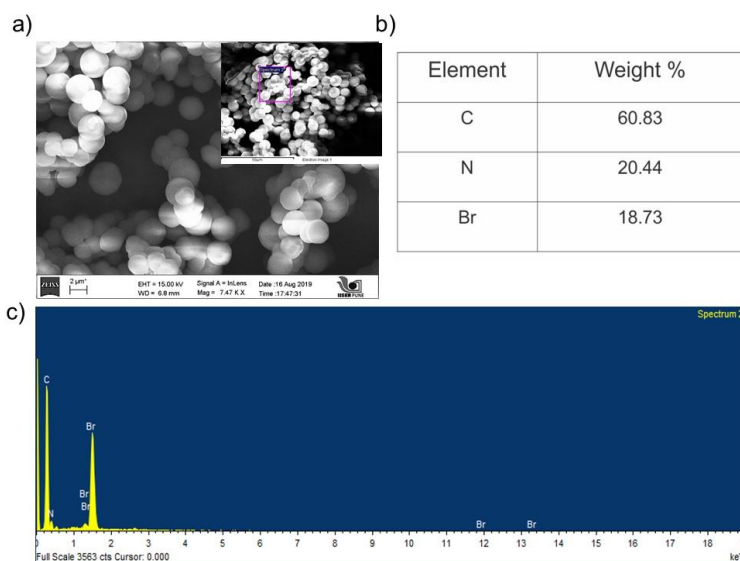
Appendix 4.3. Thermogravimetric analysis (TGA) of pristine and desolvated phase of compound-1.



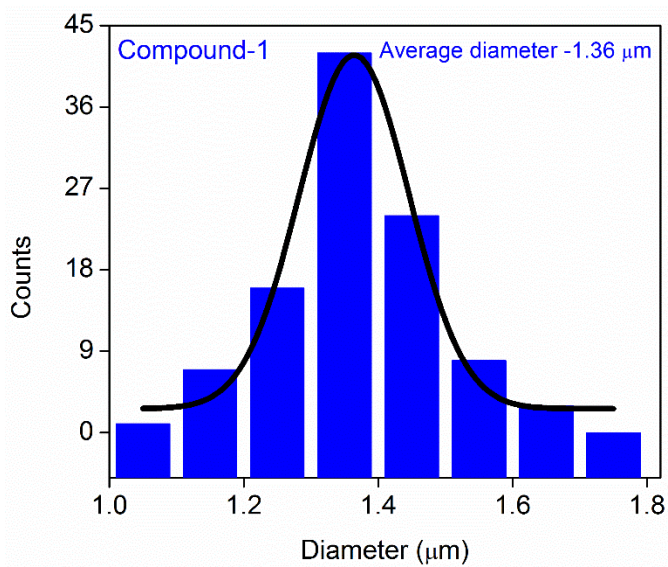
Appendix 4.4. Thermogravimetric analysis (TGA) of pristine and desolvated phase of compound-2.



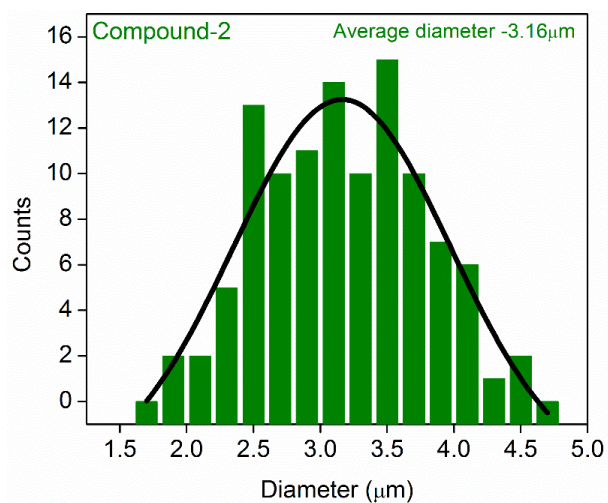
Appendix 4.5. a) FESEM image b) EDS table and c) EDS spectra of compound-1.



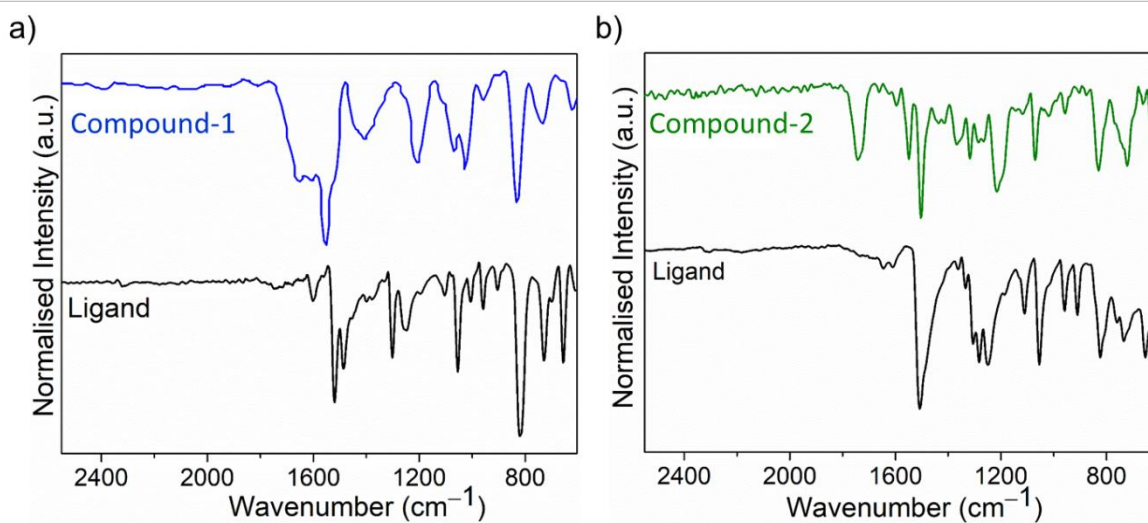
Appendix 4.6. a) FESEM image b) EDS table and c) EDS spectra of compound-2.



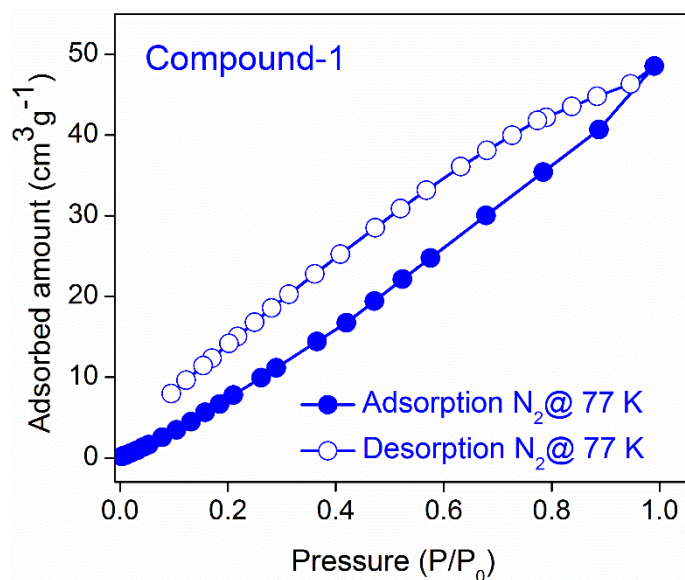
Appendix 4.7. Size distribution plot of compound-1.



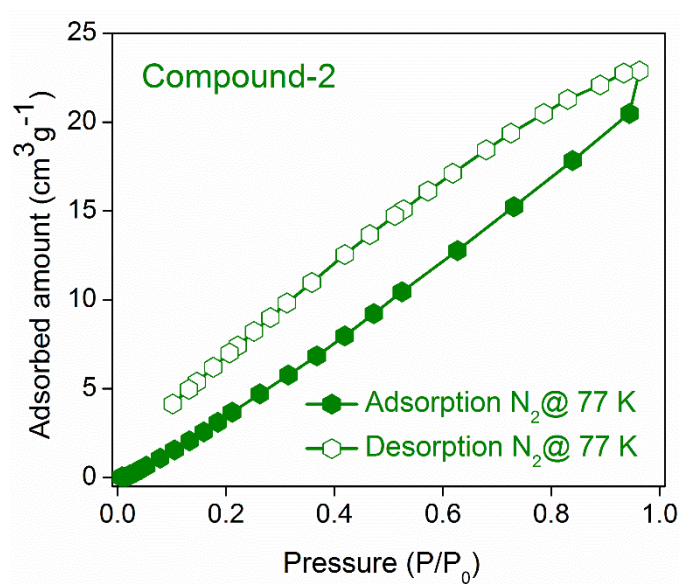
Appendix 4.8. Size distribution plot of compound-2.



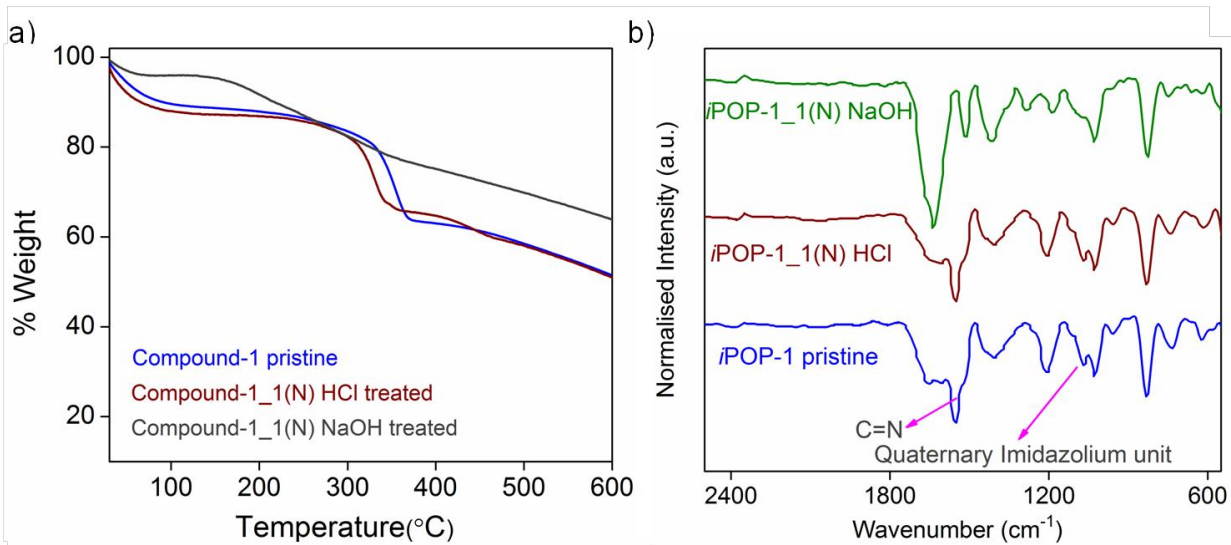
Appendix 4.9. Comparative FTIR spectra of monomeric tripodal linkers with compounds: a) For compound-1 b) For compound-2.



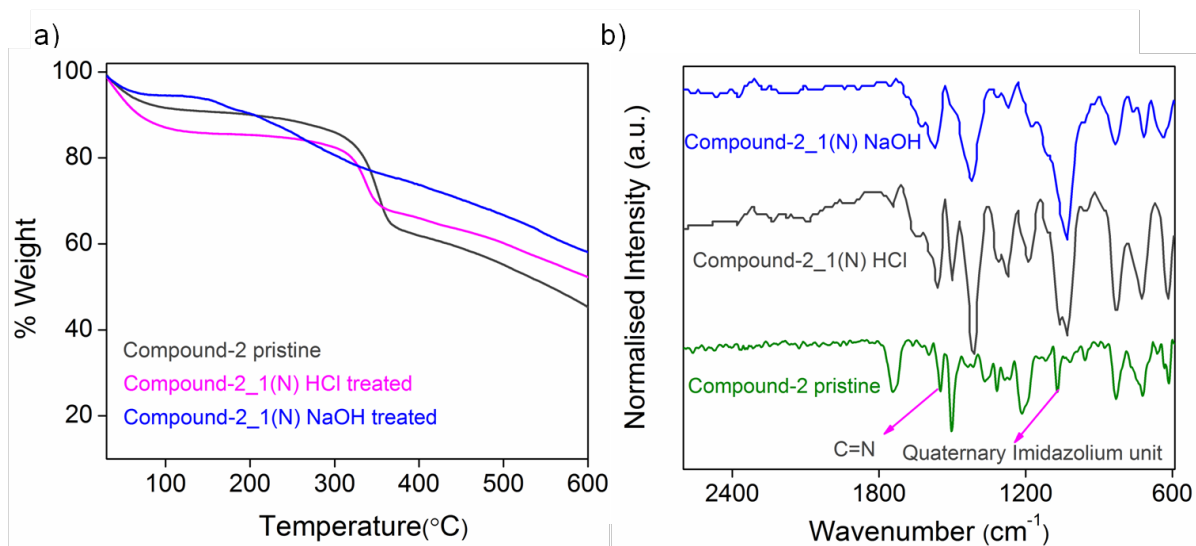
Appendix 4.10. Nitrogen sorption profile of compound-1 at 77 K.



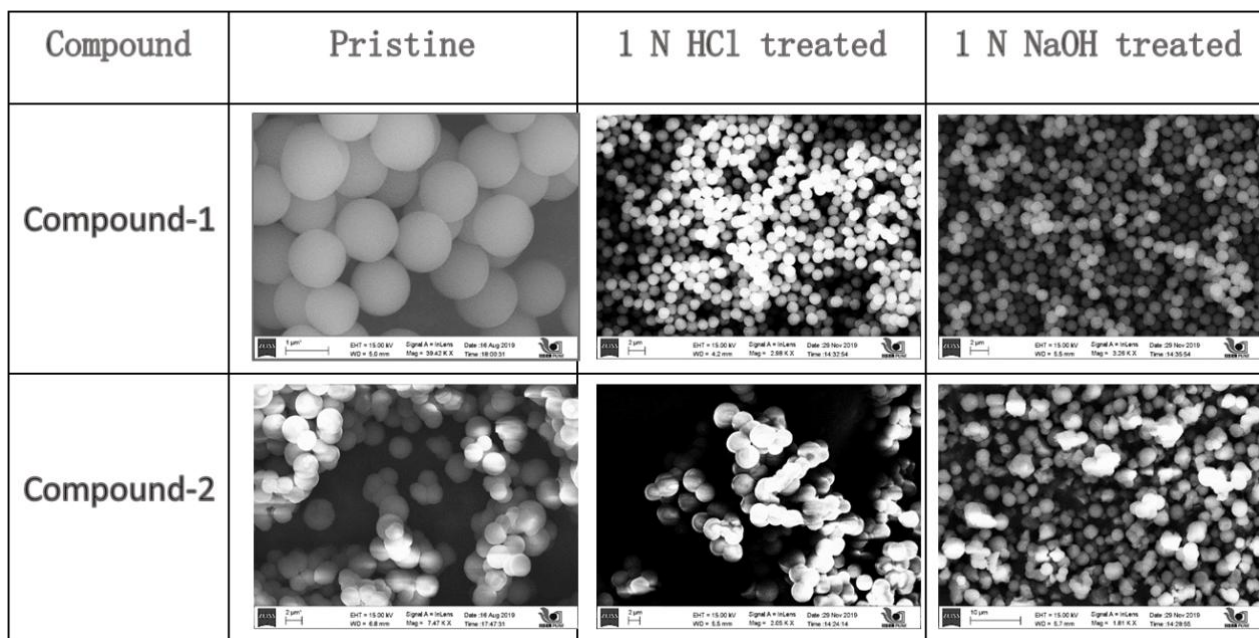
Appendix 4.11. Nitrogen sorption profile of compound-2 at 77 K.



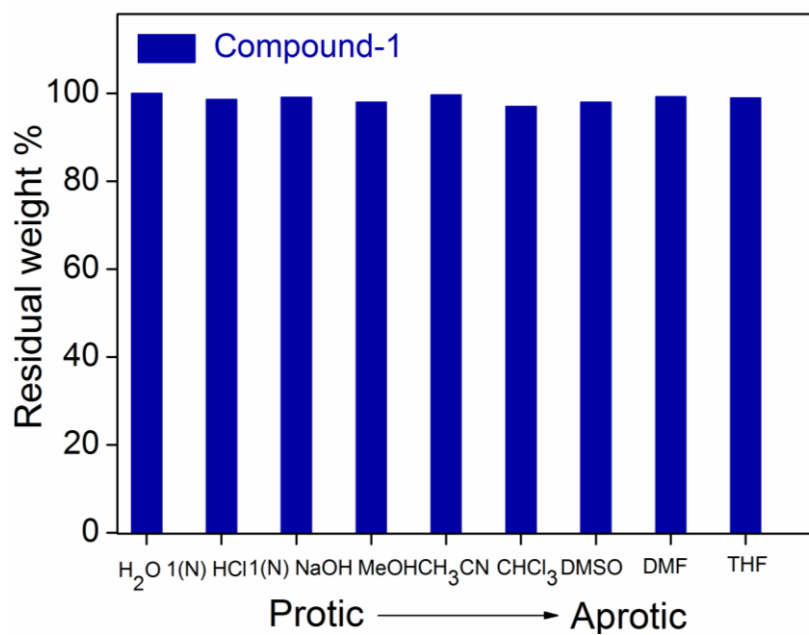
Appendix 4.12. a) Thermogravimetric analysis and b) FTIR spectra of various treated phase of compound-1.



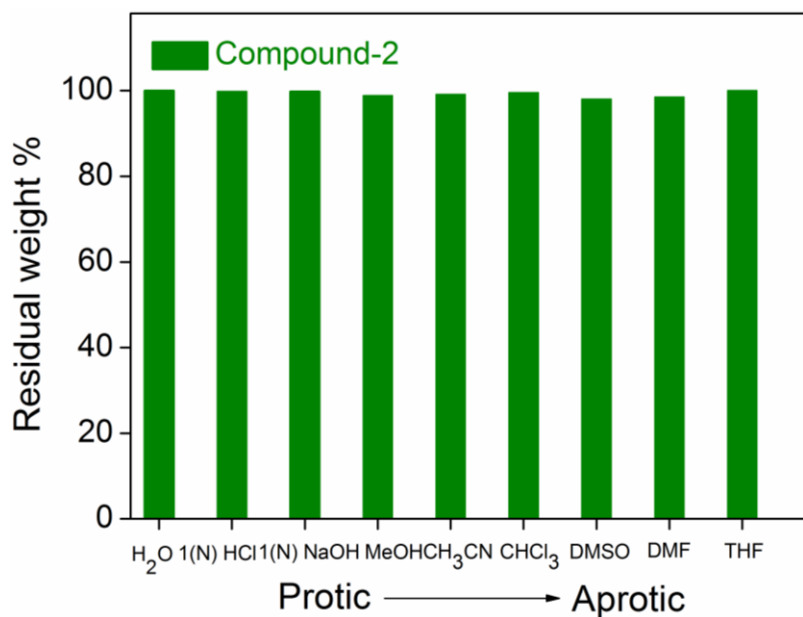
Appendix 4.13. a) Thermogravimetric analysis and b) FTIR spectra of various treated phase of compound-1.



Appendix 4.14. FESEM images of compounds after acid and base treatment.



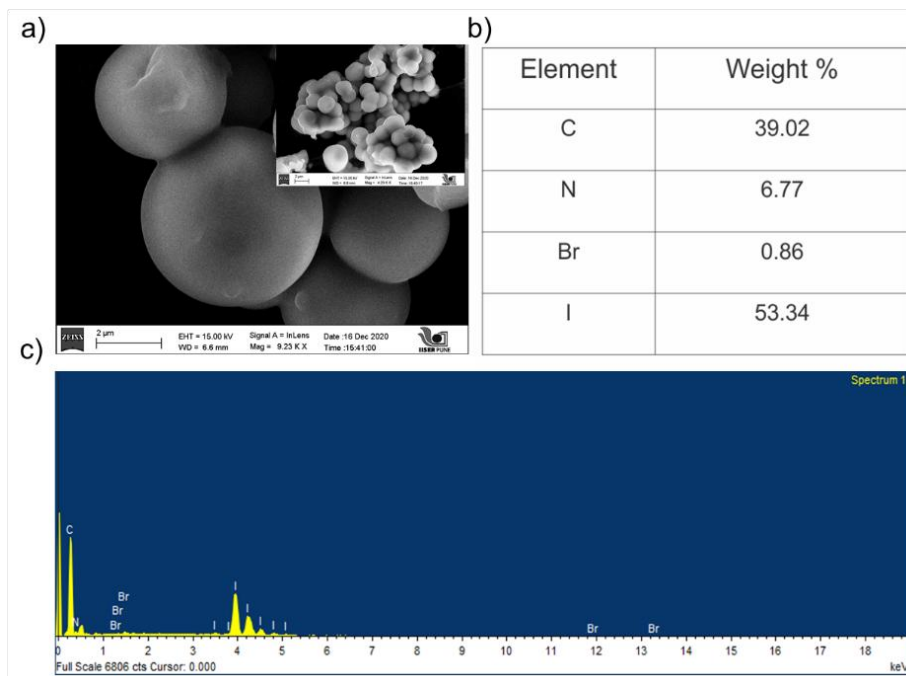
Appendix 4.15. Residual weight percentage plot of compound-1 after exposure to different solvent.



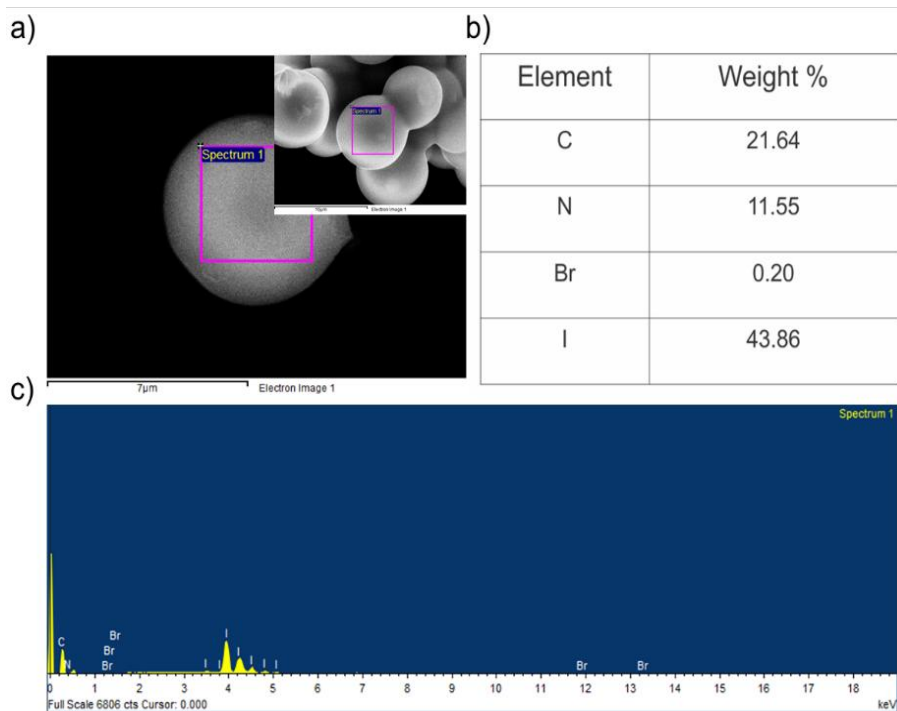
Appendix 4.16. Residual weight percentage plot of compound-2 after exposure to different solvent.

Compound	Pristine	I ₂ exposed (Under ambient light)
Compound-1		
Compound-2		

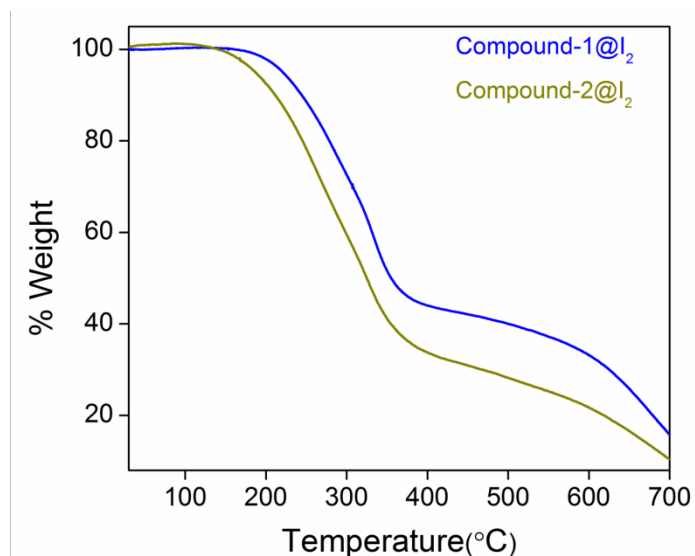
Appendix 4.17. Images of pristine and I₂ adsorbed phase of compounds under ambient conditions.



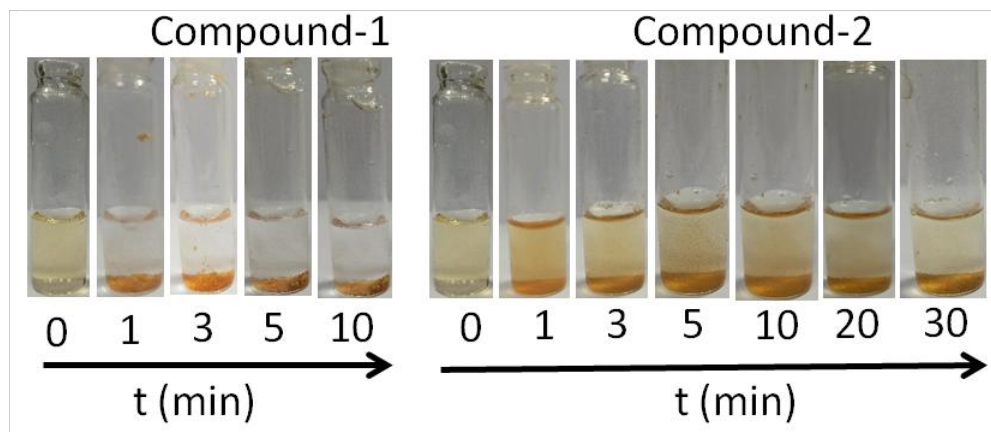
Appendix 4.18. a) FESEM image b) EDS table and c) EDS spectral data of compound-1 after I_2 adsorption.



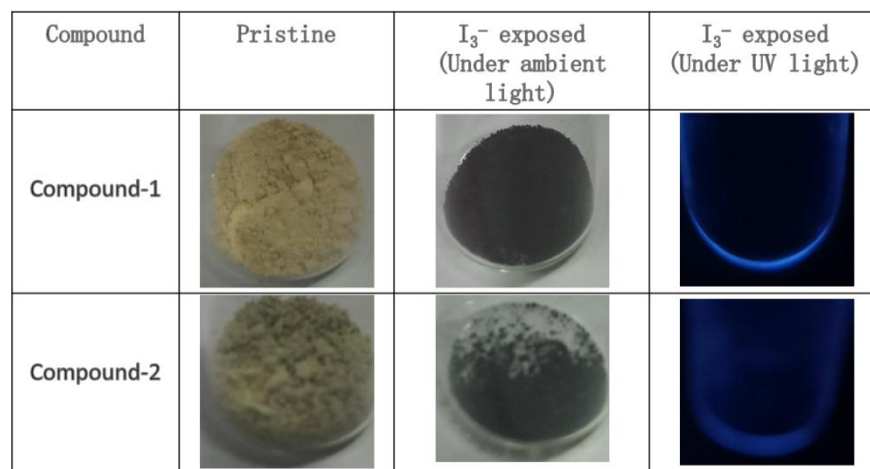
Appendix 4.19. a) FESEM image b) EDS table and c) EDS spectral data of compound-2 after I_2 adsorption.



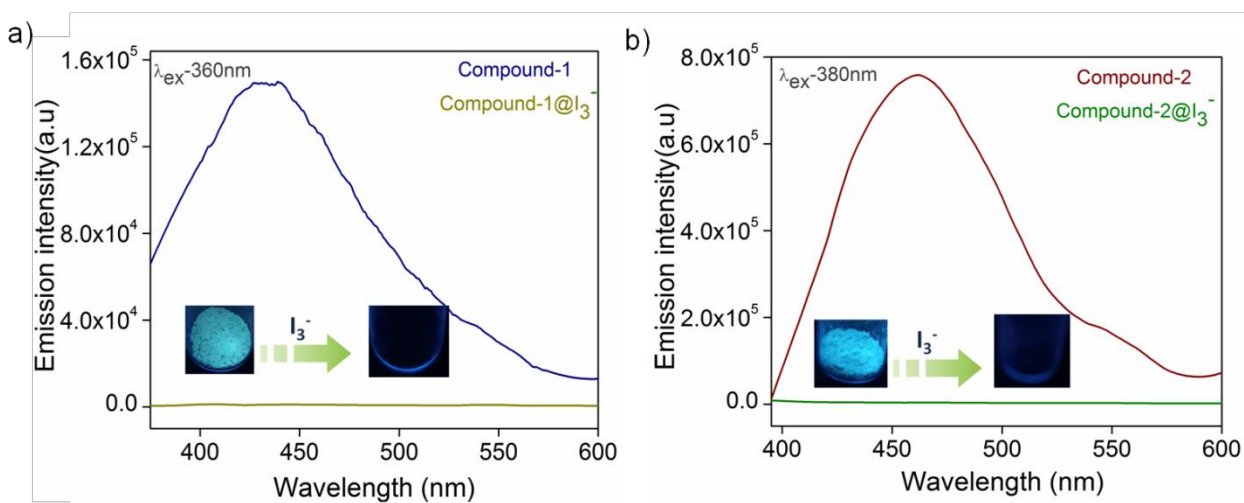
Appendix 4.20. TGA profile of compounds after I₂ adsorption.



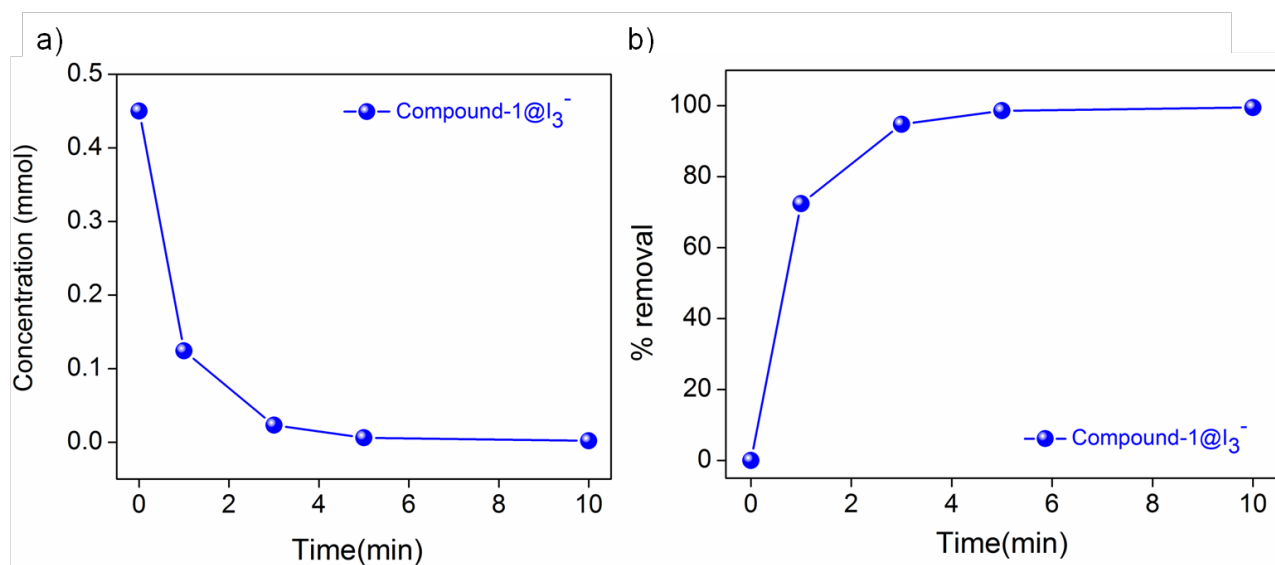
Appendix 4.21. I₃⁻ ambient temperature image showing decrease in concentration of triiodide anion for compound-1 and compound-2.



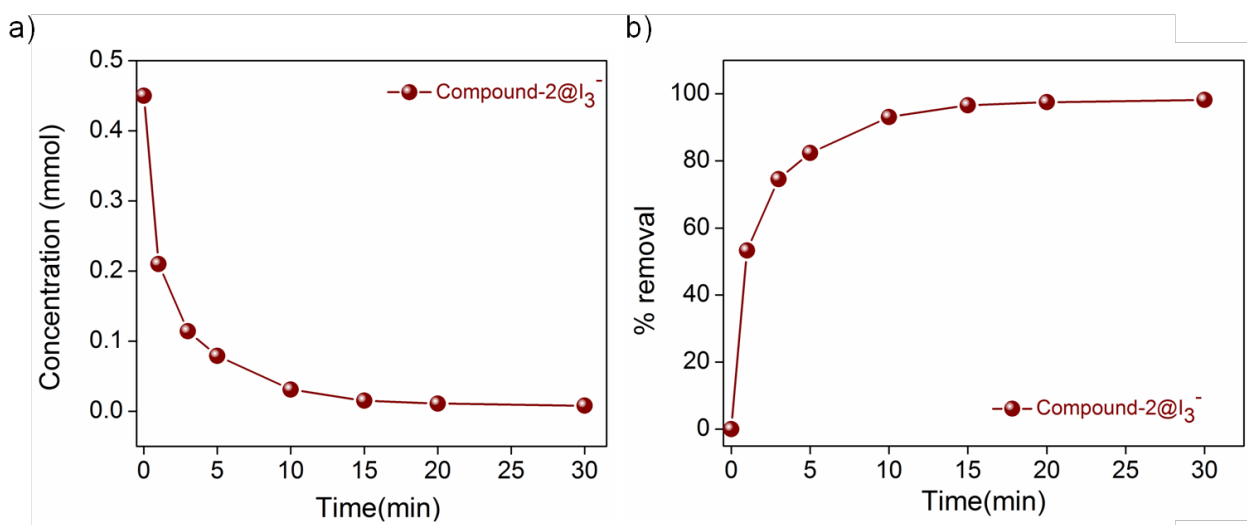
Appendix 4.22. Images of pristine and I₃⁻ adsorbed phase of compounds under ambient conditions and UV-light.



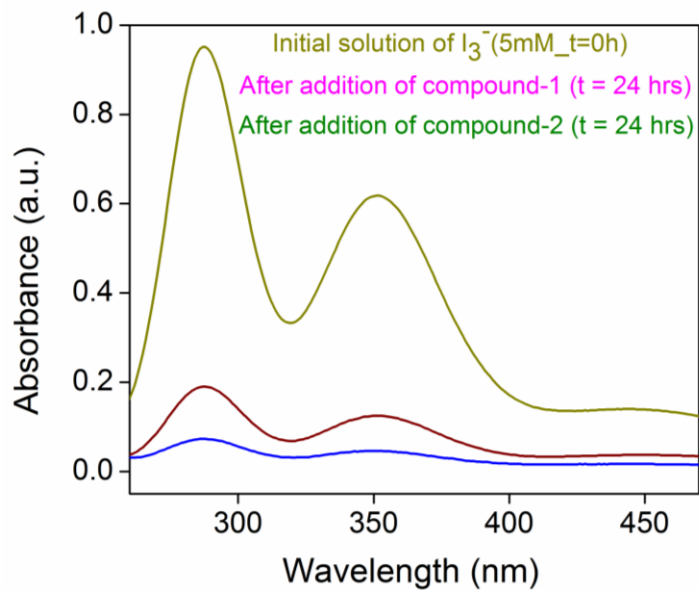
Appendix 4.23. Photoluminescence spectra of compounds pre and post iodine treatment in water. Inset photograph showing quenching of luminescence under UV lamp ($\lambda=365\text{nm}$) for a) compound-1 b) compound-2.



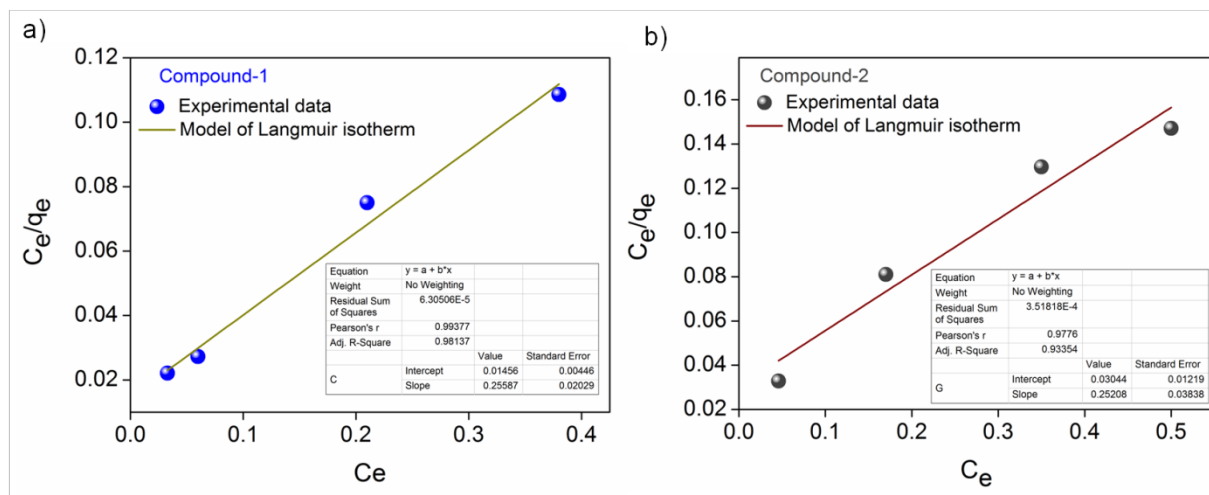
Appendix 4.24. Kinetic profiles of compound-1 for I_3^- capture (a) Concentration of I_3^- as a function of time. (b) % removal plot as a function of time.



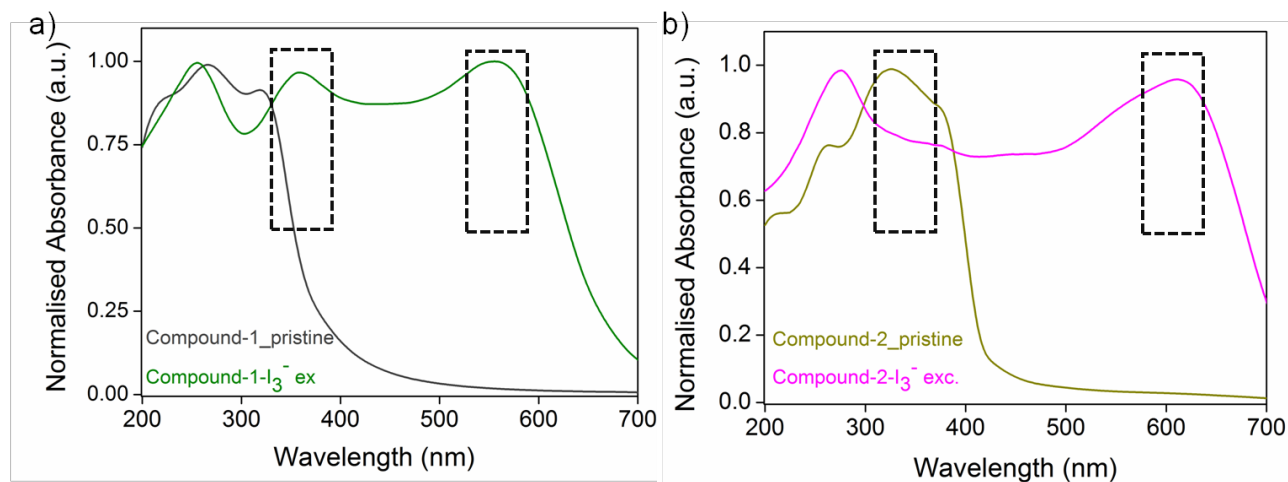
Appendix 4.25. Kinetic profiles of compound-2 for I_3^- capture (a) Concentration of I_3^- as a function of time. (b) % removal plot as a function of time.



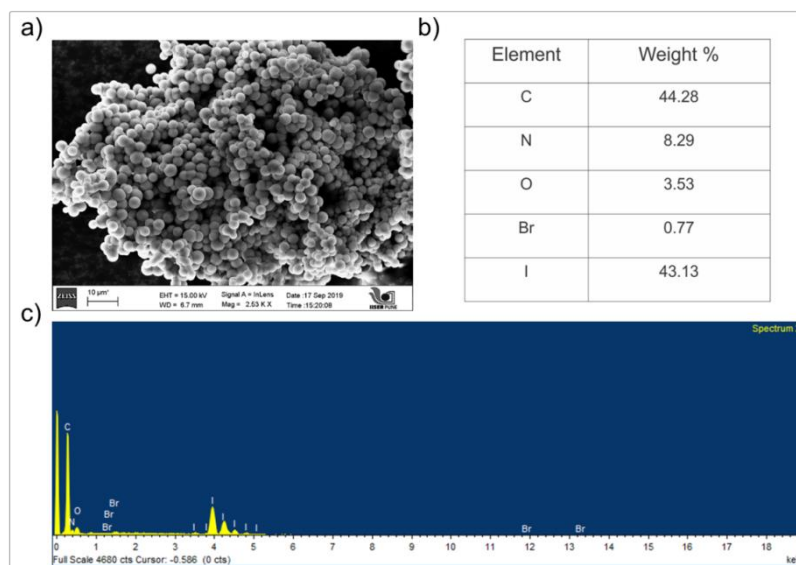
Appendix 4.26. UV-Vis spectra of 5 mM I_3^- solution, and after treatment with the compounds for 24 h (Capacity of compounds for I_3^- ion uptake in water has been calculated from this data and Langmuir model of I_3^- ion capture study).



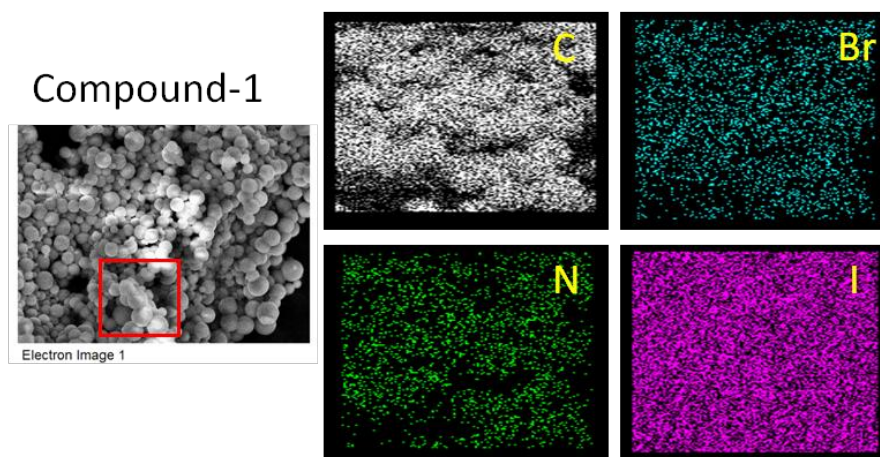
Appendix 4.27: Langmuir model of I_3^- ion capture study for (a) compound-1 and (b) compound-2 respectively.



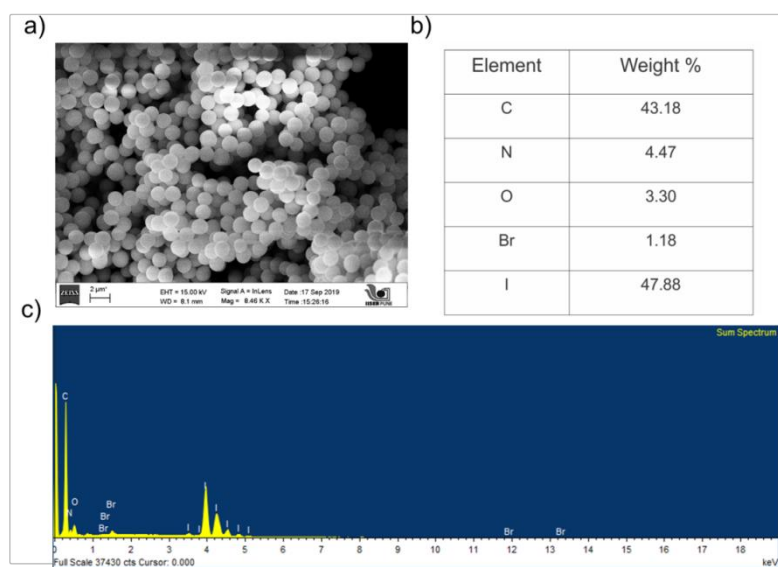
Appendix 4.28. Solid state UV spectra of pristine and I_3^- treated phase of a) compound-1 b) compound-2.



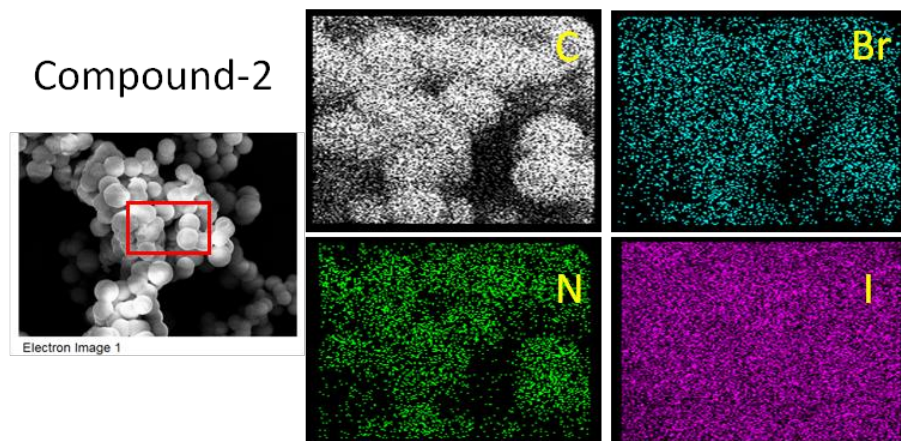
Appendix 4.29. a) FESEM image b) EDS table and c) EDS spectra of iodine treated phase of compound-1 in water.



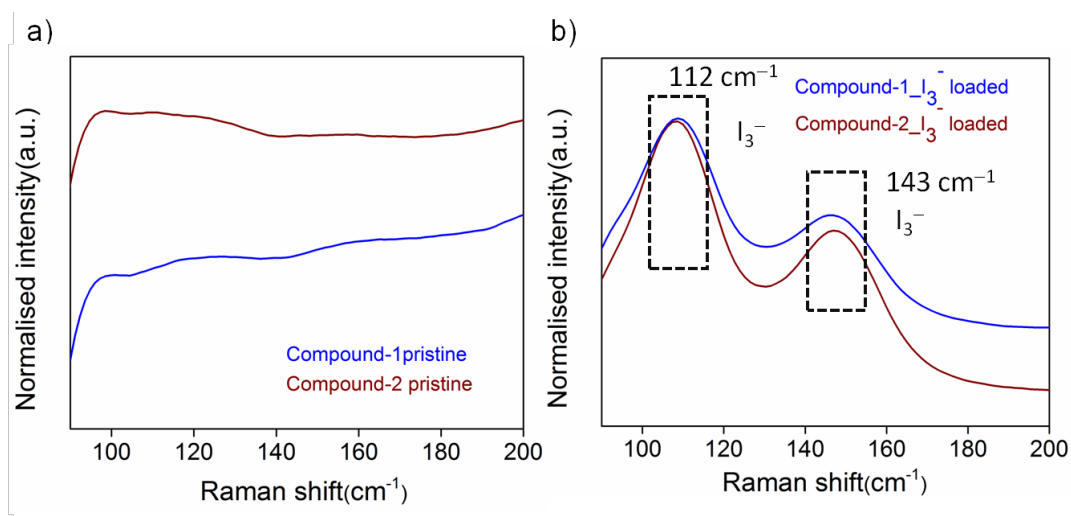
Appendix 4.30. Elemental mapping of iodine treated phase of compound-1 in water.



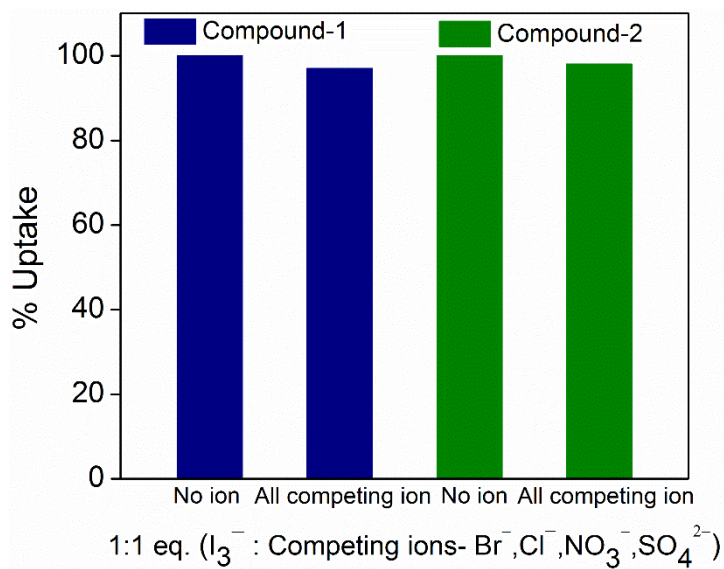
Appendix 4.31. a) FESEM image b) EDS table and c) EDS spectra of iodine treated phase of compound-2 in water.



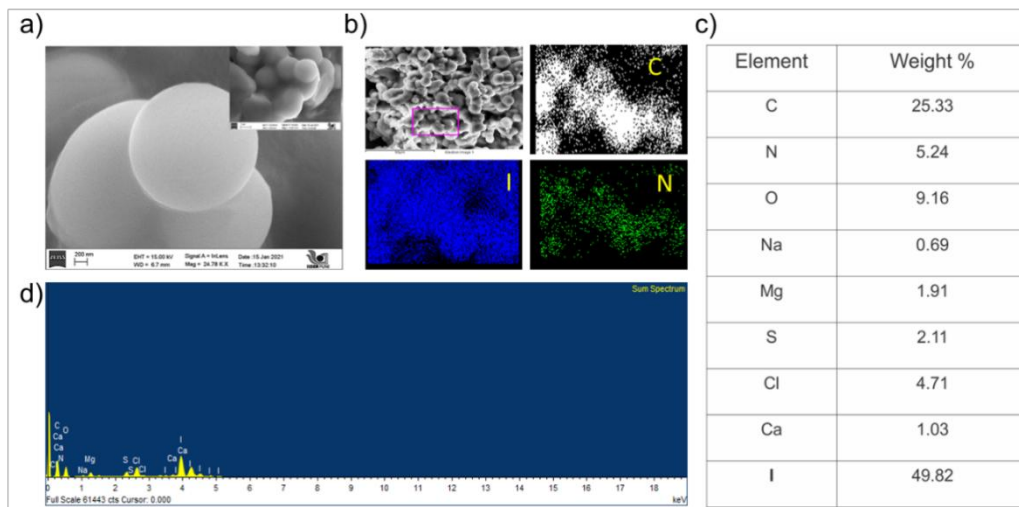
Appendix 4.32. Elemental mapping of iodine treated phase of compound-2 in water.



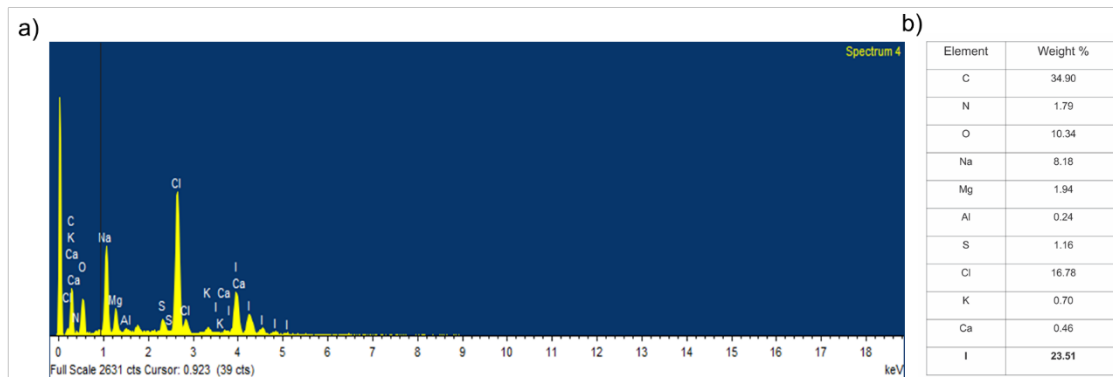
Appendix 4.33. Raman spectra of (a) pristine phase and (b) I_3^- treated phase of compound-1 and compound-2.



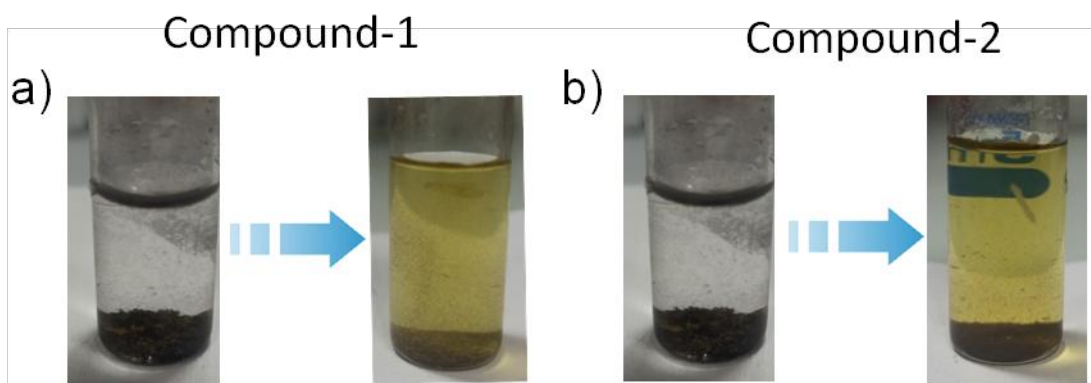
Appendix 4.34. Relative uptake for I_3^- anion in presence of all competing anions for both compound-1 and compound-2.



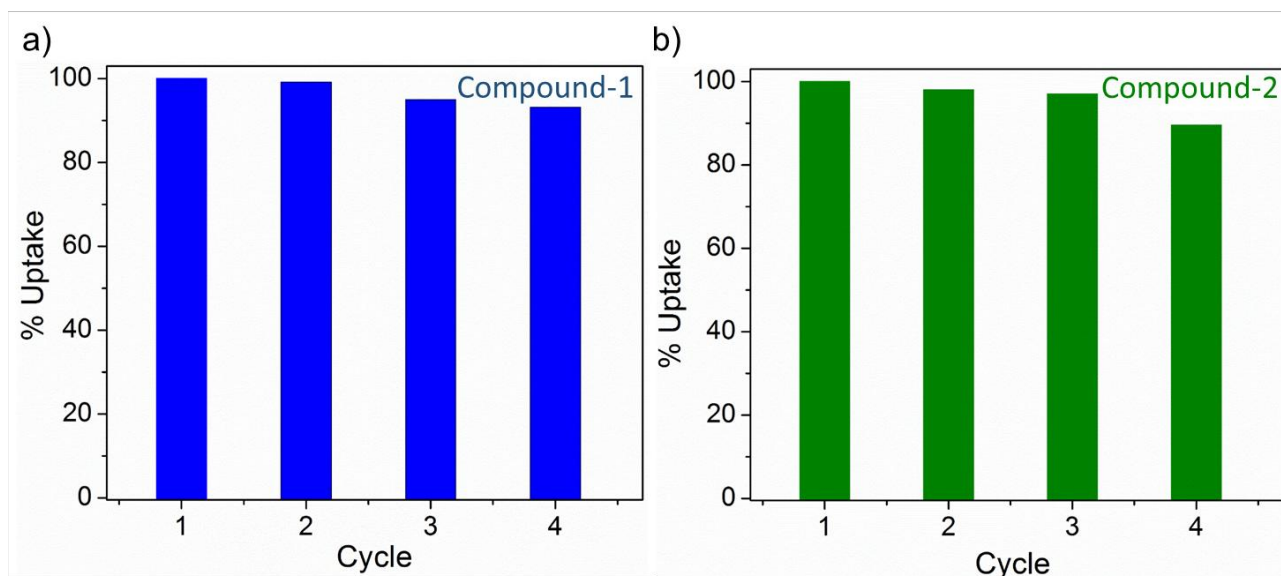
Appendix 4.35. a) FESEM b) elemental mapping profile c) EDS table and d) EDS spectra for compound-1 exposed to iodine spiked seawater samples.



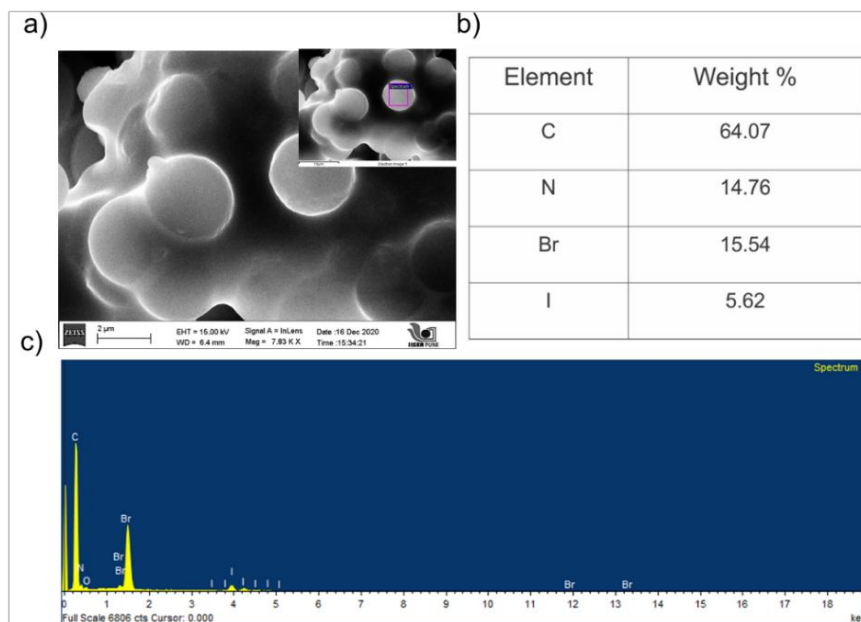
Appendix 4.36. a) EDS profile and b) EDS table for compound-2 exposed to iodine spiked seawater samples.



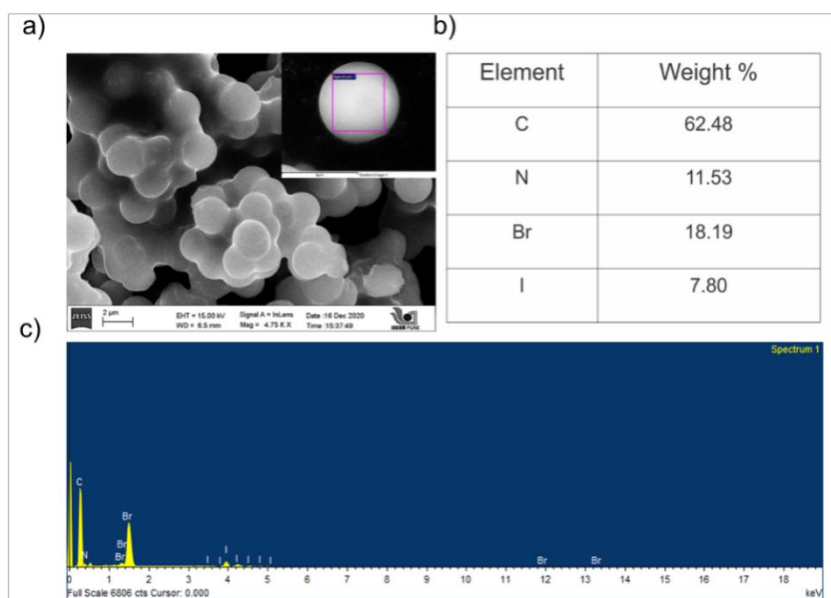
Appendix 4.37. Images showing reversibility w.r.t I_3^- capture in compounds a) compound-1 b) compound-2. (The desorption of I_3^- was achieved by utilizing tetrabutylammonium bromide in methanol).



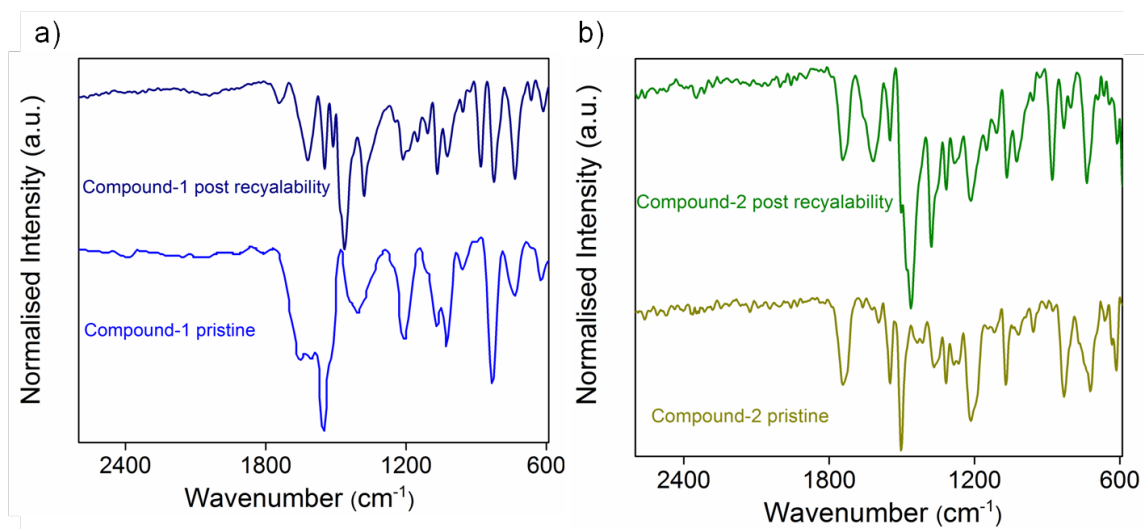
Appendix 4.38. Plot depicting cycling experiment for I_3^- by compounds by using aqueous tetrabutylammoniumbromide-methanol solution a) compound-1 b) compound-2.



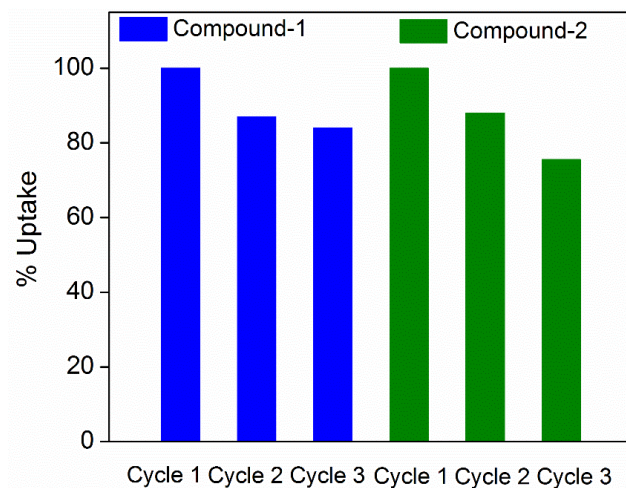
Appendix 4.39. a) FESEM image b) EDS table and c) EDS spectra of compound-1 post recyclability test of I_3^- uptake.



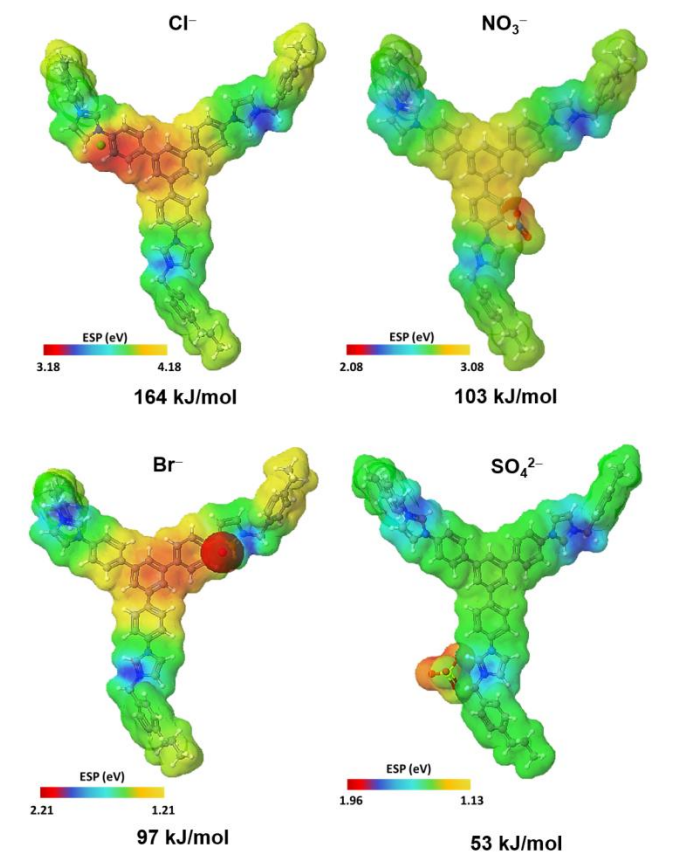
Appendix 4.40. a) FESEM image b) EDS table and c) EDS spectra of compound-2 post recyclability test of I_3^- uptake.



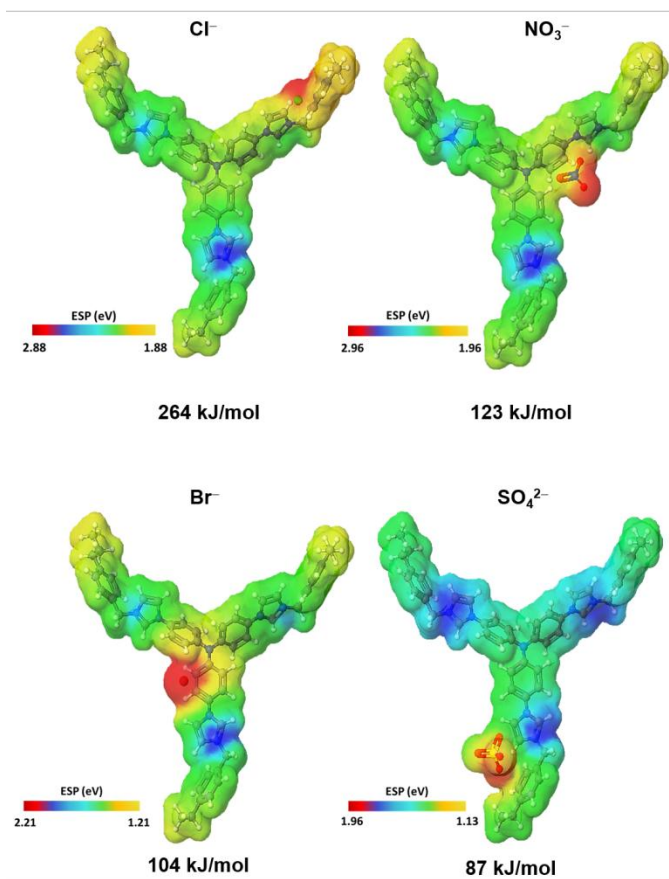
Appendix 4.41. FTIR spectra of compounds post recyclability test of I_3^- uptake; a) For compound-1 b) For compound-2.



Appendix 4.42. : Plot depicting cycling experiment for I_2 vapour by compounds by using aqueous tetrabutylammonium bromide-methanol solution.



Appendix 4.43. ESP diagram and corresponding bonding energies (in – kJ/mol) for competing ions with compound-1.



Appendix 4.36. ESP diagram and corresponding bonding energies (- kJ/mol) for competing ions with compound-2.

Appendix Table 4.1. Elemental analysis data of compounds.

Compound	C/N	C/H
Compound-1	6.62	10.56
Compound-2	4.91	10.70
Compound-1(Iodine treated)	6.55	10.41
Compound-2(Iodine treated)	4.86	9.78

Appendix Table 4.2. Comparison of uptake capacity obtained from theoretical fitting (Langmuir) and experiment (Titration).

I₃⁻ Uptake		
Compound	Theoretical (g/g)	Experimental (g/g)
Compound-1	3.9	3.55
Compound-2	3.96	3.04

Appendix Table 4.3. Sorption kinetics data for I₃⁻ uptake by compound-1 at low concentration.

C₀ (mmol)	Time (min)	C_f (mmol)	% Removal	K_d (mL/g)
0.45	1	0.124	72.4	1.1×10^4
	3	0.023	94.8	8.1×10^4
	5	0.006	98.6	3.2×10^5
	10	0.002	99.5	9.8×10^5

Appendix Table 4.4. Sorption kinetics data for I_3^- uptake by compound-2 at low concentration.

C_0 (mmol)	Time (min)	C_r (mmol)	% Removal	K_d (mL/g)
0.45	1	0.21	53.3	0.5×10^4
	3	0.11	75.5	1.2×10^4
	5	0.07	84.4	2.0×10^4
	10	0.03	93.3	5.9×10^4
	15	0.011	96.6	1.2×10^5
	20	0.015	97.5	1.7×10^5
	30	0.007	98.4	2.4×10^5

Appendix Table 4.5. Comparison of I₂ adsorbents with compound-1 and compound-2.

Adsorbent	Temperature (°C)	I ₂ uptake	Ref	Material
compound-1	70	7.3 g/g	This work	iPOP
compound-2	70	4 g/g	This work	iPOP
Bis-imiPOP@2	77	10.3 g/g	53	POP
Bis-imiPOP@1	77	9.5 g/g	53	POP
MFP	100	6.3 g/g	15	POP
TPB-DMTP COF	75	6.26 g/g	9	COF
TTA-TTB COF	75	4.95 g/g	9	COF
ETTA-TPA COF	75	4.79 g/g	9	COF
COP ₁ ⁰	60	3.8 g/g	54	COP
KOH-AC	77	3.76 g/g	55	Porous Carbon
HCMP-3	85	3.36 g/g	56	CMP
Azo PPN	77	2.9 g/g	57	PPN
PAF-23	75	2.90 g/g	33	PAF
PAF-24	75	2.76 g/g	33	PAF
PAF-25	75	2.71 g/g	33	PAF
Azo-Trip	77	2.38 g/g	58	Azo-linked porous triptycene network
NiMoSchalcogels	60	2.25 g/g	5	Chalcogenide aerogels
Cu-BTC	75	1.75 g/g	59	MOF
PAF-21	75	1.52 g/g	33	PAF
ZIF-8	75	1.20 g/g	60	MOF
HKUST-1	75	0.636 g/g	59	MOF
{[Cu ₆ (pybz) ₈ (OH) ₂] I ₅ ⁻ I ₇ ⁻ } _n	140	0.432 g/g	61	MOF
Macroreticular resins	70	0.250 g/g	62	Resins
AgX-silverexchangedfaujasite	150	0.200-1.000 g/g	62	Solid inorganic adsorbents
AgZ-silverexchanged mordenite	150	0.080-0.200 g/g	62	Solid inorganic adsorbents
AgA-silver impregnated alumina	150	0.100-0.235 g/g	62	Solid inorganic adsorbents
{[Mn ₂ (oxdz) ₂ (tpbn)(H ₂ O) ₂]·C ₂ H ₅ OH} _n	70	213(5) (wt %)	63	MOF

MFM 300(Sc)	80	154 (wt %)	69	MOF
MFM 300 (Fe)	80	129 (wt %)	69	MOF
MFM 300 (In)	80	116 (wt%)	69	MOF
SBMOF-1	-	22.6(2) wt %	70	MOF
SBMOF-2	-	42.7 (2) wt %	70	MOF

Appendix Table 4.6. Comparison of adsorbents exhibiting I_3^- capture from water and I_2 capture in humidity with compounds

Compound	Method	Equilibrium Capacity	Selectivity	Reversibility	Ref.	Material
Compound-1	Ion-exchange	3.5g/g	Cl^-, Br^-, NO_3^-, SO_4^{2-}	Yes	This work	<i>i</i>POP
Compound-2	Ion-exchange	3.04g/g	Cl^-, Br^-, NO_3^-, SO_4^{2-}	Yes	This work	<i>i</i>POP
HcOF-1	Interaction	2.01±0.1 g/g	-	Yes	37	Hydrogen-bonded cross-linked Organic Frameworks (HcOFs)
CaCOP1	Interaction	240 wt%	-	Yes	38	Covalent organic polycalix[4]arenes
CaCOP2	Interaction	281 wt%	-	Yes	38	Covalent organic polycalix[4]arenes
CaCOP3	Interaction	310 wt%	-	Yes	38	Covalent organic polycalix[4]arenes
{[Mn ₂ (oxdz) ₂ (tpbn)(H ₂ O) ₂]·C ₂ H ₅ OH} _n	Interaction	1.1±0.05 g/g	-	Yes	63	MOF
SCNU-Z4	Interaction	331.7 mg/g	-	Yes	64	MOF
CaCOP1	Physical and chemical	2.318 g/g	-	Yes	36	Triazine based

	adsorption					covalent organic polycalix[4]arenes
CalCOP2	Physical and chemical adsorption	1.758 g/g	-	Yes	36	Triazine based covalent organic polycalix[4]arenes
CalCOP3	Physical and chemical adsorption	0.346 g/g	-	Yes	36	Triazine based covalent organic polycalix[4]arenes
CalCOP4	Physical and chemical adsorption	0.156 g/g	-	Yes	36	Triazine based covalent organic polycalix[4]arenes
TNHCP1	Interaction	729 mg/g	-	Yes	65	Triptycene based nitrogen rich HCP
TNHCP2	Interaction	854 mg/g	-	Yes	65	Triptycene based nitrogen rich HCP
TNHCP3	Interaction	819 mg/g	-	Yes	65	Triptycene based nitrogen rich HCP
SBMOF-1	Exposure in 33 % Relative humidity (RH)	15 wt%	-	Yes	71	MOF
SBMOF-2	Exposure in 43 % Relative humidity (RH)	35 wt%	-	Yes	71	MOF

Appendix Table 4.7. Comparison of electrical conductivity (σ) values for conductive porous organic polymers (POPs)

Compound	Conductivity	Ref.
Compound-1_I ₃ ⁻	9.76 x 10 ⁻⁶ S cm ⁻¹	This work
Compound-2_I ₃ ⁻	2.46 x 10 ⁻⁴ S cm ⁻¹	This work

3D ep-POP	$8(1) \times 10^{-10} \text{ S cm}^{-1}$	66
3D p-POP	$5(3) \times 10^{-8} \text{ S cm}^{-1}$	66
I ₂ @3D p-POP	$6(2) \times 10^{-4} \text{ S cm}^{-1}$	66
POP-1	$2.1 \times 10^{-3} \text{ S cm}^{-1}$	67
POP-2	$6.7 \times 10^{-3} \text{ S cm}^{-1}$	67
DTT-CMP	$8 \times 10^{-5} \text{ S cm}^{-1}$	68
DTT-LP _{elec}	$3.1 \times 10^{-4} \text{ S cm}^{-1}$	68
DTT-CMP _{elec}	$1.4 \times 10^{-4} \text{ S cm}^{-1}$	68
DTT-CMP ⁺ I _x ⁻	$3 \times 10^{-2} \text{ S cm}^{-1}$	68
Iodine treated DTT-LP _{elec}	$1.2 \times 10^{-3} \text{ S cm}^{-1}$	68
Iodine treated DTT-CMP _{elec}	$9 \times 10^{-3} \text{ S cm}^{-1}$	68

Appendix Table 4.8. Comparison of binding energies of anions, I₂ and I₃⁻ with compound-1 and compound-2.

Compound	Binding Energies (-KJ/mol)					
	I ₂	I ₃ ⁻	Cl ⁻	Br ⁻	NO ₃ ⁻	SO ₄ ²⁻
Compound-1	228	430	164	97	103	53
Compound-2	289	527	264	104	123	87

4.6 References

- [1] Office of Nuclear Energy, 3 Reasons Why Nuclear is Clean and Sustainable | Department of Energy, <https://www.energy.gov/ne/articles/3-reasons-why-nuclear-clean-and-sustainable>, (accessed 9 January 2021).
- [2] International Atomic Energy Agency, *REFERENCE DATA SERIES No. 1 2015 Edition: Energy, Electricity and Nuclear Power Estimates for the Period up to 2050*, 2015, vol. 37.
- [3] D. F. Sava, M. A. Rodriguez, K. W. Chapman, P. J. Chupas, J. A. Greathouse, P. S. Crozier and T. M. Nenoff, *J. Am. Chem. Soc.*, 2011, **133**, 12398–12401.
- [4] W. Xie, D. Cui, S. R. Zhang, Y. H. Xu and D. L. Jiang, *Mater. Horiz.*, 2019, **6**, 1571–1595.
- [5] K. S. Subrahmanyam, D. Sarma, C. D. Malliakas, K. Polychronopoulou, B. J. Riley, D. A. Pierce, J. Chun and M. G. Kanatzidis, *Chem. Mater.*, 2015, **27**, 2619–2626.
- [6] F. C. Küpper, M. C. Feiters, B. Olofsson, T. Kaiho, S. Yanagida, M. B. Zimmermann, L. J. Carpenter, G. W. Luther, Z. Lu, M. Jonsson and L. Kloo, *Angew. Chem. Int. Ed.*, 2011, **50**, 11598–11620.
- [7] G. Mushkacheva, E. Rabinovich, V. Privalov, S. Povolotskaya, V. Shorokhova, S. Sokolova, V. Turdakova, E. Ryzhova, P. Hall, A. B. Schneider, D. L. Preston and E. Ron, *Radiat. Res.*, 2006, **166**, 715–722.
- [8] X. Guo, Y. Li, M. Zhang, K. Cao, Y. Tian, Y. Qi, S. Li, K. Li, X. Yu and L. Ma, *Angew. Chem. Int. Ed.*, 2020, **59**, 22697–22705.
- [9] P. Wang, Q. Xu, Z. Li, W. Jiang, Q. Jiang and D. Jiang, *Adv. Mat.*, 2018, **30**, 1801991.
- [10] A. Saiz-Lopez, J. M. C. Plane, A. R. Baker, L. J. Carpenter, R. von Glasow, J. C. Gómez Martín, G. McFiggans and R. W. Saunders, *Chem. Rev.*, 2012, **112**, 1773–1804.
- [11] P. H. Svensson and L. Kloo, *Chem. Rev.*, 2003, **103**, 1649–1684.

- [12] K. W. Chapman, P. J. Chupas and T. M. Nenoff, *J. Am. Chem. Soc.*, 2010, **132**, 8897–8899.
- [13] B. Riebe, S. Dultz and C. Bunnenberg, *App. Clay Sci.*, 2005, **28**, 9–16.
- [14] J. Huve, A. Ryzhikov, H. Nouali, V. Lalia, G. Augé and T. J. Daou, *RSC Adv.*, 2018, **8**, 29248–29273.
- [15] J. Wang, Z. Li, Y. Wang, C. Wei, K. Ai and L. Lu, *Mater. Horiz.*, 2019, **6**, 1517–1525.
- [16] J. S. Hoskins, T. Karanfil and S. M. Serkiz, *Environ. Sci. Technol.*, 2002, **36**, 784–789.
- [17] Z. Ji, H. Wang, S. Canossa, S. Wuttke and O. M. Yaghi, *Adv. Func. Mat.*, 2020, **30**, 2000238.
- [18] D. E. Jaramillo, D. A. Reed, H. Z. H. Jiang, J. Oktawiec, M. W. Mara, A. C. Forse, D. J. Lussier, R. A. Murphy, M. Cunningham, V. Colombo, D. K. Shuh, J. A. Reimer and J. R. Long, *Nat. Mater.*, 2020, **19**, 517–521.
- [19] L. S. Xie, G. Skorupskii and M. Dincă, *Chem. Rev.*, 2020, **120**, 8536–8580.
- [20] K. B. Idrees, Z. Chen, X. Zhang, M. R. Mian, R. J. Drout, T. Islamoglu and O. K. Farha, *Chem. Mater.*, 2020, **32**, 3776–3782.
- [21] A. Knebel, A. Bavykina, S. J. Datta, L. Sundermann, L. Garzon-Tovar, Y. Lebedev, S. Durini, R. Ahmad, S. M. Kozlov, G. Shterk, M. Karunakaran, I. D. Carja, D. Simic, I. Weilert, M. Klüppel, U. Giese, L. Cavallo, M. Rueping, M. Eddaoudi, J. Caro and J. Gascon, *Nat. Mater.*, 2020, **19**, 1346–1353.
- [22] J. Hou, M. L. Ríos Gómez, A. Krajnc, A. McCaul, S. Li, A. M. Bumstead, A. F. Sapnik, Z. Deng, R. Lin, P. A. Chater, D. S. Keeble, D. A. Keen, D. Appadoo, B. Chan, V. Chen, G. Mali and T. D. Bennett, *J. Am. Chem. Soc.*, 2020, **142**, 3880–3890.
- [23] Y. Sakata, S. Furukawa, M. Kondo, K. Hirai, N. Horike, Y. Takashima, H. Uehara, N. Louvain, M. Meilikhov, T. Tsuruoka, S. Isoda, W. Kosaka, O. Sakata and S. Kitagawa, *Science (80-.)*, 2013, **339**, 193–196.

- [24] Z. Bin Fang, T. T. Liu, J. Liu, S. Jin, X. P. Wu, X. Q. Gong, K. Wang, Q. Yin, T. F. Liu, R. Cao and H. C. Zhou, *J. Am. Chem. Soc.*, 2020, **142**, 12515–12523.
- [25] S. Sharma, A. V. Desai, B. Joarder and S. K. Ghosh, *Angew. Chem. Int. Ed.*, 2020, **59**, 7788–7792.
- [26] B. Li, X. Dong, H. Wang, D. Ma, K. Tan, S. Jensen, B. J. Deibert, J. Butler, J. Cure, Z. Shi, T. Thonhauser, Y. J. Chabal, Y. Han and J. Li, *Nat. Commun.*, 2017, **8**, 485.
- [27] Z. J. Li, Y. Ju, Y. Ju, B. Yu, X. Wu, H. Lu, Y. Li, J. Zhou, X. Guo, Z. H. Zhang, J. Lin, J. Q. Wang, J. Q. Wang and S. Wang, *Chem. Commun.*, 2020, **56**, 6715–6718.
- [28] J. Li, X. Dai, L. Zhu, C. Xu, D. Zhang, M. A. Silver, P. Li, L. Chen, Y. Li, D. Zuo, H. Zhang, C. Xiao, J. Chen, J. Diwu, O. K. Farha, T. E. Albrecht-Schmitt, Z. Chai and S. Wang, *Nat. Commun.*, 2018, **9**, 3007.
- [29] B. Valizadeh, T. N. Nguyen, B. Smit and K. C. Stylianou, *Adv. Func. Mat.*, 2018, **28**, 1801596.
- [30] Z. Yin, Q. X. Wang and M. H. Zeng, *J. Am. Chem. Soc.*, 2012, **134**, 4857–4863.
- [31] T. Geng, Z. Zhu, W. Zhang and Y. Wang, *J. Mater. Chem. A*, 2017, **5**, 7612–7617.
- [32] K. Jie, Y. Zhou, E. Li, Z. Li, R. Zhao and F. Huang, *J. Am. Chem. Soc.*, 2017, **139**, 15320–15323.
- [33] Z. Yan, Y. Yuan, Y. Tian, D. Zhang and G. Zhu, *Angew. Chem. Int. Ed.*, 2015, **54**, 12733–12737.
- [34] L. He, L. Chen, X. Dong, S. Zhang, M. Zhang, X. Dai, X. Liu, P. Lin, K. Li, C. Chen, T. Pan, F. Ma, J. Chen, M. Yuan, Y. Zhang, L. Chen, R. Zhou, Y. Han, Z. Chai and S. Wang, *Chem*, 2021, **7**, 699–714.
- [35] S. Yao, W.-H. Fang, Y. Sun, S.-T. Wang and J. Zhang, *J. Am. Chem. Soc.*, 2021, **143**, 2325–2330.
- [36] Z. Zhang, L. Li, D. An, H. Li and X. Zhang, *J. Mater. Sci.*, 2020, **55**, 1854–1864.
- [37] Y. Lin, X. Jiang, S. T. Kim, S. B. Alahakoon, X. Hou, Z. Zhang, C. M. Thompson, R. A. Smaldone and C. Ke, *J. Am. Chem. Soc.*, 2017, **139**, 7172–7175.

- [38] D. An, L. Li, Z. Zhang, A. M. Asiri, K. A. Alamry and X. Zhang, *Mater. Chem. Phys.*, 2020, **239**, 122328.
- [39] M. Huang, L. Yang, X. Li and G. Chang, *Chem. Commun.*, 2020, **56**, 1401–1404.
- [40] Y. Tian, J. Song, Y. Zhu, H. Zhao, F. Muhammad, T. Ma, M. Chen and G. Zhu, *Chem. Sci.*, 2019, **10**, 606–613.
- [41] Y. Su, Y. Wang, X. Li, X. Li and R. Wang, *ACS App. Mater. Int.*, 2016, **8**, 18904–18911.
- [42] D. Jung, P. Das, A. Atilgan, P. Li, J. T. Hupp, T. Islamoglu, J. A. Kalow and O. K. Farha, *Chem. Mater.*, 2020, **32**, 9299–9306.
- [43] S. Dutta, P. Samanta, B. Joarder, S. Let, D. Mahato, R. Babarao and S. K. Ghosh, *ACS App. Mater. Int.*, 2020, **12**, 41810–41818.
- [44] Y. Wang, H. Zhao, X. Li and R. Wang, *J. Mater. Chem. A*, 2016, **4**, 12554–12560.
- [45] Q.-H. Hu, W. Jiang, R.-P. Liang, S. Lin and J.-D. Qiu, *Chem. Eng. J.*, 2021, **419**, 129546.
- [46] A. V. Desai, B. Manna, A. Karmakar, A. Sahu and S. K. Ghosh, *Angew. Chem. Int. Ed.*, 2016, **55**, 7811–7815.
- [47] S. Sharma, S. Let, A. V. Desai, S. Dutta, G. Karuppasamy, M. M. Shirolkar, R. Babarao and S. K. Ghosh, *J. Mater. Chem. A*, 2021, **9**, 6499–6507.
- [48] M. J. Manos and M. G. Kanatzidis, *Chem. Sci.*, 2016, **7**, 4804–4824.
- [49] C. Wang, Y. Wang, R. Ge, X. Song, X. Xing, Q. Jiang, H. Lu, C. Hao, X. Guo, Y. Gao and D. Jiang, *Chem. Eur. J.*, 2018, **24**, 585–589.
- [50] E. Jin, M. Asada, Q. Xu, S. Dalapati, M. A. Addicoat, M. A. Brady, H. Xu, T. Nakamura, T. Heine, Q. Chen and D. Jiang, *Science*, 2017, **357**, 673–676.

- [51] T. Ben, K. Shi, Y. Cui, C. Pei, Y. Zuo, H. Guo, D. Zhang, J. Xu, F. Deng, Z. Tian and S. Qiu, *J. Mater. Chem.*, 2011, **21**, 18208–18214.
- [52] M. H. Zeng, Q. X. Wang, Y. X. Tan, S. Hu, H. X. Zhao, L. S. Long and M. Kurmoo, *J. Am. Chem. Soc.*, 2010, **132**, 2561–2563.
- [53] T. H. Niu, C. C. Feng, C. Yao, W. Y. Yang and Y. H. Xu, *ACS Appl. Poly. Mat.*, 2021, **3**, 354–361.
- [54] G. Das, T. Prakasam, S. Nuryyeva, D. S. Han, A. Abdel-Wahab, J. C. Olsen, K. Polychronopoulou, C. Platas-Iglesias, F. Ravaux, M. Jouiad and A. Trabolsi, *J. Mater. Chem. A*, 2016, **4**, 15361–15369.
- [55] H. Sun, P. La, Z. Zhu, W. Liang, B. Yang and A. Li, *J. Mater. Sci.*, 2015, **50**, 7326–7332.
- [56] Y. Liao, J. Weber, B. M. Mills, Z. Ren and C. F. J. Faul, *Macromolecules*, 2016, **49**, 6322–6333.
- [57] H. Li, X. Ding and B. H. Han, *Chem. Eur. J.*, 2016, **22**, 11863–11868.
- [58] Q. Q. Dang, X. M. Wang, Y. F. Zhan and X. M. Zhang, *Poly. Chem.*, 2016, **7**, 643–647.
- [59] D. F. Sava, K. W. Chapman, M. A. Rodriguez, J. A. Greathouse, P. S. Crozier, H. Zhao, P. J. Chupas and T. M. Nenoff, *Chem. Mater.*, 2013, **25**, 2591–2596.
- [60] D. F. Sava, T. J. Garino and T. M. Nenoff, *Ind. Eng. Chem. Res.*, 2012, **51**, 614–620.
- [61] Z. Yin, Q. X. Wang and M. H. Zeng, *J. Am. Chem. Soc.*, 2012, **134**, 4857–4863.
- [62] D. Haefner and T. Tranter, *Idaho Natl. Lab.*, , DOI:10.2172/911962.
- [63] A. Gogia, P. Das and S. K. Mandal, *ACS App. Mater. Int.*, 2020, **12**, 46107–46118.
- [64] G. Wang, J.-F. Huang, X. Huang, S. Deng, S. Zheng, S.-L. Cai, J. Fan and W.-G. Zhang, *Inorg. Chem. Front.*, 2021, **8**, 1083–1092.
- [65] A. Hassan, S. Goswami, A. Alam, R. Bera and N. Das, *Sep. Purif. Tech.*, 2021, **257**, 117923.

- [66] Y. Byun, L. S. Xie, P. Fritz, T. Ashirov, M. Dincă and A. Coskun, *Angew. Chem. Int. Ed.*, 2020, **59**, 15166–15170.
- [67] T. Li, W. Zhu, R. Shen, H. Y. Wang, W. Chen, S. J. Hao, Y. Li, Z. G. Gu and Z. Li, *New J. Chem.*, 2018, **42**, 6247–6255.
- [68] H. Bildirir, I. Oskan, T. Ozturk and A. Thomas, *Chem. Eur. J.*, 2015, **21**, 9306–9311.
- [69] X. Zhang, I. Silva, H. G. W. Godfrey, S. K. Callear, S. A. Sapchenko, Y. Cheng, I. Vitórica-Yrezábal, M. D. Frogley, G. Cinque, C. C. Tang, C. Giacobbe, C. Dejoie, S. Rudić, A. J. Ramirez-Cuesta, M. A. Denecke, S. Yang, and M. Schröder, *J. Am. Chem. Soc.*, 2017, **139**, 16289.
- [70] D. Banerjee, X. Chen, S. S. Lobanov, A. M. Plonka, X. Chan, J. A. Daly, T. Kim, P. K. Thallapally, and J. B. Parise, *ACS Appl. Mater. Interfaces*, 2018, **10**, 10622.

Chapter 5

**Imidazolium functionalized chemically
robust ionic porous organic polymers
(*i*POPs) toward toxic oxo-pollutants
capture from water**

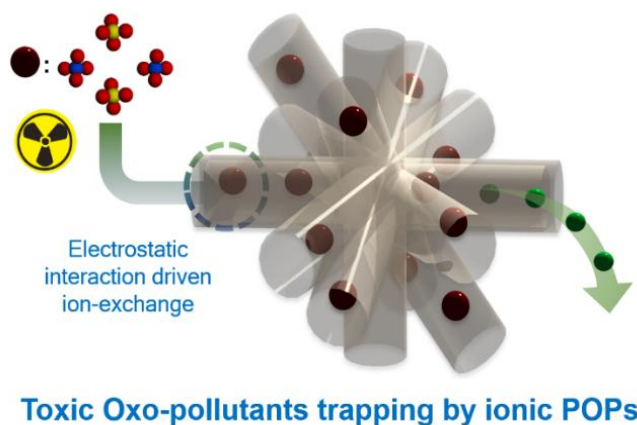
5.1 Introduction

Accessibility to fresh drinking water has become an imminent threat in the 21st century that have direct impact on human lives. The far-flung growth in industrialization and widespread urbanization across the globe are the two prime reasons behind such crisis and depletion of fresh water.^[1] This situation might become so dreadful that as many as one billion of global population will experience utmost water crisis by 2025, as predicted by United Nations.^[2] Among various contamination sources, water pollution by heavy metals (density > 5 g cm⁻³) and their oxo-anionic complexes (CrO₄²⁻, MnO₄⁻, SeO₃²⁻, AsO₄³⁻ etc.) have come forth as pressing concern, owing to their severe toxic effect on living organisms upon bioaccumulation.^[3] In addition, such toxic oxo-anions are considered as the “priority pollutants”, listed by Environment Protection Agency (EPA, United States).^[4] In this context, special attention has been directed toward Cr(VI) based oxo-anions because of their carcinogenic and mutagenic impact on living beings.^[5] Several industrial sectors including leather tanning, steel manufacturing, textile pigments & dyes, wood preservation etc. are involve in chromium usage in huge amounts for diverse applications. As is known, tanning industries generate ~35 L of chromium contaminated wastewater solely for one kilogram of leather production which subsequently pollute natural water bodies.^[6] Additionally, Cr(VI) based oxo-anions are found to weaken the integrity of nuclear waste glass during its vitrification process resulting in poor efficiency of the process.^[6] Moreover, the world has witnessed several incidents of ground water pollution because of improper disposal of Cr(VI) containing wastewater.^[7] Hinkley groundwater contamination in California is one of the famous example where ~1,400 million litres of chromium containing wastewater was disposed into the natural waterbodies.^[8] In addition, other than Cr(VI)-based water pollution issues, ground water contamination by nuclear power plant generated radioactive wastes have become another major concern.^[9] In this regard, nuclear safety has become a genuine concern as the last few decades have witnessed several nuclear accidents, which lead to contamination of radioisotopes in large scale along with their chemotoxicity and radiotoxicity to natural water bodies. Among them, pertechnetate (TcO₄⁻) anion has attracted much research attention mainly as one of its β-emitting radioactive isotope technetium (⁹⁹Tc), which possess a very prolonged half-life period of 2.1 × 10⁵ years. Moreover, nuclear fission of ²³⁹Pu and ²³⁵U result into a very large fission yield of radioactive ⁹⁹Tc and approximately 305 metric tons nuclear waste containing ⁹⁹Tc have been discharged from several nuclear power plants and weapons testing activities.^[10] The non-complexing characteristic of TcO₄⁻ along with its high mobility and solubility in water allows it to remain as low-level nuclear-waste material.^[11] Several techniques, for example, adsorption, photocatalytic reduction, chemical precipitation, ion exchange etc have been utilized to combat this concern, but among them, ion exchange based methods are preferred over other methods owing to its comparatively simple and safe processing,

high affinity and selectivity, good performance in low-concentration waste solution etc.^[12] In addition, the state of the art ion-exchangers present pitfalls such as lower uptake efficiency, poor selectivity and slow kinetics which endows possibilities to develop new alternative and more efficient ion exchange materials.^[13]

To address this demand, tremendous efforts have been employed toward the development of new sorbent materials featuring higher binding affinity and uptake efficiency.^[14] To this end, metal-organic frameworks (MOFs) and porous-organic Polymers (POPs) have strongly established themselves as the new generation ion exchangers owing to features such as tailor made tuneable pore surface, charge controllability, amenability of design etc.^[15] Although MOFs are known to offer good kinetics and selectivity towards such oxo-anion extraction, but poor physiochemical stability especially under highly acidic as well as basic conditions limits the utility of these materials as sorbents towards real-time environmental remediation and nuclear fuel processing.^[16] On the contrary, porous organic polymers fabricated from stable covalent bonds not only exhibit superior physiochemical stabilities even under extreme chemical conditions but their additional beneficial features e.g. high surface area, radiation resistibility etc. make them front runner in comparison with other contemporary porous materials.^[17] Moreover, strategic utilisation of neutral N-donor based moieties such as imidazole and benzimidazole as different crosslinking terminals with multiple halogen sites ($-\text{CH}_2\text{X}$; X-halogen) yield in cationic porous organic polymers with positive quaternized nitrogen site and exchangeable counter halide anions. The electrostatic interaction between the counter halide anions and the host framework are known to be very weak due to which the halide counter anions assist in dispersion of cationic *i*POP particles in water, resulting in rapid and efficient trapping of the aimed anionic pollutants in water via ion-exchange. Additionally, incorporation of different binding sites inside the network such as triazine core, imidazole based moieties, π electron rich surface etc. contribute in superior selectivity of these materials towards such oxo-anions^[5c-5d,11] On account of such structural diversity and physiochemical stability, cationic porous organic frameworks certainly can be an appropriate candidate for sequestration of such hazardous oxo-anionic pollutants from water.

Considering all these aspects, here we present two novel chemically stable ionic porous organic polymers (*i*POPs), *i*POP-3 and *i*POP-4 fabricated from nitrogen rich triazine core and imidazole derivatives, bearing exchangeable bromide (Br^-) anions inside the porous networks. Both the compounds are found to show highly selective and efficient capture of toxic and hazardous CrO_4^{2-} and ReO_4^- anions from water, while ReO_4^- anions were being utilized as a corresponding surrogate for radioactive TcO_4^- ions (Scheme 5.1).



Scheme 5.1. Schematic representation of toxic oxo-anion capture in *i*POPs.

5.2 Experimental

5.2.1. Materials and methods

All materials were obtained commercially until specified.

5.2.2. Synthesis

Synthesis of Tris-(4-bromomethyl-phenyl)-[1,3,5]triazine: This compound was synthesized by following a reported protocol with little modifications (Appendix scheme 5.1).^[18]

Synthesis of *i*POP-3: This compound was also synthesized following a previously reported protocol with slight modifications (Appendix scheme 5.2).^[19] Imidazole (20.83 mg, 0.306 mmol) was refluxed along with potassium carbonate (K_2CO_3) (0.306 mmol, 42.28 mg) in 10 ml dry acetonitrile for 3 hour. Subsequently, Tris-(4-bromomethyl-phenyl)-[1,3,5] triazine (0.17 mmol, 100 mg) was taken in 6 ml dry THF and was added dropwise very slowly to the refluxing reaction mixture which was further refluxed for 24 hour under inert conditions. Then the obtained white solid product was collected and washed thoroughly with different solvents (DMF, DMSO, THF, Toluene, MeOH, acetone and water) for several times to ensure the removal of any unreacted substrates and oligomers within the pores of *i*POP-3. Further, the as-obtained solids were soaked in a combination of solvents of DCM, THF and acetonitrile (1:1:1) for 72 hour and subsequently heated at 90^oC under vacuum for 24 hour to obtain the desolvated phase of the compound (Appendix scheme 5.2).

Synthesis of *i*POP-4: This compound was synthesized by following the similar protocol by using benzimidazole instead of imidazole (Appendix scheme 5.3). Benzimidazole (36.15 mg, 0.306 mmol) was refluxed along with potassium carbonate (K_2CO_3) (42.28 mg, 0.306 mmol) in 10ml dry Acetonitrile for 3 hour. Thereafter, Tris-(4-bromomethyl-phenyl)-[1,3,5]triazine (100 mg, 0.17 mmol) was taken in 60 ml

dry THF and was added dropwise very slowly to the refluxing reaction mixture which was further refluxed for 24 hour under inert conditions (Appendix scheme 5.3).

5.2.3. Oxo-anion capture study:

5.2.3.1. Time dependent oxo-anion removal study:

For the CrO_4^{2-} capture studies, we have taken 2 ml 0.5 mM aqueous solution of CrO_4^{2-} anions in a UV cuvette and subsequently collected the initial absorbance of the solution by UV-Vis spectroscopy. 1 mg each of the activated *i*POPshas been added to the cuvette individually and then we have recorded the absorbance spectra of the supernatant solutions accordingly at different time intervals. Similar experimental methods were adopted to execute the UV-Vis spectroscopic experiment for ReO_4^- anions with a solution of 2 ml 0.5 mM ReO_4^- ion. In addition, the removal %of both the oxo-anions with respect to time and decrease in concentration vs time of the oxo-anions data were calculated from the time dependent study by applying the following equation,

$$D_t = \frac{C_0 - C_t}{C_0} \times 100\% = \frac{A_0 - A_t}{A_0} \times 100\%$$

$$i. e., \quad C_t = C_0 - \frac{A_0 - A_t}{A_0} \times C_0$$

Where, D_t is the exchange capacity of both the *i*POPs, A_0 and C_0 are the absorbance and initial concentration of the supernatant solutions, A_t and C_t are the absorbance and concentration of the supernatant solution at particular times.

5.2.3.2. Oxo-anion capture study in presence of concurrent anions:

We have taken Br^- , Cl^- , SO_4^{2-} and NO_3^- anions as the contending anions in this capture study, which are ubiquitous to any regular water sources especially in waste water. Moreover, we have performed the binary capture experiments with an equimolar (1mM aqueous solution; 1:1) of various competing anions with the aimed oxo-anion. 5 mg of activated *i*POP-3 and *i*POP-4 were added to the aqueous solution mixture under stirring condition for 24 hours. The solution was further filtered off after 24 hours to separate both the compounds from the aqueous mixtures. Thus acquired oxo-anion solutions were further diluted 10 times to quantify via UV-Vis spectroscopy. Additionally, the oxo-anion removal efficiency in presence of other competing anions for both *i*POPs were calculated by comparing the different concentrations with blank solution (Blank solution: 5mM of only oxo-anion was taken instead of mixture).

5.2.3.3. Calculation of capacity:

5 mg of each activated iPOPs were dipped into 5 mM 10ml of oxo-anion solutions individually at stirring condition for 24 hours. After 24 hours, the solution dipped iPOPs were separated by filtration and the filtrates were used further for characterisation. UV-Vis experiments have been executed by diluting (0.2mM each solution has been analysed for UV-Vis) the solution. We have quantified the saturation uptake capacity of the both iPOPs in 24 hours from the initial absorbance and final absorbance data of the oxo-anion solutions by using the following equation,

$$Q_t = \frac{(C_0 - C_t) \times V}{m}$$

Where C_t , C_0 , Q_t , m and V are the concentration of the oxo-anion solution at particular times, initial concentration of oxo-anion solution, capacity of adsorbent, mass and volume of the solution applied for the adsorbent respectively.

5.2.3.4. Reversibility Studies:

Both the iPOPs were regenerated by keeping the oxo-anion loaded compounds (5 mg each) for 24 hours in tetrabutylammonium bromide solution ($[(CH_3(CH_2)_3)_4N]_2Br$) (10ml). Recyclability of the regenerated compound was performed with 5 ml, 1 mM of the oxo-anion solutions (CrO_4^{2-} and ReO_4^-). After 1 day, the concentrations of the post capture oxo-anion solutions were obtained by UV-Vis spectroscopy. Similar experiment was repeatedly performed for up to three cycles in case of both the anions (CrO_4^{2-} and ReO_4^-).

5.2.3.5. Adsorption isotherm experiment:

5 mg of each iPOPs were immersed in 10 ml of aqueous solution of both oxo-anions separately with different concentrations (in case of CrO_4^{2-} ions, concentration was taken in the range of 0-180 ppm and for ReO_4^- ions the range of concentration is 0-550 ppm). After 2 hours UV-Visible spectroscopic experiments were carried out with the respective supernatant solutions and further fitted with following equation,

Langmuir model,
$$Q_e = \frac{Q_m C_e}{K_d + C_e}$$

Where C_e (ppm) and Q_e ($mg\ gm^{-1}$) are the oxo-anion concentration at equilibrium and amount of oxo-anion adsorbed at equilibrium respectively. Q_m ($mg\ gm^{-1}$) is the maximum amount of oxo-anions per unit mass of adsorbent to form a complete monolayer. K_d (mg/L) is a constant related to the affinity of the binding sites.

Freundlich Model,
$$Q_e = K_F C_e^{1/n}$$

where, K_F and $1/n$ are the Freundlich model constants, indicating capacity and intensity of adsorption, respectively.

5.2.3.6. Simulation Details:

Electrostatic Potential Surface (ESP)

Density functional theory (DFT) computations were performed using the Discovery Studio 2016 to derive the ESP surface of *i*POP-3 and *i*POP-4 monomers. The monomer structure was constructed considering experimental parameters consist of imidazole and triazine rings. The Geometry optimization of the monomers were carried out with water as solvent using hybrid B3LYP exchange correlation function and double numeric plus polarization (DNP) basis set with SCF density convergence of 1×10^{-6} . The electrostatic potential (ESP) on the van der Waals (VDW) surfaces (isodensity = 0.001 a.u.) of *i*POP-3 and *i*POP-4 monomers was derived based on its ground state electron density.

Binding Energies

The simulated annealing technique was used to locate the initial position of the anion in the monomer unit of *i*POP-3 and *i*POP-4. The static binding energies (ΔE) at 0 K in vacuum were calculated using the following expression

$$\Delta E = E_{Compound + Anion} - E_{Compound} - E_{Anion}$$

where E_x refers, to the total energies of the *Compound+Anion* complex, the charged *Compound* + alone, and the *Anion* molecule respectively.

5.2.4 Physical Measurements:

All infra-red (IR) spectra were recorded using a NICOLET 6700 FT-IR spectrophotometer, using KBr pellets in the range of 400–4000 cm^{-1} . Thermogravimetric analysis (TGA) was recorded on a Perkin-Elmer STA 6000 TGA analyser under an N_2 atmosphere with a heating rate of $10^\circ\text{C min}^{-1}$. FESEM was performed using a FEI Quanta 3D dual beam ESEM at 30 kV. UV spectra were acquired on a Shimadzu UV 2600 Spectrophotometer.

5.3 Results and discussion

The compounds *iPOP-3* and *iPOP-4* were synthesized via one-condensation reaction between imidazole for *iPOP-3* and benzimidazole for *iPOP-4* with Tris-(4-bromomethyl-phenyl)-[1,3,5]triazine for 24 hour under inert atmosphere (Figure 5.1, Appendix scheme 5.2-5.3). The as-made compounds were thoroughly washed with different solvents (DMF, DMSO, THF, Toluene, MeOH, acetone and water) post synthesis to remove the trapped small chain oligomers as well as unreacted starting materials. Further, both compounds were dipped in DCM, THF and acetonitrile (1:1:1) mixture for 72 hour for solvent exchange with changing of solvents frequently in repeated interval of 12 hour and were kept under vacuum around 90°C for 24 hour to obtain the guest free desolvated phase of *iPOP-3* and *iPOP-4*. The guest free phases of both polymers were thoroughly characterized with ^{13}C -CP-MAS NMR (cross polarization magic angle spinning nuclear magnetic resonance), Fourier transform infra-red (FT-IR) spectroscopy, field emission scanning electron microscopy (FESEM), energy dispersive X-ray analysis (EDX) and thermogravimetric analysis (TGA). The ^{13}C -CP-MAS NMR studies exhibited peaks around ~114 ppm to ~142 ppm (d, e, f), which corresponds to presence of aromatic carbons of imidazole and benzene rings respectively.

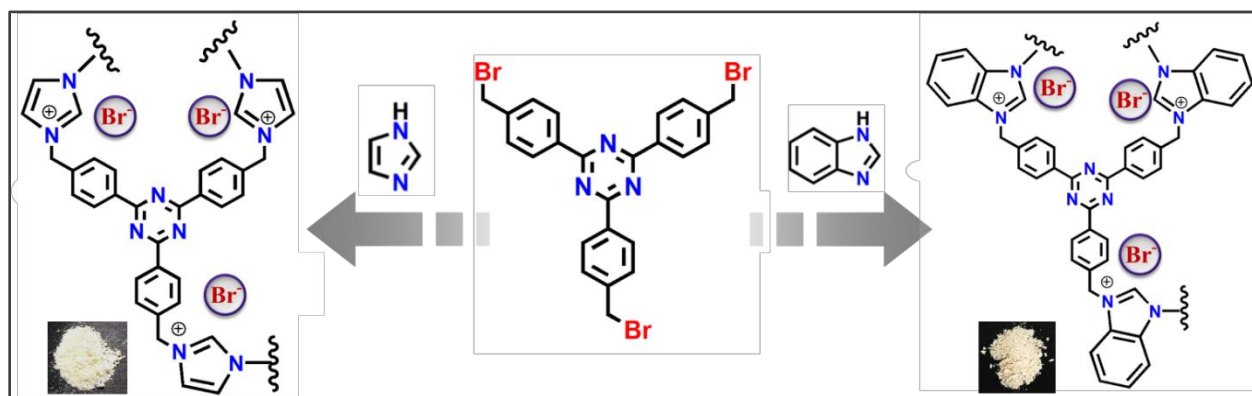


Figure 5.1. Schematic representation for synthesis of *iPOP-3* and *iPOP-4*.

The peak around ~51 ppm (a,b) corresponds to the formation of the methylene linkages attached with both the nitrogens of imidazole for *iPOP-3* and benzimidazole for *iPOP-4* for the expansion of the cationic polymeric networks. The peaks around ~169 ppm (c) corresponds to the carbon atoms of the triazine rings present at the core of *iPOP-3* and *iPOP-4* (Figure 5.2a, Appendix 5.1).^[18,20] TGA analysis of *iPOP-3* showed an initial weight loss (~8%) around 75°C in the pristine phase which might be attributed to the trapped solvent molecules which were removed via desolvation. The TGA curve for the desolvated phase of *iPOP-3* showed negligible weight loss until 300°C while the profile for *iPOP-4* shows negligible weight loss until 350°C confirming guest free nature (Figure 5.2b, Appendix 5.3). FESEM images

revealed the presence of agglomerated particles while EDX spectroscopy and elemental mapping showed the homogeneous presence of free Br^- as the counter anions in the desolvated *i*POP-3 and *i*POP-4 networks (Appendix 5.13-5.18). FTIR spectroscopy revealed peaks $\sim 1520\text{ cm}^{-1}$ corresponding to $\text{C}=\text{N}$ stretching frequency of constituent triazine and imidazol linkages. The peaks around $\sim 1150\text{ cm}^{-1}$ and 750 cm^{-1} are indicative of the presence of imidazolium based functional groups. Moreover, the peaks around $\sim 1420\text{ cm}^{-1}$ represents the stretching frequency of the methylene ($-\text{CH}_2-$) functional groups present while the peak at $\sim 1370\text{ cm}^{-1}$ represents the presence of triazine rings present in *i*POP-3 and *i*POP-4 (Figure 5.2c, Appendix 5.9).^[18,20,21]

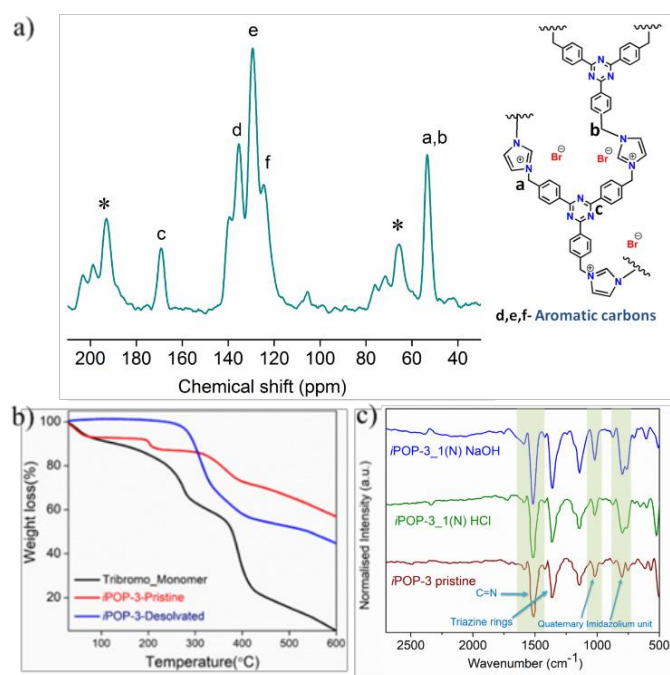


Figure 5.2. Characterization of compound 3. (a) Solid state NMR for *i*POP-3, the ‘*’ marked peaks correspond to side bands; (b) TGA profiles for compound *i*POP-3; (c) FTIR profiles for compound *i*POP-3.

To access the stability aspect of these *i*POPs, they were subjected to harsh condition treatment of acidic (1 N HCl) as well basic (1 N NaOH) solutions for 24 hour. The post treated samples were thoroughly characterized with solid state NMR (^{13}C -CP-MAS NMR), TGA and FT-IR techniques. ^{13}C -CP-MAS NMR did not show any deviation from original spectra with no emergence of any new peaks accounting for unaltered structural features (Appendix 5.10-5.11). The TGA data revealed analogous profile to that of the pristine phase of *i*POP-3 and *i*POP-4 (Figure S4-S5) confirming the retention of thermal as well as chemical stability. Moreover, FTIR measurements substantiated the presence of all the characteristic

peaks when compared with the pristine compounds (Figure 5.2c, Appendix 5.9). Further, we have performed low-temperature gas adsorption N_2 (77K) as well as CO_2 (195K) data to substantiate the porosity of both *i*POPs (Appendix 5.8). We observed very lower uptakes for N_2 (77K) for both *i*POPs whereas the CO_2 (195K) adsorption profiles substantiated the inherent porosity with an uptake of 64 mlg^{-1} for *i*POP-3 and 49 mlg^{-1} for *i*POP-4. Additionally, the chemically robust nature of these *i*POPs was further substantiated from its outstanding performance upon exposure to various chemical environments. A minimal loss in residual weight % (Appendix 5.12) was observed when both of the compounds were immersed in a wide array of solutions advocating for its highly stable nature.

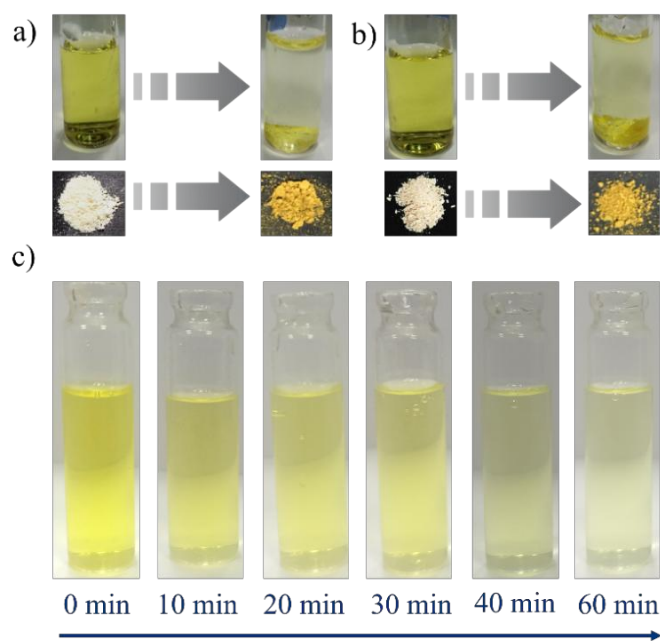


Figure 5.3. Visual color change of aqueous solution of CrO_4^{2-} and corresponding *i*POPs (a) upon addition of *i*POP-3, (b) upon addition of *i*POP-4, (c) decrease in concentration of CrO_4^{2-} with increment of time upon addition of *i*POP-3.

Such physiochemical stability along with cationic nature of both compounds propelled us to evaluate its potential towards toxic oxo-anion trapping from water. Depending upon the pH of the medium, hexavalent chromium oxo-anions, i.e. chromate (CrO_4^{2-}) and dichromate ($Cr_2O_7^{2-}$), primarily remain in interconvertible equilibrium. Hence, we further performed the capture experiments with chromate in this work. Initially, we dipped 5 mg of both *i*POP-3 and *i*POP-4 in a 5 ml 2 mM aqueous CrO_4^{2-} solution individually and monitored the trapping process via both naked eye colour change and UV-Vis spectroscopy. A gradual colour change from yellow to almost colourless for both the solutions were

observed within just 1 hour illustrating rapid capture of CrO_4^{2-} by both the compounds (Figure 5.3a-5.3c). Enthused from such fast kinetics, we have carried out in-situ titration of CrO_4^{2-} capture in water for both *i*POPs and monitored via UV-Vis spectroscopy where 2 mL 0.5 mM aqueous solution of CrO_4^{2-} anions was added to 1 mg of both compounds individually and the absorption maxima (λ_{max}) at 372 nm for CrO_4^{2-} ions was monitored (Figure 5.4a, 5.4d). The diminishing trend in UV-Vis spectra at 372 nm with increment of time affirmed trapping of CrO_4^{2-} anions in case of both compounds. As was observed, the anion trapping took place in a rapid manner with almost ~60% and ~55% removal of CrO_4^{2-} ions were observed within just 2 min while almost ~90% and ~80% removal was achieved within 60 min using 1 mg of *i*POP-3 and *i*POP-4 respectively (Figure 5.4a, 5.4d). The percentage removal vs. time study corroborated with the fast kinetics of the capture process by both *i*POP-3 and *i*POP-4 (Appendix 5.31, 5.33). In addition, the saturation uptake capacity of CrO_4^{2-} evidenced from UV-vis spectroscopy are 170 mgg^{-1} and 141 mgg^{-1} for *i*POP-3 and *i*POP-4 respectively (Appendix 5.35-5.36). It is noteworthy to mention that these saturation uptake capacities are accounted among the highest values reported in the literature of porous materials (Appendix Table 5.1). The differential efficiency toward pollutant capture performance of *i*POP-4 in comparison with *i*POP-3 may be attributed to a combination of reduced porosity as well as enhanced hydrophobicity (Appendix 5.8, 5.65). Furthermore, the post-capture phases were characterized by SS-NMR, solid state UV-vis analysis, FTIR analysis, EDX and elemental analysis studies. The SS-NMR confirmed retention of the characteristic peaks for both *i*POPs in post-capture phases (Appendix 5.19- 5.20). FTIR analysis confirmed presence of all characteristic peaks along with emergence of a new peak at $\sim 894 \text{ cm}^{-1}$ correlated with the CrO_4^{2-} anions validating the retention of the network integrity (Appendix 5.23-5.24). In addition, homogeneous distribution of chromium in EDX and elemental spectra analysis confirmed the incorporation of chromate anions inside the pores of both the compounds (Appendix 5.25-5.30).

Along the same line, pertechnetate (TcO_4^-) is another lethal oxo-anion on account of being radioactive while ^{99}Tc is β -emitting in nature. Due to radioactivity of TcO_4^- , we have used a non-radioactive surrogate viz. ReO_4^- , that have similar size-charge distribution. Further, we have performed *in-situ* titration studies ReO_4^- anions under UV-vis spectroscopy by monitoring the intensity maxima (λ_{max}) at 208 nm with increase in time intervals. Notably, both compounds exhibited similar rapid kinetics as almost ~75% and ~55% of ReO_4^- anions found to be trapped within just 2 min by *i*POP-3 and *i*POP-4 respectively (Figure 5.4b, 5.4e). The percentage removal vs. time studies further corroborated with the rapid kinetics of the capture processes (Appendix 5.41, 5.43). In addition, the saturation uptake capacities of ReO_4^- ions evidenced from UV-Vis spectroscopy are 515.5 mgg^{-1} and 350.3 mgg^{-1} for *i*POP-3 and

*i*POP-4 respectively (Appendix 5.45, 5.46), among which *i*POP-3 was found to stand tall among the highest values reported in the regime of porous materials (Appendix Table 5.2).

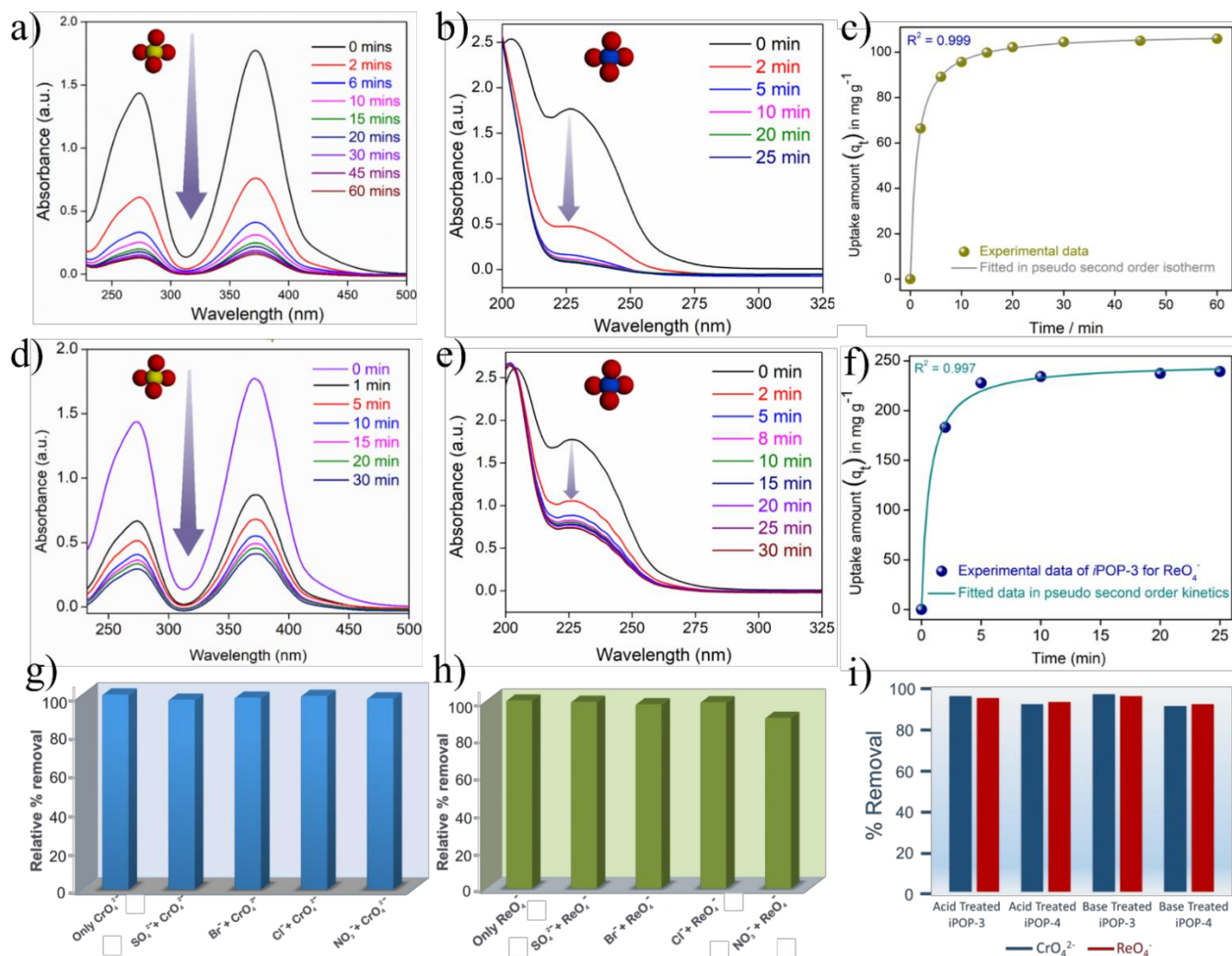


Figure 5.4. (a) UV-Vis spectra in presence of *i*POP-3 for CrO_4^{2-} , (b) UV-Vis spectra in presence of *i*POP-3 for ReO_4^- , (c) Kinetic study of CrO_4^{2-} ion capture with *i*POP-3, (d) UV-Vis spectra in presence of *i*POP-4 for CrO_4^{2-} , (e) UV-Vis spectra in presence of *i*POP-4 for ReO_4^- , (f) Kinetic study of ReO_4^- ion capture with *i*POP-3, (g) Bar diagram for CrO_4^{2-} removal efficiency of *i*POP-3 in presence of Br^- , Cl^- , NO_3^- and SO_4^{2-} ions, (h) Bar diagram for ReO_4^- removal efficiency of *i*POP-3 in presence of Br^- , Cl^- , NO_3^- and SO_4^{2-} ions, (i) Removal efficiency of acid and base treated phases of *i*POP-3 and *i*POP-4.

^{13}C -NMR data of post pollutant capture phase corroborated well with the pristine compound while FTIR spectra revealed the presence of characteristic peaks for both the compounds with a new peak at ~ 918

cm^{-1} corresponding to the ReO_4^- anions (Appendix 5.19-5.20, 5.23-5.24). Additionally, a homogeneous distribution of rhenium along with the other elements in EDX and elemental spectra analysis confirmed the incorporation of perrhenate anions inside the pores of both the compounds (Appendix 5.37-5.40).

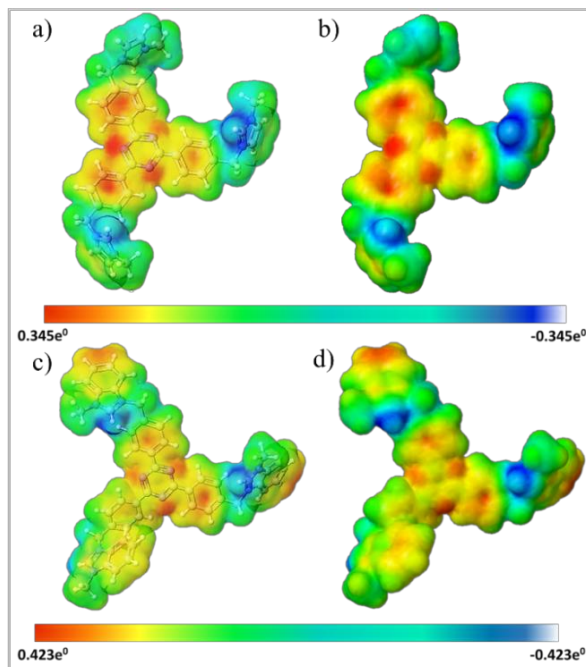


Figure 5.5. Visual Monomer unit of *iPOP-3* and *iPOP-4* showing the electrostatic potential isosurface (isodensity = 0.001 a.u.) calculated using DFT-DMOL3-B3LYP (a) and (c) represent top view of *iPOP-3* and *iPOP-4* respectively, (b) and (d) represent top view ESP diagram of *iPOP-3* and *iPOP-4* respectively.

Keeping in mind the real time applicability of our materials, we were prompted to test the competency of these compounds when subject to harsh chemical environments. To validate this, we have performed the oxo-anion capture experiments with both *iPOP-3* and *iPOP-4* after they were exposed to 1(N) HCl and 1(N) NaOH respectively. To our delight, both *iPOPs* exhibited almost intact efficiency with the acid treated phases: 99% (*iPOP-3*), 95% (*iPOP-4*) for CrO_4^{2-} and 98% (*iPOP-3*), 96% (*iPOP-4*) for ReO_4^- whereas with base treated phases: 100% (*iPOP-3*), 94% (*iPOP-4*) towards CrO_4^{2-} capture and 99% (*iPOP-3*), 95% (*iPOP-4*) towards ReO_4^- anions (Figure 5.4i). Such results indeed underscore the utility of these *iPOPs* in treatment of real-world wastewater. Moreover, anion trapping by both the *iPOPs* followed pseudo-second-order kinetics as the time dependent uptake capacity fitting profile revealed that all the capture processes was exclusively dependent upon the quantity of adsorbent and the adsorbate used (Figure 5.4c, 5.4f, Appendix 5.47-5.48). The correlation coefficient (R^2) values for *iPOP-3* were found to be 0.999 and 0.997 for CrO_4^{2-} and ReO_4^- ions respectively. On the other hand, R^2 values of *iPOP-4* were

found to be 0.995 and 0.999 for CrO_4^{2-} and ReO_4^- anions respectively. The rate constant (k_2) values were found to be 0.00728 mg/g min (CrO_4^{2-}) and 0.00621 mg/g min (ReO_4^-) in case of *i*POP-3 and 0.00938 mg/g min (CrO_4^{2-}) and 0.00735 mg/g min (ReO_4^-) in case of *i*POP-4. Further, to substantiate the potential of these *i*POPs towards removal of such oxo-anions in very low concentration, we have performed CrO_4^{2-} removal experiments with both *i*POPs in a very low concentration range (10-100ppm). To our delight, both *i*POPs have recorded almost 100% removal efficiency towards CrO_4^{2-} anions even in lower concentration of 10ppm (Appendix 5.49-5.50).

Enthused by their impressive uptake capacities, we were motivated to investigate the selectivity of these *i*POPs as real wastewater effluents contain several interfering anions (such as SO_4^{2-} , Br^- , Cl^- , NO_3^- etc.) that coexists along with the targeted oxo-anions. The competing studies were carried out in presence of various coexisting interfering anions in a 1:1 mixture of both CrO_4^{2-} and ReO_4^- oxo-anions individually. Both *i*POPs exhibited excellent selectivity towards CrO_4^{2-} and ReO_4^- as the removal performance remained almost unaltered ($\geq 90\%$) in each case confirming very high affinity of both the *i*POPs toward such oxo-anions (Figure 5.4g-5.4h, Appendix 5.51-5.52). Further, to strengthen and verify our results regarding the selectivity of *i*POPs, we have performed Density Functional Theory (DFT studies) which successfully validated our experimental findings (discussed in details later).

Reusability of the sorbent material is one of the major aspects in real-time water pollutant sequestration processes. In this regard, we have carried out reversibility experiments with both *i*POPs in which we dipped 5 mg of each oxo-anion (CrO_4^{2-} and ReO_4^-) occluded phase of *i*POP-3 (*i*POP-3@ CrO_4^{2-} , *i*POP-3@ ReO_4^-) and *i*POP-4 (*i*POP-4@ CrO_4^{2-} , *i*POP-4@ ReO_4^-) in 2 M aqueous solution of tetrabutylammonium bromide. A gradual colour change upon release of trapped CrO_4^{2-} anions from colourless to yellow was observed for both *i*POPs while the compounds went back to their initial off-white colour. Further, the concentration of the released oxo-anions was verified via UV-vis spectroscopy. The kinetics for release profile was noted to be moderate but both the *i*POPs were able to release almost all CrO_4^{2-} anions within 24hour (Appendix 5.53-5.54, 5.63). The slow kinetics indicate that both *i*POPs frameworks possess very high affinity as well as favorable binding sites towards the oxo-anions in comparison to Br^- anion, which was further confirmed by the theoretical DFT calculations. Similar results were obtained for the release of perrhenate anions by the *i*POPs. Notably, both compounds exhibited almost same efficiency in first two cycles of recyclability and it reduced to $\sim 85\%$ in 3rd cycle for both *i*POPs (Appendix 5.53-5.54). To get more insights about such excellent selectivity and affinity of both *i*POPs toward these oxo-anions, we have executed DFT calculations using Discovery Studio software package (Supporting Information contains more simulation details). According to the experimental parameters a monomeric unit of *i*POP-3 and *i*POP-4 was constructed, consisting of triazine rings along

with imidazole and benzimidazole respectively. The electrostatic potential (ESP) distribution profile of monomers corroborated well with the uniform delocalization of negative and positive charges surrounding imidazole, benzene and triazine rings which further serve as the preferential recognition sites for the incoming oxo-anions, having lower charge density (Figure 5.5).

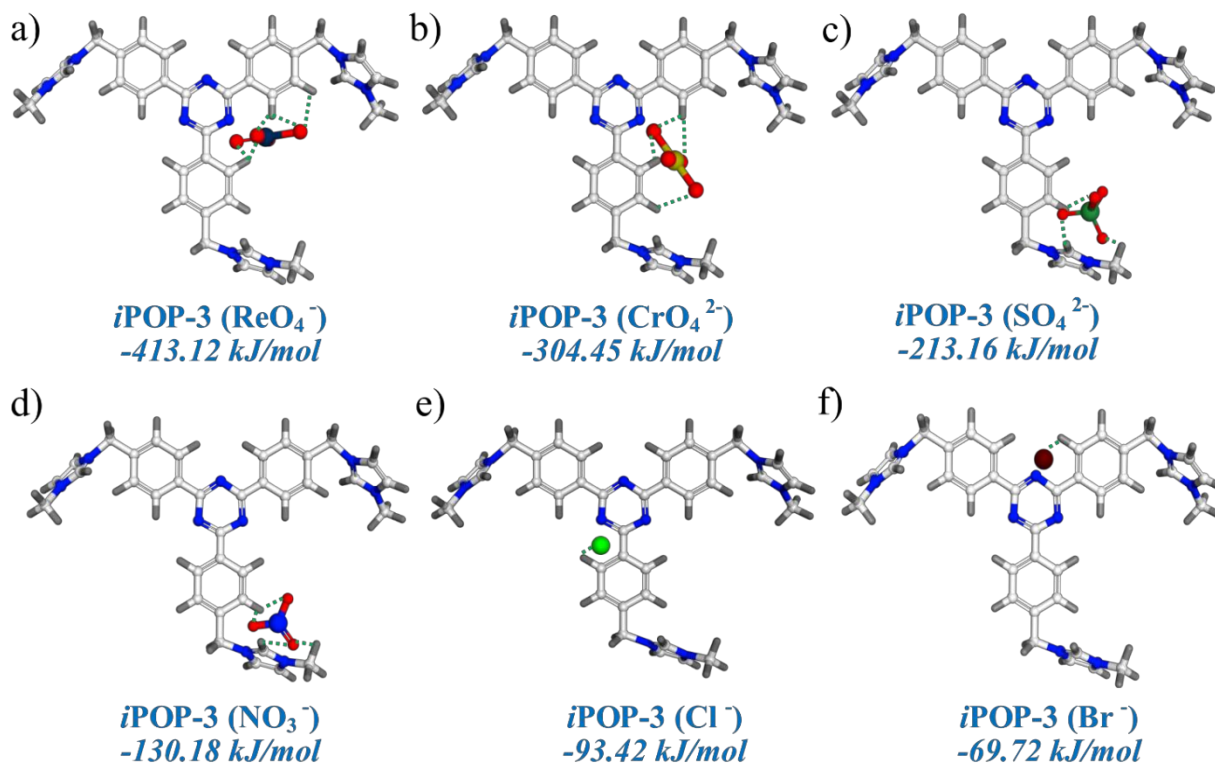


Figure 5.6. Optimized structures of monomeric unit of *iPOP-3* with different binding anions and the corresponding binding energies calculated based on DFT-DMOL3-B3LYP, (a) *iPOP-3*-(ReO_4^-), (b) *iPOP-3*-(CrO_4^{2-}), (c) *iPOP-3*-(SO_4^{2-}), (d) *iPOP-3*-(NO_3^-), (e) *iPOP-3*-(Cl^-), (f) *iPOP-3*-(Br^-)

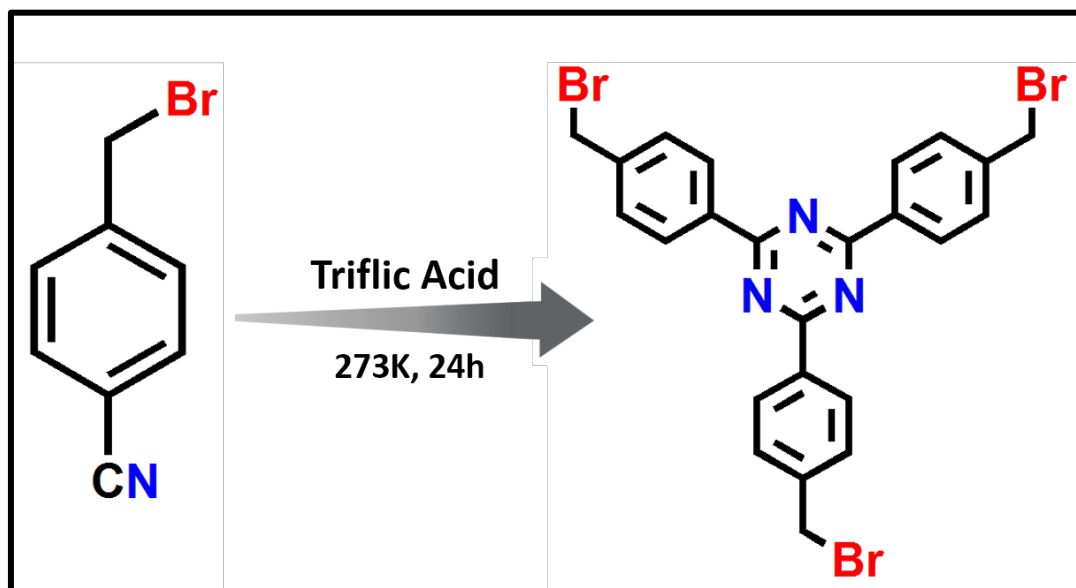
Theoretical DFT calculations provided valuable information regarding several favourable binding sites for CrO_4^{2-} and ReO_4^- over other anions that is directly reflected in the binding energy values. The binding energies of CrO_4^{2-} with the building units of *iPOP-3* and *iPOP-4* were found to be -304.45 kJ/mol and -544.45 kJ/mol respectively, which are much higher than the binding energies of other anions (Figure 5.6a-5.6f, Appendix 5.64). Similarly, the binding energies of ReO_4^- anion with the building units of *iPOP-3* and *iPOP-4* were found to be as high as -413.12 kJ/mol and -603.12 kJ/mol respectively, which indicate strong interactions as well as high affinity of both the *iPOPs* for ReO_4^- anions. The binding energies for Br^- ion with the *iPOPs* building units were found to be -69.72 kJ/mol and -74.82 kJ/mol, which are much

lower than the corresponding binding energies of the target analytes aiding both these materials in kinetics, capture efficiency and selectivity as observed in the experimental studies.

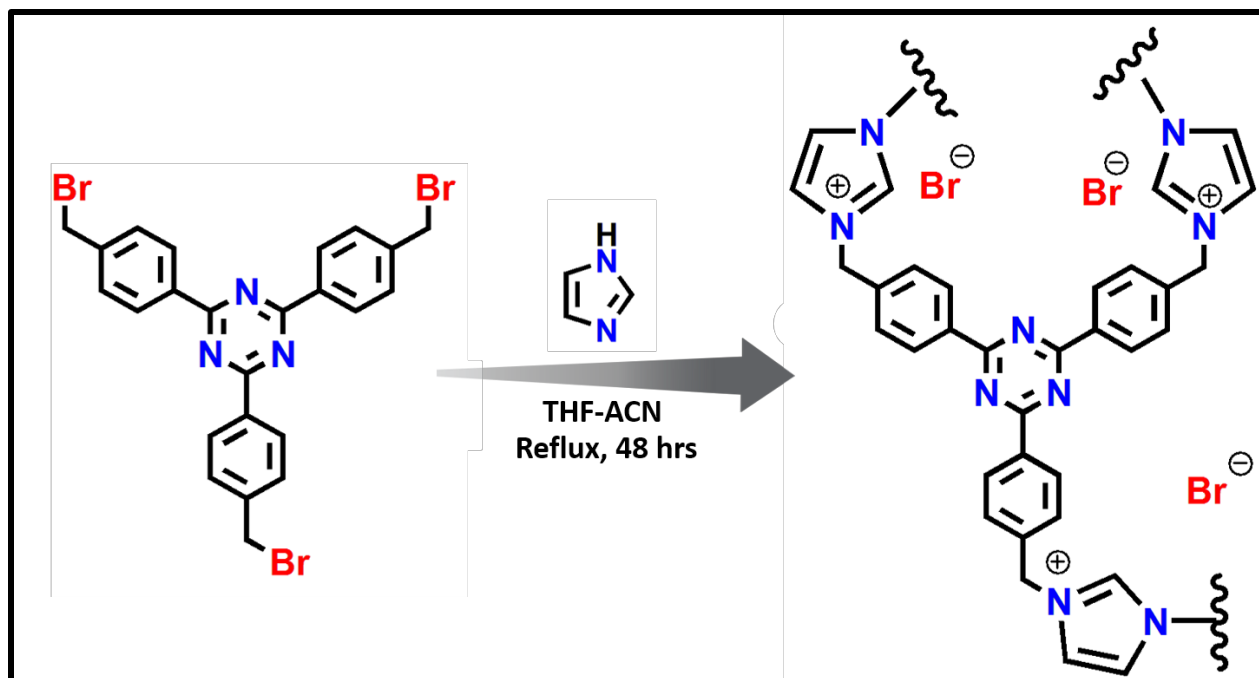
5.4 Conclusions

In conclusion, two new chemically stable cationic porous organic polymers, namely *i*POP-3 and *i*POP-4, were synthesized and thereupon utilized for sequestration of toxic oxo-anions (CrO_4^{2-} and ReO_4^-) from water. Both compounds performed remarkably well in terms of rapid kinetics, high uptake efficiency and superior selectivity toward these oxo-anions. The uptake capacities of *i*POP-3 for both CrO_4^{2-} and ReO_4^- are among the highest reported values in the arena of overall porous materials. Furthermore, the theoretical calculations along with DFT analysis brings forth insights regarding potential recognition sites for oxo-anions as well as the emergence of the exceptional selectivity and efficiency of both the *i*POPs. In addition, both compounds showed reusability up to three cycles for the oxo-anions, illustrating as potential candidates for real-time utilization in such oxo-anion sequestration applications. The experimental findings of this work highlights that *i*POPs can serve as potent adsorbents toward wastewater remediation with facile synthesis, exceptional removal efficiency and high adsorption capacity.

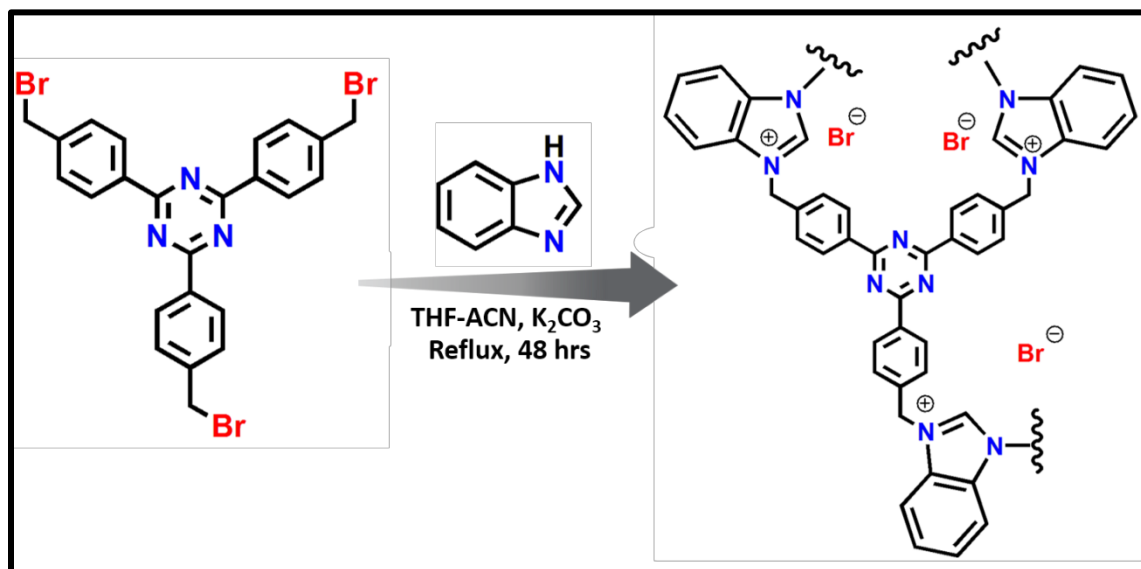
5.5 Appendix section



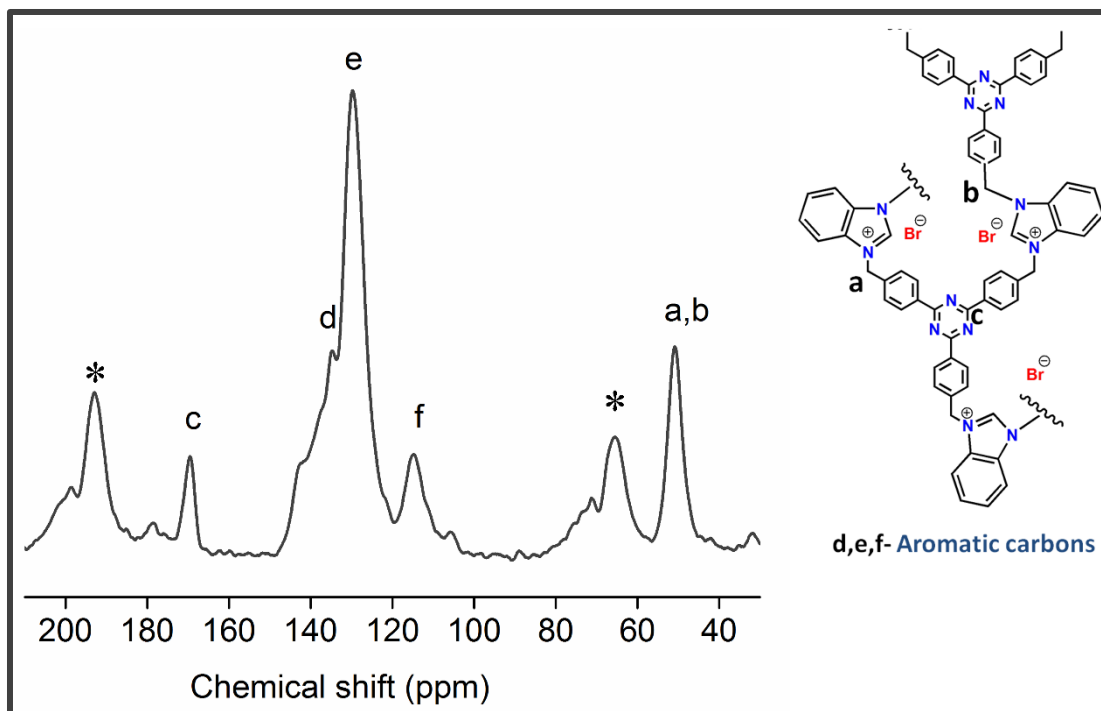
Appendix scheme 1. Representation of the protocol employed for the synthesis of Tris-(4-bromomethyl-phenyl)-[1,3,5] triazine.



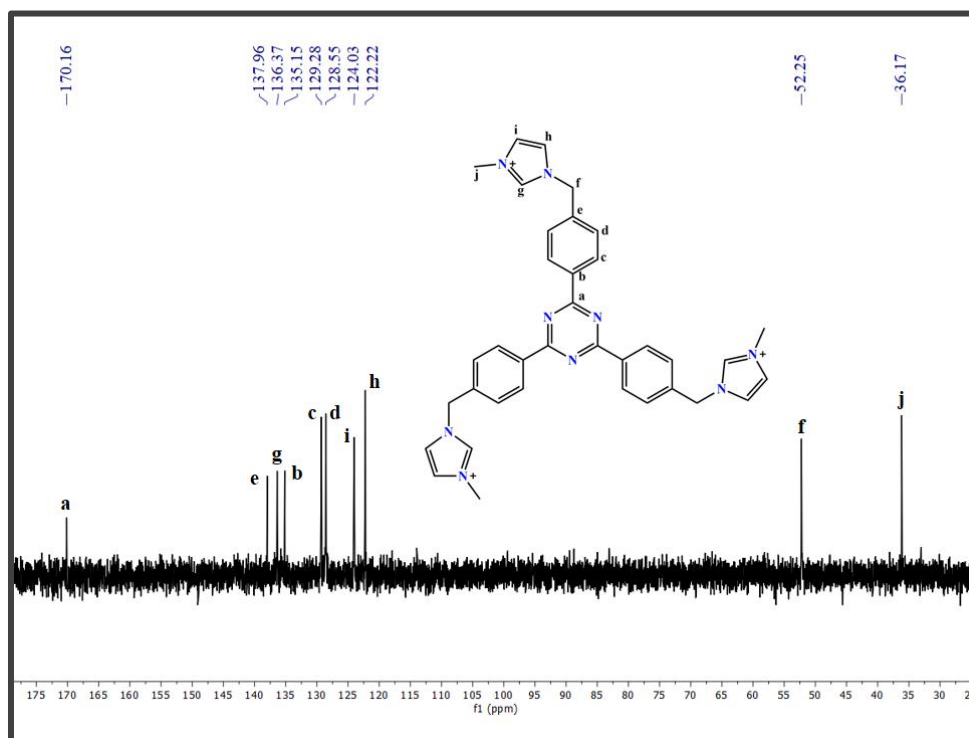
Appendix scheme 2. Representation of the protocol employed for the synthesis of *iPOP-3*.



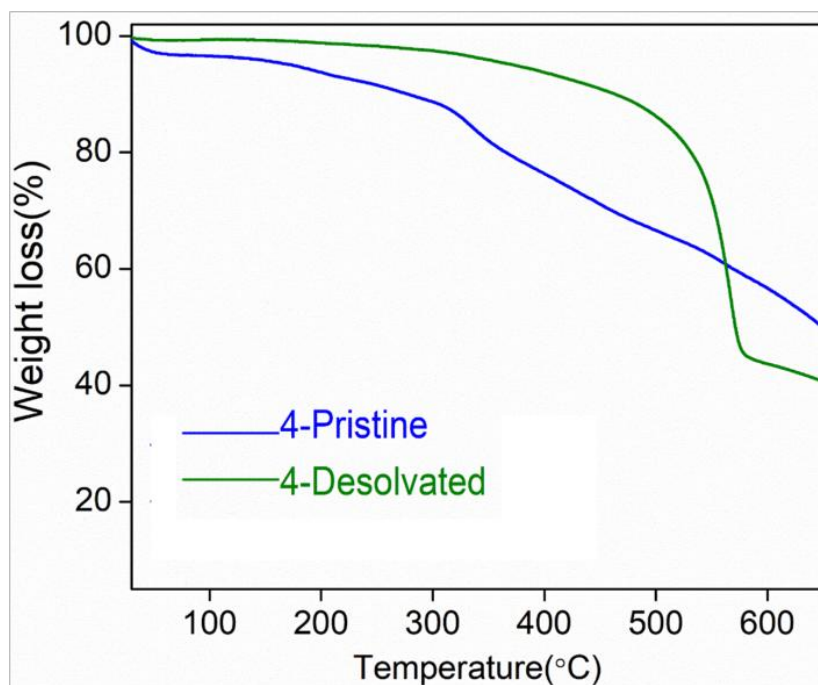
Appendix scheme 3. Representation of the protocol employed for the synthesis of *iPOP-4*.



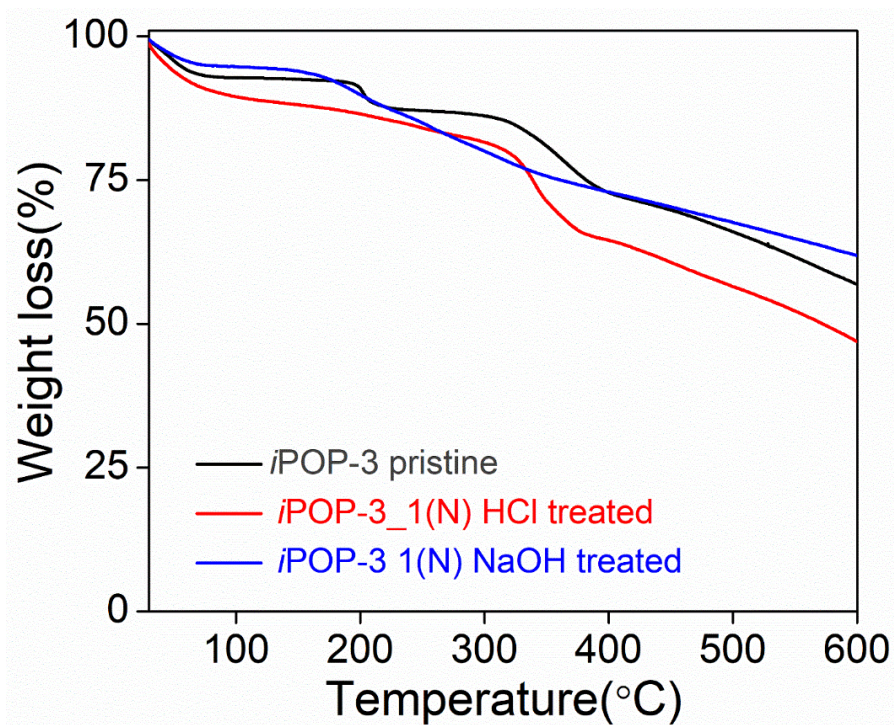
Appendix 5.1. Solid state NMR for *iPOP-4*, the * marked peaks correspond to side bands.



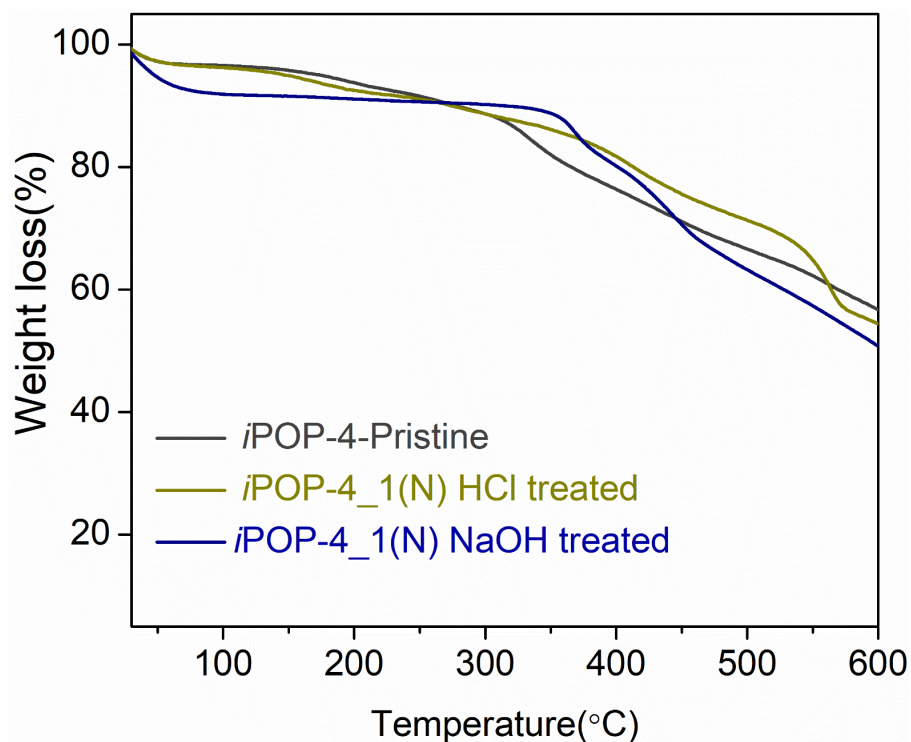
Appendix 5.2. ^{13}C NMR for the model compound of *iPOP-3*.



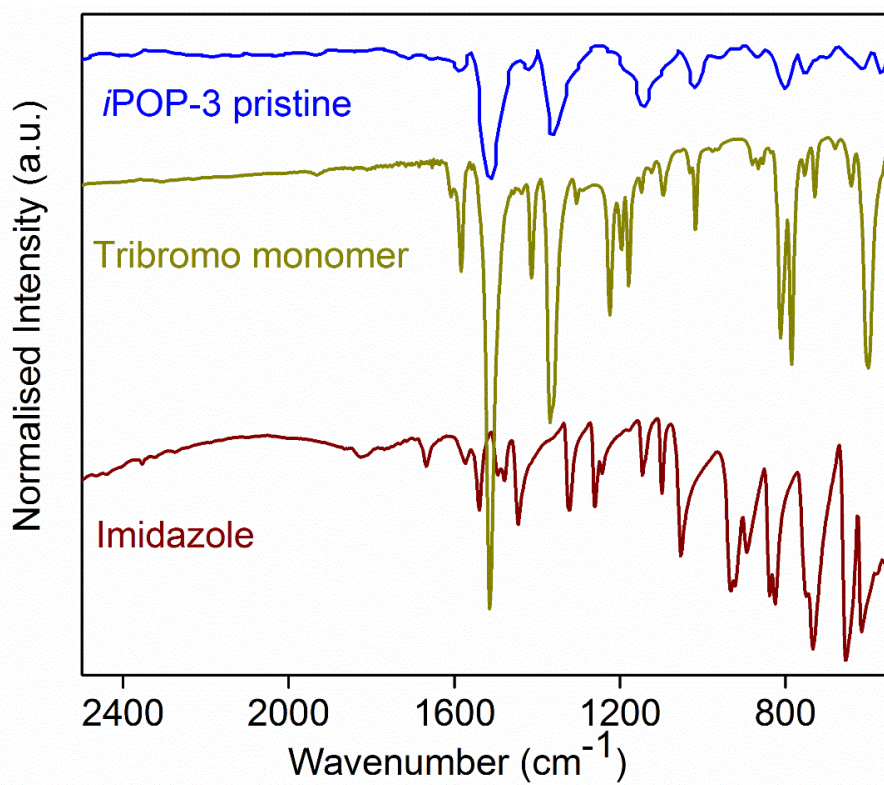
Appendix 5.3. TGA profiles for *iPOP-4*.



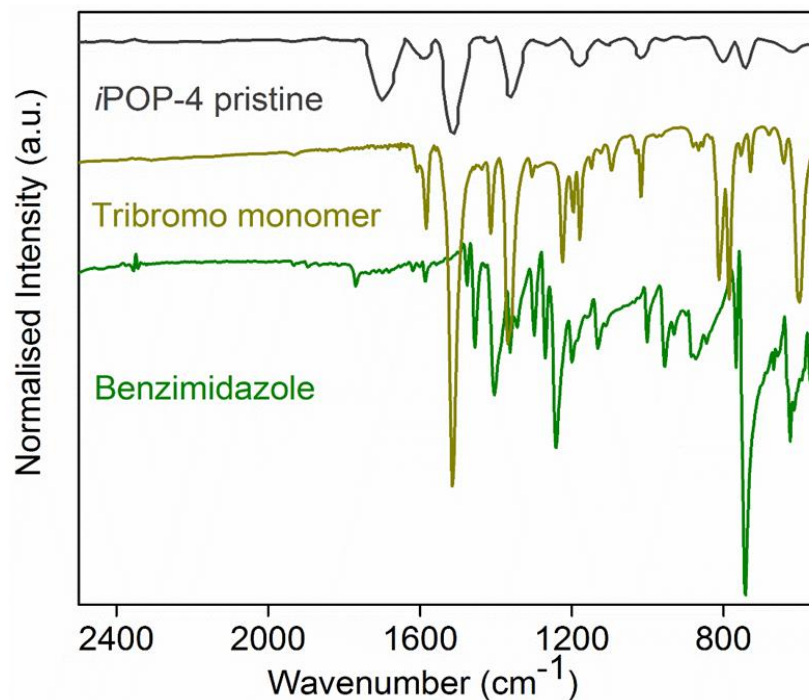
Appendix 5.4. TGA profiles for acid and base treated *iPOP-3*.



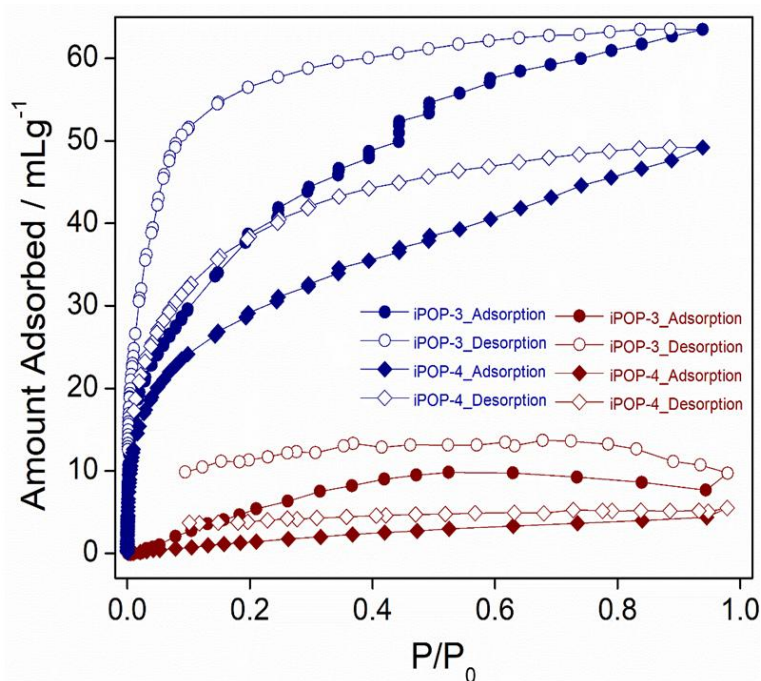
Appendix 5.5. TGA profiles for acid and base treated *iPOP-4*.



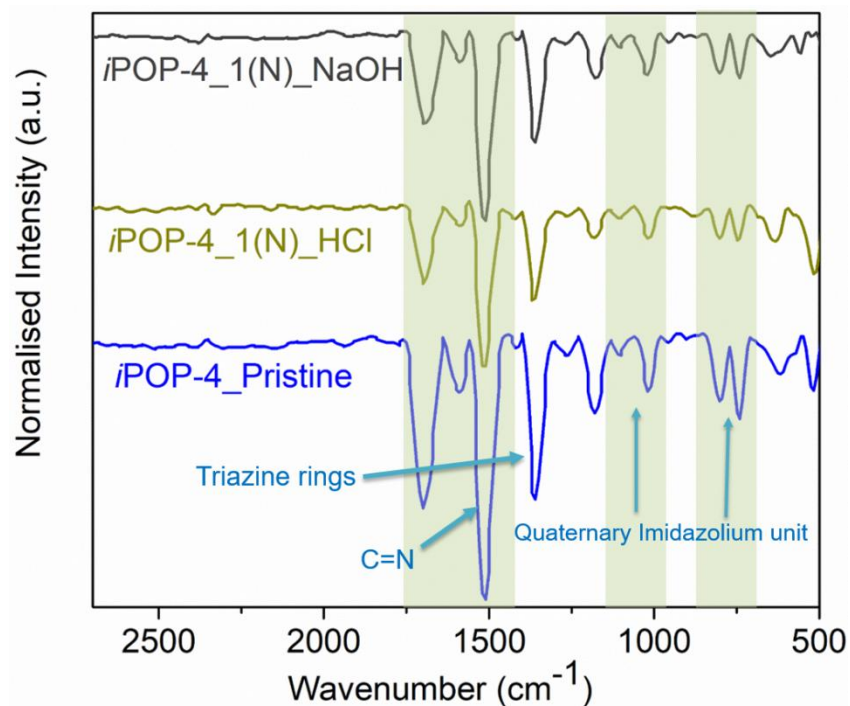
Appendix 5.6. FTIR profiles for compound *iPOP-3*.



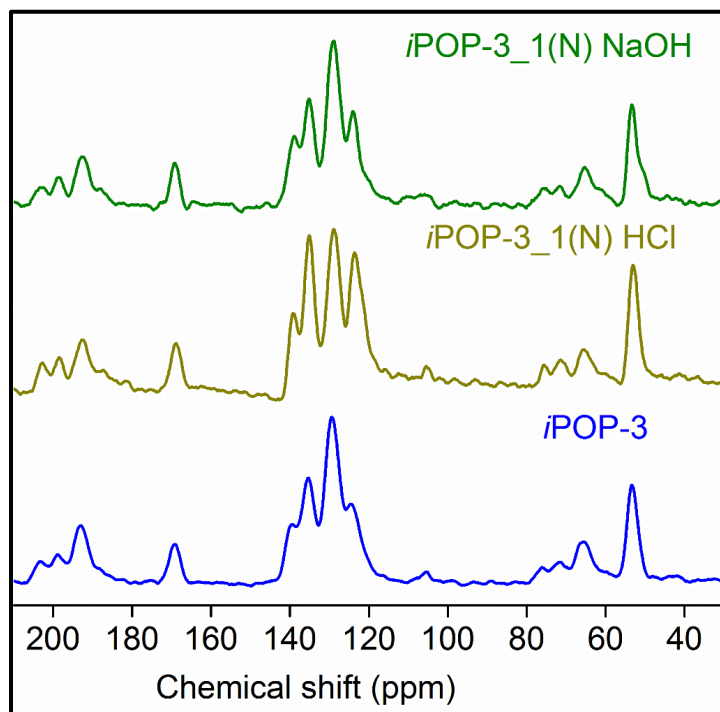
Appendix 5.7. FTIR profiles for compound *iPOP-4*.



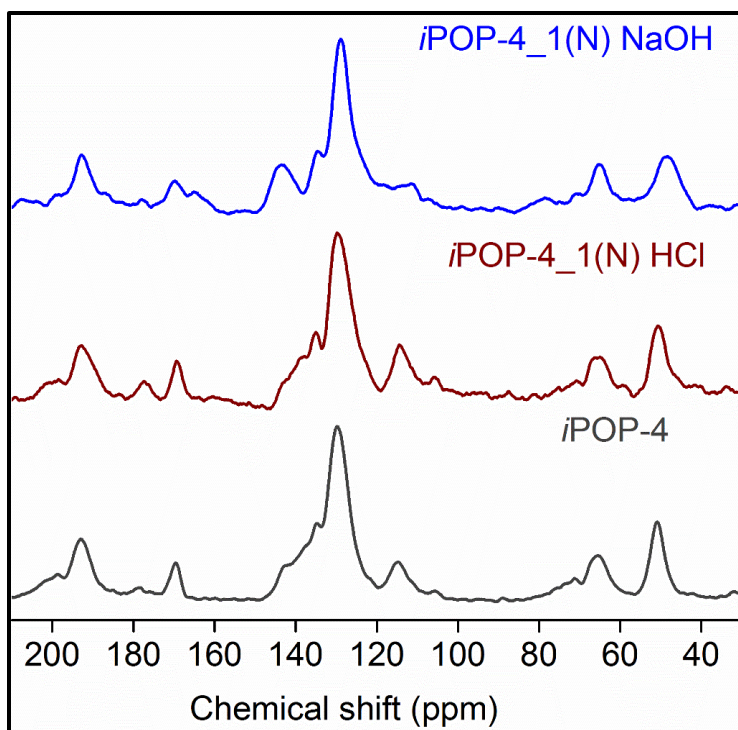
Appendix 5.8. Single component N₂ (77K) and CO₂ (195K) adsorption data for *iPOP-3* and *iPOP-4*; (colour code: Wine Red: N₂ (77K), Navy Blue: CO₂ (195K)).



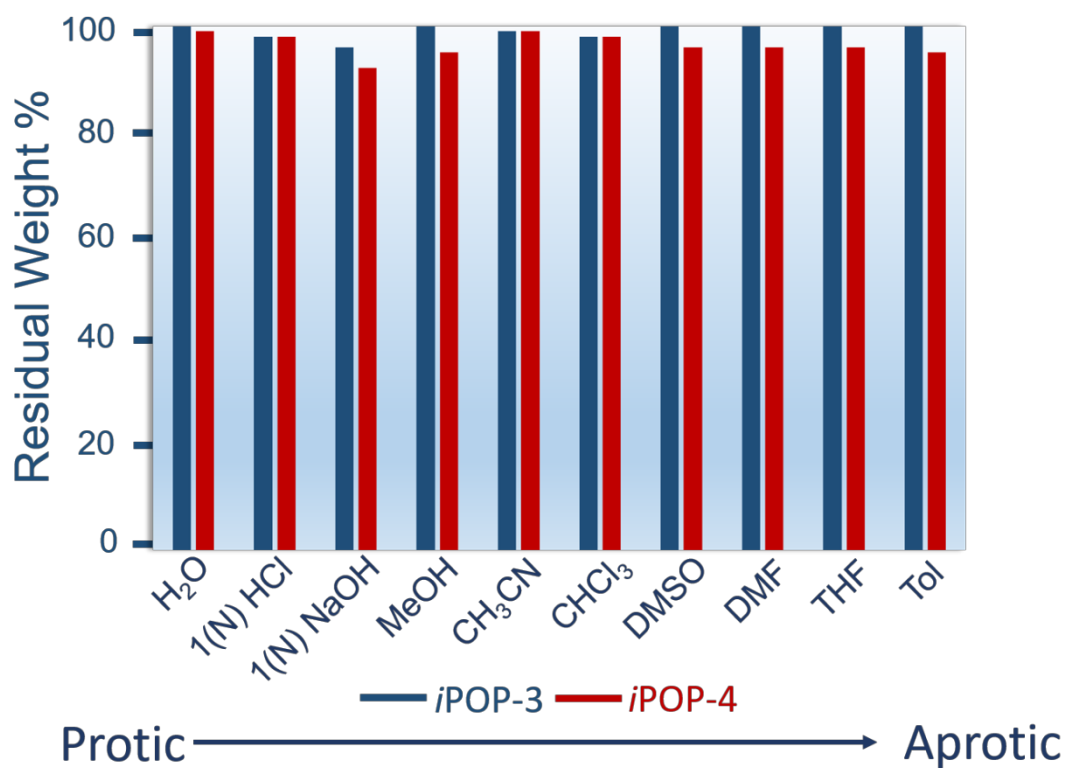
Appendix 5.9. FTIR profiles for compound *iPOP-4*.



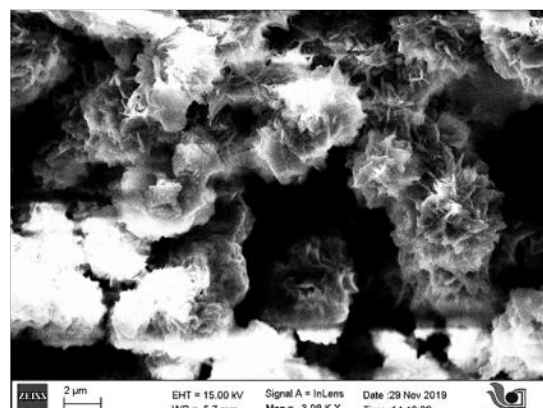
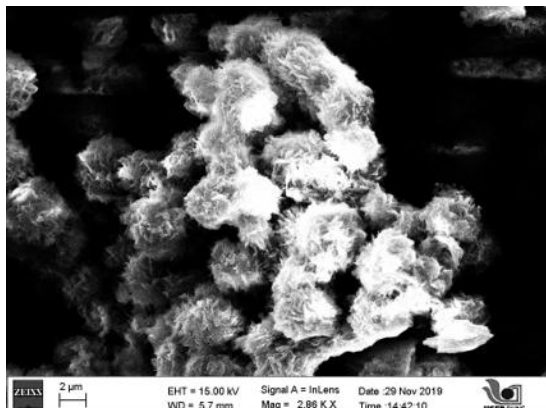
Appendix 5.10. Solid state NMR spectra for *iPOP-3*.



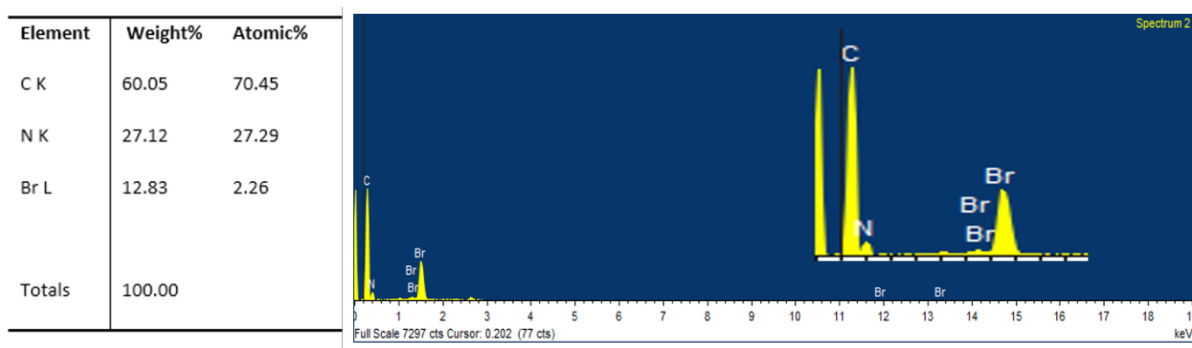
Appendix 5.11. Solid state NMR spectra for *iPOP-4*.



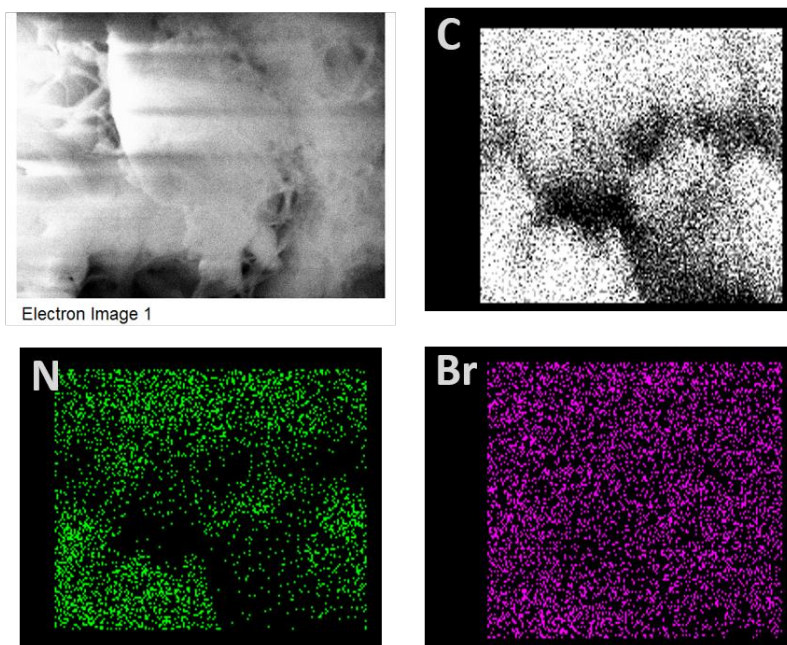
Appendix 5.12. Residual weight percentage of both *iPOPs* after exposing in different solvents.



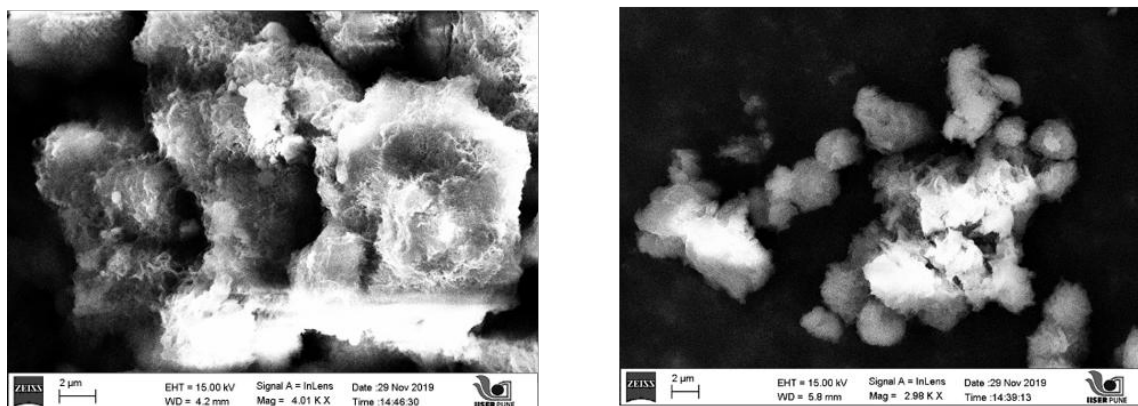
Appendix 5.13. FESEM images of *iPOP-3*.



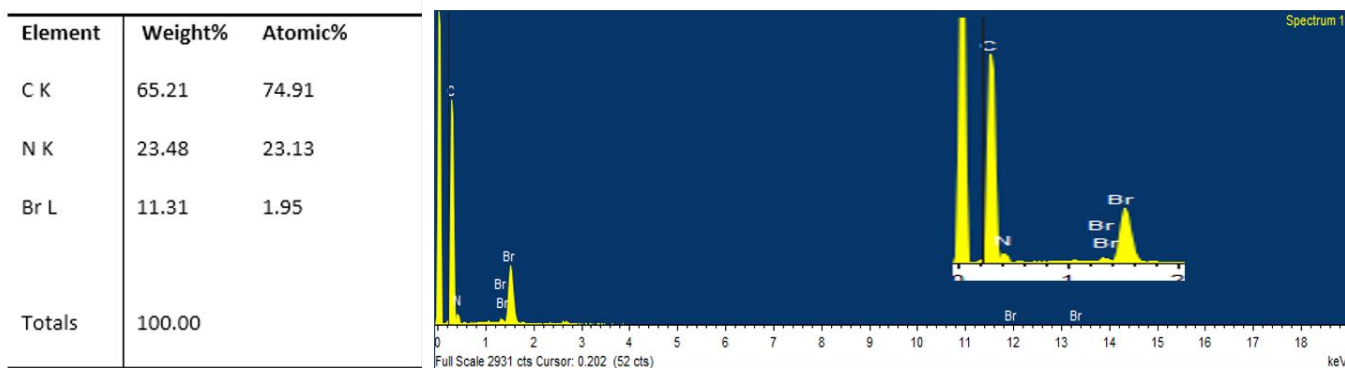
Appendix 5.14. EDX analysis of *iPOP-3*.



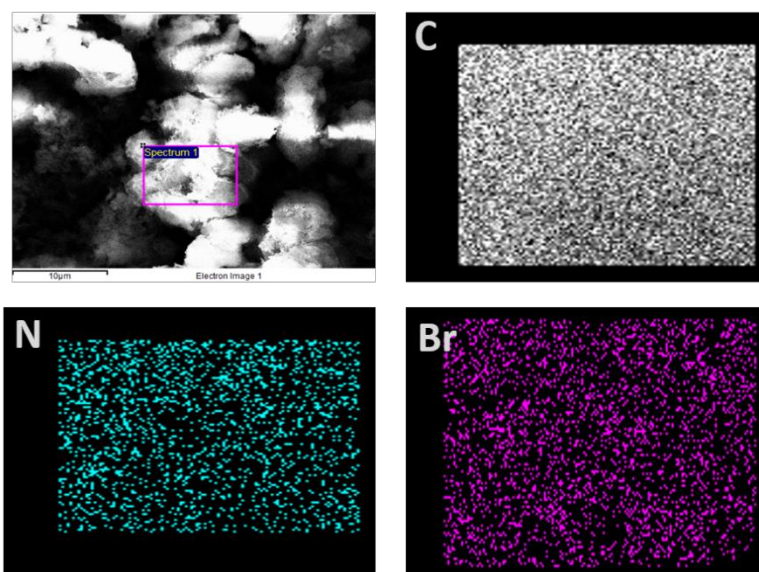
Appendix 5.15. Elemental mapping of *iPOP-3*.



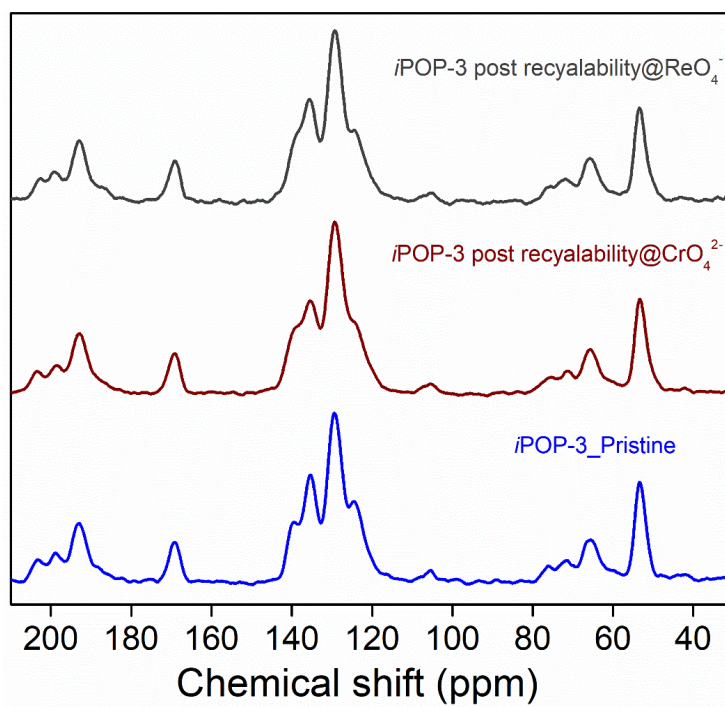
Appendix 5.16. FESEM images of *iPOP-4*.



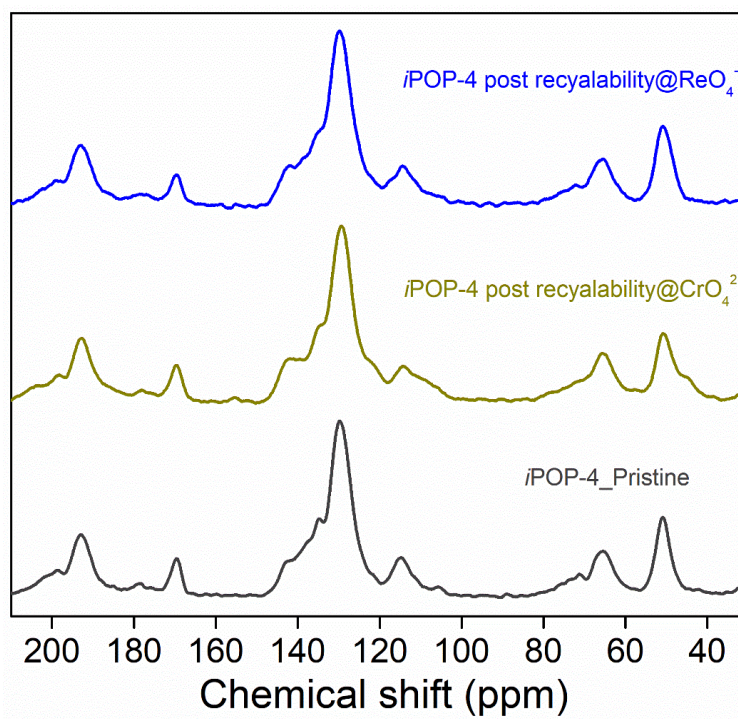
Appendix 5.17. EDX analysis of *iPOP-4*.



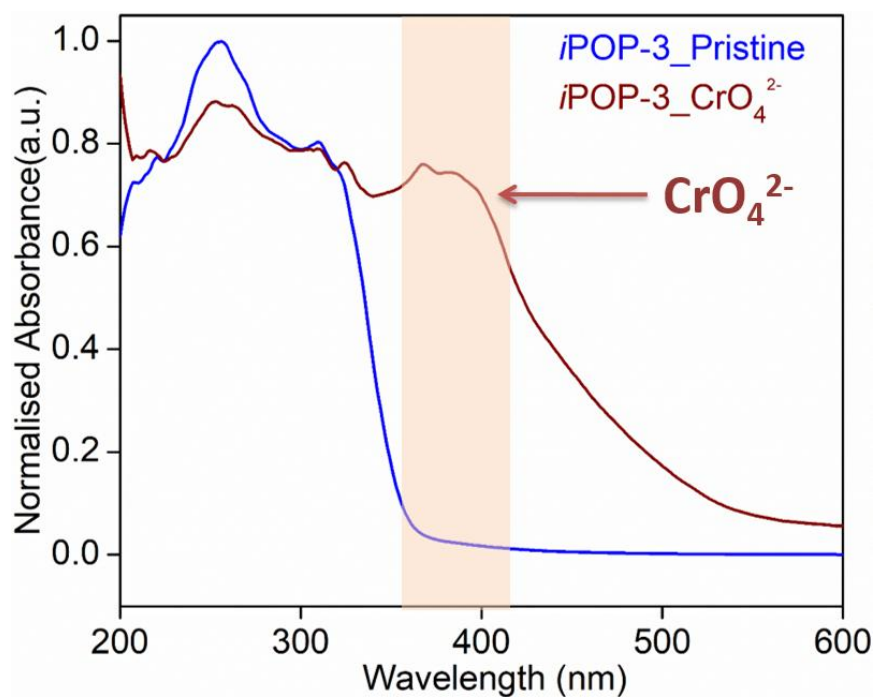
Appendix 5.18. Elemental mapping of *iPOP-4*.



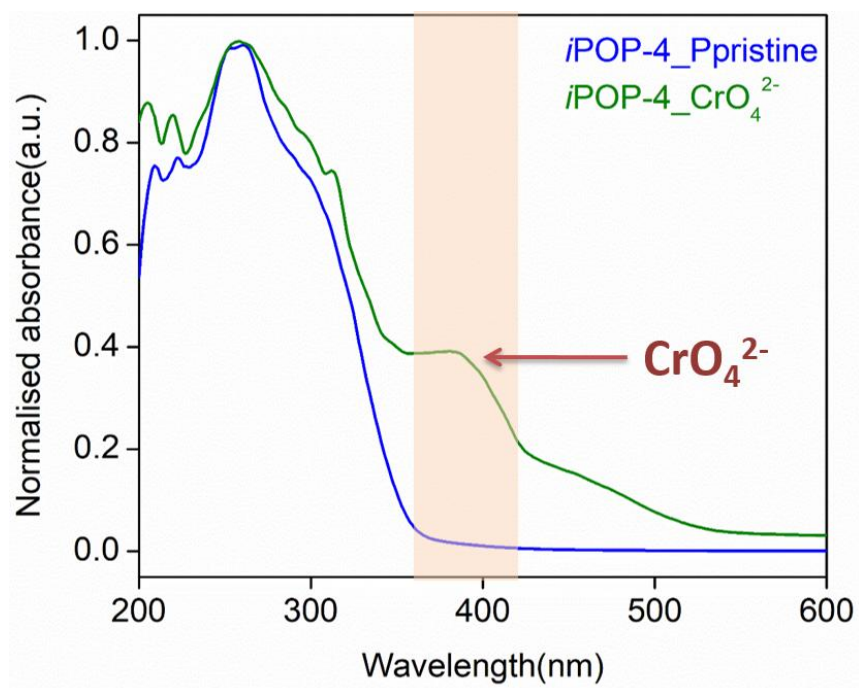
Appendix 5.19. Solid state NMR spectra of after treated phases for *i*POP-3.



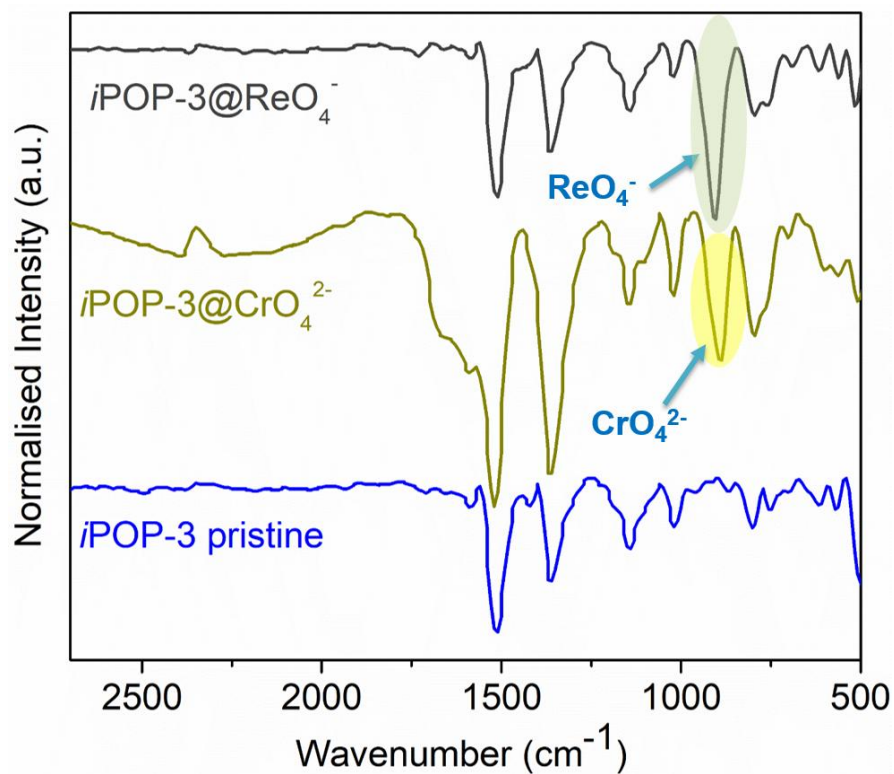
Appendix 5.20. Solid state NMR spectra of after treated phases for *i*POP-4.



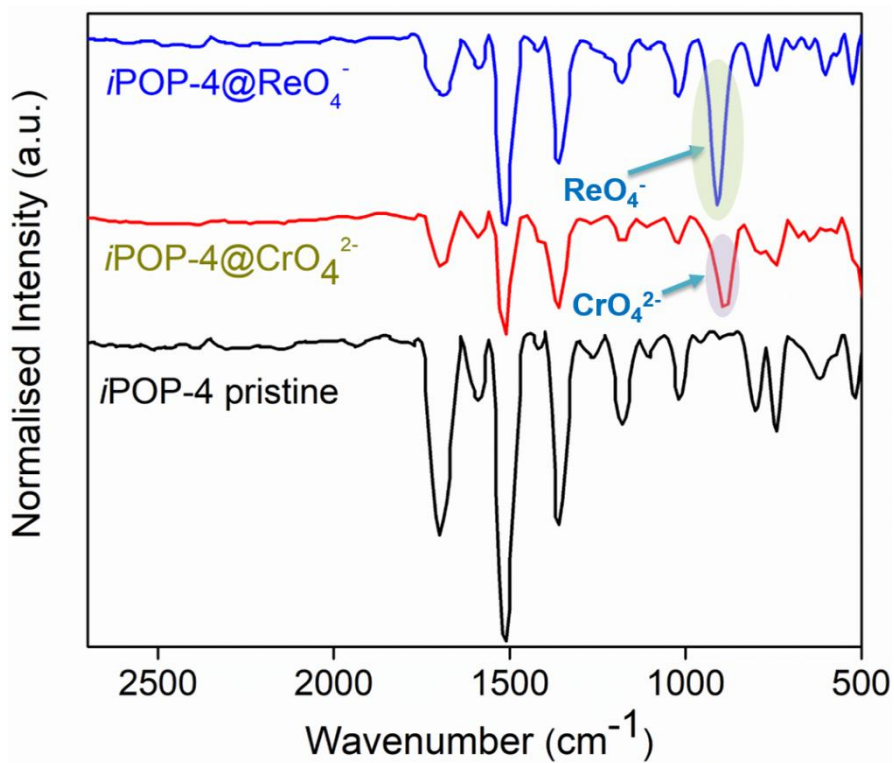
Appendix 5.21. Solid state UV-Vis spectra of *iPOP-3*.



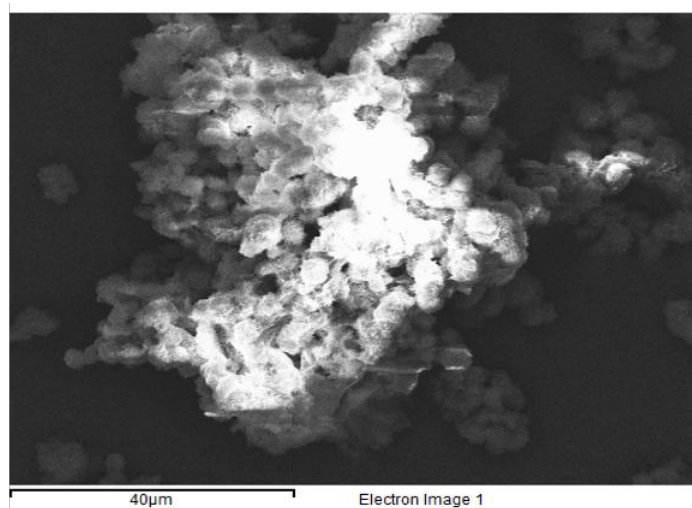
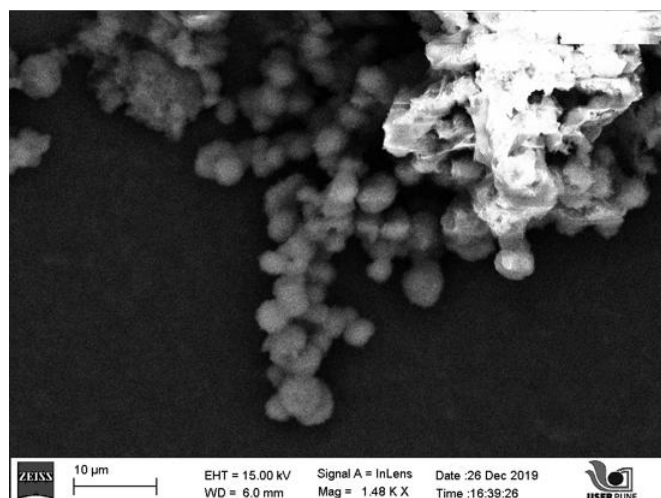
Appendix 5.22. Solid state UV-Vis spectra of *iPOP-4*.



Appendix 5.23. FTIR profiles for oxo-anion occluded phases of *iPOP-3*.

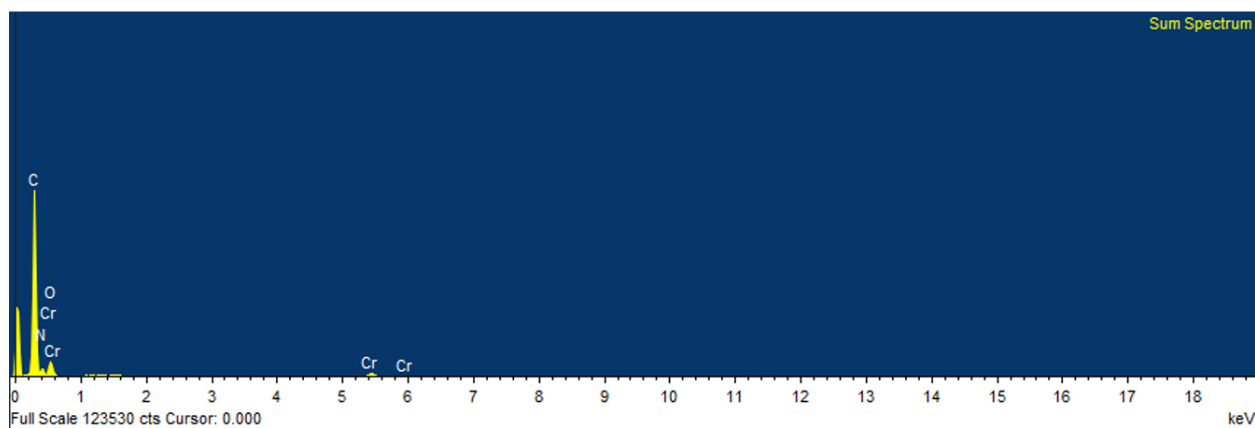


Appendix 5.24. FTIR profiles for oxo-anion occluded phases of *iPOP-4*.

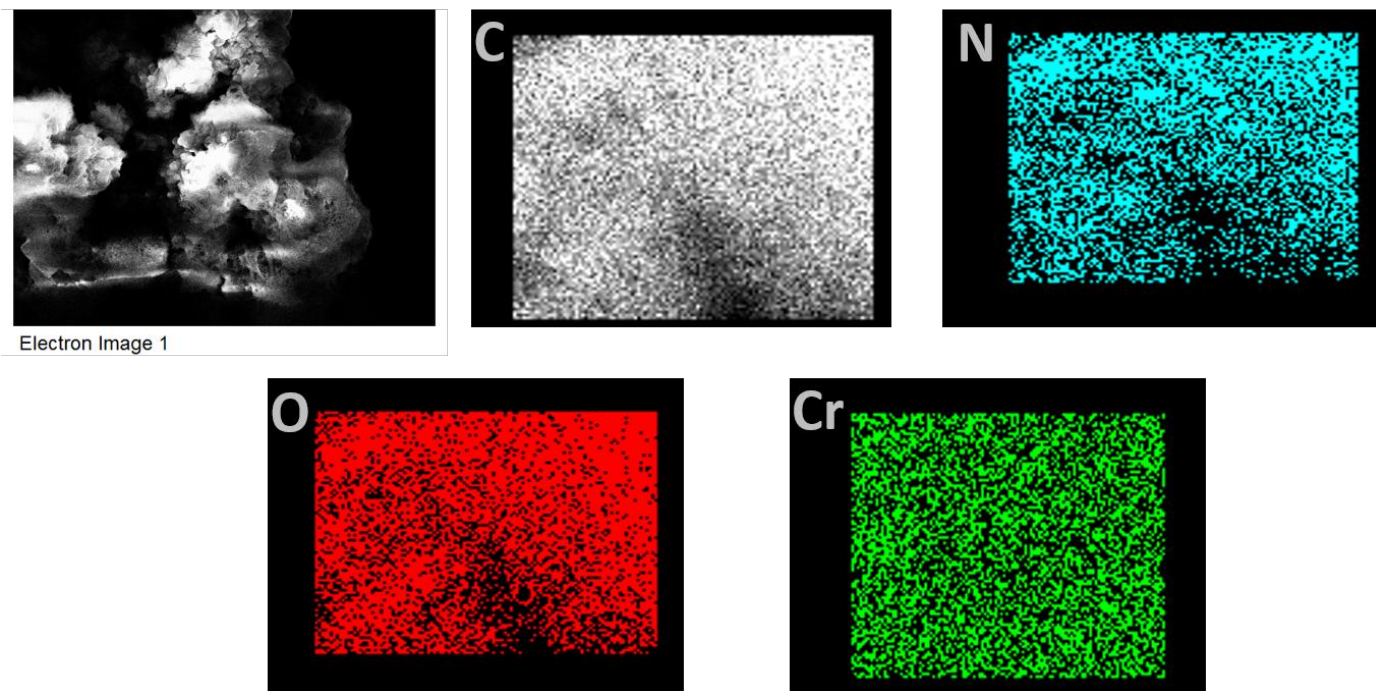


Appendix 5.25. FESEM images of $iPOP-3@CrO_4^{2-}$.

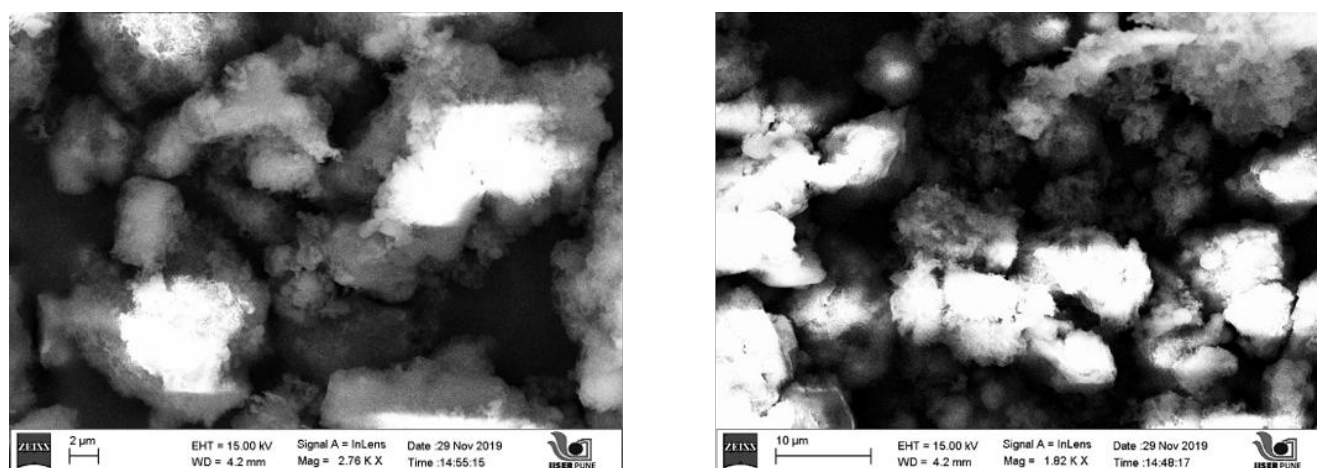
Element	% weight
C	64.09
N	17.15
O	15.31
Cr	3.45
Total	100



Appendix 5.26. Elemental mapping of $iPOP-3$ after CrO_4^{2-} exchange.

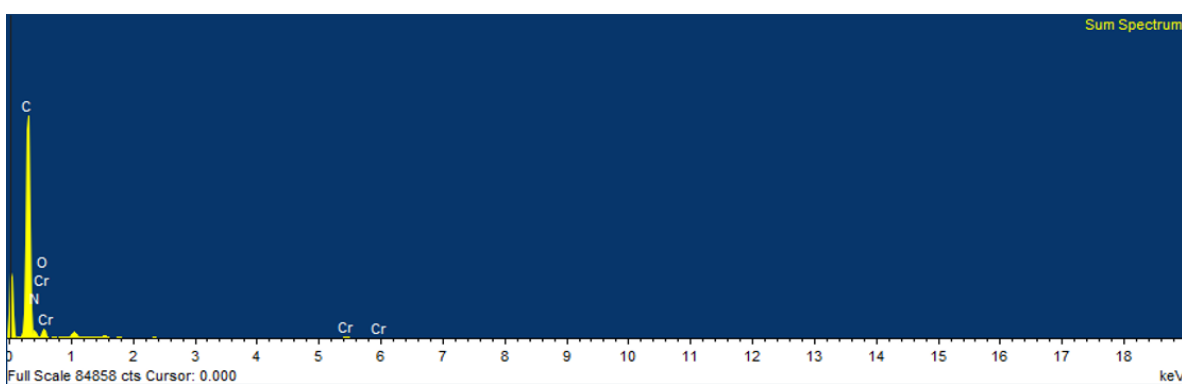


Appendix 5.27. Elemental mapping of *iPOP-3* after CrO_4^{2-} exchange.

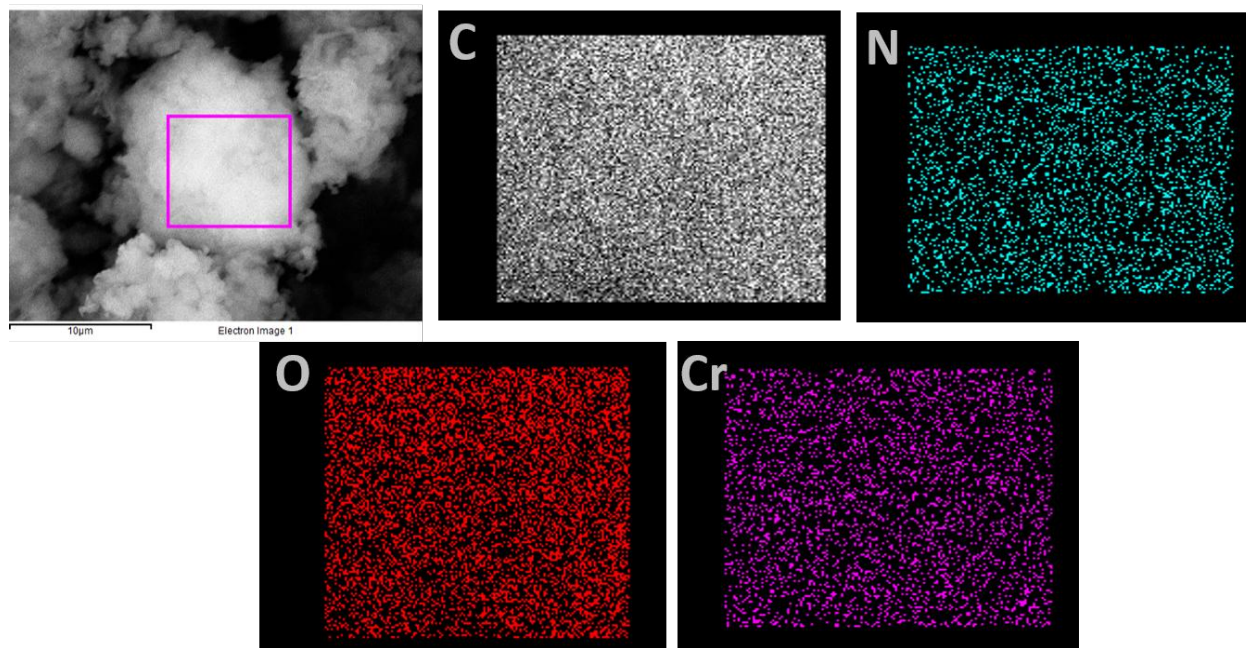


Appendix 5.28. FESEM images of *iPOP-4@CrO₄²⁻*.

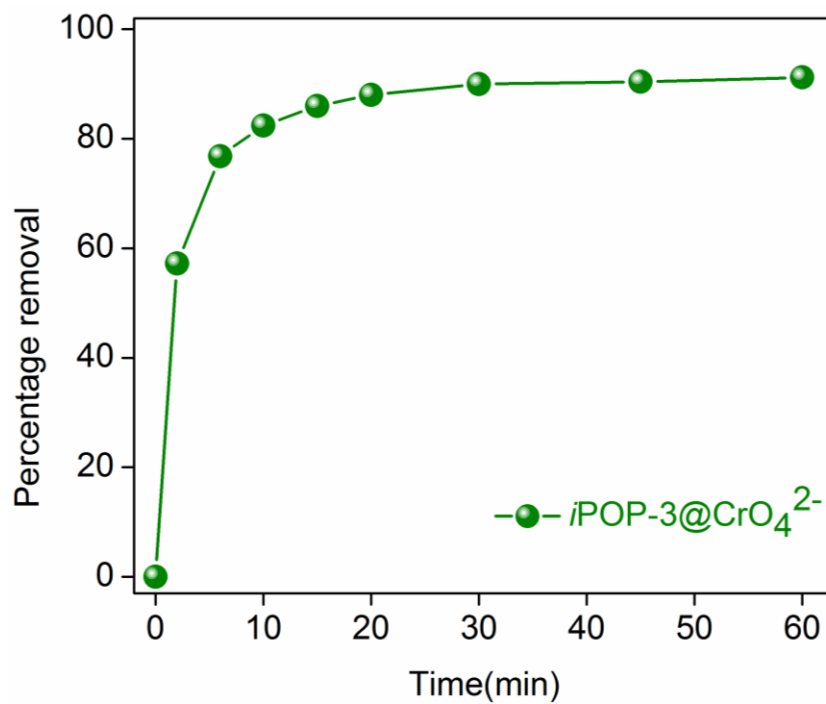
Element	% weight
C	69.67
N	17.22
O	10.74
Cr	2.38
Total	100



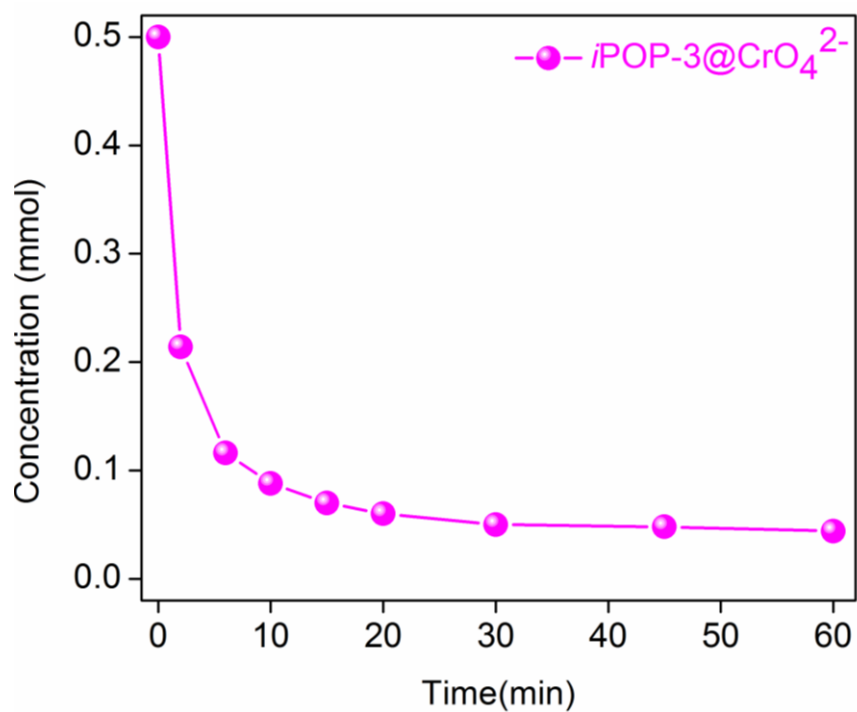
Appendix 5.29. Elemental mapping of *iPOP-4* after CrO_4^{2-} exchange.



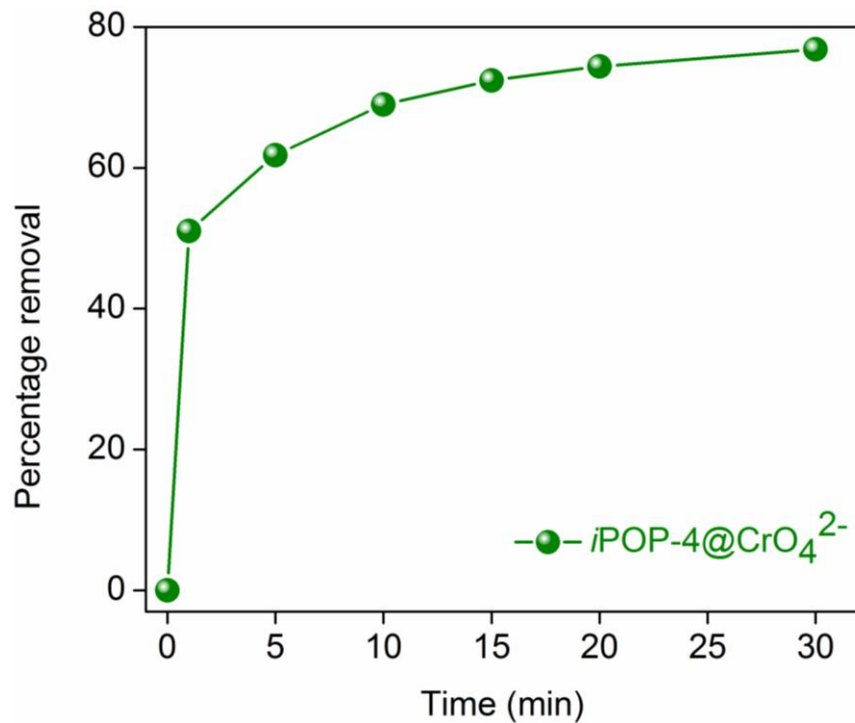
Appendix 5.30. Elemental mapping of *iPOP-4* after CrO_4^{2-} exchange.



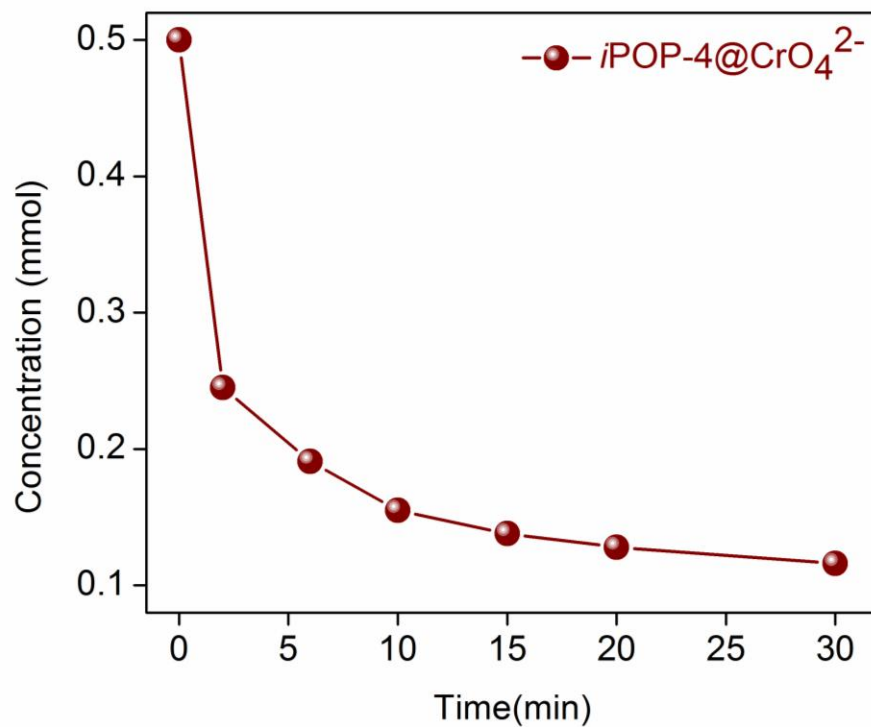
Appendix 5.31. Percentage removal of $iPOP-3@CrO_4^{2-}$.



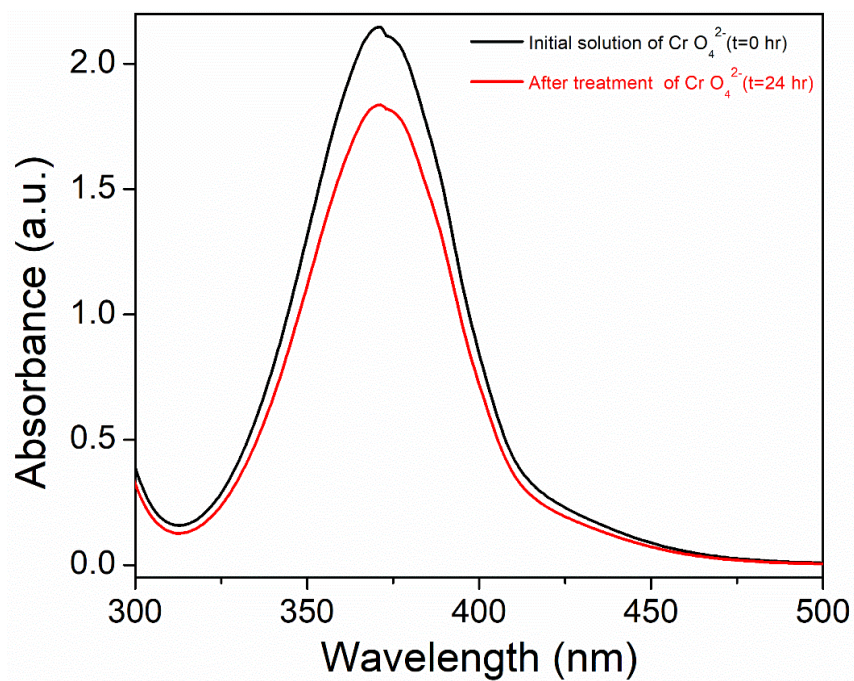
Appendix 5.32. Concentration removal with time for $iPOP-3@CrO_4^{2-}$.



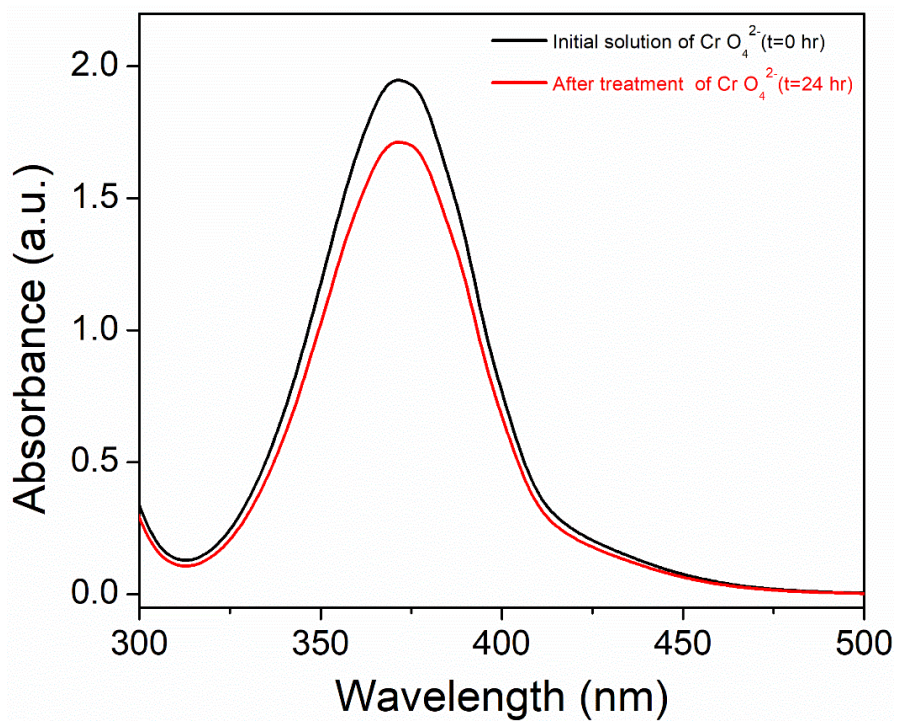
Appendix 5.33. Percentage removal of $iPOP-4@CrO_4^{2-}$.



Appendix 5.34. Concentration removal with time for $iPOP-4@CrO_4^{2-}$.

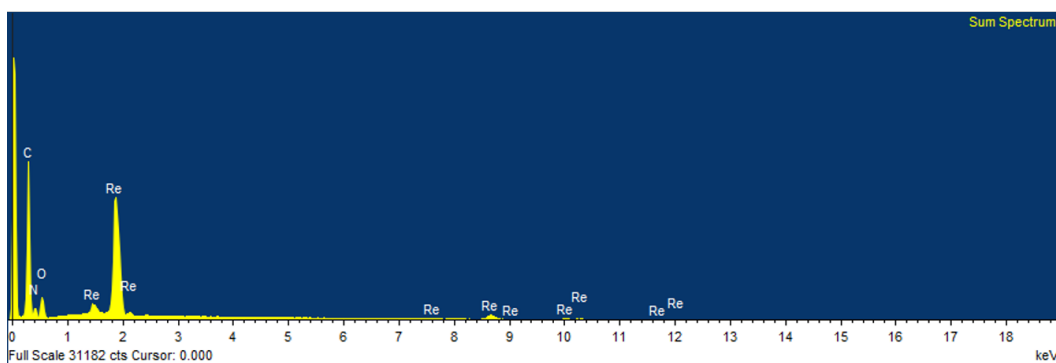


Appendix 5.35. Saturation uptake capacity for *iPOP-3@CrO₄²⁻*.



Appendix 5.36. Saturation uptake capacity for *iPOP-4@CrO₄²⁻*.

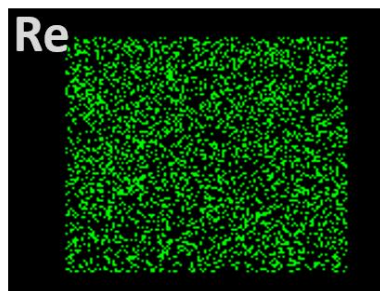
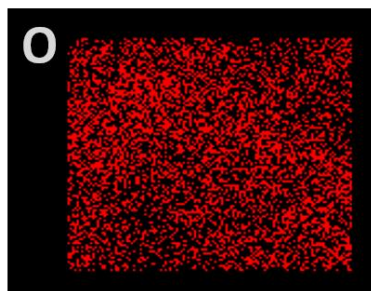
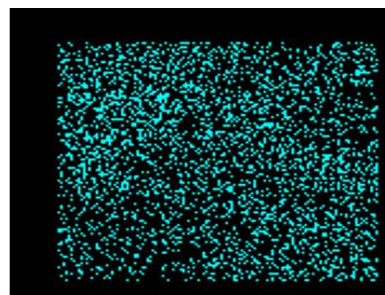
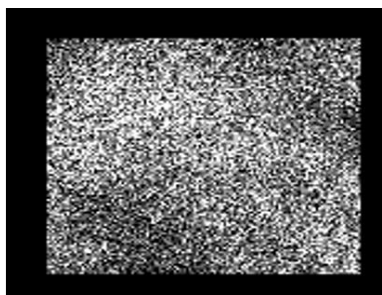
Element	% weight
C	44.87
N	8.60
O	7.99
Re	38.45
Total	100



Appendix 5.37. Elemental mapping of *i*POP-3 after ReO_4^- exchange.

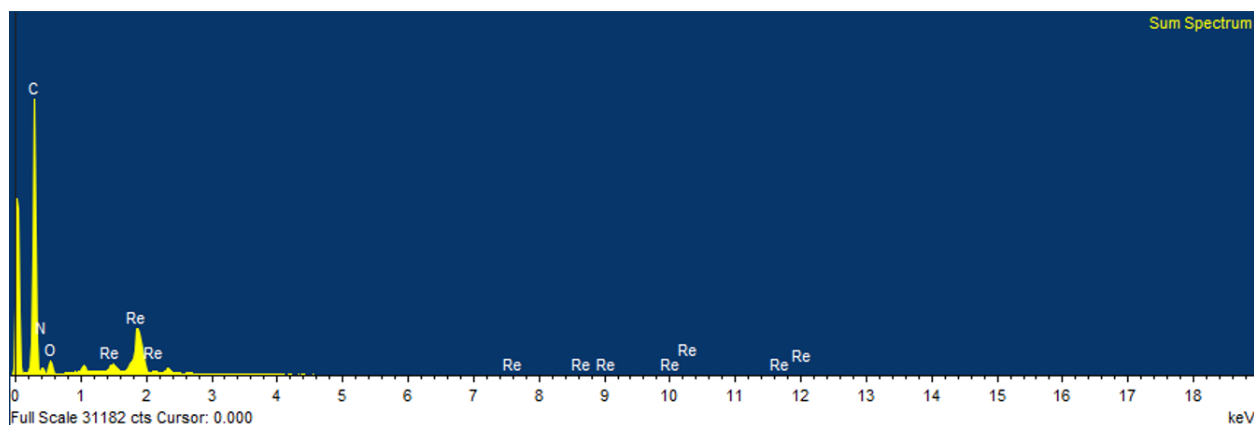


Electron Image 1

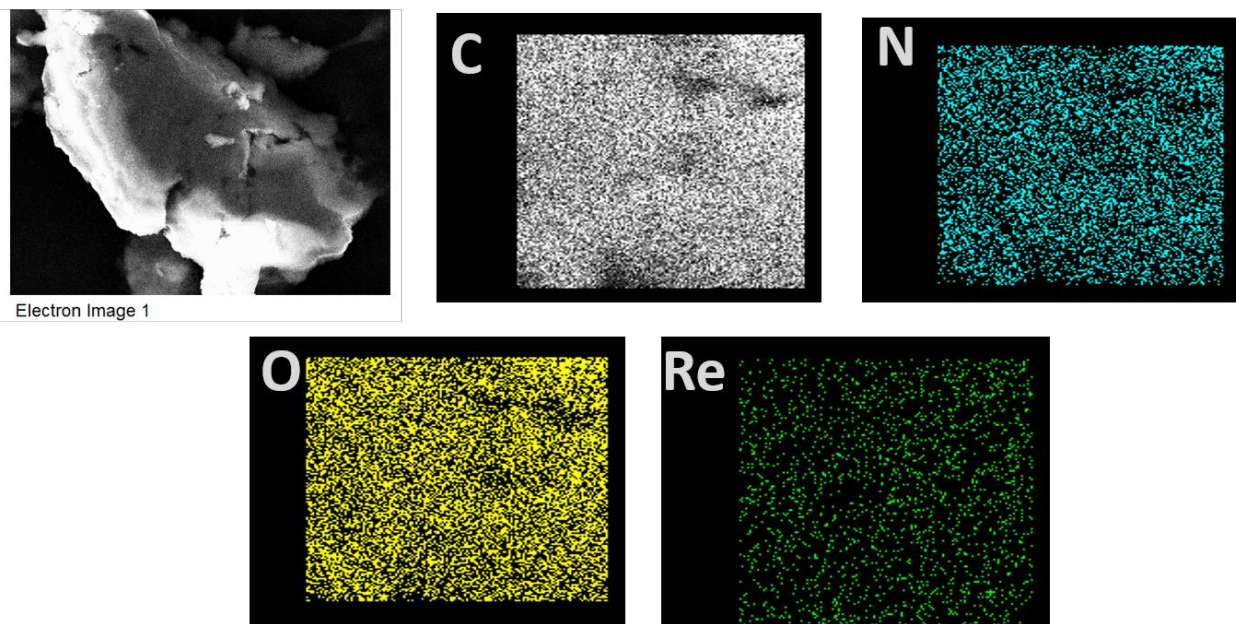


Appendix 5.38. Elemental mapping of *i*POP-3 after ReO_4^- exchange.

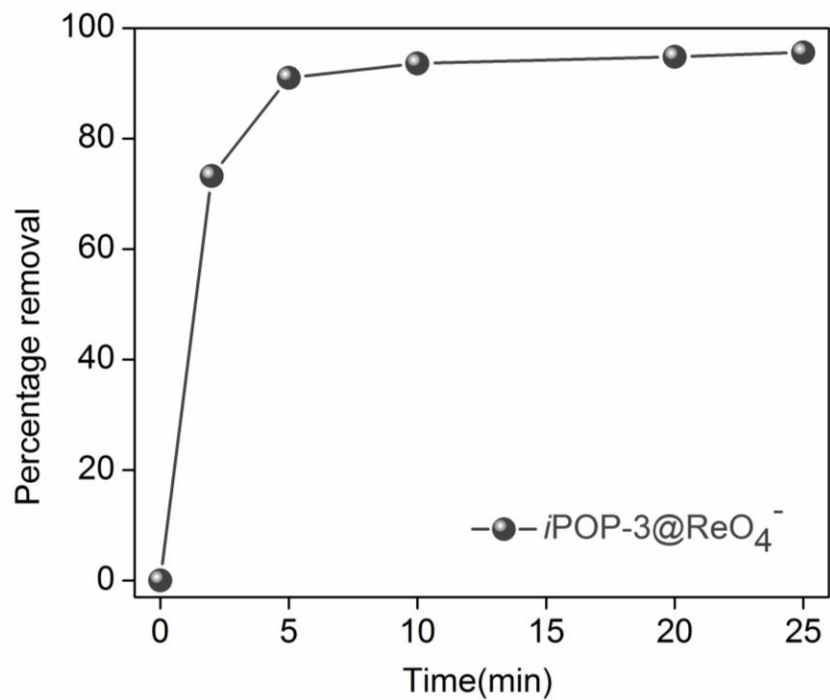
Element	% weight
C	67.40
N	7.71
O	8.30
Re	16.59
Total	100



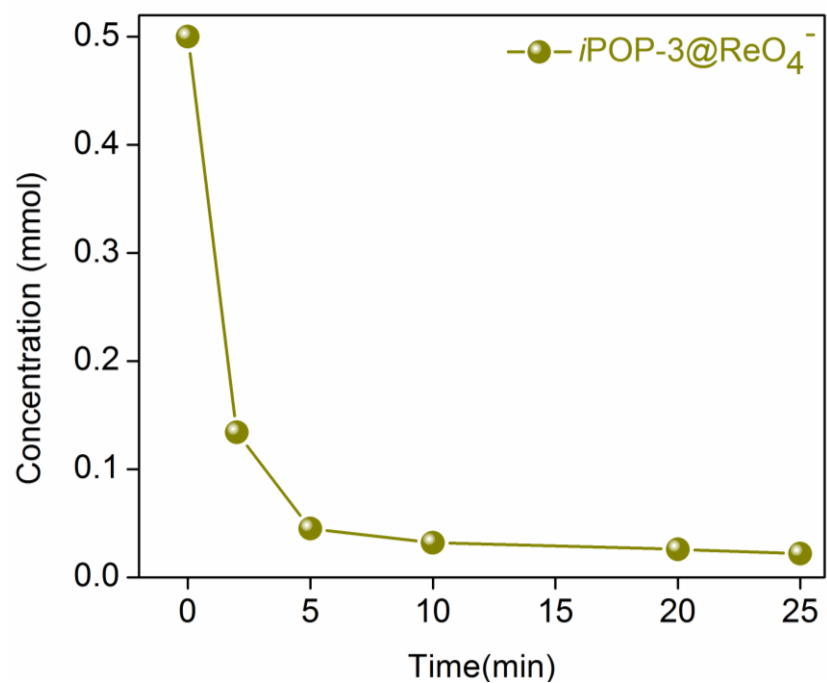
Appendix 5.39. Elemental mapping of *iPOP-4* after ReO_4^- exchange.



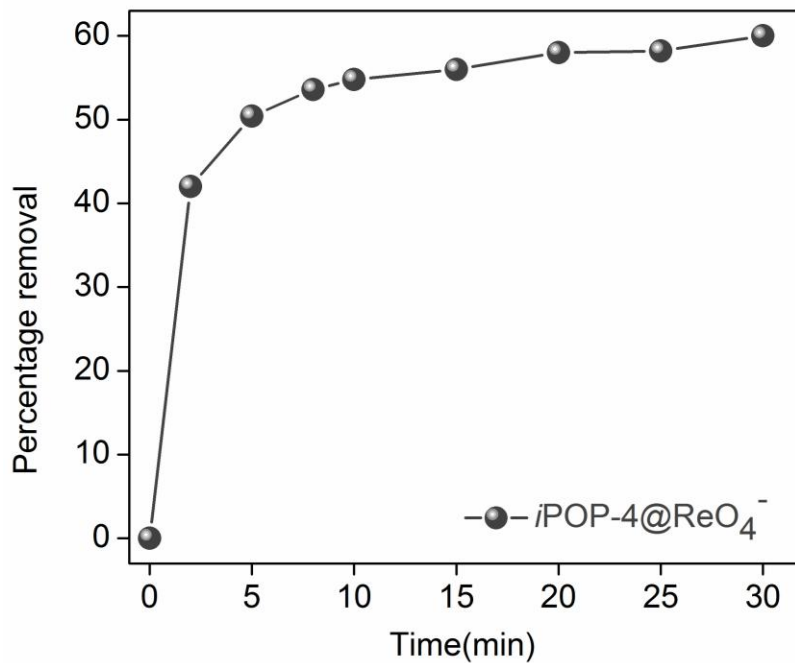
Appendix 5.40. Elemental mapping of *iPOP-4* after ReO_4^- exchange.



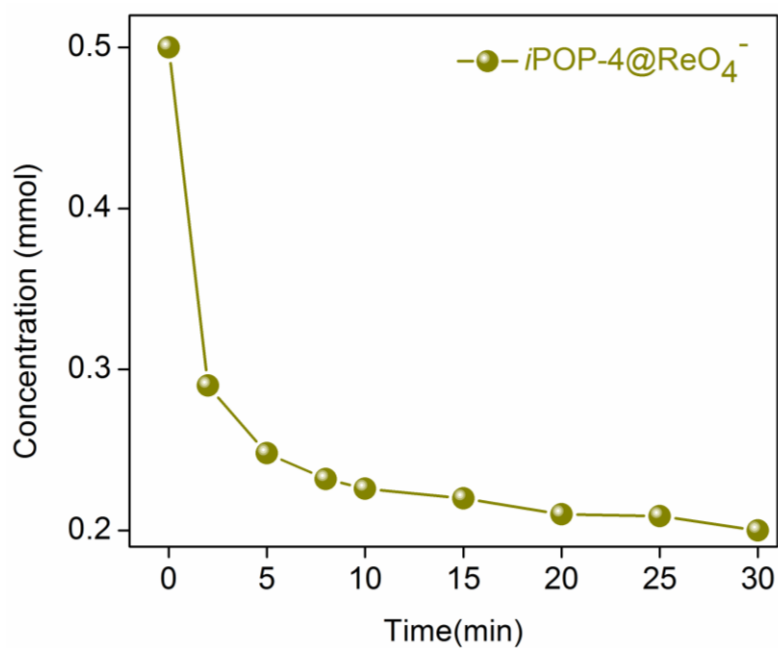
Appendix 5.41. Percentage removal of $iPOP-3@ReO_4^-$.



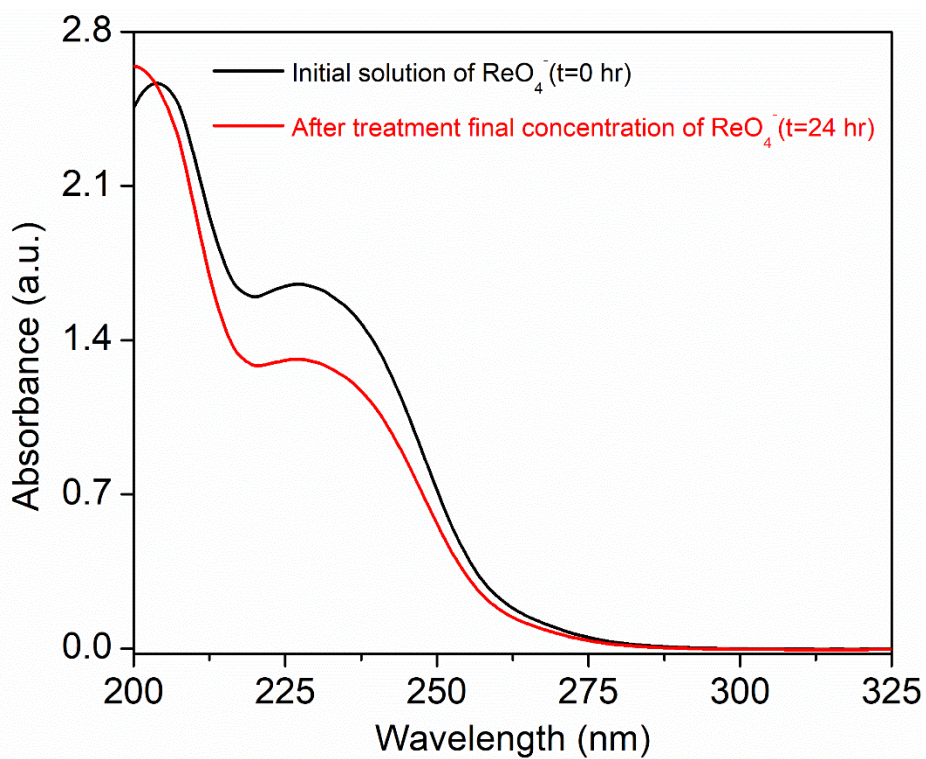
Appendix 5.42. Concentration removal with time for $iPOP-3@ReO_4^-$.



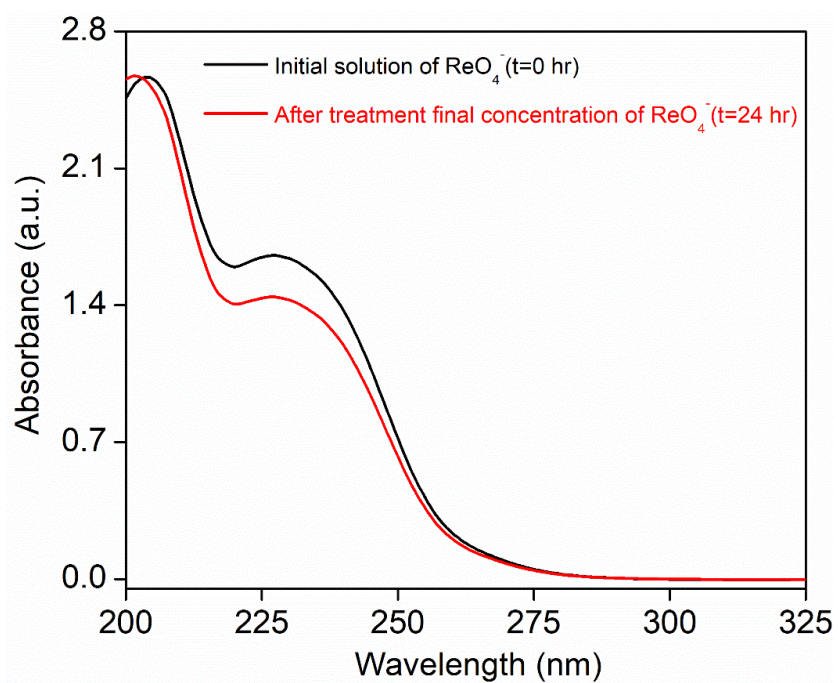
Appendix 5.43. Percentage removal of $iPOP-4@ReO_4^-$.



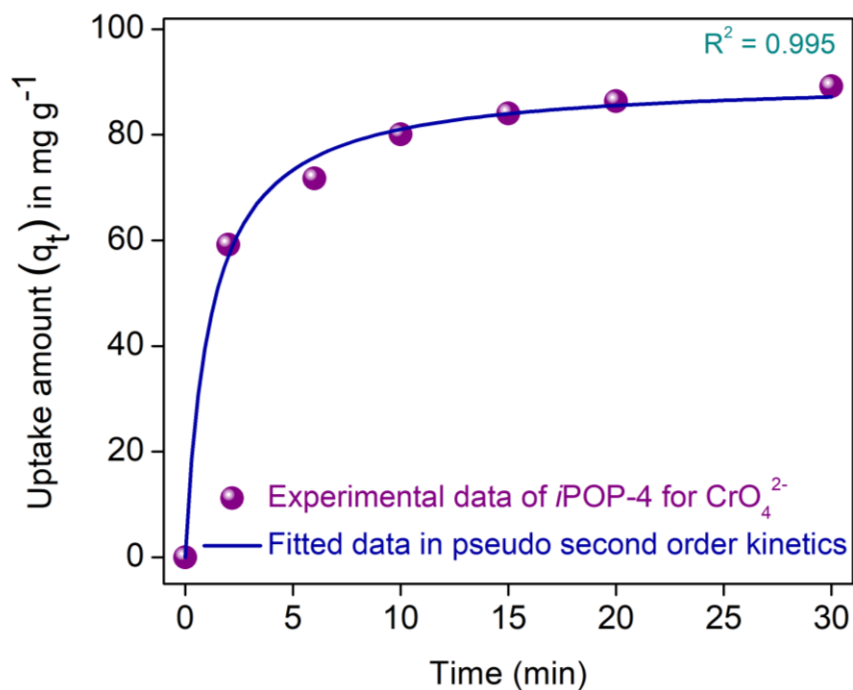
Appendix 5.44. Concentration removal with time for $iPOP-4@ReO_4^-$.



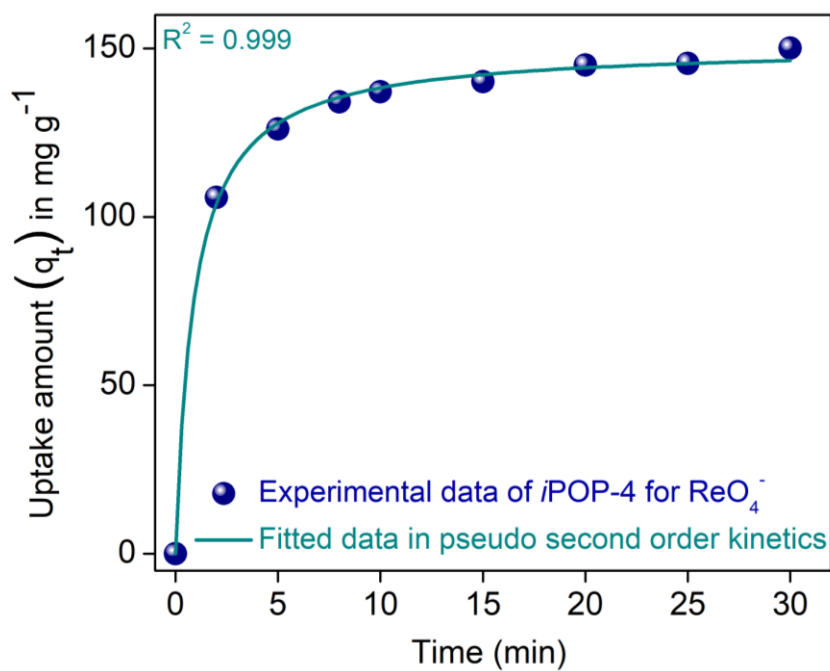
Appendix 5.45. Saturation uptake capacity for $i\text{POP-3@ReO}_4^-$.



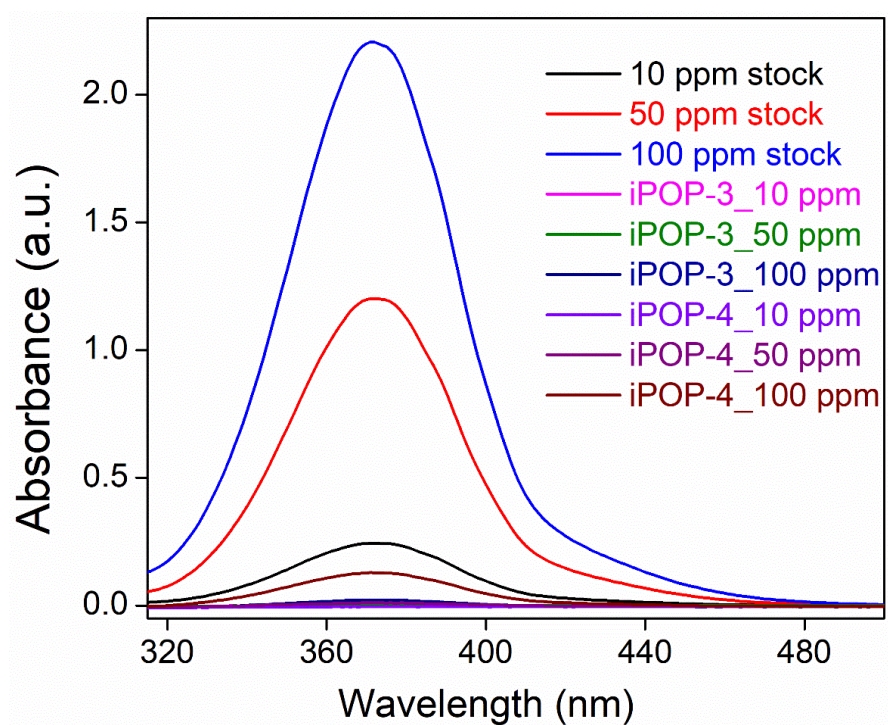
Appendix 5.46. Saturation uptake capacity for $i\text{POP-4@ReO}_4^-$.



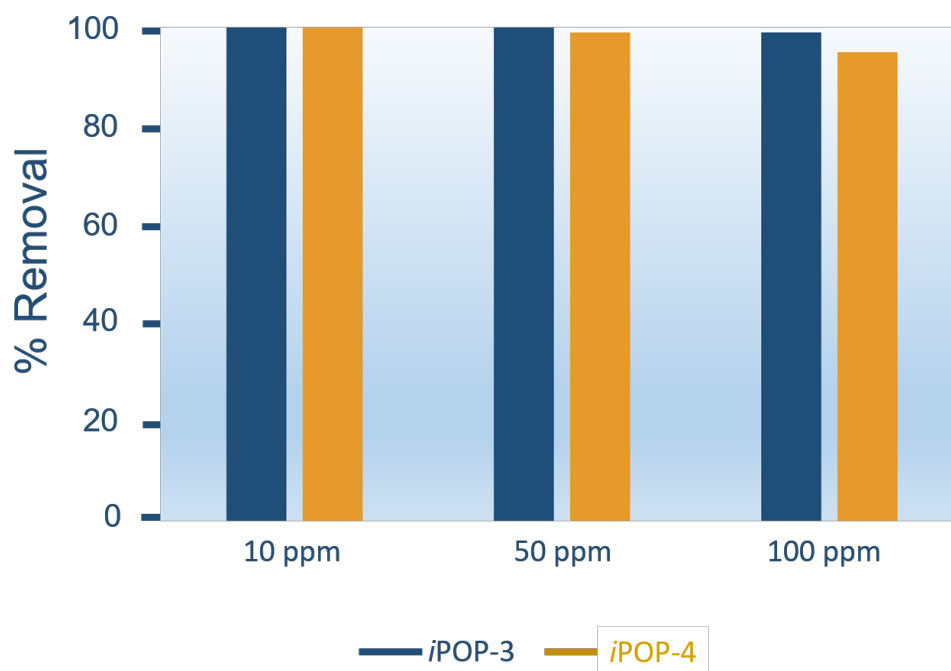
Appendix 5.47. Kinetic study of CrO_4^{2-} ion capture with *iPOP-4*.



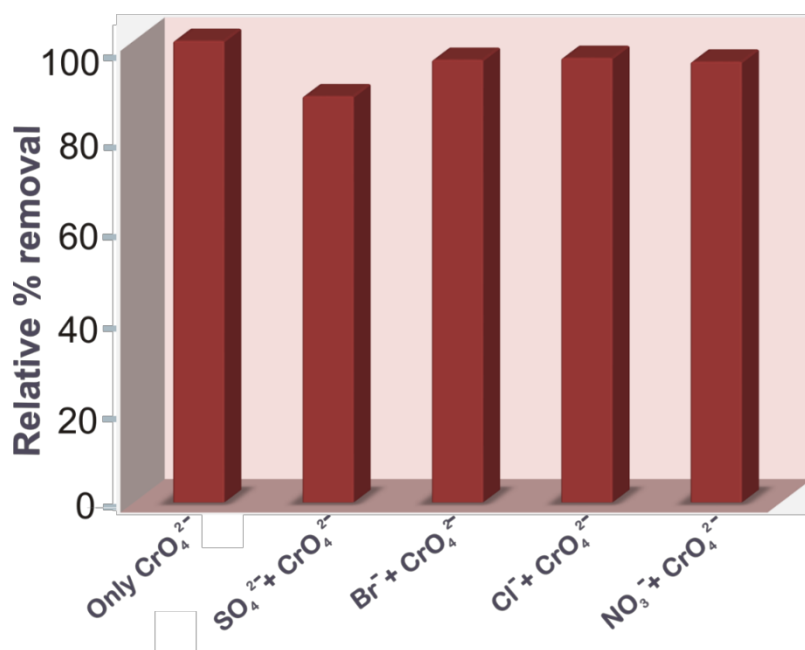
Appendix 5.48. Kinetic study of ReO_4^- ion capture with *iPOP-4*.



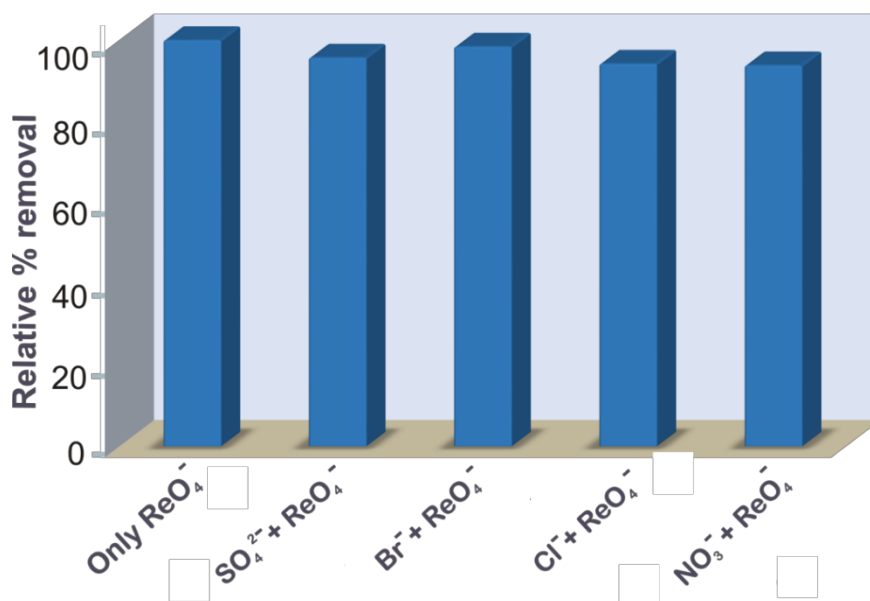
Appendix 5.49. Kinetic study of CrO₄²⁻ ion capture with *iPOP-3* and *iPOP-4*.



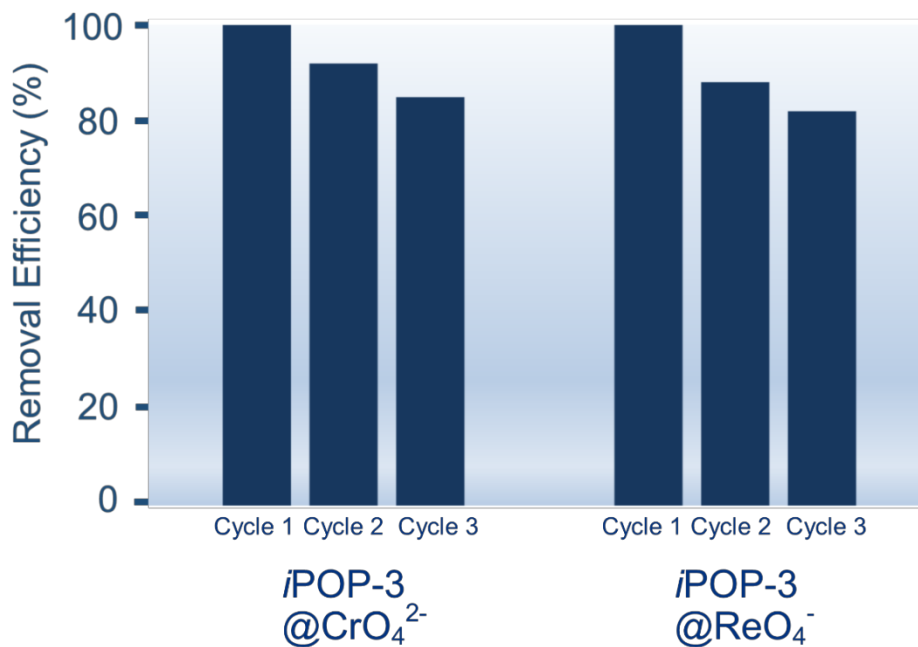
Appendix 5.50. Kinetic study of CrO₄²⁻ ion capture with *iPOP-3* and *iPOP-4*.



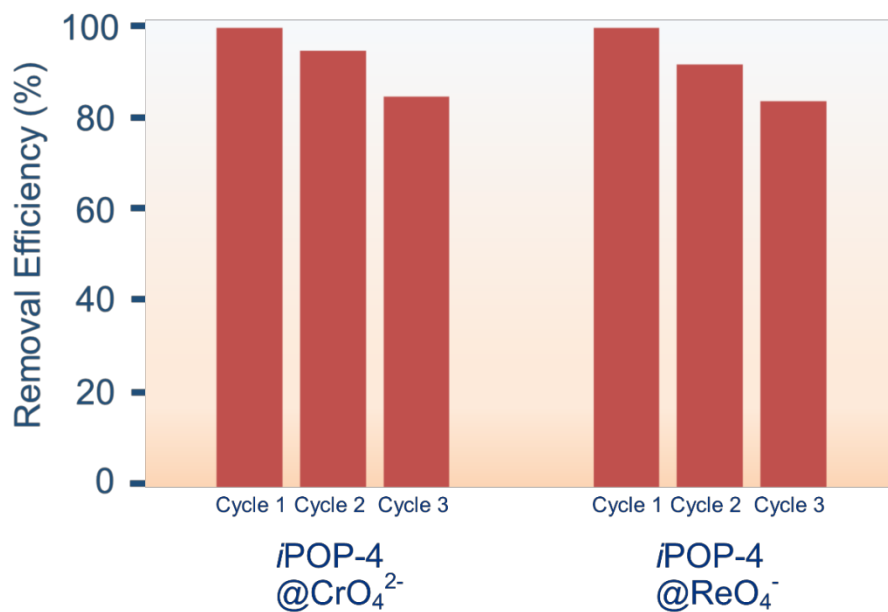
Appendix 5.51. Bar diagram for CrO_4^{2-} removal efficiency of *iPOP-4* in presence of Br^- , Cl^- , NO_3^- and SO_4^{2-} ions.



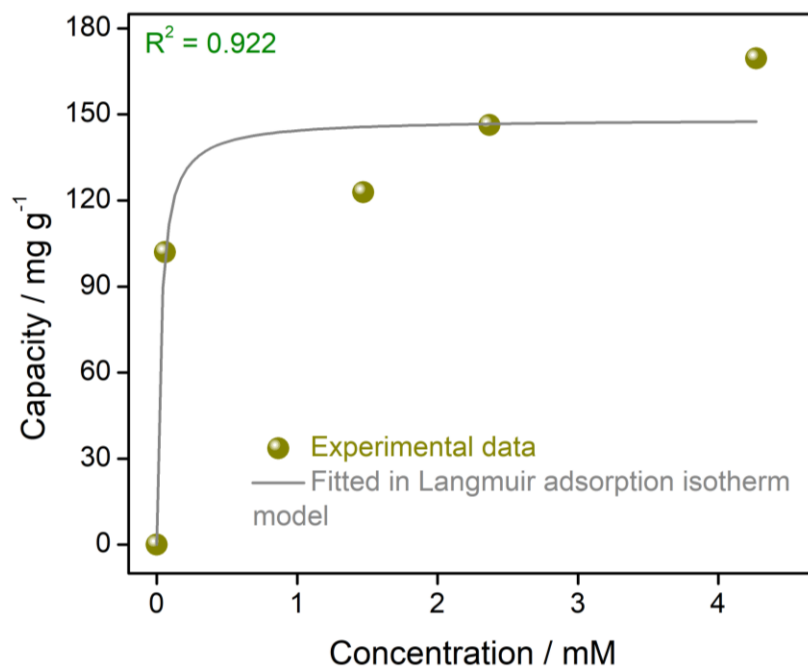
Appendix 5.52. Bar diagram for ReO_4^- removal efficiency of *iPOP-4* in presence of Br^- , Cl^- , NO_3^- and SO_4^{2-} ions.



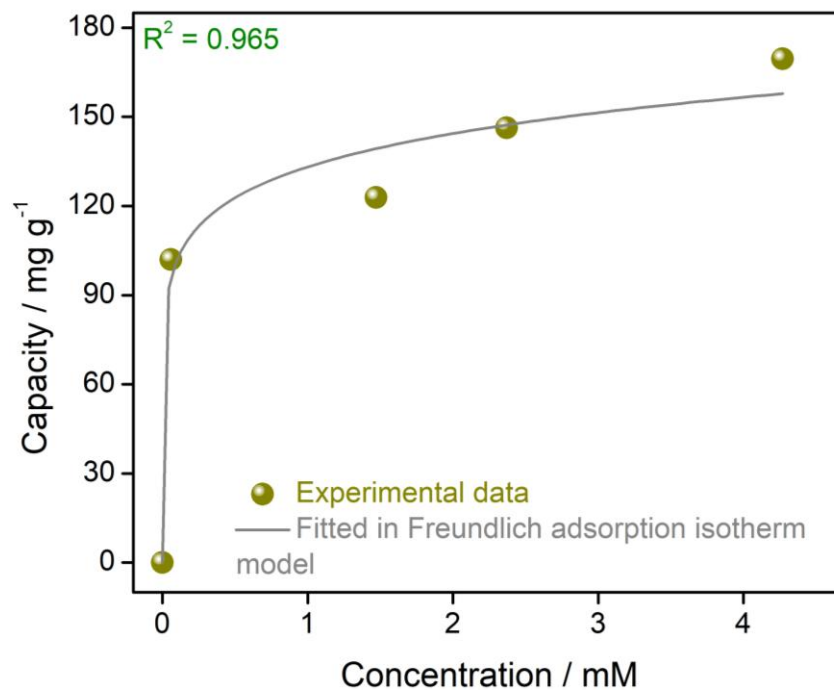
Appendix 5.53. Recyclability for *iPOP-3*@CrO₄²⁻ and *iPOP-3*@ReO₄⁻.



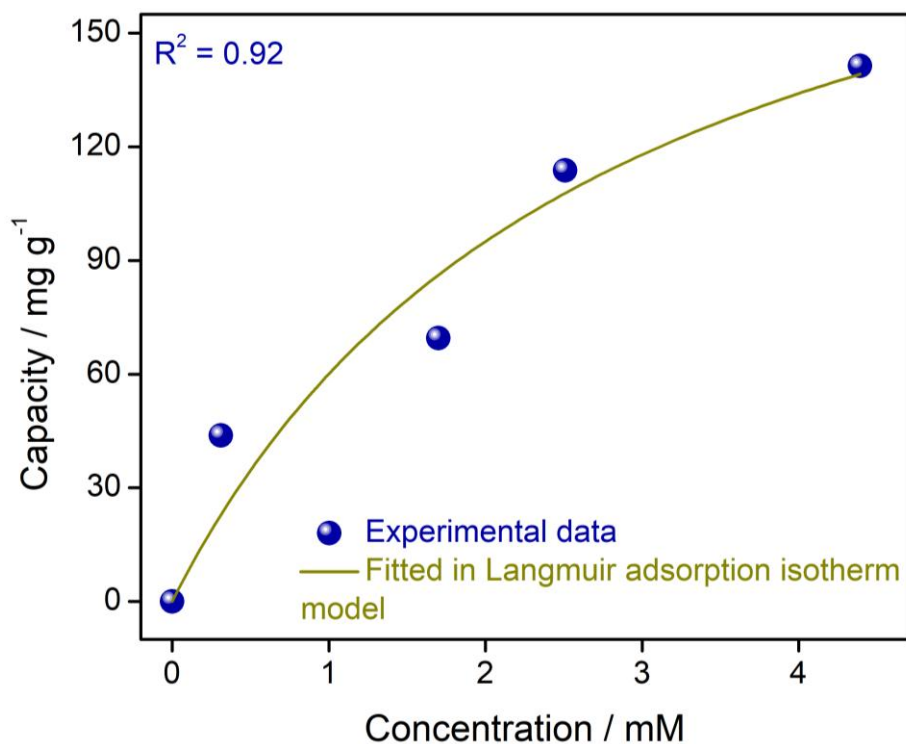
Appendix 5.54. Recyclability for *iPOP-4*@CrO₄²⁻ and *iPOP-4*@ReO₄⁻.



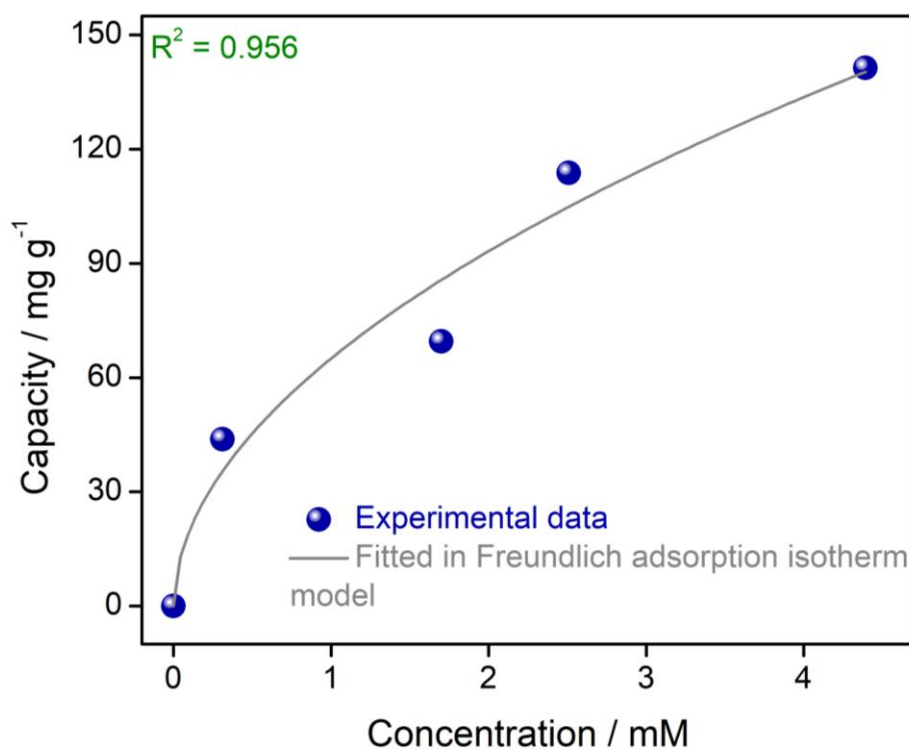
Appendix 5.55. Langmuir model of CrO_4^{2-} ion capture study with *iPOP-3*.



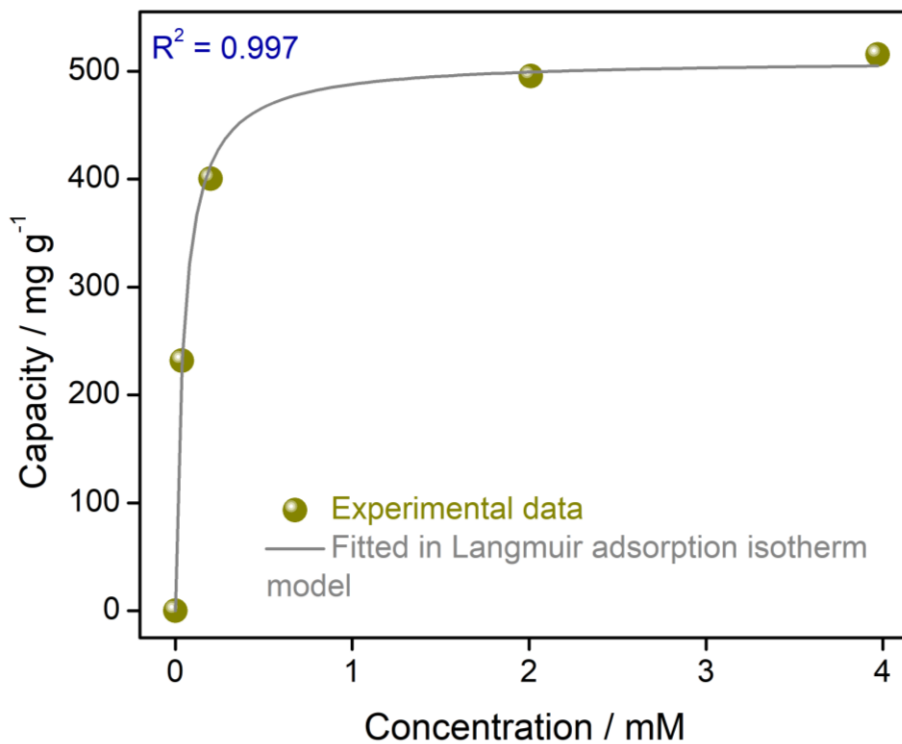
Appendix 5.56. Freundlich model of CrO_4^{2-} ion capture study with *iPOP-3*.



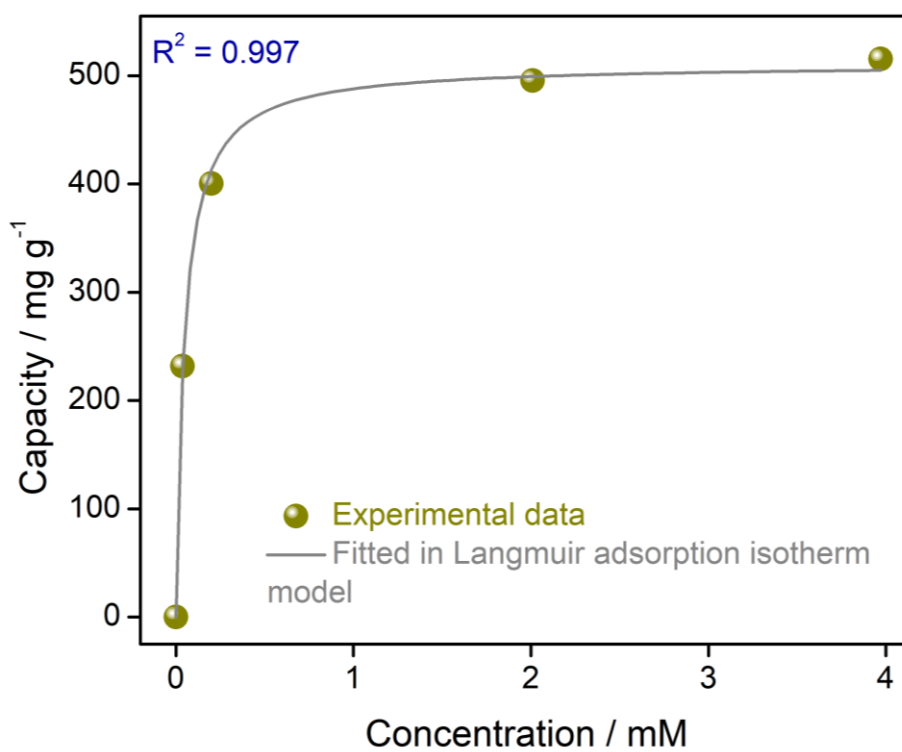
Appendix 5.57.Langmuir model of CrO_4^{2-} ion capture study with *iPOP-4*.



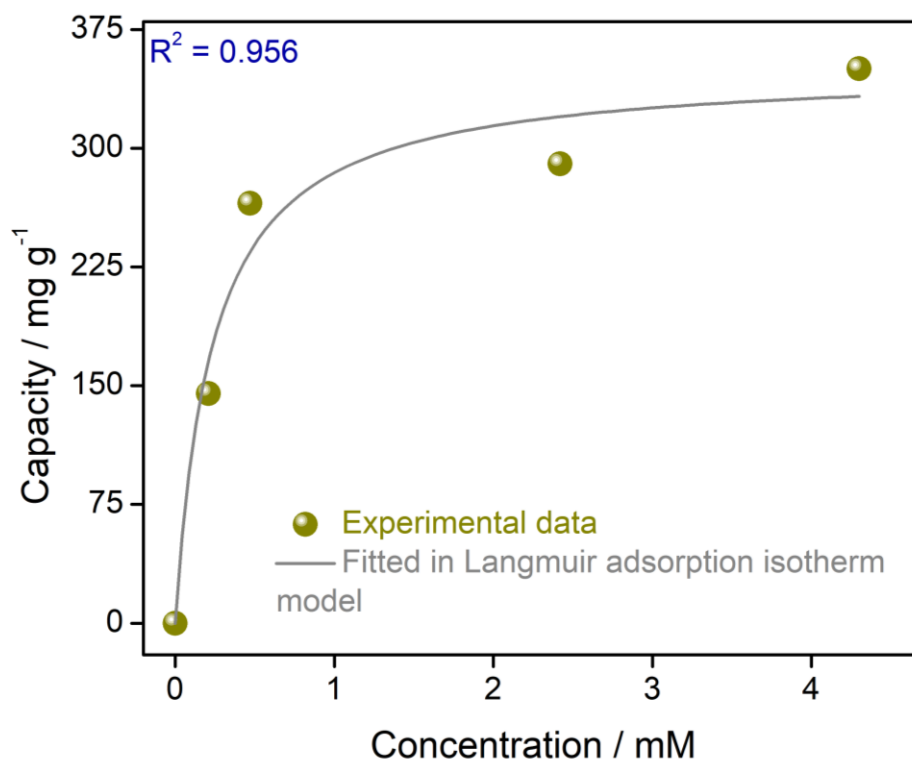
Appendix 5.58.Freundlich model of CrO_4^{2-} ion capture study with *iPOP-4*.



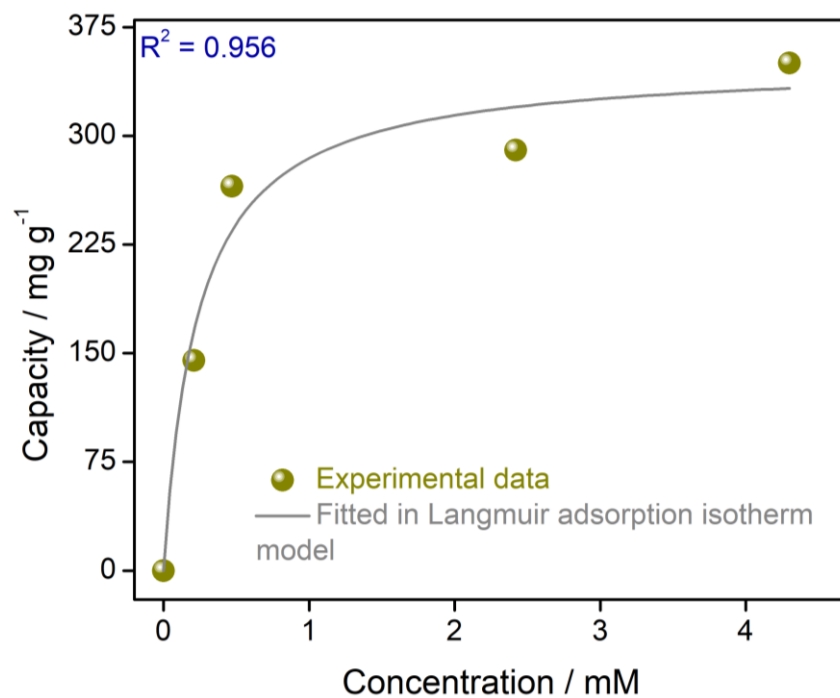
Appendix 5.59. Langmuir model of ReO_4^- ion capture study with *iPOP-3*.



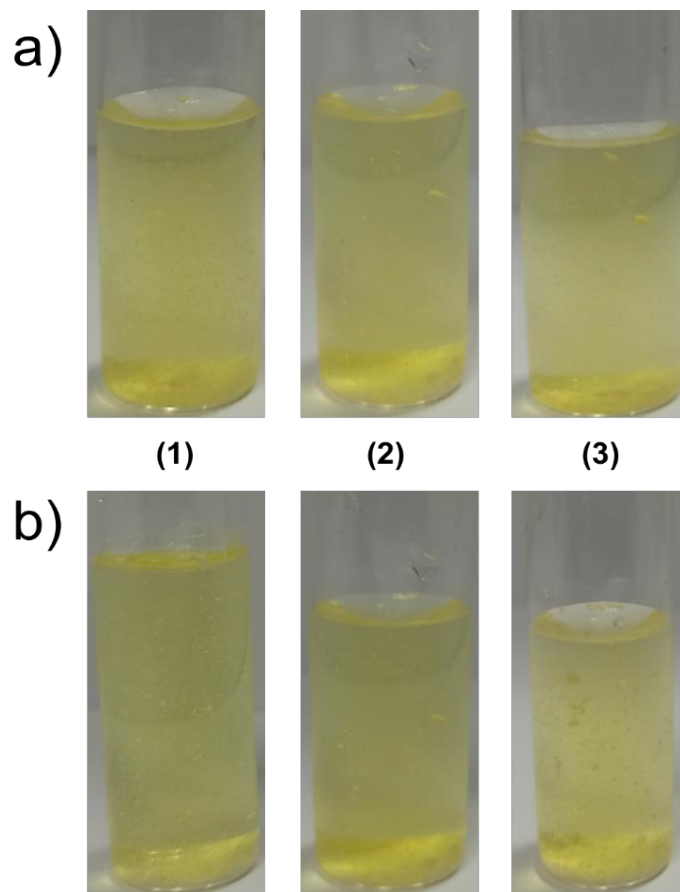
Appendix 5.60. Freundlich model of ReO_4^- ion capture study with *iPOP-3*.



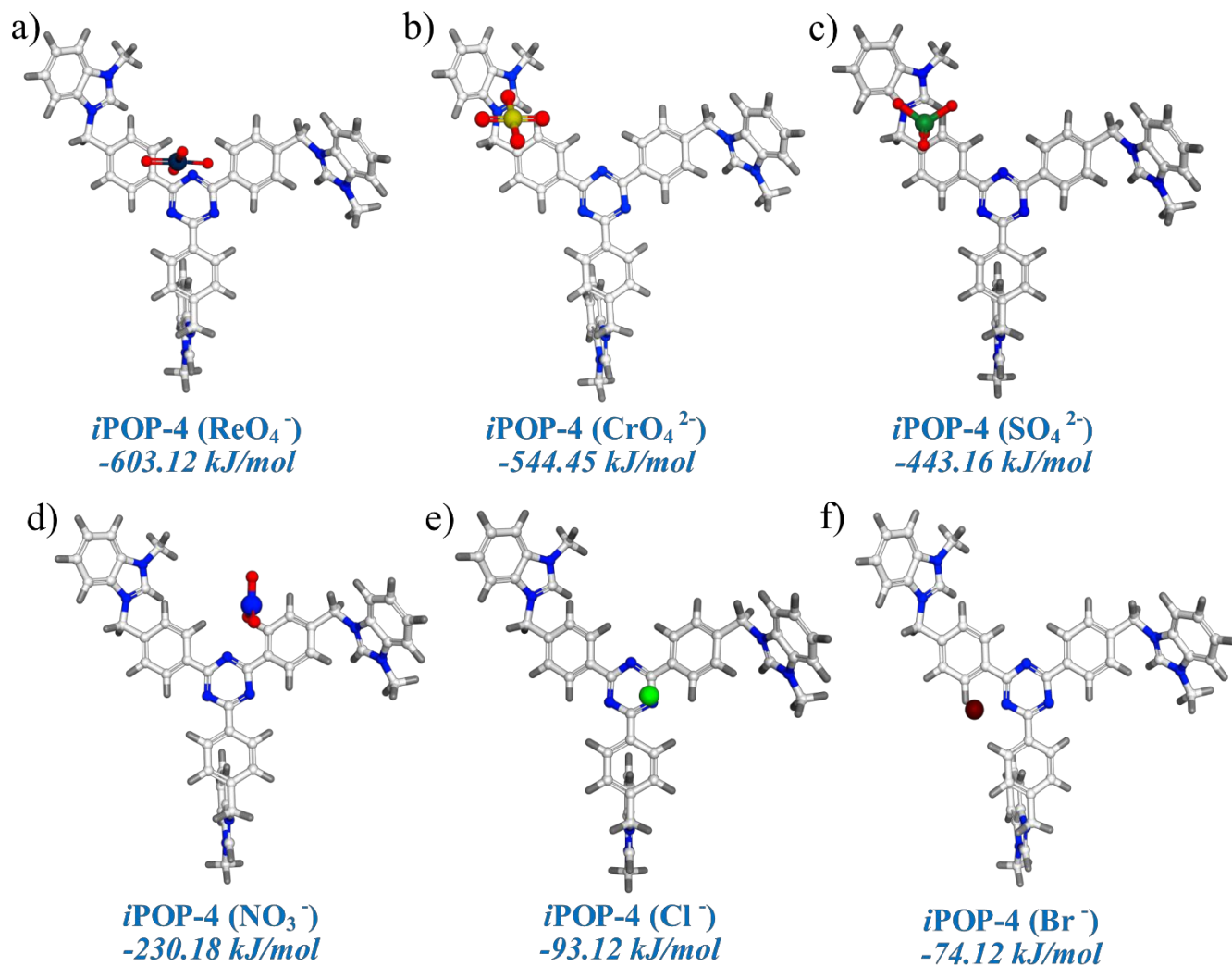
Appendix 5.61. Langmuir model of ReO_4^- ion capture study with *iPOP-4*.



Appendix 5.62. Freundlich model of ReO_4^- ion capture study with *iPOP-4*.

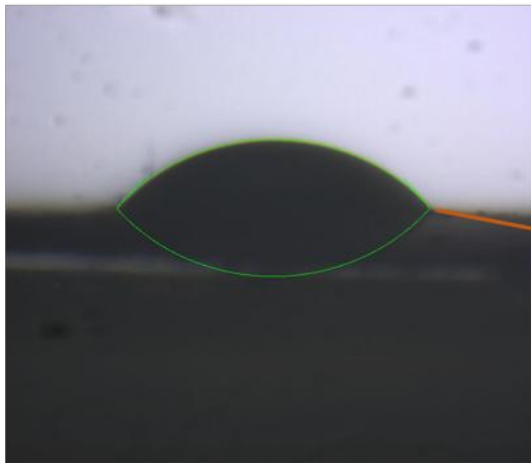


Appendix 5.63. CrO_4^{2-} anion release cycles by (a) *iPOP-3*, (b) *iPOP-4*.



Appendix 5.64. Optimized structures of monomeric unit of *iPOP-4* with different binding anions and the corresponding binding energies calculated based on DFT-DMOL3-B3LYP method, (a) *iPOP-4*@ ReO_4^- , (b) *iPOP-4*@ CrO_4^{2-} , (c) *iPOP-4*@ SO_4^{2-} , (d) *iPOP-4*@ NO_3^- , (e) *iPOP-4*@ Cl^- , (f) *iPOP-4*@ Br^- .

a)



Low Bond Axisymmetric Drop Shape Analysis

DROP PARAMETERS

Parameter	Value	Optimize
b [pixels]	423	<input checked="" type="checkbox"/>
c [m-2]	water	<input type="checkbox"/>
x0 [pixels]	766	<input checked="" type="checkbox"/>
y0 [pixels]	299	<input checked="" type="checkbox"/>
h [pixels]	132	<input checked="" type="checkbox"/>
d [pixels]	768	<input type="checkbox"/>

Relative approximation: 7 %

DROP PROPERTIES

Contact angle (Canvas): 48.410

Contact angle subpixel:

Drop Volume: 2.86E0 mm³ Drop Surface: 9.28E0 mm²

Surface of contact: 7.80E0 mm²

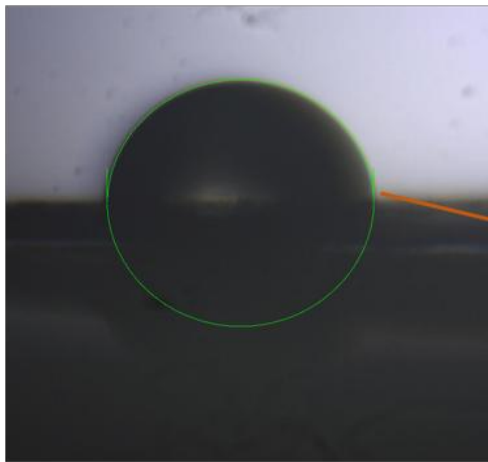
OPTIMIZATION

Region Energy Gradient Energy

Unified 50 % gradient

Table Settings About Close

b)



Low Bond Axisymmetric Drop Shape Analysis

DROP PARAMETERS

Parameter	Value	Optimize
b [pixels]	306	<input checked="" type="checkbox"/>
c [m-2]	water	<input type="checkbox"/>
x0 [pixels]	527	<input checked="" type="checkbox"/>
y0 [pixels]	181	<input checked="" type="checkbox"/>
h [pixels]	269	<input checked="" type="checkbox"/>
d [pixels]	768	<input type="checkbox"/>

Relative approximation: 43 %

DROP PROPERTIES

Contact angle (Canvas): 89.247

Contact angle subpixel:

Drop Volume: 6.69E0 mm³ Drop Surface: 1.36E1 mm²

Surface of contact: 7.23E0 mm²

OPTIMIZATION

Region Energy Gradient Energy

Unified 50 % gradient

Table Settings About Close

Appendix 5.65. Water contact angle measurements for (a) *iPOP-3* and (b) *iPOP-4*.

Appendix Table 1. A comparison table of CrO_4^{2-} capture (CrO_4^{2-} mg/g) with some well-studied examples in the literature (N.D.: Not done)

Compound	Capacity (mg/g)	Selectivity	Reference
UTSA-74 (MOF^+)	796	N.D.	6b
iMOF-2C	476.3	Cl^- , NO_3^- , Br^- , SO_4^{2-} , ClO_4^-	14d
TJU-1	279	Cl^- , HCO_3^- , NO_3^- , SO_4^{2-}	22
MOR-2	263	Cl^- , NO_3^- , HCO_3^- , etc.	6d
iPOP-3	170	Cl^-, NO_3^-, Br^-, SO_4^{2-}	This Work
iPOP-4	141	Cl^-, NO_3^-, Br^-, SO_4^{2-}	This Work
Compound-1	133	Cl^- , NO_3^- , Br^- , SO_4^{2-}	14c
Fe nanoparticles	109	N.D.	23
ED-rGO	100	N.D.	24
1- NO_3	82.5	NO_3^- , CO_3^{2-}	25
Zn-Co-SLUG-35	68.5	NO_3^- , SO_4^{2-}	26
1- ClO_4	62.9	halide anions	27
SLUG-21	60	NO_3^- , CO_3^{2-}	28
Polyaniline	18.1	N.D.	29

Appendix Table 2. A comparison table of ReO_4^- capture (ReO_4^- mg/g) with some well-studied examples in the literature (N.D.: Not done)

Compound	Capacity (mg/g)	Selectivity	Reference
PQA-pN(Me)2Py-Cl	1127	NO_3^- , SO_4^{2-}	11a
PQA-Py-Cl	849	NO_3^- , SO_4^{2-}	11a
Ag(4,4-bipyridine) NO_3	786	N.D.	30
Th-MOF	807	Cl^- , OAc^- , SO_4^{2-}	31
iMOF-2C	691	Cl^- , NO_3^- , Br^- , SO_4^{2-} , ClO_4^-	14d
SLUG-21	602	NO_3^- , CO_3^{2-}	28
SCU-100	553	CO_3^{2-} , SO_4^{2-} , PO_4^{3-}	12e
iPOP-3	515.5	Cl^-, NO_3^-, Br^-, SO_4^{2-}	This Work
iPOP-4	350.3	Cl^-, NO_3^-, Br^-, SO_4^{2-}	This Work
SCU-101	217	various anions	32
NU-1000	210	Cl^- , NO_3^- , Br^- , I^- , SO_4^{2-} ,	33
UIO-66- NH_2	159	NO_3^- , SO_4^{2-} , PO_4^{3-}	34
PQA-pNH ₂ Py-Cl	642	NO_3^- , SO_4^{2-}	11a
Compound-1	517	Cl^- , NO_3^- , Br^- , SO_4^{2-}	14c
PAF-1-F	420	SO_4^{2-} , PO_4^{3-}	35
LDHs	130	N.D.	36
Dowex 1x8	98.1	N.D.	35

Purolite 530E	96	N.D.	35
PolyDMAEMA hydrogels	30.5	N.D.	37

5.6 References

- [1] (a) R.P. Schwarzenbach, B.I. Escher, K. Fenner, T.B. Hofstetter, C.A. Johnson, U. Gunten and B. Wehri, *Science*, 2006, **313**, 1072–1077; (b) J.B. Derraik, *Mar. Pollut. Bull.*, 2002, **44**, 842–852.
- [2] E. M. Dias and C. Petit, *J. Mater. Chem. A.*, 2015, **3**, 22484–22506.
- [3] L. H. Keith and W. A. Teillard, *Environ. Sci. Technol.*, 1979, **13**, 416–423.
- [4] (a) H. Fei, D. L. Rogow and S. R. J. Oliver, *J. Am. Chem. Soc.*, 2010, **132**, 7202–7209; (b) R. Cao, B. D. McCarthy and S. J. Lippard, *Inorg. Chem.*, 2011, **50**, 9499–9507; (c) S. Abubakar, T. Skorjanc, D. Shetty and A. Trabolsi, *ACS Appl. Mater. Interfaces.*, 2021, **13**, 13, 14802–14815.
- [5] (a) Toxicological Profile for Chromium, Public Health Service Agency for Toxic Substances and Diseases Registry, U.S. Department of Health and Human Services, *Atlanta, GA*, 2012; (b) R. Vonburg and D. Liu, *J. Appl. Toxicol.*, 1993, **13**, 225–230; (c) Y. Su, Y. Wang, X. Li, X. Li and R. Wang, *ACS Appl. Mater. Interfaces.*, 2016, **8**, 29, 18904–18911; (d) Y. Wang, H. Zhao, X. Li and R. Wang, *J. Mater. Chem. A*, 2016, **4**, 12554–12560.
- [6] (a) L. Khezami and R. Capart, *J. Hazard. Mater.*, 2005, **123**, 223–231; (b) M. B. Luo, Y. Y. Xiong, H. Q. Wu, X. F. Feng, J. Q. Li and F. Luo, *Angew. Chem., Int. Ed.*, 2017, **56**, 16376–16379; (c) S. Rapti, A. Pournara, D. Sarma, I. T. Papadas, G. S. Armatas, A. C. Tsipis, T. Lazarides, M. G. Kanatzidis and M. J. Manos, *Chem. Sci.*, 2016, **7**, 2427–2436; (d) S. Rapti, D. Sarma, S. A. Diamantis, E. Skliri, G. S. Armatas, A. C. Tsipis, Y. S. Hassan, M. Alkordi, C. D. Malliakas, M. G. Kanatzidis, T. Lazarides, J. C.

Plakatouras and M. J. Manos, *J. Mater. Chem. A.*, 2017, **5**, 14707–14719; (e) S. Dutta, S. Let, S. Sharma, D. Mahato and S. K. Ghosh, *Chem. Rec.*, 2021, DOI: 10.1002/tcr.202100127.

[7] (a) W. Liu, Y. Wang, Z. Bai, Y. Li, Y. Wang, L. Chen, L. Xu, J. Diwu, Z. Chai and S. Wang, *ACS Appl. Mater. Interfaces*, 2017, **9**, 16448–16457; (b) S. R. J. Oliver, *Chem. Soc. Rev.*, 2009, **38**, 1868–1881; (c) S. Dutta, S. Let, M. M Shirolkar, A. V. Desai, P. Samanta, S. Fajal, Y. D. More, S. K. Ghosh, *Dalton Trans.*, **2021**, DOI:10.1039/D1DT01097B.

[8] C. Pellerin and S. M. Booker, *Environ. Health Perspect.*, 2000, **108**, A402–A407.

[9] C. Xiao, A. Khayambashi and S. Wang, *Chem. Mater.*, 2019, **31**, 3863–3877.

[10] S. Wang, P. Yu, B. A. Purse, M. J. Orta, J. Diwu, W. H. Casey, B. L. Phillips, E. V. Alekseev, W. Depmeier, D. T. Hobbs and T. E. Albrecht-Schmitt, *Adv. Funct. Mater.*, 2012, **22**, 2241–2250.

[11] (a) Q. Sun, L. Zhu, B. Aguila, P. K. Thallapally, C. Xu, J. Chen, S. Wang, D. Rogers and S. Ma, *Nat. Commun.*, 2019, DOI: 10.1038/s41467-019-09630; (b) X. Li, Y. Li, H. Wang, Z. Niu, Y. He, L. Jin, M. Wu, H. Wang, L. Chai, A. M. Al-Enizi, A. Nafady, S. F. Shaikh, and S. Ma, *Small*, 2021, 2007994 (DOI: 10.1002/smll.202007994).

[12] (a) T. H. Boyer and P. C. Singer, *Environ. Sci. Technol.*, 2008, **42**, 608–613; (b) B. Gammelgaard, Y. P. Liao and O. Jons, *Anal. Chim. Acta*, 1997, **354**, 107–113; (c) B. Wen, X. Q. Shan and J. Lian, *Talanta*, 2002, **56**, 681–687; (d) A. Syty, R. G. Christensen and T. C. Rains, *J. Anal. At. Spectrom.*, 1988, **3**, 193–197; (e) D. Sheng, L. Zhu, C. Xu, C. Xiao, Y. Wang, Y. Wang, L. Chen, J. Diwu, J. Chen, Z. Chai, T. E. Albrecht-Schmitt and S. Wang, *Environ. Sci. Technol.*, 2017, **51**, 3471–3479; (f) D. Banerjee, D. Kim, M. J. Schweiger, A. A. Kruger and P. K. Thallapally, *Chem. Soc. Rev.*, 2016, **45**, 2724–2739.

[13] (a) A. V. Desai, B. Manna, A. Karmakar, A. Sahu and S. K. Ghosh, *Angew. Chem. Int. Ed.*, 2016, **55**, 7811–7815; (b) J. Li, X. Dai, L. Zhu, C. Xu, D. Zhang, M. A. Silver, P. Li, L. Chen, Y. Li, D. Zuo, H.

Zhang, C. Xiao, J. Chen, J. Diwu, O. K. Farha, T. E. Albrecht-Schmitt, Z. Chai and S. Wang, *Nat. Commun.*, 2019, DOI: 10.1038/s41467-018-05380-5.

[14] (a) P. Samanta, A. V. Desai, S. Let and S. K. Ghosh, *ACS Sustainable Chem. Eng.*, 2019, **7**, 7456–7478; (b) Q. Gao, J. Xu and X.-H. Bu, *Coord. Chem. Rev.*, 2019, **378**, 17-31; (c) P. Samanta, P. Chandra, S. Dutta, A. V. Desai and S. K. Ghosh, *Chem. Sci.*, 2018, **9**, 7874–7881; (d) S. Dutta, P. Samanta, B. Joarder, S. Let, D. Mahato, R. Babarao and S. K. Ghosh, *ACS Appl. Mater. Interfaces.*, 2020, **12**, 41810–41818.

[15] (a) X. Feng, X. Ding and D. Jiang, *Chem. Soc. Rev.*, 2012, **41**, 6010–6022; (b) A. G. Slater and A. I. Cooper, *Science*, 2017, **348**, DOI: 10.1126/science.aaa8075; (c) H. M. El-Kaderi, J. R. Hunt, J. L. Mendoza-Cortés, A. P. Côté, R. E. Taylor, M. O’Keeffe and O. M. Yaghi, *Science*, 2007, **316**, 268–272; (d) A. Karmakar, A. V. Desai and S. K. Ghosh, *Coord. Chem. Rev.*, 2016, **307**, 313–341; (e) S. Furukawa, J. Reboul, S. Diring, K. Sumida and S. Kitagawa, *Chem. Soc. Rev.*, 2014, **43**, 5700–5734; (f) P. Samanta, S. Let, W. Mandal, S. Dutta and S. K. Ghosh, *Inorg. Chem. Front.*, 2020, **7**, 1801-1821; (g) A. J. Howarth, M. J. Katz, T. C. Wang, A. E. Platero-Prats, K. W. Chapman, J. T. Hupp and O. K. Farha, *J. Am. Chem. Soc.*, 2015, **137**, 7488–7494; (h) T. Kitao, Y. Zhang, S. Kitagawa, B. Wang and T. Uemura, *Chem. Soc. Rev.*, 2017, **46**, 3108–3133; (i) Z. Hu, B. J. Deibert and J. Li, *Chem. Soc. Rev.*, 2014, **43**, 5815–5840; (j) S. Sharma, S. Let, A. V. Desai, S. Dutta, G. Karuppasamy, M. M. Shirolkar, R. Babarao and S. K. Ghosh, *J. Mater. Chem. A*, 2021, **9**, 6499-6507.

[16] (a) W. Lu, D. Yuan, J. Sculley, D. Zhao, R. Krishna and H. -C. Zhou, *J. Am. Chem. Soc.*, 2011, **133**, 18126–18129; (b) S. Keskin, T. M. van Heest and D. S. Sholl, *ChemSusChem.*, 2010, **3**, 879–891.

[17] (a) W. Lu, D. Yuan, D. Zhao, C. I. Schilling, O. Plietzsch, T. Muller, S. Bräse, J. Guenther, J. Blümel, R. Krishna, Z. Li and H. -C. Zhou, *Chem. Mater.*, 2010, **22**, 5964–5972; (b) M. G. Rabbani and H. M. El-Kaderi, *Chem. Mater.*, 2011, **23**, 1650–1653; (c) G. Garai, D. Shetty, T. Skorjanc, F. Gándara, N. Naleem, S. Varghese, S. K. Sharma, M. Baias, R. Jagannathan, M. A. Olson, S. Kirmizialtin and A.

- Trabolsi, *J. Am. Chem. Soc.*, 2021, 143, **9**, 3407–3415; (d) S. P. S. Fernandes, V. Romero, B. Espiña, L. M. Salonen, *Chem. Eur. J.*, 2019, **25**, 6461-6473.
- [18] H. Zhao, L. Li, Y. Wang and R. Wang, *Sci. Rep.*, 2014, **4**, 5478.
- [19] (a) A. Kumar, E. Zangrando and P. S. Mukherjee, *Polyhedron.*, 2019, **172**, 67-73; (b) G. M. Roberts, P. J. Pierce and L. K. Woo, *Organometallics*. 2013, 32, **6**, 2033–2036.
- [20] (a) H. Pan, Z. Cheng, Z. Xiao, X. Li and R. Wang, *Adv. Funct. Mater.*, 2017, **27**, 1703936; (b) Y. Gong, H. Zhong, W. Liu, B. Zhang, S. Hu and R. Wang, *ACS Appl. Mater. Interfaces.*, 2018, 10, **1**, 776–786.
- [21] (a) D. Chen, C. Cui, N. Tong, H. Zhou, X. Wang and R. Wang, *ACS Appl. Mater. Interfaces.*, 2019, 11, **1**, 1480–1486; (b) Z.-W. Liu, C.-X. Cao and B.-H. Han, *J. Hazard. Mater.*, 2019, 367, **5**, 348-355; (c) Dr. G. Xu, Y. Zhu, Dr. W. Xie, Dr. S. Zhang, Dr. C. Yao and Prof. Dr. Y. Xu, *Chem. Asian J.*, 2019, **14**, 3259–3263.
- [22] H. Yang and H. Fei, *Chem. Commun.*, 2017, **53**, 7064–7067.
- [23] J. Cao and W. -X. Zhang, *J. Hazard. Mater.*, 2006, **132**, 213–219.
- [24] H. -L. Ma, Y. Zhang, Q. -H. Hu, D. Yan, Z. -Z. Yu and M. Zhai, *J. Mater. Chem.*, 2012, **22**, 5914–5916.
- [25] L. Li, X. Feng, R. Han, S. Zang and G. Yang, *J. Hazard. Mater.*, 2017, **321**, 622–628.
- [26] H. Fei, C. S. Han, J. C. Robins, S. R. J. Oliver, *Chem. Mater.* **2013**, 25, 647–652.
- [27] P. Shi, B. Zhao, G. Xiong, Y. Hou, P. Cheng, *Chem. Commun.* **2012**, 48, 8231–8233.
- [28] H. Fei, M. R. Bresler, S. R. J. Oliver, *J. Am. Chem. Soc.* **2011**, 133, 11110–11113.
- [29] B. Qiu, C. Xu, D. Sun, H. Wei, X. Zhang, J. Guo, Q. Wang, D. Rutman, Z. Guo, S. Wei, *RSC Adv.* **2014**, 4, 29855–29865.

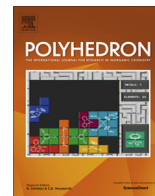
- [30] L. Zhu, C. Xiao, X. Dai, J. Li, D. Gui, D. Sheng, L. Chen, R. Zhou, Z. Chai, T. E. Albrecht-Schmitt and S. Wang, *Environ. Sci. Technol.Lett.*, 2017, **4**, 316–322.
- [31] H. Xu, C.-S. Cao, H.-S. Hu, S.-B. Wang, J.-C. Liu, P. Cheng, N. Kaltsoyannis, J. Li and B. Zhao, *Angew. Chem. Int. Ed.*, 2019, **131**, 6083-6088.
- [32] L. Zhu, V. Sheng, C. Xu, X. Dai, M. A. Silver, J. Li, P. Li, Y. Wang, Y. Wang, L. Chen, C. Xiao, J. Chen, R. Zhou, C. Zhang, O. K. Farha, Z. Chai, T. E. Albrecht-Schmitt and S. Wang, *J. Am. Chem. Soc.*, 2017, **139**, 14873–14876.
- [33] R. J. Drout, K. Otake, A. J. Howarth, T. Islamoglu, L. Zhu, C. Xiao, S. Wang and O. K. Farha, *Chem. Mater.*, 2018, **30**, 1277–1284.
- [34] D. Banerjee, W. Q. Xu, Z. M. Nie, L. E. V. Johnson, C. Coghlan, M. L. Sushko, D. Kim, M. J. Schweiger, A. A. Kruger, C. J. Doonan, P. K. Thallapally, *Inorg. Chem.* **2016**, *55*, 8241–8243.
- [35] D. Banerjee, S. K. Elsaidi, B. Aguila, B. Li, D. Kim, M. J. Schweiger, A. A. Kruger, C. J. Doonan, S. Ma and P. K. Thallapally, *Chem. Eur. J.*, 2016, **22**, 17581–17584.
- [36] H. Fei, C. S. Han, J. C. Robins and S. R. J. Oliver, *Chem. Mater.*, 2013, **25**, 647–652.
- [37] Y. Yan, M. Yi, M. L. Zhai, H. F. Ha, Z. F. Luo and X. Q. Xiang, *React. Funct. Polym.*, 2004, **59**, 149-154.

Chapter 6

Summary and Perspectives

6.1 Summary and Perspectives

Advanced functional porous materials (AFPMS) gained tremendous importance in the last several decades due to their utilization in a variety of fields including clean energy, molecular recognition and environment related applications. The scientific works carried out in this thesis were to develop task specific AFPMS to address the global problems of environment pollution. In the first part of the work, MOFs were utilised for recognition of toxic pollutants using fluorescence based detection methods. In this regard, a functional luminescent MOF was designed utilising a electron deficient naphthalene di-imide linker was utilised to recognise a toxic electron rich VOC like styrene through host guest interaction. Moreover, functional water stable MOF was designed with suitable functional groups appended through covalent post-synthetic approach to selectively detect bisulphite anion (HSO_3^-), the hydrolysed form of sulphur dioxide, in water medium. These studies will help to enrich the library of luminescent MOF and develop smart sensor materials for detection of toxic environment pollutants. The second part of the work deals with design, synthesis and applications of light-weight physio-chemically stable porous organic polymers for selective sequestration of toxic water pollutants. In that context, aromatic functionalised ionic porous organic polymers was utilised to capture I_2 and I_3^- as surrogate for radioiodine released post nuclear fission. The iodine uptake was studied in both vapour and water medium and the materials were selective to iodine due to presence of interaction sites within the architectures. The uptake process were persistent in presence of concurrent anions as well as the materials were recyclable up to three cycles with retention of performances. In this work cationic porous organic polymers are also utilised for uptake of chromate (CrO_4^{2-}), a well-known water pollutant through ion exchange strategy. The same materials were also utilised for perrhenate (ReO_4^-) uptake as a surrogate for radioactive pertechnetate (TcO_4^-) anion from water. The polymers showed appreciable uptake for both the oxoanions as well as selectivity in terms of retention of uptake performance even in presence of competing available ions in water. The uptake process was reversible depicting potential of aforementioned materials in terms of usage in real time application. The studies carried out in this thesis focuses on strategic development of AFPMS for multifunctional applications including both detection and sequestration of air and water pollutants and such materials can be utilised in workable forms in near future for remediation of environment pollutants.



Post-synthetically modified metal–organic framework as a scaffold for selective bisulphite recognition in water

Arunabha Sen^a, Aamod V. Desai^{a,1}, Partha Samanta^{a,1}, Subhajit Dutta^a, Sumanta Let^a, Sujit K. Ghosh^{a,b,*}

^a Department of Chemistry, Indian Institute of Science Education and Research (IISER), Dr. Homi Bhabha Road, Pashan, Pune 411008, India

^b Centre for Energy Science, IISER Pune, Dr. Homi Bhabha Road, Pashan, Pune 411008, India

ARTICLE INFO

Article history:

Received 9 July 2018

Accepted 29 August 2018

Available online 5 September 2018

Keywords:

Metal–organic framework

Post-synthetic modification

Sensing

Bisulfite ion

Turn-on

ABSTRACT

A metal–organic framework (MOF) based luminescent probe was strategically designed for selective recognition of bisulfite anion (HSO_3^-) in water medium. The chemically stable MOF, $\text{NH}_2\text{-MIL-68(In)}$ was decorated with specific recognition site via post synthetic modification. The post synthetically modified MOF showed a selective turn on response towards bisulfite anion retaining its structural integrity. This selective recognition is also persistent even in presence of competing anions.

© 2018 Elsevier Ltd. All rights reserved.

1. Introduction

The versatile role played by anions both in biological and environmental aspects makes anion recognition an important area of scientific interest. Hence anion recognition chemistry has seen tremendous development over the past few decades [1]. Sulphur dioxide (SO_2), a known major air pollutant further on hydrolysis produces its oxo-anion namely bisulfite (HSO_3^-) [2,3]. Bisulfite anion plays a crucial role in regulation of different cardiovascular processes in our body at low concentration [4]. Also it is used extensively in food, beverage and pharmaceutical industries as an antioxidant and antimicrobial agent [5]. However, at high concentration it is well established to have marked adverse effects [6]. This includes attack in the cells and tissues of human respiratory system leading to asthmatic and allergic tendencies [7]. Further it is also found that bisulfite anion affects the human cardiovascular and alimentary systems leading to abdominal pain, diarrhea, dermatitis, hypertension as well as other biological disorders [8]. Based on all these facts some countries have imposed serious restrictions on usage of bisulfite in food products either to a very low level or prohibited it [9]. So from a bigger perspective recognition of bisulfite in water medium is very important. Many analytical techniques which include electrophoresis and electrochemical methods, chromatography etc., have been developed for

determination of bisulfite [10]. Due to lack of simplicity to a great extent and time consuming procedure have hindered the application of aforementioned techniques. On the other hand fluorescence spectroscopy is a simple, cost effective and sensitive technique with fast response time and can be an alternate powerful tool to serve this purpose [11]. Various luminescent organic probes with specific functionalities have been designed in the past for selective sensing of bisulfite anions. This includes inclusion of functional moieties like aldehyde and levulinate group or group containing unsaturated covalent bonds into the probe [12]. The reason behind choice of such groups is the facile chemical reactions of the bisulfite anion with all these functionalities which results in achieving a fast and accurate response in fluorescence intensity. But low water solubility often causes difficulty for such organic probes to detect bisulfite in water medium [13]. So designing luminescent probes for selective anion recognition in water medium is indeed required.

Metal–organic frameworks (MOFs) are a distinguished class of crystalline porous material that has emerged over the last decade [14]. Constructed from organic struts and metal nodes, MOFs represent an excellent tunable structure–property co-relationship. The choice of metal nodes as well as the design of the organic counterpart can be devised strategically to target and obtain any specific functionality. This can be utilized for the usage of MOFs in terms of molecular storage and separation, sensors, ion-conduction, molecular transport and various other applications [15]. Luminescent MOFs (LMOFs) are a subclass of MOFs with wide range of applications in terms of molecular sensing, fabrication of optical devices etc [16]. The long range ordering and porosity generated from the coordination

* Corresponding author at: Department of Chemistry, Indian Institute of Science Education and Research (IISER), Dr. Homi Bhabha Road, Pashan, Pune 411008, India.

E-mail address: sgghosh@iiserpune.ac.in (S.K. Ghosh).

¹ These authors contributed equally.

RESEARCH ARTICLE

Imidazolium Functionalized Chemically Robust Ionic Porous Organic Polymers (*i*POPs) toward Toxic Oxo-pollutants Capture from Water

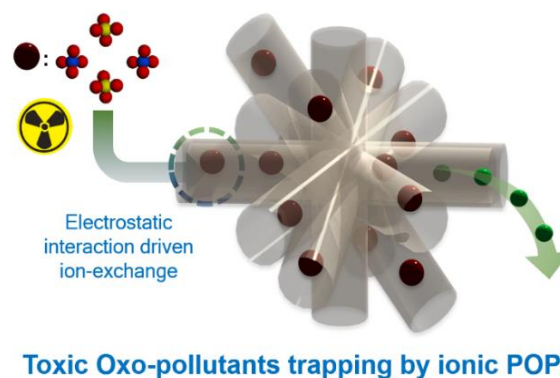
Arunabha Sen,^{[a]†} Subhajit Dutta,^{[a]†} Gourab K. Dam,^[a] Dr. Partha Samanta,^[a] Sumanta Let,^[a] Dr. Shivani Sharma,^[a] Dr. Mandar M. Shirolkar,^[b] Prof. Sujit K. Ghosh*^[a]

Abstract: Fabricating new and efficient materials aimed at containment of water contamination, in particular removing toxic heavy metal based oxo-anions (for example CrO_4^{2-} , TcO_4^-) holds paramount importance. In this work, we report two new highly stable imidazolium based ionic porous organic polymers (*i*POPs) decorated with multiple interaction sites along with electrostatics driven adsorptive removal of such oxo-anions from water. Both the *i*POPs (namely, *i*POP-3 and *i*POP-4) exhibited rapid sieving kinetics and very high saturation uptake capacity for CrO_4^{2-} anions (170 and 141 mg g^{-1} for *i*POP-3 and *i*POP-4 respectively) and ReO_4^- (515.5 and 350.3 mg g^{-1} for *i*POP-3 and *i*POP-4 respectively), where ReO_4^- anions being the non-radioactive surrogate counterpart of radioactive TcO_4^- ions. Noticeably, both *i*POPs showed exceptional selectivity towards CrO_4^{2-} and ReO_4^- even in presence of several other concurrent anions such as Br^- , Cl^- , SO_4^{2-} , NO_3^- etc. The theoretical binding energy calculations via DFT method further confirmed the preferential interaction sites as well as binding energies of both *i*POPs towards CrO_4^{2-} and ReO_4^- over all other competing anions which corroborates with the experimental high capacity and selectivity of *i*POPs towards such oxo-anions.

Introduction

Accessibility to fresh drinking water has become an imminent threat in the 21st century that have direct impact on human lives. The far-flung growth in industrialization and widespread urbanization across the globe are the two prime reasons behind such crisis and depletion of fresh water.^[1] This situation might become so dreadful that as many as one billion of global population will experience utmost water crisis by 2025, as predicted by United Nations.^[2] Among various contamination sources, water pollution by heavy metals (density > 5 g cm^{-3}) and their oxo-anionic complexes (CrO_4^{2-} , MnO_4^- , SeO_3^{2-} , AsO_4^{3-} etc.) have come forth as pressing concern, owing to their severe toxic effect on living organisms upon bioaccumulation.^[3] In addition, such toxic oxo-anions are considered as the “priority pollutants”, listed by Environment Protection Agency (EPA, United States).^[4] In this context, special attention has been directed toward Cr(VI)

based oxo-anions because of their carcinogenic and mutagenic impact on living beings.^[5] Several industrial sectors including leather tanning, steel manufacturing, textile pigments & dyes, wood preservation etc. are involve in chromium usage in huge amounts for diverse applications. As is known, tanning industries generate ~35 L of chromium contaminated wastewater solely for one kilogram of leather production which subsequently pollute natural water bodies.^[6] Additionally, Cr (VI) based oxo-anions are found to weaken the integrity of nuclear waste glass during its vitrification process resulting in poor efficiency of the process.^[6] Moreover, the world has witnessed several incidents of ground water pollution because of improper disposal of Cr (VI) containing wastewater.^[7] Hinkley groundwater contamination in California is one of the famous example where ~1,400 million litres of chromium containing wastewater was disposed into the natural waterbodies.^[8] In addition, other than Cr(VI)-based water pollution issues, ground water contamination by nuclear power plant generated radioactive wastes have become another major concern.^[9] In this regard, nuclear safety has become a genuine concern as the last few decades have witnessed several nuclear accidents, which lead to contamination of radioisotopes in large scale along with their chemotoxicity and radiotoxicity to natural water bodies. Among them, pertechnetate (TcO_4^-) anion has attracted much research attention mainly as one of its β -emitting radioactive isotope technetium (^{99}Tc), which possess a very prolonged half-life period of 2.1×10^5 years. Moreover, nuclear fission of ^{239}Pu and ^{235}U result into a very large fission yield of radioactive ^{99}Tc and approximately 305 metric tons nuclear waste containing ^{99}Tc have been discharged from several nuclear power plants and weapons testing activities.^[10] The non-complexing characteristic of TcO_4^- along with its high mobility and solubility in water allows it to remain as low-level nuclear-waste material.^[11] Several techniques, for example, adsorption, photocatalytic reduction, chemical precipitation, ion exchange etc.



Scheme 1. Schematic representation of toxic oxo-anion capture in *i*POPs.

[a] Department of Chemistry, Indian Institute of Science Education and Research (IISER), Pune. Dr. Homi Bhabha Road, Pashan, Pune-411008, India. E-mail: sghosh@iiserpune.ac.in

[b] Symbiosis Center for Nanoscience and Nanotechnology (SCNN), Symbiosis International (Deemed University) (SIU), Lavale, Pune 412115, Maharashtra.

† These authors contributed equally to this work. Supporting information for this article is given via a link at the end of this document.

Functionalized Ionic Porous Organic Polymers Exhibiting High Iodine Uptake from Both the Vapor and Aqueous Medium

Arunabha Sen,[§] Shivani Sharma,[§] Subhajit Dutta, Mandar M. Shirolkar, Gourab K. Dam, Sumanta Let, and Sujit K. Ghosh*



Cite This: <https://doi.org/10.1021/acsami.1c07178>



Read Online

ACCESS |



Metrics & More



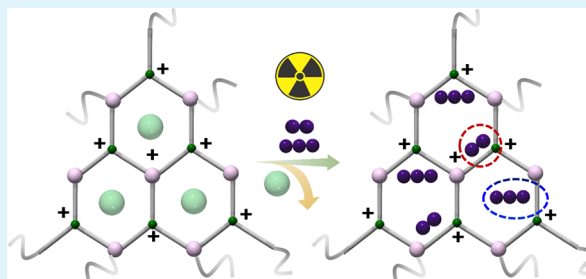
Article Recommendations



Supporting Information

ABSTRACT: Large-scale generation of radioactive iodine (^{129}I , ^{131}I) in nuclear power plants pose a critical threat in the event of fallout, thus rendering the development of iodine sequestering materials (from both the vapor and aqueous medium) highly pivotal. Herein, we report two chemically stable ionic porous polymers containing multiple binding sites, including phenyl rings, imidazolium cations, and bromide anions, which in synergy promote adsorption of iodine/triiodide anions. In brief, exceptional iodine uptake (from the vapor phase) was observed at nuclear fuel reprocessing conditions. Furthermore, the ionic nature propelled removal of $>99\%$ of I_3^- from water within 30 min. Additionally, benchmark uptake capacities, as well as unprecedented selectivity, were observed for I_3^- anions. The excellent affinity (distribution coefficient, $\sim 10^5$ mL/g) enabled iodine capture from seawater-spiked samples. Moreover, iodine-loaded compounds showed conductivity (10^{-4} S/cm, 10^{-6} S/cm), placing them among the best known conducting porous organic polymers. Lastly, DFT studies unveiled key insights in coherence with the experimental findings.

KEYWORDS: ionic porous organic polymers (iPOPs), radioactive iodine, capture, cationic network, distribution coefficient, real-world samples, DFT studies



INTRODUCTION

Nuclear energy is regarded as an efficient zero emission-based clean energy source.¹ Recent projection estimate a substantial rise of $\sim 80\%$ in nuclear energy by the year 2050, reaching a massive ~ 715 GW(e)/annum.² Typically, nuclear energy generated via uranium (^{235}U) fission produces several harmful radioactive isotopes alongside, which includes selenium (^{79}Se), technetium (^{99}Tc), iodine (^{129}I , ^{131}I), krypton (^{85}Kr), and so on.³ Among them, ^{129}I is regarded as extremely dangerous because of its large half-life ($\sim 1.57 \times 10^7$ years) and high volatility.^{4,5} Also, ^{131}I , although exhibiting a shorter half-life span (~ 8 days),⁶ is even more problematic as it can interfere with metabolic processes causing various adverse effects such as coma and untimely death as witnessed during the tragic Chernobyl nuclear disaster.^{4,7} Moreover, a significant spike in concentrations of volatile radionuclides (^{131}I , ^{129}I , and ^{137}Cs) was observed all across Europe, especially in water bodies after the Chernobyl nuclear disaster.^{6,7} Furthermore, ^{131}I shows utility in cancer therapy and is regularly generated in hospitals, which is unequivocally risky as well.⁸ Classically, iodine exists as molecular iodine (I_2) in the vapor phase;⁹ however, recent studies have also hinted at the presence of iodide (I^-) and triiodide anions (I_3^-) in the vapor phase.^{6,10} While, in the aqueous medium, iodine tends to form polyiodides, among which triiodide (I_3^-) is one of the most predominant species.^{6,11}

The state-of-the-art materials employed for iodine sequestration include silver-based zeolites (Ag-Z), activated carbons, zerovalent iron (ZVI), and clays.^{12–14} Although displaying high chemical stability, these traditional sorbents fail to reach high sorption capacity and selectivity on account of low surface areas and weak interactions.¹⁵ Additionally, the incorporation of expensive silver metal lowers the cost-effectiveness, thus making them unsustainable for the long-term use.¹⁶ This renders development of cost-efficient and highly selective sorbents for radioactive iodine capture from both vapor and aqueous phases of high topical relevance.

As a seminal class of porous materials, metal-organic frameworks (MOFs), covalent-organic frameworks (COFs), porous organic polymers (POPs), porous organic materials (POMs), and others have shown vast potential in several applications, including molecular recognition-based capture studies.^{17–25} In particular, recent literature reflects an upsurge in researcher's interest globally in developing advanced porous

Received: April 19, 2021

Accepted: July 7, 2021